EUROPEAN COMMISSION

European Research Area

The design of avalanche protection dams

Recent practical & theoretical developments

EUR 23339

PROJECT REPORT

Climate Change and Natural Hazard Research - Series 2

COOPERATION

Interested in European research?

Research*eu is our monthly magazine keeping you in touch with main developments (results, programmes, events, etc.).
It is available in English, French, German and Spanish. A free sample copy or free subscription can be obtained from:

European Commission

Directorate-General for Research

Communication Unit

B-1049 Brussels

Fax (32-2) 29-58220

E-mail: research-eu@ec.europa.eu

Internet: http://ec.europa.eu/research/research-eu

EUROPEAN COMMISSION
Directorate-General for Research
Directorate I — Environment
Unit I.5 — Climate Change and Environmental Risks

E-Mail: rtd-climate-change@ec.europa.eu
Contact: Denis PETER
Sub-activity: Natural Hazards

European Commission
Office CDMA 3/120
B-1049 Brussels
Tel. (32-2) 29-58446
Fax (32-2) 29-95755
E-mail: denis.peter@ec.europa.eu

EUROPEAN COMMISSION

The design of avalanche protection dams

Recent practical and theoretical developments




Edited by T. Jóhannesson[1], P. Gauer[2], P. Issler[2] and K. Lied[2]

Contributions by M. Barbolini[4], U. Domaas[2], T. Faug[3], P. Gauer[2], K. M. Hákonardóttir[1,6], C. B. Harbitz[2], D. Issler[2], T. Jóhannesson[1], K. Lied[2], M. Naaim[3], F. Naaim-Bouvet[3] and L. Rammer[5]

[1] Icelandic Meteorological Office
[2] Norwegian Geotechnical Institute
[3] CEMAGREF, Research Division on Torrents, Snow and Avalanches, ETNA
[4] FLOW-ING s.r.l.
[5] Austrian Institute for Avalanche and Torrent Research
[6] VST Consulting Engineers Ltd.

Directorate-General for Research

2009 Environment Directorate EUR 23339

Photographs on the title page:
Top left: Mounds and catching dam in Neskaupstaður, eastern Iceland, photo: Tómas Jóhannesson.
Top right: A catching dam, deflecting dam, and concrete wedges at Taconnaz, near Chamonix, France, photo: Christopher J. Keylock.
Bottom left: Two deflecting dams at Gudvangen, near Voss in western Norway, after successful deflections of consecutive avalanches on both dams, photo: Ulrik Domaas.
Bottom right: A catching dam and braking mounds at Arzleralm-Lawine near Innsbruck, Tirol, Austria, photo: A. Gwercher.

Cataloguing data can be found at the end of this publication.

Luxembourg: Office for Official Publications of the European Communities, 2009

ISBN 978-92-79-08885-8
ISSN 1018-5593
DOI 10.2777/12871

Printed in Belgium
PRINTED ON WHITE CHLORINE-FREE PAPER

Contents

List of Tables

List of Figures

Foreword

Snow avalanches represent a serious problem for society. During the last decade, catastrophic avalanches in Europe focused the attention of the public and politicians on avalanche danger and the associated risks. An adequate level of avalanche safety is a prerequisite to further development of mountain regions as habitable areas, prime destinations of tourism, and the critical segments of some of the most important European traffic routes.

Therefore, avalanche protective measures have become increasingly important due to population growth and increasing tourism in many avalanche-prone areas in the Alps and elsewhere. Furthermore, higher safety and risk awareness is required from modern societies.

Extensive avalanche protective measures have been constructed in several countries in recent decades. The effectiveness of the different types of protective measures is still an open question. Properly designed supporting structures in the starting zones are considered sound protection against avalanches, as conclusively demonstrated in the Alps during the avalanche winter of 1999. During the same winter, several avalanches overran avalanche dams, underlining the need for further research in this field.

The European Commission (EC) is supporting Natural Hazards research efforts through its Environment research programme. In the field of avalanche research, and in particular related to avalanche dynamics and avalanche dams, the research projects CADZIE and SATSIE have furthered the state of the art. Based on laboratory experiments and theoretical analyses, these projects have led to an improved understanding of the flow of snow avalanches against dams and other obstructions, and made it possible to take a step forward in the formulation of design criteria for protective measures in the run-out zones of avalanches. Performing this work at a European level in order to share know-how and make maximum use of the large cost of operating full-scale experimental sites was essential.

This book brings together the main results of this development and combines them with traditional design principles to form a new framework for the design of avalanche dams. Although uncertainties remain, the book represents an important improvement. It is therefore important that these results are disseminated effectively to potential users, including the community of avalanche professionals in Europe and elsewhere.

I do hope that the book will increase awareness about avalanche risks, improve the prevention capacity and enable efficient avalanche mitigation options and measures to be put in place for the benefit of all.

Manuela Soares
Director
Research Directorate-Environment

1 Introduction

Protective measures against snow- and landslides are widely used to improve the safety of settlements in avalanche-prone areas. Measures to manage snow- and landslide danger and protect settlements include:

Land use planning: With proper hazard zoning and long term planning of building activity, this is undoubtably the safest and most cost-effective way to manage danger due to snow- and landslides. It does, however, not solve problems associated with settlements that have already been developed in hazard areas.

Evacuations: Moving people from threatened areas can be either *permanently*, usually with some assistance from the government or local authorities to relocate settlements, or *temporarily*, by evacuating people from their homes and work places during avalanche cycles. Temporary evacuations during avalanche cycles are usually not considered a viable long-term solution for ensuring the safety of settlements.

Supporting structures: Supporting structures in the starting zones of avalanches are the most widely used protective measures in the Alps and have also been used to a lesser extent in many other countries. There is firm evidence that properly designed supporting structures reduce the avalanche hazard substantially, in particular the experience gained during the harsh avalanche winter of 1999 in the Alps.

Deflecting dams: If there is sufficient space in the run-out zone and if the endangered area is suitably located with respect to the direction of the avalanches, deflecting dams may be used to divert avalanches away from objects at risk. Deflecting dams are often a cost-effective solution and several examples of successful deflections of medium-sized avalanches have been documented.

Catching dams: Catching dams are intended to stop dense avalanches or the dense part of mixed-type avalanches completely before they reach objects at risk. They are typically used for extended areas along the foot of the slope where there is insufficient space for deflecting dams. Large avalanches flowing at high speed can hardly be stopped by catching dams and there are many examples of avalanches overtopping such dams. The effectiveness of catching dams is therefore dependent upon a location near the lower end of the run-out zone of the avalanches.

Wedges for the protection of individual buildings: Individual buildings may be protected by short deflecting constructions that are either built a short distance away from the building or constructed as a part of the building. Such wedges are widely used and have proven to be an effective protection method against avalanches.

Braking mounds: Braking mounds are used to retard avalanches by breaking up the flow and causing increased dissipation of kinetic energy. There is not much observation evidence for the effectiveness of braking mounds for natural avalanches, but laboratory experiments with granular materials indicate that they can reduce the speed and run-out distance of avalanches.

Reinforcement of buildings: Specially designed buildings to withstand the impact pressures of avalanches can increase the safety of the inhabitants considerably. Because of the very high impact pressure of snow avalanches, such buildings must either be built into the slope, so that the avalanches overflow them, or constructed near the lower end of the run-out zone, where the flow velocity has been reduced to lower levels than higher up the path.

Measures to reduce snow accumulation in starting areas: Snow fences in catchment areas for snow drift may be used to collect snow that would otherwise be carried into an adjacent starting zone, thereby decreasing the volume and thus the run-out of the avalanches.

This book discusses the design of dams and other protective measures in the *run-out zones of wet- and dry-snow avalanches*. It summarises recent theoretical developments and the results of field and laboratory studies, combining them with traditional design guidelines and principles to formulate design recommendations. Not discussed are hazard zoning, land use planning, evacuations, supporting structures in starting zones, snow fences in catchment areas, and other safety measures outside the run-out zone. Reinforcement of individual buildings also falls outside the scope of the book, as do protective measures against landslides and slushflows.

The book is organised as follows. Section 2 describes the dialogue between avalanche experts, local authorities and the public during the design of avalanche protective measures. This is an important aspect of the preparation of protective measures, where decision makers and the public have a chance to come forward with their views on the problem and are informed about *possible alternatives*, *rest risk*, *hazard zoning after measures have been implemented* and other key concepts.

Sections 3 and 4 give an overview of traditional design principles for avalanche dams and a summary of avalanche dynamics, with an emphasis on the interaction of avalanches with obstacles.

The design of deflecting dams, catching dams and braking mounds is discussed in Sections 5 to 9, which are followed by Section 10 about the effect of dams on powder-snow avalanches.

Sections 11 and 12 deal with impact loads on walls and on masts and narrow obstacles, and point loads due to impacts of solid bodies and static snow loads are treated in Sections 13 and 14.

Geotechnical aspects of dam design are discussed in Section 15, followed by a discussion of unresolved issues and open questions in Section 16.

The book concludes with seven appendices: Appendix A: A summary of the proposed dam design requirements; Appendix B: Definitions of the variables used in the book; Appendix C: Examples of the design of deflecting and catching dams; Appendix D: An example of integrated protective measures; Appendix E: Examples of loads on structures; Appendix F: A summary of existing Swiss and Norwegian recommendations about loads on structures; and Appendix G: A summary of laws and regulations about avalanche protective measures and hazard zoning after the completion of protective measures in several European countries.

The design of protective measures in the run-out zones of avalanches needs to be based on an understanding of the dynamics of granular flows against obstructions that lead to a change in the flow direction, slow the flow down or cause it to stop. In spite of advances in the understanding of the dynamics of avalanches against obstacles in recent years, there remains

considerable uncertainty regarding the effectiveness of deflecting dams, catching dams, braking mounds, wedges and other defence structures in run-out zones. In particular, analyses of run-up against man-made dams and natural obstacles, on the one hand (see Section 5.9), and overrun over the catching dam at Ryggfonn in western Norway (see Section 7.2), on the other, give quite misleading indications about the effectiveness of dams to bring avalanches to a halt or shorten their run-out. *This uncertainty about the effectiveness of dams must be borne in mind in all planning of protective measures in run-out zones.*

Traditionally, one of the most important and difficult steps in the design of dams and other protective measures in the run-out zones of snow avalanches is the definition of an appropriate *design avalanche*. This is intimately linked with *hazard zoning*, which in most cases is the background for the decision to implement protective measures in the first place. This book will only indirectly touch upon hazard zoning and the choice of a design avalanche, assuming in most places that the velocity, flow depth and other relevant properties of the oncoming avalanche under consideration have already been decided. However, some properties of the design avalanche will be considered where appropriate. The section about deflecting dams, for example, contains practical considerations regarding the choice of the deflecting angle for deflecting dams. Hazard zoning below avalanche dams is also briefly discussed in the sections about deflecting dams and catching dams.

The book is written as a part of the research project SATSIE (grant EVG1-CT-2002-00059), with support from the European Commission, and is partly based on results of theoretical analyses, field measurements, and laboratory experiments that have been carried out within that project and its predecessor CADZIE (grant EVG1-1999-00009), which was also supported by the European Commission. The book has also benefited from various national research projects in the countries participating in SATSIE and CADZIE that have contributed to the results summarised here. Support to finalise the book was provided by the Icelandic Avalanche and Landslide Fund.

Stefan Margreth from the Swiss Federal Institute for Snow and Avalanche Research in Davos gave useful comments on the sections on impact loads. Jón Snorri Ásgeirsson, member of the Association of Certified Court Interpreters and Translators in Iceland, and Nikolai Nawri, meteorologist at the Icelandic Meteorological Office, read the whole manuscript and suggested many improvements to the English language and to the presentation of the material.

2 Consultations with local authorities and decision makers

Karstein Lied

When avalanche dams are planned, the clients are usually municipalities, other public authorities or public institutions, building consultants, contractors, architects or private persons. Few, if any of these stakeholders are experts in avalanche dynamics or avalanche-dam construction, and it is of importance to the builder or client to get an overview of and realistic plans and cost estimates for the project as early as possible.

Very few people are aware of the large size of a dam needed to stop or deflect an avalanche, and this point should be discussed in detail. The avalanche expert must illustrate the speeds, snow volumes, and impact forces that need to be considered in an attempt to change avalanche run-out by means of dams, walls or similar constructions, and what this means with respect to heights, lengths and volumes of the constructions.

The preferred location of the dam in the path must be discussed thoroughly. Many considerations must be taken into account in this respect. From a technical point of view, it is usually a clear advantage to locate the dam as far down the path as possible, mainly to reduce flow speeds before avalanches hit the dam. The client or landowner, on the other hand, might prefer to locate the dam higher up the path, outside of the economically most valuable area, or far away from existing buildings, so that the dam does not disturb the view or limit land use or access to the area.

As a first step, the experts should present their preliminary plans to the client, for instance the administration of a municipality, and discuss the basic layout and viable alternatives. If a dam is built to protect a housing area, the residents must be informed about the planning and decision process as early as possible. Public meetings for the people involved should be arranged where the experts and the decision makers should present their plans. If possible, more than one alternative should be worked out and presented.

The environmental and visual impact of avalanche dams can be large. This needs to be taken into account in the design process, and should be discussed and explained to the local authorities and the public. Landscape architects should be involved in the design process from the start, especially for constructions in close proximity to settlements, in order to integrate the dams into the environment as well as possible (Vilhjálmsson and Ingþórsson, 2008).

Avalanche calculations, design criteria and the most important dimensions, such as height, length and width of the dam(s), should be presented. Advantages and drawbacks of the plans should be discussed, together with possible means of financing the defence structures.

The experts must be open and frank, and explain in non-technical terms what is known about the effect of the proposed defence structures, and what is not known. They should point out uncertainties in the design criteria, as well as explain what is thought to be an appropriate design avalanche with respect to magnitude and frequency. This last point must reflect the national safety demands and regulations concerning natural hazards and avalanches.

If possible, a rest risk should be calculated or at least discussed, as no defence structure will in principle be able to guarantee a 100% safety.

The experts must be prepared to meet strong arguments, both in favour and disfavour of their plans. People often have good knowledge and clear views about how things should be in their own neighbourhood, and about avalanche hazards. However, irrelevant arguments are

sometimes also brought forward. The experts must be patient and willing to listen to various arguments, since avalanche hazards often evoke strong emotions.

An avalanche hazard zoning is usually worked out before the planning and construction of defence structures commences. In some cases, avalanches unexpectedly hit buildings, roads and other types of infrastructure. In many such cases, no hazard zoning was available before the avalanche fell, so that planning of protective measures must start by an evaluation of the hazard.

As a consequence of the planned defence structures, an updated or new hazard zoning must be made for the area in question. The revised hazard zones should reflect the effect of the defence structures, as the run-out of the avalanches will be altered. Whether the adjusted hazard zones should take into account the full expected effect of a dam, *i.e.* whether the actual hazard line is moved uphill to the dam, or to a location a certain distance downhill from the dam, must be based on the calculated rest risk, as well as other elements such as human factors (the perceived risk), environmental conditions, and in some cases political decisions. In some countries, hazard zones are not to be adjusted after defence structures are built, because of the uncertainty about the effectiveness of such structures. In that case, the structures are only intended to increase the safety of already existing settlements, but do not lead to an expansion of the settlement into the previously endangered area.

3 Overview of traditional design principles for avalanche dams

Tómas Jóhannesson

Several methods have been used to design avalanche dams, based either on simple point-mass considerations pioneered by Voellmy (1955) and widely used in Alpine countries (Salm and others, 1990), a description of the dynamics of the leading edge of the avalanche (Chu and others, 1995), or on numerical computations of the trajectory of a point-mass on the upstream facing sloping side of the dam (Irgens and others, 1998; Harbitz and others, 2001). Traditional design methods for avalanche dams are described by Salm and others (1990), Norem (1994), Lied and Kristensen (2003) and Margreth (2004).

The height of avalanche dams, H_D, is usually determined from the formula

$$H_D = h_u + h_f + h_s \,, \tag{3.1}$$

where h_u is the required height due to the kinetic energy or the velocity of the avalanche, h_f is the thickness of the flowing dense core of the avalanche, and h_s is the thickness of snow and previous avalanche deposits on the ground on the upstream side of the dam before the avalanche falls (Fig. 3.1). The terms h_f and h_s in the equation for H_D are typically assumed to be a few to several metres each for unconfined slopes, and must be estimated based on a knowledge of snow accumulation conditions and the frequency of avalanches at the location of the dam.

The term h_u is usually computed according to the equation

$$h_u = \frac{u^2}{2g\lambda} \tag{3.2}$$

for *catching dams*. Here, u is the velocity of the chosen design avalanche at the location of the dam, $g = 9.8\,\mathrm{m\,s^{-2}}$ is the acceleration of gravity, and λ is an empirical parameter intended to reflect the momentum loss when the avalanche hits the dam, as well as the effect of friction

Figure 3.1: A schematic figure of a catching dam showing the contributions of the velocity of the avalanche, h_u, the thickness of the flowing dense core, h_f, and the thickness of snow and previous avalanche deposits on the ground, h_s, to the dam height, H_D. The figure is adapted from Margreth (2004).

Figure 3.2: A catching dam at Brún in Bjólfur in Seyðisfjörður, eastern Iceland. An avalanche that fell on 9 February 2008 and stopped just at the dam face can be seen. The dam is 20 m high with a 10 m high very steep upper part. (Photo: Emil Tómasson.)

on the flow of the avalanche during run-up along the upstream side of the dam. The value of λ for catching dams is usually chosen to be between 1 and 2 (and sometimes even higher), with the higher values used for dams with steep upstream faces. Higher values of λ (lower dams) are chosen where the potential for large avalanches is considered rather small, whereas lower values of λ (higher dams) are chosen for avalanche paths where extreme avalanches with large volumes may be released. Figure 3.2 shows an example of a catching dam from Seyðisfjörður in eastern Iceland.

In addition to the requirements expressed by Equations (3.1) and (3.2), the *storage capacity* above a catching dam must be large enough to hold the assumed volume of the design avalanche and the volume of snow on the ground prior to the avalanche. The storage capacity depends on the *terrain slope upstream of the dam*, the *inclination of avalanche deposits*, which have piled up above the dam, and the relative *compaction of the snow* from the release density to the deposit density. The inclination of the avalanche deposits is sometimes assumed to be between 5–10° for slow, moist and dense avalanches. However, the storage capacity can be much smaller than this for dry, fast flowing avalanches (Margreth, 2004). A value of about 1.5 for the compaction factor from release to deposition density is sometimes used (Stefan Margreth, personal communication 2006), but this factor is often not specified, which is equivalent to adopting a compaction factor of unity.

The height of *deflecting dams* is traditionally calculated using Equation (3.1), as for a catching dam, with the term h_u determined according to the equation

$$h_u = \frac{(u \sin \varphi)^2}{2g\lambda} \,, \tag{3.3}$$

where φ is the *deflecting angle* of the dam. The terms h_f and h_s are determined in the same manner as for catching dams. The λ parameter for deflecting dams is often chosen to be 1. This choice of λ is equivalent to neglecting momentum loss when the avalanche hits the dam and the effect of friction of the avalanche against the dam. This leads to higher dams compared with $\lambda > 1$. This may partly be considered as a safety measure to counteract the

Figure 3.3: Two deflecting dams and a catching dam at Flateyri, northwestern Iceland. The deflecting dams are 15–20 m high and the small catching dam between them is 10 m high. The dams were built after a catastrophic avalanche in 1995 that killed 20 people. (Photo: © Mats Wibe Lund.)

uncertainty, which is always present in the determination of the deflecting angle, and for taking into account internal pressure forces, which may lead to higher run-up than assumed in point-mass dynamics. Figure 3.3 shows an example of deflecting dams from Flateyri in northwestern Iceland.

There exist no accepted design guidelines for braking mounds for retarding snow avalanches although they are widely used as a part of avalanche protective measures (see Fig. 3.1). Laboratory experiments have been performed in recent years in order to shed light on the dynamics of avalanche flow over and around braking mounds and catching dams and to estimate the retarding effect of the mounds. These experiments and the resulting design criteria for braking mounds have been described by Hákonardóttir (2000), Hákonardóttir (2004), Hákonardóttir and others (2003c), Jóhannesson and Hákonardóttir (2003) and in papers and reports referenced therein, and form the basis for the treatment of braking mounds in Section 9 of this book.

A fundamental problem with the point-mass view of an avalanche for the design of deflecting dams is the neglect of the transverse width of the avalanche. As a consequence of this simplification, the lateral and longitudinal interactions between different parts of the avalanche are ignored. Point-mass trajectories corresponding to adjacent lateral parts of an avalanche that is deflected by a dam inevitably intersect as already deflected material on its way down the dam side collides with material heading towards the dam farther downstream. Similarly, it is not realistic to consider the flow of snow in the interior of an avalanche hitting a catching dam without taking into account the snow near the front that has already been stopped. The effect of this interaction on the run-up cannot be studied based on point-mass considerations, and a more complete physical description of lateral and longitudinal interactions within the avalanche body during impact with an obstacle must be developed. These flaws of the point-

mass dynamics are most clearly seen by the fact that no objective method based on dynamic considerations can be used to determine the empirical parameter λ in equations (3.2) and (3.3), which nevertheless has a large effect on the design of both catching and deflecting dams.

4 Avalanche dynamics

Tómas Jóhannesson and Peter Gauer

Natural dry-snow avalanches are believed to consist of a dense core with a fluidised (saltation) layer on top, and possibly in front of it, surrounded by a powder cloud (suspension layer) (Fig. 4.1). The dense core is characterised by a frictional contact between the snow particles, where each particle is in persistent contact with other particles (Issler, 2003). The density is on the order of 300 kg m^{-3}, and a typical flow depth is 1–3 m, although channelised flow may in many cases reach much greater flow depth. The fluidised or saltation layer consists of particles with mean-free-paths up to several particle diameters that interact in pairwise collisions, where the dynamics of the interstitial air may be assumed to play a rather limited role and persistent particle–particle contacts do not arise. The density is in the range of 10–100 kg m^{-3}, and a typical depth of this layer is 2–5 m. The fluidised layer can precede the dense core of the avalanche by many tens of metres. The powder cloud is a turbulent suspension of snow particles in air, where particle collisions are comparatively unimportant and the dynamics are dominated by turbulent entrainment, settlement of snow particles and air flow. The density is on the order of 3 kg m^{-3}, and the flow depth can range from a few tens of metres to 100 m or more.

These flow regimes can be distinguished in impact measurements on structures. The loading due to the dense core shows up as rapid fluctuations that rarely drop to zero or near-zero between peaks. The fluidised layer, on the other hand, is characterised by irregular peaks in the loading, which are interpreted as being due to impacts of individual snow clods, with near-zero loading between the peaks, or as having a higher fluctuation intensity than the dense core. The powder cloud has a much lower impact pressure, which tends to zero over a comparatively large vertical distance compared with the depth of the dense core or the fluidised layer.

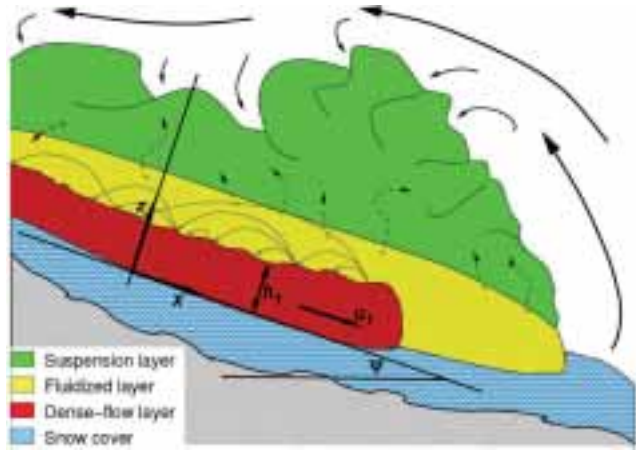

Figure 4.1: A schematic figure of a dry-snow avalanche showing the dense core, the fluidised (saltation) layer and the powder cloud. The depth-averaged quantities u_1 and h_1 apply to the dense core in the sloping (x,z)-coordinate system. The figure is adapted from Issler (2003).

The classification of a snow avalanche into three flow regimes is of course an abstraction and the boundaries between the regimes are not sharp. In particular, the transition between the dense core and the fluidised layer takes place over a range of flow depths rather than at a well-defined distance from the bottom of the flow. In Sections 11 and 12, for an analysis of loading of constructions due to snow avalanches, it is for simplicity assumed that the transition from the dense core to the fluidised layer takes place where the density has dropped considerably from the characteristic density of the dense core, such that the magnitude of the impact pressure within the fluidised layer decreases rapidly with height.

As mentioned in the previous section, the traditional design criteria for catching and deflecting dams (Eqs. (3.1), (3.2) and (3.3)) are based on viewing the avalanche as a point-mass whereby important lateral and longitudinal interactions within the avalanche body cannot be studied. The simplest description of a snow avalanche that takes these interactions into account is based on a depth-averaged formulation of the dynamic equations for the flow of a shallow layer of granular material down inclined terrain. This description is intended to represent the dynamics of the dense core, but the fluidised and powder components of the avalanche are omitted.

In the depth-averaged formulation, the dense core is modelled as a shallow, free-surface, granular gravity current (*cf.* Eglit, 1983), which can be described by a flow depth h and a depth-averaged velocity $\mathbf{u}$. The dynamics of shallow, free-surface gravity flows are characterised by the *Froude number*

$$\mathrm{Fr} = \frac{u}{\sqrt{g\cos(\psi)\,h}}\,, \tag{4.1}$$

where $u = |\mathbf{u}|$, ψ is the slope of the terrain and of the coordinate system, and g is the acceleration of gravity. The flow depth and velocity are here defined in the directions approximately normal to and parallel with the terrain, respectively, as indicated by the z- and x-axes in Figure 4.1. The Froude number is the ratio of the flow velocity to the speed of small-amplitude free-surface gravity waves and corresponds to the Mach number in gas flows. The Froude number of the dense core of natural dry-snow avalanches is approximately in the range 5–10 (Issler, 2003), which implies that such avalanches are well within the supercritical range defined by $\mathrm{Fr} > 1$.

The depth-integrated conservation equations for mass and momentum for incompressible, shallow flows may, in the absence of entrainment, be written as

$$\frac{\partial h}{\partial t} + \nabla\cdot(h\,\mathbf{u}) = 0\,, \tag{4.2}$$

and

$$\frac{\partial(h\,\mathbf{u})}{\partial t} + \nabla\cdot(h\,\mathbf{u}\,\mathbf{u}) = g\sin(\psi)\,h\,\mathbf{a}_\psi - g\cos(\psi)\,h\,\nabla z_s - \rho^{-1}\tau_\mathbf{b}\,, \tag{4.3}$$

where $h = z_s - z_b$ is the flow depth perpendicular to the xy-plane (see Fig. 4.1), z_b and z_s are the z-coordinates of the bedrock and the surface of the flow, respectively, $h\,\mathbf{u}$ is volume flux and ∇ denotes the gradient operation in the x- and y-directions only (the z-direction has been taken care of by the depth-averaging). $\mathbf{u}\,\mathbf{u}$ denotes the tensor product of $\mathbf{u}$ with itself, which is sometimes denoted by $\mathbf{u}\otimes\mathbf{u}$. ρ is the density of the dense core, $\mathbf{a}_\psi = \cot\psi\,(\tan\psi_x\,\mathbf{a}_x + \tan\psi_y\,\mathbf{a}_y)$ is a unit vector in the direction of the slope of the coordinate system, ψ_x and ψ_y are the slopes along the x- and y-axes, $\mathbf{a}_x$ and $\mathbf{a}_y$ are unit vectors in the x-direction and y-direction, respectively, and $\tau_\mathbf{b}$ is shear stress at the bottom of the flow. The first term on the

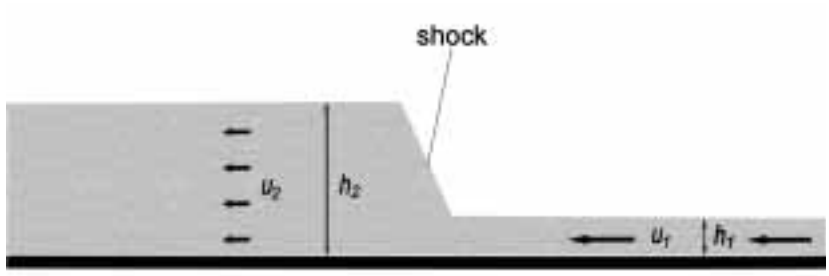

Figure 4.2: A schematic figure explaining the notation used to describe a shock in shallow granular flow. The subscript "1" denotes quantities upstream of the shock and "2" denotes quantities on the downstream side.

right-hand-side of the momentum equation represents the component of gravity in the sloping (x,y,z)-coordinate system, the second term is due to internal stresses within the moving body, which are assumed to be given by a hydrostatic pressure distribution, $p = g\cos(\psi)(z_s - z)$, due to the component of gravity normal to the bed, and the last term on the right-hand-side represents retardation due to bottom friction, which is further discussed in the next section. The basis vectors $\mathbf{a}_x$ and $\mathbf{a}_y$ point in the local x- and y-directions, which are defined in the tangent plane of the terrain. If the slope angle is variable, additional terms related to the curvature of the terrain arise (Gray and others, 1999), but these are disregarded here.

Sharp gradients in the flow depth and velocity are now believed to be an important aspect of the dynamics of the dense core during interactions with obstacles (Hákonardóttir and Hogg, 2005; Gray and others, 2003). Such gradients are represented in the depth-averaged description, Eqs. (4.2) and (4.3), as mathematical discontinuities in the flow depth and velocity across so-called *shocks*, which are formed upstream of the obstacle. The discontinuities are of course mathematical abstractions but they are believed to reflect real physical aspects of shallow, supercritical flow. "Information" about obstructions can only propagate a short distance upstream in supercritical flows and sharp gradients in flow depth and velocity occur in the transition between the undisturbed flow and flow that is affected by the obstacle. In the following, the subscripts "1" and "2" will be used to denote quantities upstream and downstream of shocks, respectively (Fig. 4.2). Undisturbed flow in the absence of obstacles will thus be denoted by the subscript "1" as in Figure 4.1. Shock dynamics will be used in the following sections as an important, but until recently ignored, aspect of snow avalanche dynamics to formulate design criteria for avalanche dams.

The conservation equations for mass and momentum for shallow, incompressible flow in 2D may be shown to lead to jump conditions across shocks (Whitham, 1999)

$$-[\![h]\!]c + [\![h\mathbf{u}]\!]\cdot\mathbf{n} = 0 \tag{4.4}$$

and

$$-[\![h\mathbf{u}]\!]c + \left[\!\left[h\mathbf{u}\mathbf{u} + \frac{1}{2}g\cos(\psi)h^2\mathbf{I}\right]\!\right]\cdot\mathbf{n} = 0\,, \tag{4.5}$$

where the brackets are used to express the discontinuity in a quantity across the shock, for example $[\![h]\!] = h_2 - h_1$, with the subscripts 1 and 2 denoting the upstream and downstream sides, respectively, as mentioned above. $\mathbf{n}$ is a unit normal vector to the shock pointing in the

direction of movement of the shock or in the upstream direction if the shock is stationary, c is the propagation speed of the shock in the direction of $\mathbf{n}$ and $\mathbf{I}$ denotes the unit tensor. These equations can be solved to obtain the flow depth and velocity near catching and deflecting dams that are high enough for shocks to form on their upstream side as further described in Section 5.

The depth-averaged formulation cannot represent some processes that may be important in the flow of snow avalanches against obstacles. Among such processes are splashing during the initial impact (see Hákonardóttir and Hogg, 2005), overflow of the saltation and powder components, and the transfer of snow from the dense core into suspension during the impact. Processes related to two-phase dynamics and air pressure in the interstitial air in the avalanche that may cause "hydroplaning" or "aeroplaning", may also be important during overflow, as well as shearing flow over the dam, where a deep avalanche overflows a dam over a part of the flow depth. These aspects of the dynamics will not be considered in the dam design criteria proposed here.

5 Deflecting and catching dams

Tómas Jóhannesson, Kristín Martha Hákonardóttir, Carl B. Harbitz, Ulrik Domaas and Mohamed Naaim

5.1 Introduction

A substantial improvement in the understanding of the flow of snow avalanches against dams and other obstructions has taken place over the last 5–10 years. This improved understanding has been achieved by theoretical analyses, chute experiments, numerical simulations with a new generation of 2D depth-averaged snow avalanche models, and an interpretation of flow marks of snow avalanches that have hit man-made dams and natural obstructions. This development makes it possible to formulate improved design criteria for catching and deflecting dams based on more advanced dynamic concepts, which solve some of the inconsistencies that are associated with the traditional criteria for the design of such dams. In spite of this progress, understanding of the dynamics of the impact of snow avalanches with obstacles remains incomplete, so that the formulation of the new criteria is to some degree based on subjective or partly justifiable considerations.

The new criteria are based on the concepts of *supercritical overflow* and *flow depth downstream of a shock*. They are formulated in terms of a description of the geometry of the terrain and the dam and an analysis of the dynamics of the flow of avalanches against dams. A summary of the proposed dam design procedure is given in Appendix A. This section describes the dynamics of avalanche flow against obstructions and common aspects of the dam height criteria that apply to both deflecting and catching dams. Aspects that are particular to either deflecting or catching dams, such as the determination of the deflecting angle and storage space above a catching dam, are treated in Sections 6 and 7.

The description of the dam design criteria below is intentionally brief, and most of the results are presented without derivations or detailed arguments. Derivations and more detailed arguments are given in a separate report (Jóhannesson and others, 2008), which is intended as an accompanying document to the description presented here. The fluid dynamics background of the design criteria and various laboratory experiments that they are based on has been described by Hákonardóttir and others (2003a), Hákonardóttir and others (2003d), Hákonardóttir (2004) Hákonardóttir and Hogg (2005) and Baillifard (2007), see also the references cited therein.

There is considerable uncertainty about the effectiveness of dams to deflect and, particularly, to stop snow avalanches. Validation of the proposed design criteria based on observed run-up of natural avalanches is discussed below in Subsection 5.9 and in more detail in the abovementioned accompanying report. Overflow over catching dams is, additionally, discussed in Section 7 and in more detail by Gauer and Kristensen (2005).

5.2 Dam geometry and notation

Except in the last stage of the design, flow depth, dam height and run-up on the dam side facing the avalanche path are defined here in the direction normal to the terrain upstream of the dam (see Fig. 5.1). Terrain slope at the dam location in the direction of steepest descent is denoted by ψ and the slope of the terrain normal to the dam axis in the map plane by $\psi_\perp$.

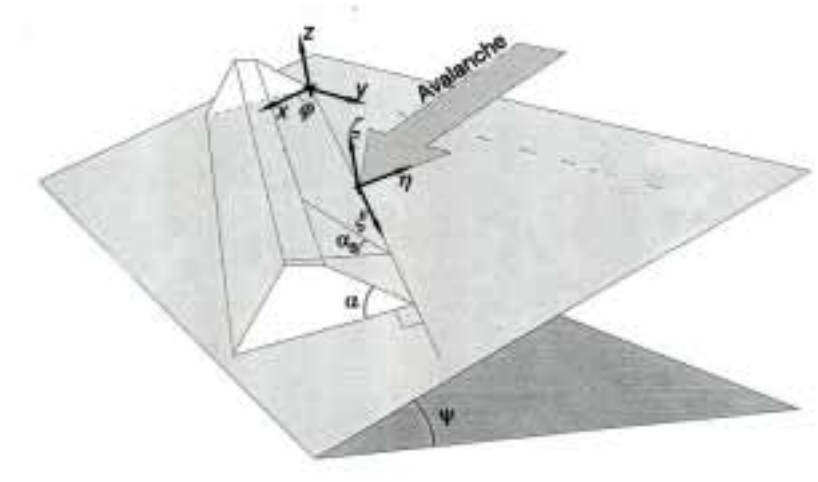

Figure 5.1: A schematic figure of a deflecting dam showing the (x,y,z)- and (ξ,η,ζ)-coordinate systems the deflecting angle, φ, the slope of the terrain, ψ, and the angle between the upper dam side and the terrain, α. The figure is adapted from Domaas and Harbitz (1998).

The (dense core of the) design avalanche has flow depth h_1 and depth-averaged velocity u_1 at the dam location (that is directly upstream of the dam before the dam has any effect on the flow) (see Figs. 4.1 and 4.2). The shape of the terrain and the avalanche flow upstream of the dam are assumed to be sufficiently uniform so that spatial variations in ψ, u_1 and h_1 may be ignored. A sloping coordinate system is aligned with the terrain upstream of the dam with the x-axis along the flow direction, which is assumed to be directly in the downslope direction. The y-axis points away from the dam, and the z-axis points upwards in a direction normal to the terrain (see Fig. 5.1). The deflecting angle of the dam is denoted by φ and the angle between the upper dam side and the terrain, in the direction normal to the dam axis, is α.

Vertical dam height (and vertical run-up) will in general be slightly different from the corresponding height measured normal to the terrain and may be computed from the following geometric identity

$$H_D = \frac{\cos\psi - \sin\varphi \sin\psi \cot\alpha}{1 - \cos^2\varphi \sin^2\psi} H \ , \tag{5.1}$$

where H is measured normal to the terrain and H_D is measured in a vertical section normal to the dam axis in a horizontal plane as shown in Figure 5.2. Protection dams are typically built in the run-out areas of avalanches, where terrain slopes are small and this difference in most cases is not important. Since vertical dimensions are slightly shorter than the corresponding dimensions normal to the terrain, values found for H may be used to determine vertical dam heights with a small error on the safe side for moderate values of the terrain slope ψ. For dams in steep terrain, Equation (5.1) should be used to compute H_D after H has been determined. In the discussion that follows, all quantities are expressed in a coordinate system that is aligned with the terrain unless otherwise stated.

In a geotechnical analysis of the stability of the dam, it is often necessary to find the steepest inclination of the dam side or the upstream facing side of a natural obstacle, α_s. For given values of φ, ψ, and α, α_s may be derived from the geometric identity (see Domaas and

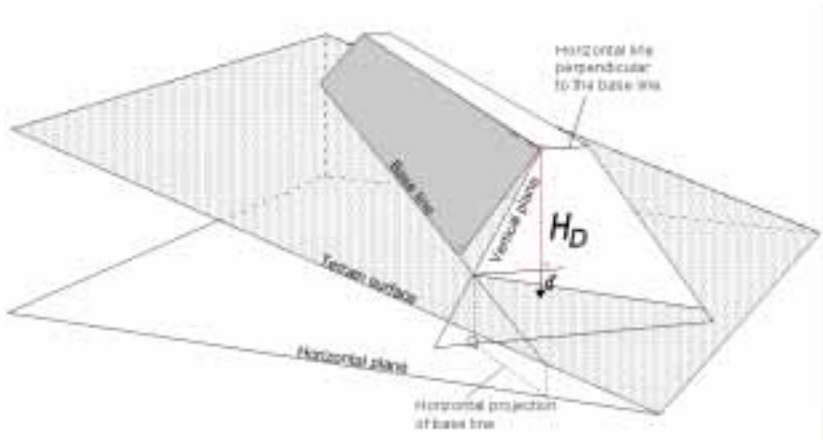

Figure 5.2: A schematic figure explaining the definition of vertical dam height, H_D. The figure is adapted from Domaas and Harbitz (1998).

Harbitz, 1998)

$$\sin^2\alpha_s = (\cos\varphi\sin\psi)^2 + (\cos\psi\sin\alpha - \sin\varphi\sin\psi\cos\alpha)^2 \,. \tag{5.2}$$

Run-up of the avalanche above the snow cover normal to the terrain on the upstream side of the dam is denoted by h_r. The snow depth on the terrain, h_s, is only briefly considered below and is simply added to find the dam height after h_r has been determined, assuming that h_s is sufficiently uniform in space that this is appropriate

$$H = h_r + h_s \,. \tag{5.3}$$

5.3 Dynamics of flow against deflecting and catching dams

A dry-snow avalanche will typically flow towards a dam in a supercritical state, *i.e.* with a Froude number $\mathrm{Fr} > 1$.[1] The first determining factor for the design height of both catching and deflecting dams is that uninterrupted, *supercritical flow over the dam must be prevented*. If supercritical overflow is impossible, shallow fluid dynamics predicts the formation of a shock upstream of the dam. This theoretical prediction has been confirmed for fluid and granular flow in several chute experiments, and may have been observed for natural snow avalanches. The second criterion for the design height of avalanche dams is that the *flow depth downstream of the shock must be smaller than the dam height*. These two requirements in combination constitute the core of the design requirements that are proposed here.

The dynamics of the *formation* of a shock upstream of a dam is not well understood. In many, but not all, practical cases, the downstream flow depth, h_2, is smaller than the dam height required to prevent supercritical overflow, assuming no loss of momentum during impact with the dam. Therefore, if the generation of a shock could be guaranteed by enough momentum dissipation, the dam could be built substantially lower than required for preventing

[1]This criterion for supercritical flow applies to internal stresses described by a hydrostatic pressure distribution, *cf.* Eq. (4.3). Other rheologies may lead to different criteria separating subcritical and supercritical flow.

supercritical overflow. However, there are indications from natural snow avalanches, which have overflowed or scaled high natural terrain obstacles, that avalanches can flow over dams higher than the flow depth downstream of a shock, assuming probable values of the upstream velocity and flow depth. Therefore, it is proposed here to adopt a worst case scenario. Firstly, supercritical overflow must be prevented during the initial interaction such that a shock may form, and secondly, overflow downstream of a shock must be prevented.

Despite an obvious difference between the flow of avalanches against catching and deflecting dams, there is a fundamental dynamic similarity. This similarity is manifest in traditional expressions for the kinetic energy component of the dam height, h_u, for catching and deflecting dams, Equations (3.2) and (3.3). The λ-factor in these equations represents loss of kinetic energy in the interaction with the dam beyond the potential energy needed to scale the dam. These equations indicate that a deflecting dam is equivalent to a catching dam being hit by an avalanche with a speed equal to the velocity component normal to the dam axis. The equations have an intuitively clear meaning for dams on horizontal terrain in terms of the kinetic and potential energy of a point-mass that moves over the dam. In that case, the vertical dam height, H_D, is equal to the run-up normal to the upstream terrain, H. However, for dams on sloping terrain, the equations do not have a similarly clear interpretation. This is evidenced by the fact that there are "potential streamlines" along the side of deflecting dams in sloping terrain that maintain the same altitude. If avalanches could flow along such streamlines, they would be able to overflow the dam without any loss of kinetic energy due to the scaling of the dam.

If friction is approximately balanced by the downslope gravity component, the total contact force between the terrain and the bottom of the avalanche may be assumed to be normal to the terrain (within the framework of the depth-averaged description). Relative motion parallel to the terrain between the avalanche and the terrain, has then no influence on the flow of the avalanche. Even when friction has some effect, this will be approximately true for regions with sharp gradients in the flow such as shocks, if the residence time of particles in the region is very short compared with the time needed for frictional forces to have a significant effect. The conservation equations for mass and momentum for shallow fluid flow are equally valid in a uniformly moving coordinate system under these conditions. Let ξ, η and ζ be the coordinates of a right-handed Cartesian coordinate system such that the ξ-axis is aligned with the downstream axis of a deflecting dam, the η-axis points in the direction normal to the dam axis in the upstream direction, the ζ-axis points in the direction normal to the terrain, and the origin moves along the dam axis with speed $u_1 \cos\varphi$ (see Figs. 5.1 and 5.3). It is easy to show that, for supercritical flow over the dam, the dynamics in the (ξ,η,ζ)-coordinate system are *exactly equivalent* to normal flow with uniform velocity $u_1 \sin\varphi$ towards a catching dam. This fact may be used to recast the criterion for supercritical flow over a catching dam for flow against a deflecting dam (see Jóhannesson and others, 2008).

To a good approximation, the shock relations for a stationary, oblique hydraulic jump upstream of a deflecting dam may similarly be shown to be equivalent to a moving normal shock above a catching dam (see Jóhannesson and others, 2008). In a fundamental sense, avalanches that flow against catching and deflecting dams are, therefore, dynamically similar, and theoretical derivations and results of laboratory experiments for catching dams may be used to improve design criteria for deflecting dams and vice versa.

Frictional forces are not considered explicitly in the derivation of the design criteria. However, they are implicitly assumed to balance the downslope component of gravity so that the

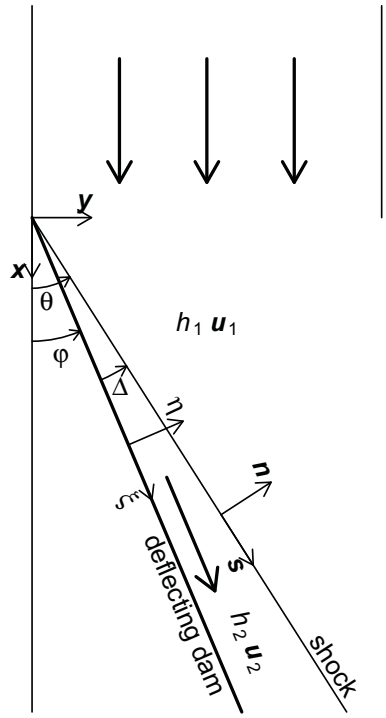

Figure 5.3: A schematic figure of an oblique shock above a deflecting dam showing the deflecting angle, φ, the shock angle, θ, their difference $\Delta = \theta - \varphi$, and the ($x$,$y$)- and ($\xi$,$\eta$)-coordinate systems.

oncoming flow can be assumed to be non-accelerating and spatially uniform. The role of terrain friction on the dynamics of avalanche impact onto a dam is not well understood, as evidenced by the fact that the Coulomb friction coefficient μ appears in some expressions for the design height of dams but not in others. However, one may expect terrain friction to be comparatively unimportant during impact of dry-snow avalanches with obstacles. For each part of the avalanche body, the impact does not last long enough for frictional forces to reduce the momentum of the avalanche significantly. In addition, many dams are located in gently sloping terrain, where friction is partially balanced by downslope gravity. Assuming that frictional forces are approximately balanced by downslope gravity may not be realistic in some situations, in particular for long deflecting dams with acute deflecting angles, where the deflecting process lasts relatively long for each part of the avalanche body. The simplified results where friction is assumed to be balanced by gravity may, however, be expected to provide an upper bound for design dam height even when the effect of friction cannot be omitted.

Entrainment of snow from the snow cover into the avalanche, and deposition of snow from the avalanche onto the terrain are also omitted here. These are poorly understood processes that may affect avalanche–dam interactions. In particular, deposition may be an important process under some circumstances in which part of the avalanche piles up in front of a dam and forms a platform for the remainder of the avalanche to flow over the dam. This aspect of avalanche–dam interactions is, however, not considered in the dam design criteria described here.

Figure 5.4: A schematic figure of supercritical overflow showing the critical dam height H_{cr} and the critical flow depth h_{cr}.

Many of the above simplifying assumptions may be relaxed in numerical simulations of the depth-averaged shallow fluid equations with shock-capturing algorithms, whereby complex terrain and dam shapes, as well as frictional forces and possibly entrainment/deposition, may be taken into account (see for example Gray and others, 2003). An insight into the simple situation analysed here is, nevertheless, useful for the interpretation of results from numerical simulations. The analytical expressions for dam height that are provided by the simplified analysis are also useful for developing initial ideas for dam geometry in more complex situations that may subsequently be refined by numerical simulations.

5.4 Supercritical overflow: $H_{cr} + h_{cr}$

The height at which the avalanche changes from a supercritical flow state to a subcritical state when it hits a dam will be referred to here as *critical dam height* and denoted by H_{cr} (Fig. 5.4). It can be derived from a conservation equation for the energy of the flow over the dam (see Hákonardóttir, 2004)

$$H_{cr}/h_1 = \frac{1}{k} + \frac{1}{2}(k\,\mathrm{Fr}\sin\varphi)^2 - \frac{3}{2}(\mathrm{Fr}\sin\varphi)^{2/3}\,, \tag{5.4}$$

which is valid if friction is balanced by gravity and as long as shocks are not formed. The critical dam height is the maximum height of a dam over which supercritical flow may just be maintained. The coefficient k represents the loss of momentum normal to the dam axis during impact and is discussed in Subsection 5.6 below. The momentum loss specified by k is only meaningful for dams that are higher than several times the upstream flow depth h_1. In the derivation of Equation (5.4), the momentum loss is assumed to take place immediately as the flow crosses the foot of the dam.

The flow depth at height H_{cr}, above the snow cover at the base of the dam, here termed *critical flow depth* (Fig. 5.4), is given by

$$h_{cr}/h_1 = (\mathrm{Fr}\sin\varphi)^{2/3}\,. \tag{5.5}$$

The flow changes from a supercritical state to a subcritical state at the height H_{cr}, where the flow depth is h_{cr}, and the surface of the flow is at height $H_{cr} + h_{cr}$ above the snow cover. If the dam height above the snow cover is lower than H_{cr}, the main core of the avalanche may overflow or "jump" over the dam in a supercritical state, and if the dam height is lower

than $H_{cr}+h_{cr}$, the front of the avalanche may partly overflow the dam, while a shock is being formed. In order to prevent such overflow, the dam height above the snow cover should be larger than $H_{cr}+h_{cr}$, which is given by

$$(H_{cr}+h_{cr})/h_1 = \frac{1}{k}+\frac{1}{2}(k\,\mathrm{Fr}\sin\varphi)^2-\frac{1}{2}(\mathrm{Fr}\sin\varphi)^{2/3}\,, \tag{5.6}$$

according to Equations (5.4) and (5.5).

The requirement expressed by Equation (5.6) may perhaps lead to some overdesign because a dam height of H_{cr} above the snow cover should be enough to generate the shock. Overflow should then only occur temporarily and the bulk of the avalanche should be stopped or deflected. If some overflow is acceptable, for example if the protected area is some distance away from the dam, it may be possible to require a dam height of only H_{cr} above the snow cover rather than $H_{cr}+h_{cr}$. It should, however, be borne in mind that overflow may occur in the initial impact of the avalanche front with the dam due to splashing for a dam height of $H_{cr}+h_{cr}$, so that even this dam height may not prevent some overflow of the dense core during the initial impact. In addition, some overflow will occur over most avalanche dams due to the saltation and powder components if the dams are hit by large avalanches. Whether H_{cr} or $H_{cr}+h_{cr}$ is the most appropriate dam height cannot be decided without more detailed understanding of the dynamics of the initial impact with the dam. Here, the more conservative choice is made and $H_{cr}+h_{cr}$ is adopted as a minimum dam height.

Equation (5.6) may be rewritten in dimensional form as

$$H_{cr}+h_{cr} = \frac{h_1}{k}+\frac{(u_1\sin\varphi)^2}{2g\cos\psi}k^2(1-k^{-2}(\mathrm{Fr}\sin\varphi)^{-4/3})\,, \tag{5.7}$$

which facilitates comparison with the traditional dam height expressions (3.2) and (3.3).

If a "Froude number" normal to the dam axis, $\mathrm{Fr}_\perp$, is defined as

$$\mathrm{Fr}_\perp = \mathrm{Fr}\sin\varphi = \frac{u_1\sin\varphi}{\sqrt{g\cos(\psi)\,h_1}} = \frac{|u_\eta|}{\sqrt{g\cos(\psi)\,h_1}}\,, \tag{5.8}$$

one may rewrite Equation (5.6) as

$$(H_{cr}+h_{cr})/h_1 = \frac{1}{k}+\frac{1}{2}(k\,\mathrm{Fr}_\perp)^2-\frac{1}{2}(\mathrm{Fr}_\perp)^{2/3}\,, \tag{5.9}$$

which shows that the same fundamental expression, in terms of the component of the velocity normal to the dam axis, $|u_\eta| = u_1\sin\varphi$, may be used for both catching and deflecting dams. The equations are based on an assumption of energy conservation of the flow over the dam. The equations are thus only valid while the flow hitting the dam is supercritical and no shocks are generated in the initial interaction that is assumed to take place at the foot of the dam, *i.e.* $(k^{3/2}\mathrm{Fr}_\perp) > 1$.

Figure 5.5 shows the run-up for a deflecting dam according to Equation (5.6) as a function of the deflecting angle, φ, for several values of the upstream Froude number, Fr, as well as the run-up for a catching dam as a function of Froude number, Fr, (solid curves). The figure also shows run-up according to the traditional Equations (3.1) to (3.3) for the height of deflecting and catching dams (above the snow cover) with $\lambda = 1$ (dashed curves). The lowering of the run-up derived from Equation (5.6), relative to the corresponding run-up according to the

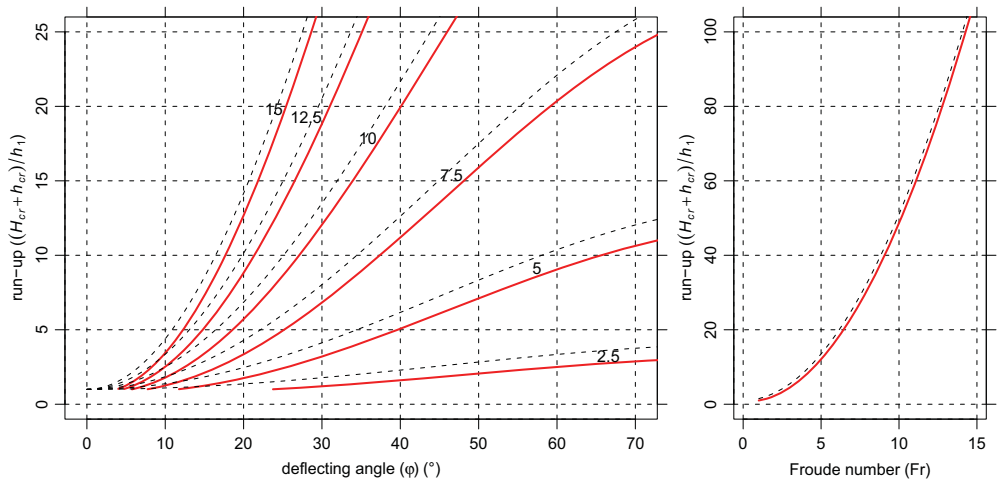

Figure 5.5: *Left:* Supercritical run-up, $(H_{cr}+h_{cr})/h_1$, according to Equation (5.6), for a deflecting dam as a function of deflecting angle, φ, and Froude number, Fr. *Right:* Supercritical run-up for a catching dam as a function of Froude number. No momentum loss is assumed during impact ($k=1$) (solid red curves). Dashed curves show run-up according to the traditional Equations (3.1) to (3.3) for the height of avalanche dams (above the snow cover) for horizontal terrain ($\psi=0$), also for no friction and no momentum loss during impact ($\lambda=1$). The curves for the deflecting dam are labelled with the Froude number.

traditional formulae, is due to the thickening of the flow as it overflows the dam, and the requirement that the overflow must be supercritical, which leads to a minimum flow velocity at the top of the dam. The resulting reduction in the required dam height is largest in a relative sense for low Froude numbers and low deflecting angles.

5.5 Upstream shock: h_2

If the dam is high enough to prevent supercritical overflow, a propagating normal shock will form upstream of a catching dam and a semi-stationary, oblique shock may form upstream of a deflecting dam. The velocity and flow depth will change discontinuously across the shock according to the depth-averaged dynamics.

The conservation equations for mass (4.4) and momentum (4.5) across a jump in shallow, incompressible flow in 2D (Whitham, 1999; Hákonardóttir and Hogg, 2005) may be shown to have the following solution for the flow depth downstream of the shock (Jóhannesson and others, 2008)

$$h_2/h_1 = (2\sqrt{(6\mathrm{Fr}_\perp^2+4)}\cos\delta+1)/3\,, \tag{5.10}$$

where δ is defined as

$$\delta = \frac{1}{3}\left(\frac{\pi}{2} - \tan^{-1}\left(\frac{9\mathrm{Fr}_\perp^2-8}{\mathrm{Fr}_\perp\sqrt{27(16+13\mathrm{Fr}_\perp^2+8\mathrm{Fr}_\perp^4)}}\right)\right)\,. \tag{5.11}$$

This solution is exact for normal shocks and a good approximation for oblique shocks. The

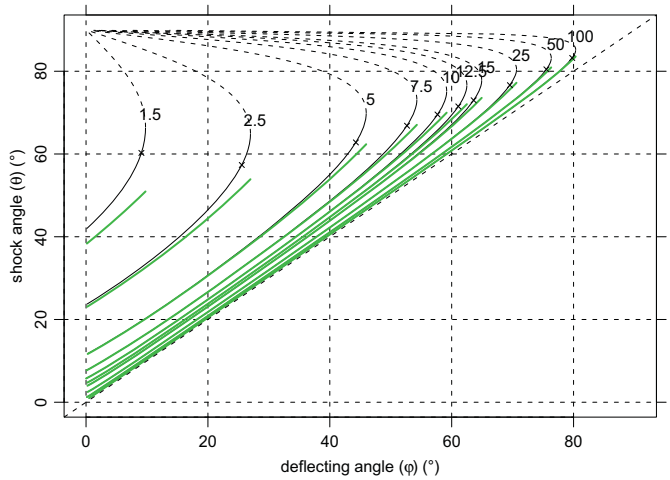

Figure 5.6: Shock angle θ as a function of deflecting angle, φ, and Froude number, Fr, for an oblique shock. Thin solid (weak shock) and dashed (strong shock) curves show the shock angle given by the exact oblique shock relations (see Jóhannesson and others, 2008). Thick green curves show the approximate solution defined by Equations (5.10) to (5.12). The curves are labelled with the Froude number and the ×-symbols show the values of the deflecting angle at which the flow downstream of the shock becomes critical.

widening of the oblique shock, Δ, above a deflecting dam is approximately given by

$$\Delta = \frac{\cos\varphi \sin\varphi}{\cos^2(\varphi)\,(h_2/h_1) - 1}\,, \tag{5.12}$$

from which the shock angle $\theta = \varphi + \Delta$ may be found (see Fig. 5.3).

Figures 5.6 and 5.7 show the shock angle, θ, and the downstream flow depth, h_2, as functions of the deflecting angle, φ, for fixed values of the Froude number, Fr. The figures show both the exact oblique shock solution (see Jóhannesson and others, 2008) (thin solid and dashed curves), and the explicit, approximate solution given by Equations (5.10) to (5.12) (thick curves). Figure 5.6 shows that two shock angles are possible for each pair of values of the deflecting angle and the Froude number. The shocks corresponding to the smaller and larger deflecting angle are called "weak" (thin solid curves) and "strong" (thin dashed curves) shocks, respectively (Chapman, 2000). The strong shock typically does not occur in real fluid or granular flow, but it has recently been observed in chute experiments with granular flow by adjusting the downstream flow conditions below the lower end of the dam (Xinjun Cui and Nico Gray, personal communication). The normal shock approximation given by (5.10) to (5.12) only gives the solution corresponding to the weak shock. Figures 5.6 and 5.7 show that the normal shock dynamics provide a good approximation to the exact oblique shock solution for $\mathrm{Fr} \geq 2.5$ and deflecting angles, φ, somewhat below the boundary between the weak and strong shocks. Thus, the normal shock approximation more or less covers the range in Fr and φ that is relevant for deflecting dams.

For each value of the Froude number, Fr, an attached, stationary, oblique shock is not dynamically possible for deflecting angles, φ, larger than a maximum, $\varphi_{\max}$, which represents the boundary between the weak and strong shocks in Figures 5.6 and 5.7. The deflecting angle

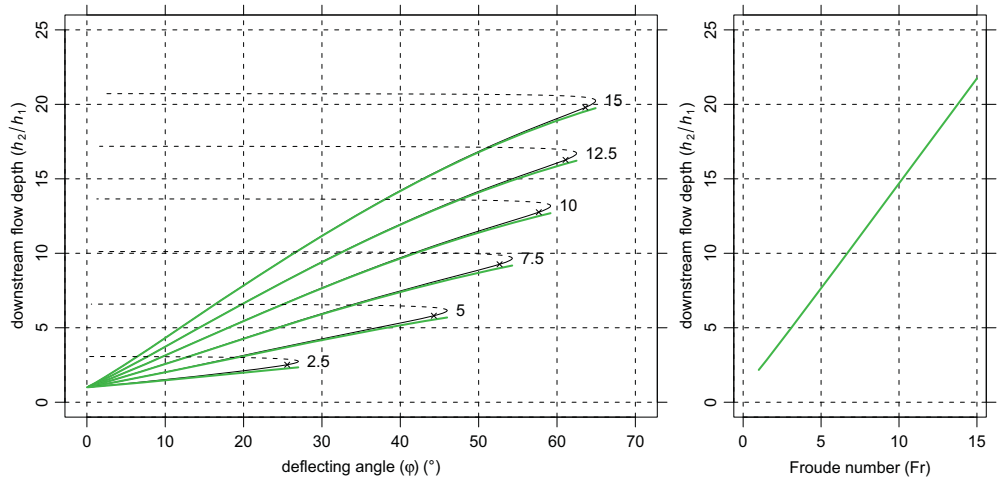

Figure 5.7: *Left:* Flow depth downstream of an oblique shock for a deflecting dam as a function of deflecting angle, φ, and Froude number, Fr. *Right:* Flow depth downstream of a normal shock for a catching dam as a function of Froude number. Thin solid (weak shock) and dashed (strong shock) curves show the solutions given by the exact oblique shock relations (see Jóhannesson and others, 2008). Thick green curves show the approximate solution defined by Equations (5.10) and (5.11). The curves for the deflecting dam are labelled with the Froude number and the ×-symbols show the values of the deflecting angle at which the flow downstream of the shock becomes critical.

corresponding to this maximum may be approximately evaluated as (Hákonardóttir and Hogg, 2005)

$$\varphi_{\max} = \frac{\pi}{2} - \frac{2^{3/4}}{\mathrm{Fr}^{1/2}} - \frac{2^{1/4}}{6\mathrm{Fr}^{3/2}} + O\left(\frac{1}{\mathrm{Fr}^{5/2}}\right) . \tag{5.13}$$

The maximum deflecting angle is shown as a function of the Froude number, Fr, in Figure 5.8. Chute experiments with granular materials indicate that an attached, stationary shock may perhaps not be maintained for deflecting angles close to the theoretical maximum, $\varphi_{\max}$. Therefore, it is recommended here that dam deflecting angles should be at least 10° lower than $\varphi_{\max}$. An avalanche hitting a dam with a deflecting angle φ that does not satisfy this requirement may not remain attached and start to propagate upstream to form a detached, semi-stationary shock (see Chapman, 2000). The detached shock will form a larger angle with respect to the oncoming flow than an attached shock and, therefore, the jump in flow depth across the shock will also be larger. It is recommended here that the downstream shock depth for a dam that does not satisfy the above requirement for an attached, semi-stationary oblique shock be computed as for a catching dam with $\varphi = 90°$. The criterion based on supercritical overflow is, however, computed with the original value of φ as before (see Subsection 5.4).

Shallow fluid shock theory has not been applied to the design of avalanche dams until recently. In hydraulics, however, this theory has been in use for many decades and is the basis of the design of numerous hydraulic structures of different types and scales (see for example Chow, 1959; Hager, 1992). In this context, the theory has been thoroughly verified. Somewhat unexpectedly, recent chute experiments indicate that the shallow fluid shock theory provides an even better approximation for granular flows than for fluid flows, for which the

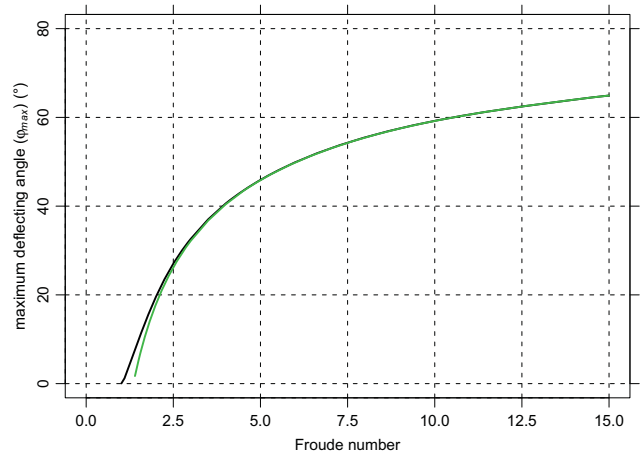

Figure 5.8: Maximum deflecting angle of an attached, stationary, oblique shock. The thick green curve shows the approximate solution defined by Equation (5.13).

theory was originally developed (see Hákonardóttir and Hogg, 2005). This is due to rapid frictional dissipation in the interaction between grains that can occur in shocks in granular media, which appears to be a more efficient dissipation mechanism than viscous and turbulent fluid friction. Transition zones with deviations from the theoretically predicted discontinuities in velocity and flow depth are, therefore, narrower in granular flows than in fluid flows. There are of course many aspects of snow avalanche dynamics that are not adequately described by shallow fluid dynamics applied to the dense core as mentioned in Section 4. Nevertheless, it is clear from the theoretical and experimental studies that have been summarised here that dam height requirements derived from shallow fluid dynamics should be viewed as minimum requirements.

5.6 Loss of momentum during impact with a dam: k

The above discussion has assumed no loss of momentum (or equivalently of kinetic energy) during impact with the dam ($k = 1$ in Equations (5.6) and (5.7)). This is a worst case scenario and leads to the highest dams. It is a pessimistic design assumption where the flow of granular material is forced to change direction abruptly. Chute experiments with granular materials, including a few experiments with snow (Hákonardóttir and others, 2003d; Hákonardóttir, 2004, section 6.4), indicate that a substantial reduction in flow velocity occurs in overflowing impacts with steep catching dams. This reduction in kinetic energy is greater than the potential energy needed to overflow or scale the dam. These experiments indicate that approximately 50%, or even more (see Hákonardóttir and others, 2003d), of the kinetic energy of an avalanche is lost in impacts with dams that are positioned normal to the bottom of the experimental chute and have heights greater than 2 to 3 times the flow depth. Furthermore, dams that have steep upstream faces with $\alpha \geq 60^\circ$ seem to be as, or almost as, efficient energy dissipators as dams with upstream faces normal to the terrain, at least for the granular material that was used in these experiments (glass beads). Dams with $\alpha = 30^\circ$ were, on the other hand, found to be less efficient.

The results from chute experiments provide an estimate of the velocity reduction that takes place as a consequence of the abrupt change in flow direction at the upstream foot of a dam. As such, they can be used to estimate the relative reduction in velocity between the oncoming flow and the avalanche as it flows up the dam side after leaving the impact region at the bottom of the dam. The relative reduction in velocity, when an avalanche scales a catching dam and continues along the path on the other side, is considered in Section 7. There is, however, a considerable uncertainty associated with applying the results to natural-scale snow avalanche defence dams. The chute experiments indicate a somewhat *greater* reduction in velocity than can easily be reconciled with some field observations of run-up of snow avalanches on dams and obstacles in the natural terrain (see discussion at the end of the section). They are, however, the only available direct evidence on the basis of which values of k can be estimated.

It is important to note that the choice of k only affects the run-up requirement corresponding to supercritical overflow (Eq. (5.6)). The dam height requirement arising from the flow depth downstream of the shock is not affected by the choice of k. In fact, chute experiments have shown that the flow depth downstream of the shock for deflecting dams with sloping sides ($\alpha < 90^\circ$) is the same as for steep dams (see Hákonardóttir, 2004). Therefore, the change in the required dam height by adopting a value of $k < 1$ is most important for catching dams, but the design height of deflecting dams is much less affected.

The λ-factor in the traditional design formula for catching dams (3.2) has often been specified as 1.5, for catching dams built from loose materials with a slope of the upstream side close to 1:1.5 ($\alpha = 34^\circ$ on horizontal terrain), and as 2, for steep dams with a reinforced upstream side with a slope greater than 2:1 ($\alpha = 63^\circ$ on horizontal terrain) (see for example Margreth, 2004). For deflecting dams it is often assumed that $\lambda = 1$, that is that no momentum is lost during impact. These λ-values for catching dams are in rough agreement with the results of the chute experiments described above. The λ-value 1.5 corresponds to $k \approx 0.85$, for catching dams from loose materials with a slope of 1:1.5, and $\lambda = 2$ corresponds to $k \approx 0.75$, for steep catching dams with a slope of 2:1 or greater, in the dam height expression (5.6). These values take into account the effect of the thickening of the flow during run-up, which leads to $\lambda > 1$ according the supercritical overflow criterion, even when $k = 1$.

Momentum loss during impact is not well understood dynamically, and little guidance for the determination of k can be obtained from theory. However, the approximate dynamic equivalence of catching and deflecting dams, which was discussed in the previous subsection, indicates that the momentum loss should be applied to both catching and deflecting dams. On the basis of the chute experiments described above, and based on observations of run-up of natural snow avalanches (see below), it is proposed here that for dry-snow avalanches $k = 0.75$ is used for dams with $\alpha > 60^\circ$, and $k = 0.85$ for dams with $\alpha = 30^\circ$, with a linear interpolation for slopes between these points. This variation of k is expressed with the following equation

$$k = 0.75 \text{ for } \alpha > 60^\circ \ , \quad k = 0.75 + 0.1(60^\circ - \alpha)/30^\circ \quad \text{for} \quad 30^\circ \leq \alpha \leq 60^\circ \ , \tag{5.14}$$

and shown graphically in Figure 5.9. Dams with side slopes less than $\alpha = 30^\circ$ should, in general, not be built, so that it is not necessary to choose k for lower values of α.

The above recommended values of k are intended for dry-snow avalanches. Similar explicit recommended values of k for wet-snow avalanches are not given here and need to be decided on a case-by-case basis. There may be less energy dissipation at the foot of the dam for wet-snow avalanches due to the greater cohesion of wet snow compared with dry snow

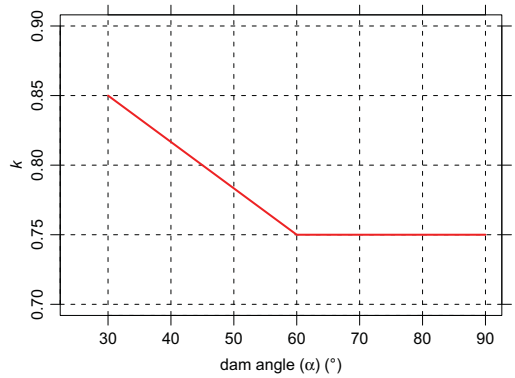

Figure 5.9: Momentum loss factor k as a function of dam angle α according to Equation (5.14). k is not defined for $\alpha < 30°$.

and, therefore, a k-value equal to 1 would perhaps be an appropriate conservative choice. Since wet-snow avalanches tend to move slower than dry-snow avalanches, avalanche speed, and thus the choice of k, is not a determining factor for the dam height in many cases. Flow depth of wet-snow avalanches downstream of a shock formed along a dam side (to the extent that such a shock is formed) may be expected to be governed by the same dynamics as for dry-snow avalanches. The requirements arising from shock dynamics should, therefore, be equally valid for wet- and dry-snow avalanches, and should be considered as a lower bound on the dam height. Qualitative considerations about dams intended as protection against wet-snow avalanches are given in Section 8.

5.7 Combined criteria: supercritical overflow and shock flow depth: $\max(H_{cr}+h_{cr}, h_2)$

Figures 5.5 and 5.7 represent the two dam height requirements proposed in these guidelines. The figures for deflecting dams have the same scales and can therefore be compared easily. Since both requirements must be satisfied, the larger dam height corresponding to a given pair of a Froude number and a deflecting angle must be chosen for each dam under consideration. For high Froude numbers and large deflecting angles, the criterion derived from supercritical overflow leads to the higher dam, but for low Froude numbers and small deflecting angles, the shock criterion leads to the higher dam.

The right panels of Figures 5.5 and 5.7 that show run-up height for catching dams have different scales for the y-axis. Figure 5.10 shows both the supercritical run-up, $(H_{cr}+h_{cr})/h_1$, according to Equation (5.6), and the flow depth downstream of a normal shock, h_2/h_1, according to Equations (5.10) and (5.11), for a catching dam as functions of the Froude number, Fr. The figure shows that supercritical run-up is the determining factor for the design height of catching dams for Froude numbers above approximately 3, but flow depth downstream of the shock determines the dam height for lower Froude numbers.

The combined requirements derived from supercritical overflow and flow depth downstream of a shock are expressed graphically in Figure 5.11 for both dams from loose materials ($k = 0.85$, upper panel) and steep dams ($k = 0.75$, lower panel). The design dam height above

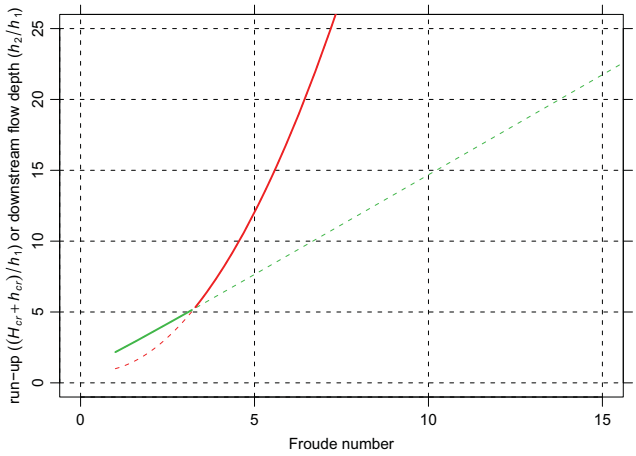

Figure 5.10: Supercritical run-up, $(H_{cr}+h_{cr})/h_1$, according to Equation (5.6) (red curve), and flow depth downstream of a normal shock, h_2/h_1, according to Equations (5.10) and (5.11) (green curve), as functions of Froude number, Fr, for a catching dam. The curve for supercritical run-up is drawn assuming no momentum loss during impact ($k = 1$). The part of each curve corresponding to larger dam height is drawn as a solid thick curve.

the snow cover, $h_r = H - h_s$, corresponding to given values of h_1 and $|u_\eta| = u_1 \sin\varphi$, may be read directly from the higher one of two curves in each figure that represent supercritical overflow (red curves) and flow depth downstream of a shock (green curves), respectively. The same curves may be used for both catching and deflecting dams because of the use of the normal shock approximations (5.10) and (5.11), according to which run-up on a deflecting dam depends only on the component of the velocity normal to the dam axis in the same manner as for a catching dam. For convenience, labelled axes at the top of Figure 5.1 show the upstream velocity u_1 corresponding to three deflecting angles.

The dependence of the dam height on the upstream flow depth, h_1, according to the dam height criteria illustrated in Figure 5.11, is somewhat different from the traditional criteria (3.1) to (3.3). According to the traditional criteria, the upstream flow depth affects the dam height simply as an additional term equal to $h_f = h_1$. The flow depth enters the new criteria in a different way, and apparently only as a multiplicative quantity in both the criteria for supercritical overflow, and as well as for flow depth downstream of the shock (Eqs. (5.7) and (5.10)). Figure 5.11 shows, however, that the expression arising from supercritical overflow predicts a weak dependency of the required dam height on flow depth, particularly for high velocities. This is due to a partial cancellation of terms in the dam height expression (5.7). The dam height derived from flow depth downstream of the shock for a given Froude number depends linearly on h_1, but approximately linearly on the square root of h_1 for a given upstream velocity u_1.

Figure 5.11 shows that supercritical run-up is the determining factor for the dam height for normal velocities above a certain critical value depending on the upstream flow depth, at which the required dam height based on supercritical overflow becomes larger than that based on shock dynamics (in the figure this is the point where the colour of the thick curve changes from green to red). Flow depth downstream of the shock determines the dam height for lower

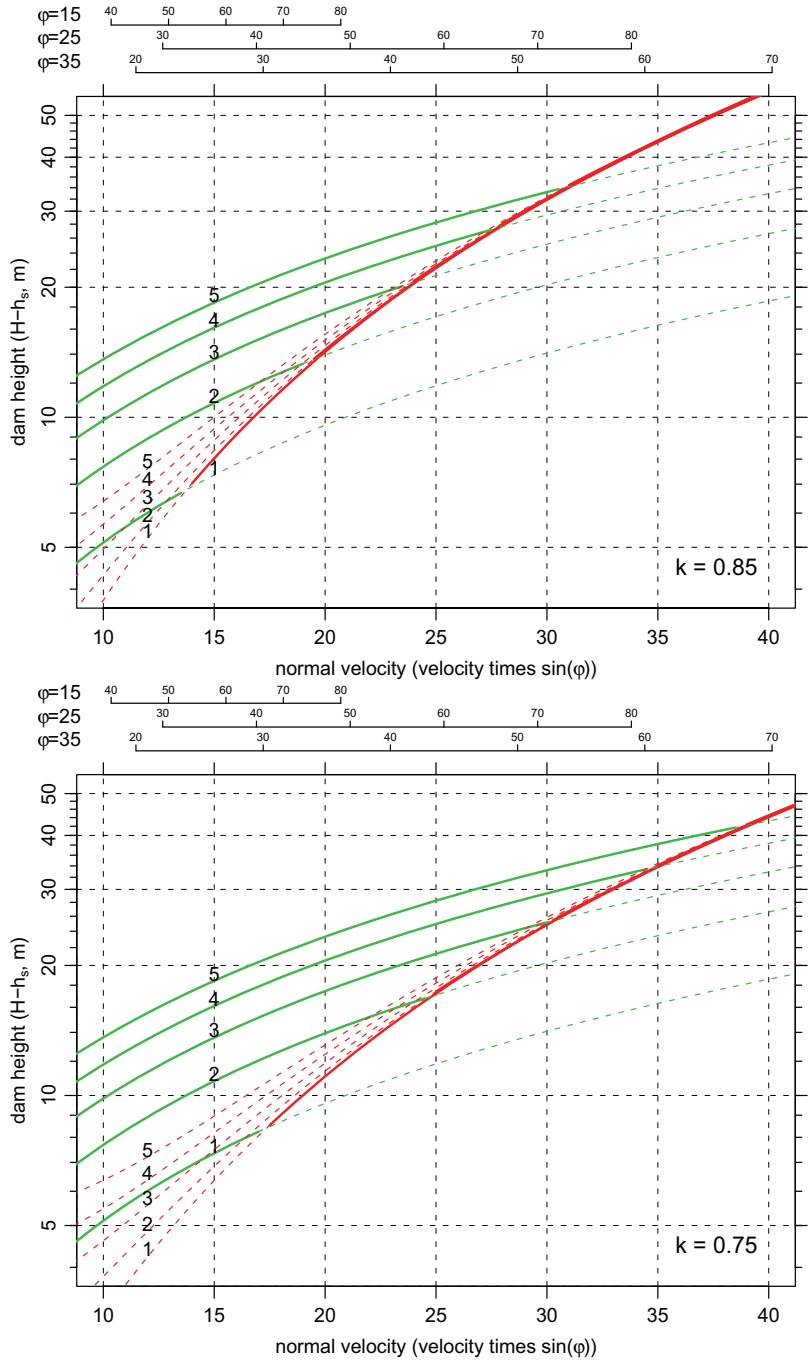

Figure 5.11: Figure caption follows on the next page.

Figure 5.11 (on the previous page): Design dam height (normal to the terrain) above the snow cover, $H - h_s$, as a function of the component of the velocity normal to the dam axis, $|u_\eta| = u_1 \sin\varphi$, for several different values for the depth of the oncoming flow h_1. Momentum loss during impact with the dam is assumed to be such that $k = 0.85$ (upper panel, corresponding to dams built from loose materials) and $k = 0.75$ (lower panel, corresponding to steep dams). The figures show curves derived from both supercritical overflow (red curves) and shock dynamics (green curves) labelled with the flow depth h_1. The design dam height should be picked from the higher of the two curves corresponding to the estimated design flow depth. The part of each family of curves corresponding to the higher dam is drawn with solid, thick curves. The labelled axes at the top of the figures show velocity corresponding to the deflecting angles $\varphi = 15$, 25 and 35°. Dam height normal to the terrain determined from the figures must be transformed to vertical dam height using Equation (5.1).

normal velocities. Supercritical overflow becomes less important for low Froude numbers and low deflecting angles, whereas the reverse it true for overflow according to shock dynamics.

A comparison of the new criteria with the traditional dam height formulae (Eqs. (3.1) to (3.3)) given in Jóhannesson and others (2008) shows that considerably higher dams are required for low deflecting angles at relatively low Froude numbers. As an example, deflecting dams with $\varphi = 20°$ and flow at $\mathrm{Fr} = 5$ (or $\varphi = 10°$ and $\mathrm{Fr} = 10$) need to be built approximately one third higher according to the new criteria compared with the traditional formulae. The change in the absolute value of the dam height is, however, not great, because the run-up component of the dam height is much smaller for these combinations of φ and Fr than for larger deflecting angles. The difference between the new and old criteria may, for example, lead to an increase in run-up, h_r, above the snow cover from 6–8 m to 9–10 m.

5.8 Snow depth on the terrain above the dam, h_s

The snow depth on the terrain above the dam, h_s, needs to be determined based on the snow climatology of the area and on the location of the dam within the avalanche path. Snow depth corresponding to a 50–100 year return period is often considered to be appropriate. This is much shorter than the return period of the design avalanche that is typically needed for the dam to provide the required safety in the protected area. This difference in the return periods of design snow depth and design avalanche arises because the statistical distributions of avalanche run-out and snow depth are partly independent so that catastrophic avalanches may fall when snow depth above the dam is at an intermediate level.

In some cases, particularly for dams high up the avalanche path, snow deposits of earlier avalanches from the same winter need to be taken into consideration in the determination of h_s. The choice of h_s is always difficult in such circumstances and can only be made on a subjective basis by an expert. Overflow due to earlier avalanche deposits above the dam is sometimes considered a part of the rest risk and may perhaps in part be dealt with by temporary measures such as evacuations. This is particularly relevant in cases in which earlier deposits would most likely be noticed by inhabitants so that reduced effectiveness of the dam could be taken into account by civil defence authorities managing the situation when avalanche danger arises. Such interplay between permanent and temporary safety measures is less feasible for dams that are often reached by avalanches, say once every few years or more, or for dams that need to be located high up the avalanche path or in inaccessible locations, where avalanches piling up against the dam would often not be noticed until long after they fall.

Snow drift can locally lead to much more accumulation of snow than indicated by regional values of snow depth on unconfined terrain. The dam itself can, in addition, influence the accumulation of drift snow. Although some guidance may be obtained by numerical air-flow simulations and scale-model experiments in wind tunnels, the effect of snow drift on snow depth above avalanche dams must chiefly be assessed subjectively by the avalanche expert. The main points to consider in this respect are:

- The dam must be formed such that the wind can blow along the upper dam side without encountering obstructions that lead to deposition of blowing snow. Complicated dam geometries with corners or bends that may lead to slowing of the wind and consequently to deposition of drift snow should be avoided. This aspect must be considered especially carefully when several dams, or dams and mounds, are built in the same area.

- To the extent this is possible, dams should not be built normal to the main wind direction at the dam location.

- The excavation area above the dam should be wide and merge smoothly with the surrounding terrain in order to prevent preferential deposition of drift snow near the dam.

5.9 Comparison of the proposed criteria with observations of natural avalanches that have hit dams or other obstacles

There are few observations of run-up of natural avalanches on man-made dams that can be used to validate the proposed dam height criteria. The largest data set is from Norway, where information about the run-up of 15 snow avalanches on dams and natural obstacles has been gathered together with data about the geometry of the obstacles and model estimates of the velocity of the oncoming flow. Similar data about four avalanches in Iceland and the Taconnaz avalanche in France in 1999, which hit three obstacles on its way down the mountainside, were combined with the Norwegian data set when compiling this book, creating a data set with a total of 22 events. The avalanches have estimated volumes ranging from about 15.000 m^3 to 800.000 m^3, and modelled impact velocities in the range of 20–70 $m\,s^{-1}$. The vertical run-up ranges from 7 to 90 m. Based on these field observations, Figure 5.12 shows a comparison of the measured run-up with run-up estimates derived from supercritical overflow (with k according to Eq. (5.14) for paths with an abrupt change in slope at the foot of the obstacle) and the flow depth downstream of a shock. The field observations are further described by Jóhannesson and others (2008) and in the references quoted in the figure caption.

Many of the obstacles are situated on rather steep terrain with a significant difference between run-up normal to the upstream terrain (here denoted by h_r) and vertical run-up (here denoted by r and traditionally measured in a vertical cross section normal to the dam axis in the map plane). Figure 5.12 shows vertical run-up since this is the quantity reported in reports on the avalanches. The theoretically predicted run-up normal to the terrain has been transformed to the corresponding vertical run-up using Equation (5.1). The flow depth, h_1, and velocity, u_1, of the oncoming flow are unknown as regards all the avalanches, and are therefore associated with a significant amount of uncertainty. The velocity was estimated by numerical simulations and the flow depth subjectively, with some assistance from computer models for some of the avalanches. In order to highlight the uncertainty due to these estimates, the model results are depicted as ranges corresponding to subjectively chosen ranges in h_1 (most often

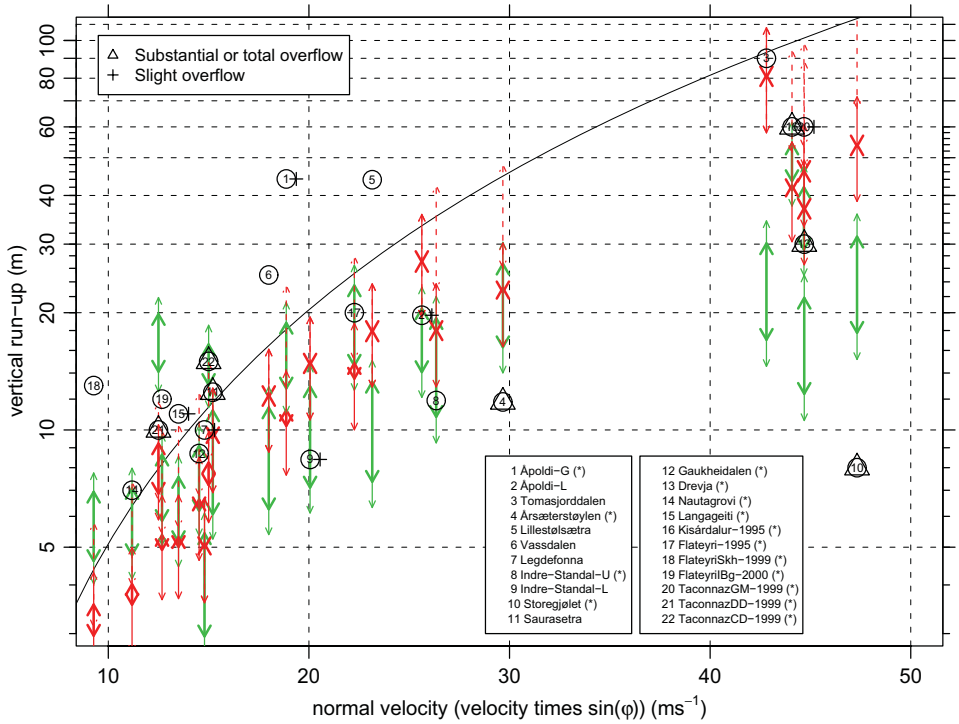

Figure 5.12: Figure caption follows on the next page.

1–3 m) and u_1 ($\pm$15%) rather than as single values. As seen in Figure 5.12, the ranges in computed run-up corresponding to "moderate" variations in h_1 and u_1 are quite large.

The theoretically computed run-up for deflecting dams does not take into account the effect of terrain slope towards the dam and curvature of the dam axis (the terms $\Delta H_{\psi_\perp}$ and ΔH_κ, see Eqs. (6.2) and (6.3) in Section 6), because the parameters $\psi_\perp$, R_κ and ξ (see Section 6) needed to estimate these terms are unavailable for most of the avalanches in the data set. These run-up terms are, for example, estimated to be several metres each for the Innra-Bæjargil dam at Flateyri for a somewhat higher velocity of the avalanche (35–55 m s^{-1} instead of 30 m s^{-1}) in a design example described in Appendix C (see Table C1). These run-up terms in combination are also estimated to amount to several metres for the Nautagrovi and Langageiti dams in another design example in Appendix C (see Table C4). A part of the discrepancy between the theoretical predictions and the observed run-up for these avalanches and some of the others could therefore be explained by the omission of these terms in the analysis that underlies Figure 5.12. Snow depth on the ground before the avalanche falls, h_s, is also omitted in the run-up analysis for all the dams and terrain obstacles.

The run-up of several of the avalanches is higher than the theoretically predicted maximum run-up, but many of them fall within the predicted ranges as further discussed by Jóhannesson and others (2008). Momentum loss during impact is only assumed for paths with an abrupt change in slope at the foot of the obstacle (marked with "(*)" in the legend of Fig. 5.12). This is the case for all the man-made dams (six avalanches in total), for six of the Norwegian

Figure 5.12 (on the previous page): Run-up of natural snow avalanches in Norway, Iceland and France on dams and terrain features compared with results of the run-up expressions derived from supercritical overflow (Eq. (5.6) with k determined from Eq. (5.14) for the avalanches where momentum loss during impact is assumed) and the flow depth downstream of a shock (Eqs. (5.10) and (5.11)) (Norway: Harbitz and Domaas, 1997; Domaas and Harbitz, 1998; Harbitz and others, 2001; Harbitz and Domaas, in prep.), (Iceland: Jóhannesson, 2001), (France: Mohamed Naaim and Francois Rapin, personal communication 2006). Momentum loss during impact with the obstacle is only assumed for paths with an abrupt change in slope at the foot of the obstacle (marked with "(*)" in the figure legend). Symbols with numbers denote observed vertical run-up. Overflow with a substantial part or all of the avalanche passing the obstacle, is denoted with $\triangle$, and slight overflow is denoted with $+$ besides the $\bigcirc$-symbol. Double arrows denote (somewhat arbitrary) ranges in the estimates for the flow depth, h_1 (typically 1–3 m), and velocity, u_1 ($\pm 15\%$), of the oncoming avalanche. Thick arrows correspond to the range in h_1 only, using the central estimate for u_1 from the studies referred to above. Thin arrows correspond to ranges in both h_1 and u_1. For the avalanches in which momentum loss is assumed during impact, the run-up range corresponding to zero momentum loss is shown with dashed thin arrows. Run-up ranges derived from supercritical overflow are shown by red arrows, and ranges derived from flow depth downstream of a shock by green arrows. Run-up ranges corresponding to ranges in u_1 are drawn at the location corresponding to the central estimate for u_1, so that the symbol indicating the observed run-up, and both arrows for each avalanche are drawn at the same location on the x-axis in the figure (same value of the normal velocity $u_\eta = u_1 \sin\varphi$). For comparison, the solid curve shows the velocity component of the vertical run-up, $r = (u_1 \sin\varphi)^2/(2g)$, given by the traditional Equations (3.2) and (3.3)) without momentum loss ($\lambda = 1$) on horizontal terrain ($\psi = 0$).

avalanches hitting natural obstacles, the Kisárdalur and Flateyri avalanches in Iceland in 1995, and the Taconnaz avalanche hitting the glacier moraine (see Jóhannesson and others (2008) for further reference). Two of those avalanches (nos. 4 and 10) overflowed obstacles that are considerably lower than the theoretically predicted run-up. The high run-up on the deflecting dams at Flateyri in 1999 and 2000 (nos. 18 and 19) may perhaps be explained by the run-up marks on loose snow on the dam sides being caused by the saltation layer of the avalanche rather than by the dense core. Three of the remaining eleven avalanches (nos. 13, 21 and 22) overflowed obstacles with height within or lower than the theoretically predicted ranges, five avalanches (nos. 8, 12, 14, 17, 20) produced run-up marks within the ranges or close to them, one avalanche (no. 15, Langageiti) slightly overflowed an 11 m high dam for which the upper limit of the predicted ranges is approximately 8.5 m, one avalanche (no. 1, Åpoldi-G) produced *much higher* run-up marks than theoretically predicted, even when no momentum loss is assumed, and one avalanche (no. 16, Kisárdalur) *completely overflowed an obstacle*, which is *higher than the predicted run-up range*, when momentum loss during impact is assumed.

The run-up data can, thus, only partially be reconciled with the theoretically predicted run-up ranges. Dashed arrows in Figure 5.12 show the run-up range corresponding to no momentum loss during impact for the avalanches hitting abrupt obstacles. The difference between the dashed and solid ranges clearly shows the large effect of the assumed momentum loss. Similarly, relatively small modifications in the assumed velocity of the avalanches can result in substantial changes in the predicted run-up ranges. Uncertainty in the flow depth, on the other hand, has little effect on the predicted run-up, except for the Kisárdalur and Taconnaz avalanches, which are estimated and/or modelled to have been unusually thick. The

Kisárdalur avalanche (no. 16) is in the lower part of the dashed range but the Åpoldi-G avalanche (no. 1) is far above the dashed range and is very difficult to reconcile with the theoretical predictions. According to NGI reports, the run-up marks of the Åpoldi-G avalanche are likely to have been produced by the powder part of the avalanche. It is, therefore, not certain whether the dense core reached this high level. Except for the Åpoldi-G avalanche, the assumed momentum loss leads to run-up ranges that are approximately in agreement with this limited data set, with some avalanches within or at the lower end of the ranges, and some above them. On the other hand, excluding momentum loss leads to much higher ranges for avalanches that hit abrupt obstacles. The Taconnaz avalanche hitting the glacier moraine in 1999 is in the upper part of the range corresponding to supercritical overflow when momentum loss is assumed. The run-up predictions are reasonable for this very large avalanche with a large deflecting angle ($\approx 40^\circ$), indicating that the theory is valid for some very large events with large normal velocities, and thus is not limited to laboratory-scale granular flows or to small snow avalanches. The avalanche at Flateyri in 1995 is also quite large and hits a steep gully wall at a large deflecting angle ($\approx 30^\circ$) with a run-up that falls within the predicted range.

On the other hand, the rather wide spread of the data points compared with the assumed uncertainty of the theoretical predictions clearly indicates an incomplete understanding of the dynamics of the impact process. The Åpoldi-G and the Kisárdalur avalanches are of particular concern. Another worrisome observation is provided by a medium-sized avalanche at Seyðisfjörður in eastern Iceland in April 2006, which overflowed a 20 m high catching dam, leaving little stopped snow on the upstream side of the dam. The uppermost 10 m of the upstream side of the dam are very steep with a slope of 4:1 but the lowest 10 m have a slope of 1:1.5. This avalanche has not yet been modelled and is, therefore, not included in the data set shown in Figure 5.12. Two other avalanches with the largest run-up in excess of the theoretically predicted run-up ranges (nos. 5 and 6) did not hit abrupt obstacles. These avalanches and the Åpoldi-G avalanche stand out due to their very high run-up, exceeding the theoretical predictions by a factor on the order of 2. These avalanches are further discussed in Jóhannesson and others (2008).

On the positive side, Figure 5.12 shows that the run-up marks of several medium-sized and large avalanches are in rough agreement with the proposed criteria, and that the overall variation of the run-up with normal velocity is in general agreement with the criteria (except of course for the four abovementioned avalanches with higher run-up and the avalanches at Flateyri in 1999 and 2000). The avalanche at Taconnaz in France in 1999 represents important data points. It *did not overflow* the approximately 60 m high glacier moraine, as evidenced by the symbol in Figure 5.12 near the upper limit of the range corresponding to supercritical overflow, assuming momentum loss during impact. This interpretation of the Taconnaz event indicates that the validity of the criteria is not limited to low speeds or acute deflecting angles, or as mentioned above to small laboratory scales and only the granular materials that were used in laboratory experiments. Farther down the path, the Taconnaz avalanche *overflowed* a 10 m high deflecting dam and a 15 m high catching dam, which is shown by two symbols in Figure 5.12 that fall well within the theoretically predicted ranges. In Figure 5.12, the location of the symbols corresponding to the three events at Taconnaz with respect to the theoretically predicted ranges indicates that the theory does not systematically underestimate or overestimate run-up.

The high observed run-up of some of the avalanches does, however, indicate a larger uncertainty in the estimated velocity than assumed here, or a run-up mechanism that is not

accounted for in the theoretical analysis. As mentioned above, some of the highest run-up marks may be caused by the impact of the saltation or powder components of the avalanches. In that way, damage may occur considerably higher than the highest point reached by the dense core. Pressure from the saltation or powder layers can, however, not account for the complete overflow of the Kisárdalur avalanche, which left very little snow in the gully at the foot of the obstacle. These events need to be taken as reminders of the imperfect dynamic basis of the proposed run-up criteria, indicating that natural avalanches are perhaps of several different types, which are not adequately described by a single dynamic framework.

Another source of information for validating the theoretical run-up ranges are measurements of avalanche flow over the 16 m high catching dam at the full-scale experimental site at Ryggfonn in western Norway (Gauer and Kristensen, 2005). These data are summarised in Section 7. They show long overrun distances compared with the inferred velocity at the impact with the dam and are difficult to reconcile with the theoretical run-up ranges described in this section. Available data about run-up and overrun of natural avalanches on obstacles and man-made dams thus appear to be partly inconsistent and cannot be explained within one conceptual framework. The effectiveness of catching dams to completely stop snow avalanches seems to be particularly uncertain, as discussed further in Section 7. These inconsistencies may to some extent be explained by the uncertainty of the data and the calculated velocities and flow depths, but this is unlikely to be the only explanation. Further full-scale experiments and improved theoretical analyses are required to resolve the inconsistencies and improve the incomplete state of knowledge of dam design.

6 Special considerations for deflecting dams

Tómas Jóhannesson, Carl B. Harbitz and Ulrik Domaas

6.1 Location and configuration of the dam

An optimal deflecting dam is built in steep terrain and adjusts the course of an avalanche without a substantial reduction of flow speed, thereby avoiding deposition of masses along the dam wall and maintaining the effective height for subsequent events.

The easiest way to control an avalanche is to guide it along a gently curving channel. However, this often requires a very long dam along a steep talus. On the upper part of the talus, the dam may need to be very wide due to the steepness of the underlying terrain.

Preferably, loose materials from the talus should be utilised to reduce the dam height above the original terrain, provided the channel width is maintained down the talus. An existing creek channel can be excavated and widened and the dam built on one side of the creek, using the material from the excavation. If possible, a deflecting dam in steep terrain should be designed in such a manner that the masses of the fill, all the way along the dam axis, are resting on lower-lying parts of the dam (see examples in Harbitz and others, 2001). The global stability of a dam in steep terrain may easily be insufficient if the dam axis does not approximately follow the steepest descent of the terrain. Too high dams in steep terrain should also be avoided in order to prevent new release zones for avalanches on the dam walls themselves.

The design of the channel on the upstream side of the dam is important for the deflecting angle. Typically, loose materials and blasted rock from an excavation area on the upstream side of the dam are used in the dam fill. The excavated area must, as far as possible, be designed to divert the avalanche away from the dam. Care should be taken to avoid a deep and narrow excavated channel by the dam, as this will have the tendency to divert the avalanche flow towards the dam. A deep and narrow channel will also accumulate more drift snow, resulting in less effective height of the dam at times of large snow depths at the dam location.

The terrain of the avalanche paths in Vassdalen and Gaukheidalen in Nordland, northern Norway, illustrates the importance of the geometry of the terrain upstream of the dam (Fig. 6.1). In Vassdalen, the contour lines are not curved upstream of the natural deflecting dam, giving a rather large angle of incidence, $\varphi \approx 40^\circ$, and a comparatively high vertical run-up, $r \approx 25\,\mathrm{m}$, of an avalanche that fell in 1986. In contrast, the upstream contour lines in Gaukheidalen are curved and end up perpendicular to the centre line of the natural deflecting dam. Hence, the effective angle of incidence at the point of impact, $\varphi \approx 25^\circ$, and the run-up height, $r \approx 9\,\mathrm{m}$, of an avalanche in 1996 are reduced because the avalanche is partly deflected before the impact and a larger part of the avalanche is guided away from the dam without climbing it. More information about these avalanches is given by Irgens and others (1998) and Harbitz and Domaas (1997, in prep.).

It is worth noting that the maximum run-up in both these cases is reached downstream of the location at which the avalanche first meets the deflecting landscape. Therefore, a detailed simulation of avalanche flow along a dam may make it possible to reduce the dam height of the upper and lower parts of the dam.

For narrow snow avalanches, for example, avalanches flowing out of narrow gullies, the flow depth, h_2, downstream of a shock along a deflecting dam, based on Equations (5.10) and (5.11), may be an overestimate of the actual flow depth. Experiments with snow in the Col

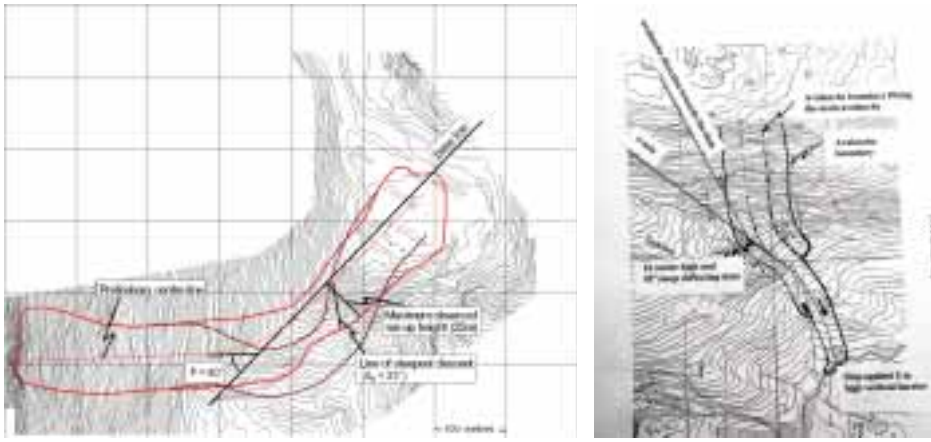

Figure 6.1: Maps of Vassdalen with 2 m contour line interval (left) and Gaukheidalen with 5 m contour line interval (right), Nordland, northern Norway, with outlines of avalanches that occurred in 1986 and 1996, respectively. The red curve on the Vassdalen map is the outline of the avalanche. The brown curves on the same map show the results of the quasi three-dimensional continuum avalanche model by Irgens and others (1998). The areas shown correspond to 800x600 m^2 and 625x925 m^2, respectively.

du Lac Blanc chute in France by Faug and others (2007) for narrow avalanches with a depth to width ratio in the approximate range of 0.2–0.5 showed that the shock theory consistently overpredicted the run-up on deflecting dams by approximately 20–50%. This may be due to the limited lateral width of the oncoming stream, which may to some extent be pushed to the side as a whole by internal pressure forces. Transverse, internal pressure forces generated during the impact with the dam are partly counteracted by the mass of the avalanche flow farther away from the dam in the case of an infinitely wide stream as assumed in the derivation of the shock theory. For narrow streams, this lateral support is weaker and the downstream shock depth may for this reason be smaller than theoretically predicted. This effect has not been quantitatively analysed in detail, but may be assumed to lead to an improved efficiency of deflecting dams for narrow oncoming avalanches compared with wide avalanches. Here, it is recommended that this effect is not used as an argument to build lower dams, but rather that it is considered an extra safety margin to partly balance the overall uncertainty regarding the effectiveness of avalanche dams.

6.2 Determination of the deflecting angle: φ

The deflecting angle in the map plane, φ_h, will in most cases be determined graphically on a map from an estimate of the flow direction of the avalanche and the direction of the dam axis. The deflecting angle in a plane aligned with the terrain, φ, which is the quantity needed in the determination of the dam height, may then be computed from the geometric identity

$$\tan\varphi = \tan\varphi_h \cos\psi \,, \tag{6.1}$$

where ψ is the slope of the upstream terrain. An example showing the determination of deflecting angles for the deflecting dams at Flateyri in Iceland is described in Appendix C.

The determination of the deflecting angle is straightforward in most cases but can be non-trivial in case of complicated terrain geometries, for example, if the terrain in the run-out zone slopes laterally with respect to the main flow direction out of the track. It is then advisable to use 2D numerical avalanche modelling to analyse the flow towards the dam and to calculate the deflecting angle from the numerically determined flow direction at the dam site. It is also possible in some cases to use simple dynamic analysis to compute corrections to the flow direction that to first approximation take into account lateral slopes upstream of the dam. It is of course important in this case to calculate the deflecting angle from the estimated flow direction rather than from the direction of steepest descent of the upstream terrain.

The run-up estimates described in Section 5, as well as the geometrical identities used to compute the vertical dam height (Eq. (5.1)) and the steepest inclination of the dam wall (Eq. (5.2)), are derived based on the assumption that the avalanche travels towards the dam directly in the direction of steepest descent of the upstream terrain. If the direction of the avalanche is at an angle to the direction of steepest descent of the upstream terrain, the assumption that friction is approximately balanced by the downslope component of gravity is not valid. The analytical solutions to the dynamic flow equations and the geometrical identities, on which the run-up estimates are based, are then not strictly valid. In this case, the terrain slope, ψ, should be estimated as the slope along the flow direction rather than the slope in the direction of steepest descent of the upstream terrain. If the difference between the flow direction and the direction of steepest descent of the upstream terrain is not large, the error arising from this difference is small compared with other uncertainties associated with the design recommendations.

Finally, the deflecting angle should be determined on the basis of the reshaped terrain after the dam construction, taking into consideration the modified geometry of the excavation area.

6.3 Maximum deflecting angle: φ_{max}

As described in the previous section, an avalanche hitting a deflecting dam with a deflecting angle φ close to or greater than the maximum deflecting angle φ_{max} corresponding to the Froude number of the flow (see Fig. 5.8), may not remain attached and may start to propagate upstream to form a detached, semi-stationary shock with a larger jump in flow depth across the shock than for an attached shock. As described before, it is recommended that deflecting dams should have deflecting angles at least 10° smaller than φ_{max}, as approximately determined from Equation (5.13).

6.4 Terrain slope towards the dam: $\Delta H_{\psi_\perp}$

It is implicitly assumed in the preceding analysis that friction is approximately balanced by the downslope component of gravity. Thus, all formulae describing supercritical overflow and formation of a shock by the dam have been derived without considering friction and the downslope component of gravity. For supercritical overflow, one may assume that for each part of the avalanche the impact does not last long enough for frictional forces to reduce the momentum of the flow significantly. For a normal shock upstream of a catching dam, where the terrain slope is smaller than the internal friction angle of avalanching snow, ϕ, the propagation of the shock away from the dam will not be much affected by the slope of the terrain, because the snow downstream of the shock is stopped. As regards flow downstream

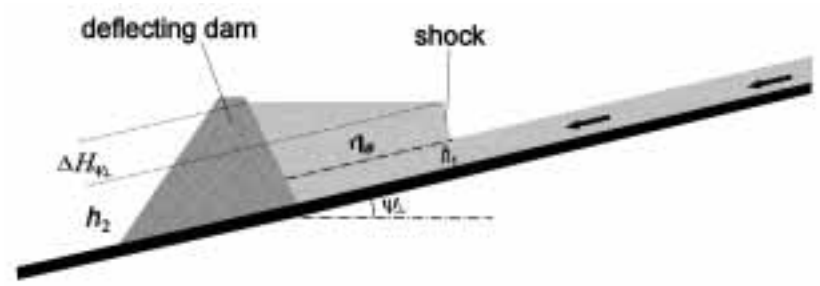

Figure 6.2: A schematic cross section of a shock formed along a deflecting dam built on terrain sloping towards the dam. In a coordinate system moving with the avalanche along the dam, the shock is propagating away from the dam. Material flows across the shock and tends to form a horizontal surface in the direction normal to the dam axis. $\psi_\perp$ is the slope of the terrain in the direction normal to the dam axis, and η_s is the width of the shock.

of an oblique shock caused by a deflecting dam on sloping terrain one may, however, expect failure of the assumption of approximate balance of downslope gravity by friction. This arises because the direction of the flow downstream of the shock is parallel to the dam, and friction in such cases cannot balance the component of gravity normal to the dam axis. Furthermore, the material does not stop at the dam as in the case of a catching dam. In general, there should be sufficient agitation in the flow for the material to flow towards the dam and form an approximately horizontal profile from the shock towards the dam in the direction normal to the dam axis (Fig. 6.2).

The effect of terrain slope towards the dam on shock height is analysed by Jóhannesson and others (2008) taking into account the flow of material across the shock towards the dam that is needed to form a horizontal profile. The flow surface will not become fully horizontal, but would do so in a worst case scenario with respect to the required dam height. With zero terrain slope towards the dam, the distance of the shock from the dam is $\eta_s = \tan(\theta - \varphi)\,\xi \approx \sqrt{2}/(2\,\mathrm{Fr}\cos\varphi)\,\xi$, where ξ is distance along the dam from its upstream end. The approximate expression for the shock widening $(\theta - \varphi)$, correct to $O(\mathrm{Fr}^{-2})$, is taken from Hákonardóttir and Hogg (2005). This width is an upper bound on the shock width for dams on a sloping terrain because the effect of the slope towards the dam is to narrow the shock. This estimate for the shock width may be used to express an approximate upper bound on the extra run-up on the dam side (normal to the terrain) as

$$\Delta H_{\psi_\perp} = \tan\psi_\perp\,\eta_s \approx \frac{\sqrt{2}\tan\psi_\perp}{2\,\mathrm{Fr}\cos\varphi}\,\xi\,. \tag{6.2}$$

In most cases, the increased dam height specified by Equation (6.2) is not appreciable, but it needs to be taken into account in rare cases when $\psi_\perp > 5^\circ$, especially if the flow depth is large or the velocity is low, so that the Froude number is small.

6.5 Curvature of the dam axis: ΔH_κ

The analysis has so far been based on the simple geometry of a straight dam that is hit by a flow with uniform thickness and velocity. Avalanche dams frequently need to be curved along

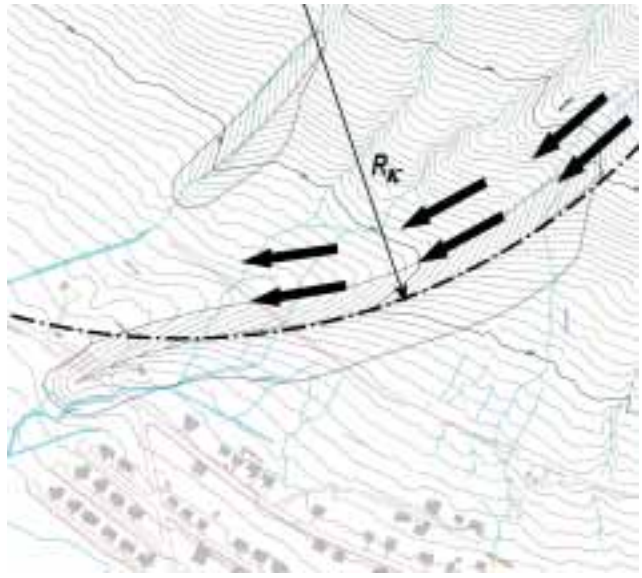

Figure 6.3: The deflection of an avalanche alongside the 700 m long, curved deflecting dam below Ytra-Strengsgil at Siglufjörður, northern Iceland. A circle with a radius of curvature $R_\kappa \approx 700$ m has been fitted to the curved dam axis.

the dam axis in order to protect as large an area as possible. The curvature of the dam axis then affects the run-up of the avalanche due to the centripetal acceleration that is introduced as the flow bends around the curved dam geometry (Fig. 6.3). The run-up requirement derived from supercritical overflow is not affected by the curvature of the dam axis, because the possibility of overflow is determined based on the local dam height and deflecting angle at each point along the dam axis. However, as for terrain slope towards the dam (see the previous subsection), the run-up height corresponding to the flow depth downstream of a shock along the dam needs to be reconsidered when the dam is curved.

Assuming that, over the width of the shock that has been formed along the dam, the centripetal acceleration is counteracted by a slope of the surface of the flow away from the dam, the extra run-up on the dam side that needs to be taken into account is given by

$$\Delta H_\kappa = \frac{(u_1 \cos\varphi)^2}{g \cos(\psi) R_\kappa} \eta_s \approx \frac{\sqrt{2}\,(u_1 \cos\varphi)^2}{2\,\mathrm{Fr} \cos(\varphi)\, g \cos(\psi) R_\kappa} \xi \,, \tag{6.3}$$

where g is the acceleration of gravity, R_κ is the radius of curvature of the dam axis, η_s is the width of the shock in the direction normal to the dam axis, and ξ is the distance along the dam axis measured from its upstream end. The same approximations have been used to express the width of the shock as in the preceding section about terrain slope towards the dam. The term ΔH_κ due to the curvature of the dam axis may come in addition to $\Delta H_{\psi_\perp}$ due to the terrain slope towards the dam, as described in the previous subsection, in the case that the upstream terrain slopes towards a curved dam (Fig. 6.3).

Avalanches hitting curved deflecting dams often flow out of gullies or confined avalanche paths, where the flow towards the dam has a limited width. The deflecting dam may, however,

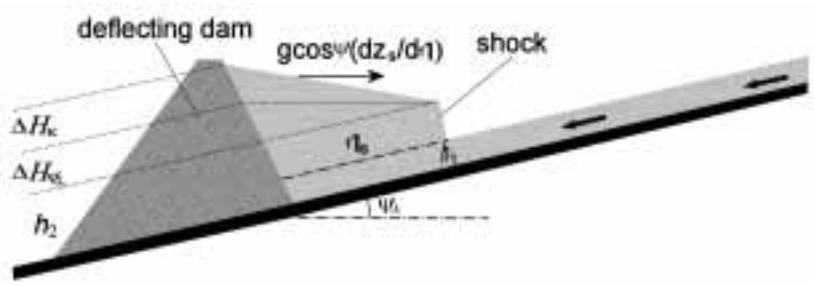

Figure 6.4: A schematic cross section of a shock formed along a curved deflecting dam built on terrain sloping towards the dam. In a coordinate system moving with the avalanche along the dam, the shock is propagating away from the dam. Material flows across the shock and for a straigt dam would tend to form a horizontal surface in the direction normal to the dam axis (*cf.* Fig. 6.2), as indicated by the horizontal dotted line below the surface of the flow downstream of the shock. The centripetal acceleration, arising from the curvature of streamlines, tends to push the flowing material towards the dam and is counteracted by the gravitational force $g\cos(\psi)(\partial z_s/\partial\eta)$. Here, $\psi_\perp$ is the slope of the terrain in the direction normal to the dam axis, η_s is the width of the shock and z_s is the vertical height of the surface of the flow.

extend out of the avalanche stream to divert the avalanche flow away from an area that needs to be protected. In such cases, the length ξ along the dam in Equation (6.3) only needs to be considered up to a maximum value corresponding to the distance along the dam, where there is flow towards the dam upstream of the shock (see Fig. 6.3). Beyond this point, the maximum value of ξ and the corresponding distance of the shock from the dam, η_s, may be used along the entire downstream length of the dam. If the dam extends a considerable distance beyond the boundaries of the oncoming flow upstream of the shock, the shock will spread out away from the dam and it will be possible to design the dam with a higher curvature without overflow. The same consideration also applies to the extra dam height $\Delta H_{\psi_\perp}$ due to the terrain slope towards the dam, as determined from Equation (6.2). The distance along the dam, ξ, only needs to be considered up to a maximum corresponding to upstream flow towards the dam.

The simple derivations presented here and in the preceding section, taking into account dam curvature and the slope of the terrain towards the dam, are sometimes inappropriate when dam and terrain geometry are complex. In such cases, it is advisable to use 2D avalanche modelling with a shock capturing algorithm to investigate these effects in more detail, possibly with guidance from the simple results presented here. In particular, 2D avalanche simulations are appropriate to analyse the effect of terrain slope towards the dam and curvature of the dam axis for long, curved dams that are hit by comparatively narrow avalanches flowing out of gullies or confined avalanche paths.

6.6 Increased run-out because of channelised flow along the dam

Avalanche flow along deflecting dams is channelised along the dam, possibly leading to a substantial increase in run-out in the direction of the deflected flow (Jóhannesson, 2001) (Fig. 6.5). The construction of a deflecting dam, therefore, leads to increased avalanche risk in

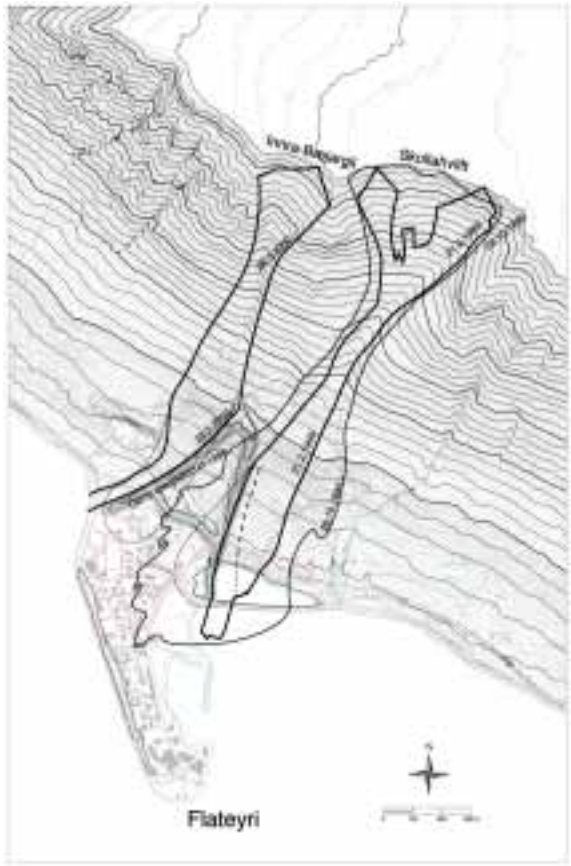

Figure 6.5: Outlines of avalanches that were deflected by the deflecting dams at Flateyri, northwestern Iceland, in 1999 and 2000. The outline of the catastrophic avalanche in 1995 is also shown. The channelised flow of the 1999 avalanche from Skollahvilft along the deflecting dam is indicated by a dashed curve. Hypothetical outlines of the avalanches in 1999 and 2000 in the absence of the deflecting dams are shown as dotted curves. Due to the channelised flow along the dam, the run-out of the 1999 avalanche may have been increased by a distance on the order of 100 m.

this direction. If possible, the increased run-out should be analysed by 2D numerical avalanche modelling (see Cui and others, 2007), and needs to be explicitly pointed out in the reassessment of avalanche hazard made following the construction of a deflecting dam.

6.7 Lateral spreading of the flow below the downstream dam end

Snow avalanches will spread out laterally when they flow past the downstream end of deflecting dams. In some cases, particularly for wet-snow avalanches (see Fig. 8.4), an avalanche or part of an avalanche may turn abruptly when it flows past the end of a dam, whereas in other cases (see Fig. 6.5), the avalanche continues in the direction of the dam axis and almost no spreading of the flow downstream of the dam can be seen. As for the increased run-out due to

channelised flow along the dam, as discussed in the previous subsection, the widening of the flow below the dam should be analysed by 2D numerical avalanche modelling if possible.

The spreading of granular materials at the end of the lateral constraints provided by a dam has been estimated analytically based on shallow fluid theory by Hogg and others (2005). The theory predicts that the maximum lateral spreading (in terms of the angular width of a fan beyond the dam axis formed at the downstream end of the dam) is a decreasing function of the Froude number of the flow and is approximately given by

$$\phi_{\mathrm{lsp}} = \frac{2}{\mathrm{Fr}} - \frac{5}{3\,\mathrm{Fr}^3} + O\left(\frac{1}{\mathrm{Fr}^5}\right) . \tag{6.4}$$

The theory predicts a spreading of 11–21° for Fr in the range of 5–10, which is consistent with a value of 20° that has sometimes been adopted in Switzerland for this type of widening (Stefan Margreth, personal communication 2006). It should be noted that smaller and slower avalanches than the design avalanche may need to be taken into account when the effect of this widening below the dam is considered, because such avalanches are predicted to form a wider fan than larger and faster avalanches. As discussed further in Section 8, wet-snow avalanches may make much sharper turns around dam ends than dry-snow avalanches, so this estimate cannot be used for dams intended as protection against wet-snow avalanches.

6.8 Empirical run-up height adjustment

Harbitz and others (2001) analysed observed run-up height of avalanches on man-made dams and natural obstructions, using a centre-of-mass dynamic avalanche model. They found that the maximum run-up height simulated by the model, r_{max}, systematically underestimates the observed run-up, r_{obs}, so that the modelled height needs to be corrected with the empirical formula

$$r_{\mathrm{obs}} = 3.43\, e^{0.136\, r_{\mathrm{max}}} , \tag{6.5}$$

to account for the bias. This equation provides a good fit to run-up observations from several Norwegian and Icelandic avalanches in the range of 7–25 m, as described by Harbitz and others. However, it may lead to very high run-up predictions for large avalanches with high velocity, such as the Taconnaz avalanche in 1999, which hit a glacier moraine at a deflecting angle of $\approx 40^\circ$ with a velocity on the order of $70\,\mathrm{m\,s^{-1}}$ producing a vertical run-up of $\approx 60\,\mathrm{m}$ (Mohamed Naaim and Francois Rapin, personal communication 2006) (Jóhannesson and others, 2008). For such avalanches, the modelled run-up with the centre-of-mass model may be substantially greater than 25 m, depending on the choice of the restitution coefficient k, which is one of the independent model parameters. The exponential variation specified by Equation (6.5) then leads to very large run-up predictions. The great sensitivity of the adjusted run-up computed using Equation (6.5) on the assumed value of restitution coefficient k also makes it hard to apply this equation in some cases, particularly for high avalanche velocities and steep dam sides. Further analysis of a larger data set is needed to determine whether empirical adjustments of modelled run-up can be used to improve run-up predictions. In particular, the flexibility provided by the currently rather arbitrarily chosen model parameters needs to be reduced, so that the model prediction is less dependent on a subjective choice of parameters.

7 Special considerations for catching dams

Peter Gauer and Tómas Jóhannesson

7.1 Storage above the dam: S

For a design avalanche to be successfully stopped by a catching dam, there must be sufficient space above the dam to store the entire volume of the snow deposit. According to traditional dam design principles in Switzerland and some other countries (Margreth, 2004), and as described in Section 3, the storage space per unit width upstream of a catching dam is computed as the area between the snow covered terrain and a line from the top of the dam with a slope of 5–10° away from the mountain (see Fig. 7.1) This requirement is primarily intended for slow, moist and dense avalanches, and the storage capacity for fast, dry-snow avalanches can be much smaller. A compaction factor of approximately 1.5 describing the ratio of deposit density to release density is, furthermore, sometimes used (Stefan Margreth, personal communication 2006). In some cases, the storage space above a catching dam must be dimensioned so that more than one avalanche per season can be stopped by the dam. This procedure for designing the storage space is not based on dynamic principles and is, therefore, not consistent with the overall framework described in the previous sections for determining the dam height.

Catching dams are usually built in the run-out zone of avalanches, where terrain slope may be expected to be smaller than the internal friction angle ϕ of avalanching snow, which is, however, not well known and probably dependent on the type of snow. In this case, one may expect a shock propagating upstream from the dam to maintain its thickness (see Hákonardóttir, 2004), even when the terrain slopes towards the dam. There is, however, considerable uncertainty regarding the propagation of the shock over possibly uneven terrain. For many dams on sloping terrain, the storage volume thus computed from shock dynamics would be larger than the volume found by the traditional procedure, since the deposit thickness would not decrease much with distance away from the dam.

Observations from the catching dam at Ryggfonn indicate that dry-snow avalanches do not pile up much against the dam, so that the avalanche deposit, in many cases, slopes away from the dam rather than towards it (see Fig. 7.2).

For lack of a better choice, it is proposed here to continue to use the traditional methodology with a deposit slope of 0–10° (see Fig. 7.1), and without a compaction factor. The storage

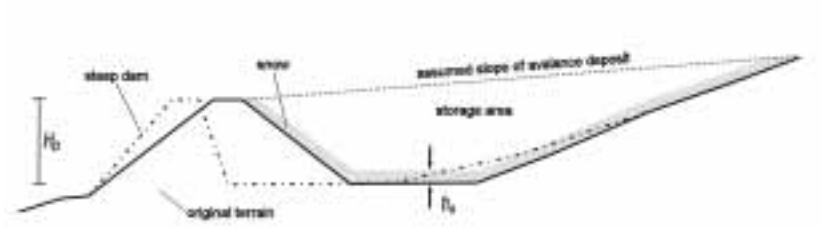

Figure 7.1: A schematic figure of the snow storage space above a catching dam. h_s is the thickness of snow and previous avalanche deposits on the ground on the upstream side of the dam. H_D is the vertical height of the upstream dam side. The figure is adapted from Margreth (2004).

volume may then be found from the equation

$$S = \int_{x_0}^{x_1} (z_l - (z_s + h_s))dx \,, \tag{7.1}$$

where x is the horizontal distance from the dam, z_l is the elevation of a straight line from the top of the dam towards the mountain with a chosen slope in the range 0–10°, $z_s + h_s$ is the elevation of the top of the snow cover before the avalanche falls, and x_0 and x_1 are the locations of the dam and the point where the line intersects the snow covered mountainside, respectively. For locations at which dry-snow avalanches are expected, deposit slopes close to 0° should be used, but for locations where wetter avalanches are typical, slopes up to 10° may be chosen. This procedure is not very satisfactory because it is not based on dynamic principles and needs to be refined by future studies. It should be noted that the storage space above the dam is typically not the determining factor in the choice of the dam height.

7.2 Overrun of avalanches over catching dams, Ryggfonn measurements

As described in Section 5, laboratory experiments and theoretical analyses have advanced our understanding of the dynamics of avalanche flow against obstructions. However, measurements of overrun length and velocity of avalanches at the catching dam at Ryggfonn (Gauer and Kristensen, 2005; Faug and others, 2008) indicate that avalanches under some conditions are able to overflow or scale dams more easily than would theoretically be expected. At other locations, observations of run-up marks on man-made dams and natural obstacles for many natural snow avalanches are in better agreement with the theory, although some natural avalanches have produced run-up marks that are difficult to explain. As yet, this discrepancy is the most important unresolved question regarding avalanche–dam interactions. Therefore, the Ryggfonn measurements are described and interpreted in this subsection and compared with results from chute experiments in the next subsection.

It will rarely be possible to design a catching dam that stops all avalanches on the upstream side. Some avalanches will partially overflow. An important question in connection with the effectiveness of catching dams is the extent to which such dams reduce the run-out of avalanches that are not fully stopped. An understanding of the shortening of run-out is clearly necessary for a reassessment of the avalanche hazard following the construction of a dam. It is also of great practical importance for the design of catching dams. An avalanche that partially overflows, but runs out before reaching the protected area, is relatively harmless. It may, therefore, be appropriate under some circumstances to design dams that are partially overflowed by the design avalanche. Both these potential applications of a theory of overflow are, however, hardly realistic in view of our current understanding of avalanche flow over obstructions.

Observations from full-scale experiments on a 16 m high and 70 m long (crown) dam at Ryggfonn, western Norway, imply that in those cases when the avalanche topped the dam, the overrun length of the avalanche can be expressed by a simple relationship as a function of the flow velocity upstream of the dam (Gauer and Kristensen, 2005; Faug and others, 2008). The slope angle of the dam is between 35 and 40°. Figure 7.3 shows the normalised overrun length as a function of the normalised kinetic energy. The overrun length of the avalanches

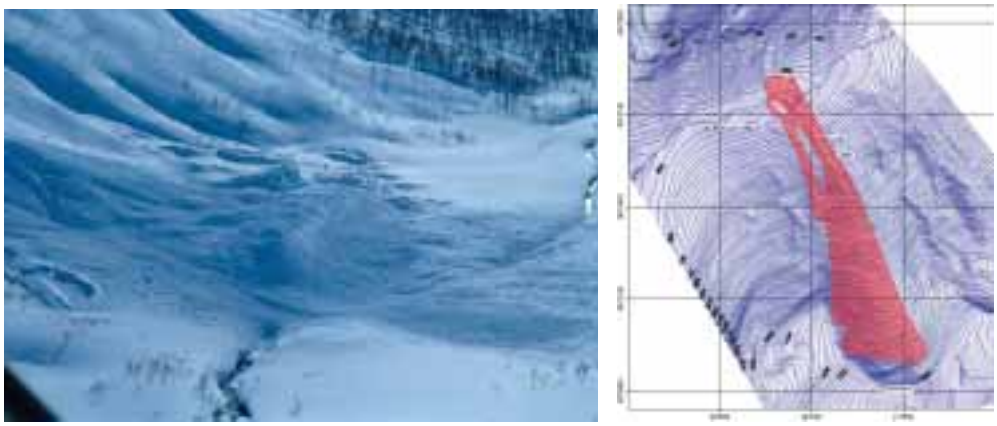

Figure 7.2: Deposition pattern of the 19970208 12:38 avalanche at Ryggfonn. *Left:* Photograph of the deposit. *Right:* Map of the deposit. Due to deposits of previous avalanches the effective free board height was only 5 m. The estimated front velocity was $40\,\mathrm{m\,s^{-1}}$. (Photo NGI.)

that surpassed the dam crown can be fitted by the line

$$\frac{l_{ovr}}{h_{fb}} \approx b_1 \frac{u_b^2}{2\,g\,h_{fb}} + b_0 \,, \tag{7.2}$$

where l_{ovr} is the overrun length measured from the top of the dam, h_{fb} the free board height, u_b the front velocity at the upstream base of the dam, and g is the gravitational acceleration. $u_b^2/(2\,g\,h_{fb})$ is the kinetic energy, E_n, normalised by the potential energy (the energy a point-mass would need to climb the effective dam height). The parameters b_0 and b_1 by linear regression analysis are found to be $b_0 = -1.41$ and $b_1 = 2.56$. The ratio $b_0/b_1 \approx 0.55$ may be interpreted as a measure of the energy, E_c, dissipated by the "effective" dam. It is the kinetic energy of the largest avalanche that is stopped by the dam divided by the potential energy corresponding to the free board of the dam. It may to some extent be compared with the energy dissipation parameter λ that is traditionally used in the design of catching dams (Eq. (3.2)). As described in Section 3, the λ-parameter is usually given a value between 1 and 2 (and sometimes even higher), with the higher values used for dams with steep upstream faces. The Ryggfonn measurements, however, indicate that λ-values close to one half may be more appropriate for natural dry-snow avalanches! Similar linear relations between overrun length and kinetic energy as in Figure 7.3 can also be found in granular experiments (*cf.* Gauer and Kristensen, 2005; Faug and others, 2008), but in that case they correspond to substantially greater loss of kinetic energy, as discussed further in the next subsection.

Equation (7.2) can also be motivated physically by rewriting it in the form of an energy balance,

$$\frac{u_b^2}{2} = -\frac{b_0}{b_1}\,g\,h_{fb} + \frac{g}{b_1}\,l_{ovr} \,. \tag{7.3}$$

The term on the left hand side corresponds to the kinetic energy of the incoming avalanche front. The first term on the right hand side is the energy dissipation of the front during the ascent of the dam, and the second term on the right describes the dissipation of the remaining

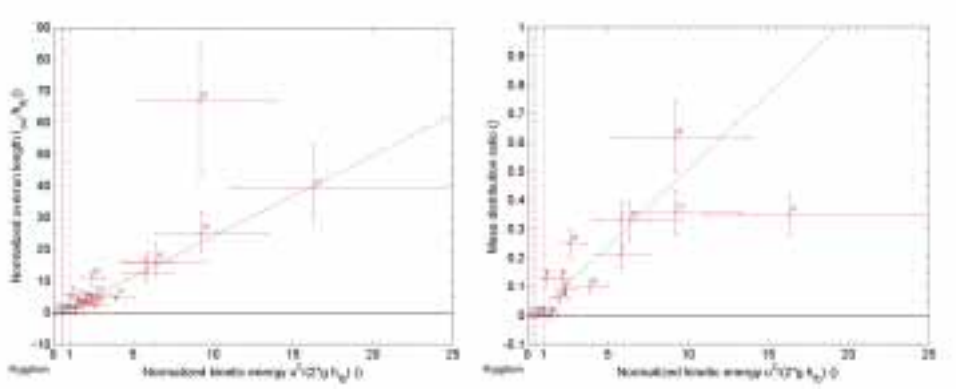

Figure 7.3: Normalised overrun length (left panel) and mass distribution ratio (right panel) as functions of normalised kinetic energy. In both panels, $\diamond$ marks the best estimates for avalanches that surpassed or overtopped the dam crown ($l_{ovr} \geq 0$), crosses indicate the range of uncertainty, numbers mark individual avalanches, the dashed lines represent the best linear relationships derived with robust fitting, and the dash-dotted red lines mark the critical energy E_c.

energy due to friction. In this sense, $1/b_0$ corresponds to an effective dissipation parameter in a Coulomb friction parameterisation.

Figure 7.3 also shows the mass distribution ratio, m_r, as a function of the normalised kinetic energy, E_n. The mass distribution ratio is defined as the estimated fraction of the total deposit mass that surpasses the dam crown, M_{ovr}. It is based on the measured deposit mass above the dam and the total mass, M_{tot} from the field surveys. The best linear fit (dashed line) is given by

$$m_r = \frac{M_{ovr}}{M_{tot}} = c_1 \frac{u_b^2}{2\,g\,h_{fb}} + c_0 \,, \tag{7.4}$$

with the regression coefficients $c_0 = -0.0254$ and $c_1 = 0.053$. Again, the ratio c_0/c_1 is a measure of the energy, E_c, dissipated by the "effective" dam.

Although Equation (7.2) is derived only from observations of those avalanches that overtopped the dam, the observations from the full-scale experiments imply that energy dissipation by the dam is less efficient than traditionally assumed (at least for dams with low steepness). Due to limited information about the avalanches that did not overflow, it is impossible to say whether they were stopped by the dam or just at the end of their natural run-out. However, from a total of about 70 to 80 observed avalanches since the dam at Ryggfonn was built in 1982, 16 are known to have surpassed the dam crown.

If one calculates the required dam height to stop an avalanche based on Equation (7.2), one finds that only avalanches with $u_b < 13\,\mathrm{m\,s^{-1}}$ could have be stopped by the dam at Ryggfonn, provided there are no previous deposits and little snow on the ground. Figure 7.4 shows further example calculations for the catching dam at Ryggfonn based on Equation (7.3). The left panel shows the calculated overrun length versus the front velocity for given effective dam heights. The right panel depicts the required dam height if a certain overrun length can be permitted. Taken at face value, this example indicates that the use of dams as protective measures for endangered areas is limited to the end of the run-out zone, or against small avalanches with typically low speeds, *e.g.* against small slides along roads to reduce road

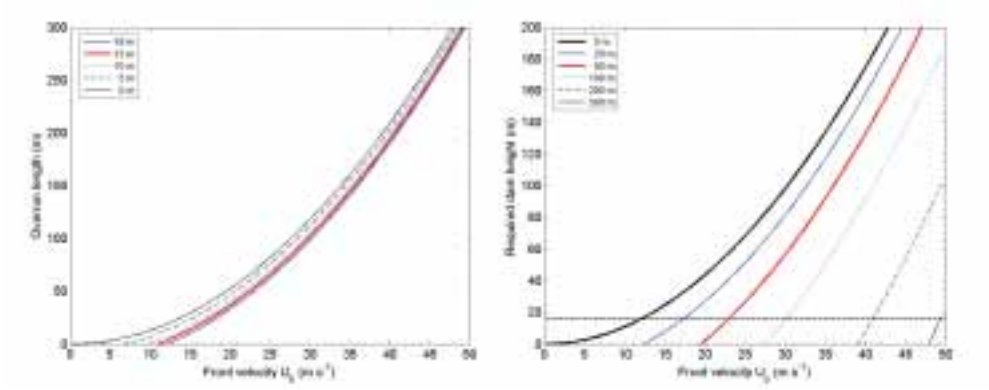

Figure 7.4: Overrun length (left panel) and required dam height given an allowed overrun length (right panel) as functions of front velocity calculated for the catching dam at Ryggfonn. The dashed line in the right panel indicates the height of the dam at Ryggfonn.

clearing work. This conclusion is clearly not consistent with the dam design recommendations described in Section 5, and it is difficult to reconcile it with observations of run-up of natural avalanches on dams and other obstacles that are described in Subsection 5.9. This discrepancy reflects our current lack of understanding of the dynamics of natural snow avalanches that hit obstacles. It indicates considerable uncertainty regarding the effectiveness of avalanche dams, and it casts doubt, particularly, on the effectiveness of catching dams to stop or reduce the run-out of rapid dry-snow avalanches.

7.3 Overrun of avalanches over catching dams, chute experiments

A number of laboratory experiments with granular materials have been performed in recent years in order to investigate the retarding effect of braking mounds and catching dams on avalanches, and to determine the degree to which their run-out is reduced (Hákonardóttir, 2000; Hákonardóttir and others, 2001, 2003d,c; Hákonardóttir, 2004; Faug and others, 2003, 2004, 2008). Here, some results about dissipation of kinetic energy and run-out reduction caused by catching dams are summarised and compared with the Ryggfonn measurements described in the previous subsection. The obstacle heights are comparatively low so that upstream shocks are not formed. The experiments are further described and illustrated in Section 9, and in the references quoted here and in Section 9.

The energy dissipation in an overflowing avalanche is hard to determine directly, due to the technical difficulties associated with measurements of the flow speed. This is particularly true for natural avalanches, but even detailed measurements of the speed of granular materials in chute experiments are non-trivial, particularly measurements of the flow speed downstream of the landing point of the jet that is often formed during the impact with an obstacle (see Figs. 9.1 and 9.2). In most of the chute experiments carried out in the abovementioned studies, the speed reduction was not directly measured. Instead, the effect of the mounds and dams to reduce the run-out distance beyond the location of the obstacles was measured, as regards both the reduction in maximum run-out and the reduction in the run-out corresponding to the centre of mass.

The relative run-out reduction may be crudely interpreted as a relative reduction in the kinetic energy of the granular material, by assuming that the slowing down of the avalanche in the run-out zone is brought about by frictional forces between the bed and the moving material that are approximately proportional to the weight of the material (Coulomb friction). The slowing down of the avalanche in a control experiment without a dam is then described by the energy balance equation

$$\frac{u_b^2}{2} + g\tan(\psi)\, l_{cont} = \mu g\, l_{cont}\ , \tag{7.5}$$

where, as in the previous subsection, u_b is used to denote the avalanche velocity at the entrance to the run-out area of the chute, at which the obstacle will be placed. ψ is the slope of the run-out area. l_{cont} is the horizontal run-out distance of either the tip of the avalanche or the centre of mass beyond the location of the dam in experiments with dams. A similar semi-quantitative interpretation of experiments with a catching dam mounted at the entrance to the run-out area results in the equation

$$\frac{u_b^2}{2} - \lambda g H + g\tan(\psi)\, l_{ovr} = \mu g\, l_{ovr}\ , \tag{7.6}$$

where l_{ovr} is overrun distance, H is the height of the dam, and λ is the ratio between the dissipation of kinetic energy caused by the dam and the potential energy corresponding to the dam height, as described in Section 3 and in the previous subsection about the Ryggfonn measurements. In laboratory experiments at different scales and with different types of granular materials, it is found that the relative run-out reduction, $1 - l_{ovr}/l_{cont}$, is often well described as an approximately linear function increasing with the dam height. Equations (7.5) and (7.6) may be used to express the dissipation of kinetic energy, as described by the parameter λ in Equation (7.6), as

$$\lambda = \frac{1}{2}\frac{u_b^2}{g h_b}\frac{1 - l_{ovr}/l_{cont}}{H/h_b} = \frac{1}{2}\mathrm{Fr}^2\frac{1 - l_{ovr}/l_{cont}}{H/h_b}\ , \tag{7.7}$$

where H/h_b is the dam height relative the upstream flow depth, h_b, and Fr is the Froude number of the flow (neglecting the effect of the small slope of the run-out area on the Froude number). This equation states that the reduction in kinetic energy caused by a dam, relative to the potential energy corresponding to the dam height, may be found from the slope of the line representing the relationship between run-out distance and dam height.

This interpretation of run-out reduction in terms of reduction in kinetic energy is too crude to determine whether it would be more appropriate to use the relative reduction in the maximum run-out, or in the run-out corresponding to the centre of mass. Therefore, we will consider both. The small-scale experiments with catching dams on run-out zones with slopes in the range 10–15° and Froude numbers near 10 described in the studies cited above, may be interpreted as corresponding to λ-values in the range of 6–14 when maximum run-out is considered, and in the range of 10–20 for centre-of-mass run-out. Experiments with dams on run-out zones with slopes in the range 20–30° and Froude numbers in the range 6–10 correspond to maximum run-out λ-values in the range 2–6 and an experiment with a run-out zone slope in this latter range and a Froude number of 3.6 corresponds to a maximum run-out λ-value of 1.2. Faug and others (2008, *cf.* their Fig. 6b) show that λ-values derived from small-scale laboratory experiments are well approximated by a linear function of the square of the Froude number, $\lambda \approx \alpha \mathrm{Fr}^2$ with $\alpha = 0.057$. For Fr in the range 5–10, this relationship

implies λ-values in the range 1.5–6. These λ-values are much greater than indicated by the Ryggfonn measurements described in the previous subsection, which correspond to λ-values approximately equal to 0.5, in particular for experiments on comparatively flat run-out zones with high Froude numbers.

The λ-values derived from small-scale experiments are also much greater than the apparent dissipation of kinetic energy during the impact of natural snow avalanches as derived from run-up marks on man-made dams and natural obstacles described in Section 5. Although the steepness of the upstream dam side differs between the different laboratory experiments described here (normal to the bottom of the chute) and the dam at Ryggfonn (slope of 40°), the difference in the λ-values is much greater than can be accounted for by the difference in steepness.

These discrepancies are hard to explain. They may partly be due to a difference in physical properties between snow and the granular materials used in laboratory experiments (glass beads and sand). It is also possible that the difference in scale between natural avalanches and laboratory experiments leads to a difference in the ability of the material to overflow obstacles. This may perhaps be due to a run-up mechanism that is not important at the laboratory scale and not accounted for in the theoretical analysis described in Section 5. Whatever the reason, the situation that estimates of the dissipation of kinetic energy by dams from different sources differ by more than an order of magnitude is highly unsatisfactory. The design recommendations given in Section 5 take into account *much less dissipation of kinetic energy than is found in laboratory experiments*, but *much greater dissipation than indicated by measurements at Ryggfonn*.

It should be noted that the validity of Equation (7.3) derived from the Ryggfonn overrun measurements must be limited to the lower end of the dam heights shown in the right panel of Figure 7.4. A substantial overrun of the dense core of avalanches travelling with a speed of 35–50 $\mathrm{m\,s^{-1}}$, say, over dams or ridges considerably higher than 100 m, is not consistent with the principle of the conservation of energy, assuming that reasonable physical bounds on the internal friction angle of snow limit longitudinal internal forces in the avalanching mass. This is, however, not much of a consolation regarding the effectiveness of practical avalanche dams that would in most or all cases fall in the lower range of required dam heights shown of Figure 7.4. Conversely, the large dissipation of kinetic energy by dams observed in small-scale laboratory experiments is not likely to apply to natural, full-scale snow avalanches because run-up marks indicate much lower dissipation during impacts with man-made dams and natural obstacles. Thus, it seems likely that dissipation of kinetic energy during the impact of natural snow avalanches with obstacles may in some cases fall between the limits indicated by the Ryggfonn measurements and small-scale laboratory experiments. However, given the current understanding of avalanche flow, it is impossible to specify under which circumstances the dissipation will be greater than indicated by the Ryggfonn measurements, or to quantify the dissipation with reasonable accuracy.

7.4 Hazard zoning below catching dams

Revision of hazard zoning below catching dams is non-trivial considering the uncertainty concerning the effectiveness of such dams, as discussed in the preceding subsection. Reduction of avalanche run-out by dams has sometimes been estimated based on Equation (3.2) for dam design, which is called *Salm's rule of thumb* (Salm and others, 1990; Baillifard, 2007). It is

then assumed that the kinetic energy of an avalanche that overflows or scales a dam is reduced by the potential energy corresponding to the dam height multiplied by the coefficient λ that is traditionally used in the design of catching dams. For λ-values in the range of 1 to 2, as are most often used, this procedure leads to much greater reduction in run-out than indicated by the Ryggfonn measurements, but to much less run-out reduction than indicated by small-scale laboratory experiments with granular materials. This may be expected from the preceding discussion. The outlined procedure for estimating run-out reduction is sometimes used in Switzerland, and has been used in the revision of hazard zoning below recently constructed catching dams in Iceland (using $\lambda = 1.5$ for dams built from loose materials, and $\lambda = 2$ for dams with steep upstream sides). It is clearly based on weak physical arguments and should, therefore, perhaps more appropriately be used to *indicate possible hazard reduction in existing settlements, rather than for justifying expansion of settlements into previously unsettled areas*. The details of how this assumption about the reduced run-out is applied, depend on the hazard zoning methodology. If the zoning is based on a design avalanche with a certain return period, the run-out of this avalanche and therefore the location of the hazard line, will be reduced accordingly. If the hazard zoning is risk-based, the contributions to the risk from avalanches with different run-out need to be computed based on the estimated run-out reduction beyond the location in question.

8 Special considerations for wet-snow avalanches

Ulrik Domaas and Carl B. Harbitz

The flow of wet-snow avalanches differs from the flow of dry-snow avalanches in several ways. Wet snow contains moisture to a varying degree and may have much more internal cohesion than dry snow. Wet-snow avalanches move relatively slowly compared with dry-snow avalanches, but they may have a long tail with a large volume of snow, and they sometimes pile up at obstructions. The avalanches may fill the storage space above dams, and they can spread sideways if they encounter obstructions or lateral changes in path geometry, such as the downstream end of deflecting dams. They can carry large amounts of loose materials and rocks, and may cause both erosion and accumulation at deflecting dams and in flow channels. These special aspects of wet-snow avalanche dynamics can be important in the design of avalanche dams, but they cannot be treated in a quantitative manner, because an adequate theory so far is lacking. In the following, we will discuss subjective considerations based on observations of wet-snow avalanches that may be of importance in the design of dams.

Since wet-snow avalanches move slower than dry-snow avalanches, they tend to follow depressions in the terrain more strongly. Sometimes minor obstructions can cause diversion and splitting of wet avalanches and they may spread out in fingers in the run-out zone, ploughing and making their own levees. The direction of flow is often unpredictable, and if a change in direction is initiated the turning may continue (Fig. 8.1). This can be especially severe at the lower end of deflecting dams, where a part of the area to be protected may be endangered by an avalanche that spreads or turns sideways after passing the dam.

Wet-snow avalanches will pile up to considerable heights in front of dams as at Ryggfonn in 2006 (Fig. 8.2). Avalanches may then continue to pile up for a significant period of time. The avalanche volume may in these cases be the determining factor for the dam dimensions, rather than flow height and velocity.

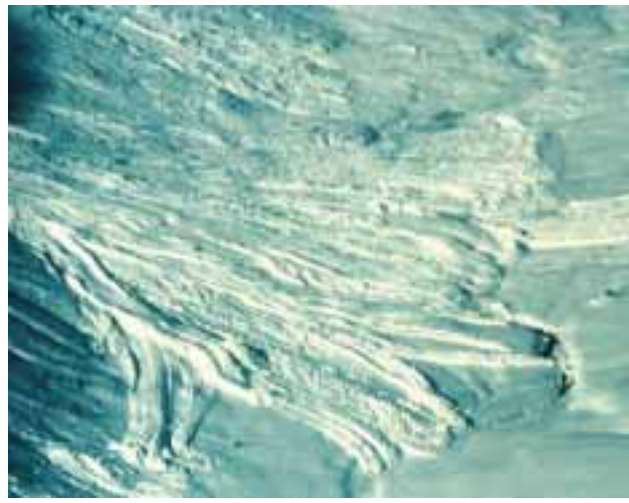

Figure 8.1: A wet-snow avalanche with fingers that spread almost perpendicular to the original flow direction (photo: NGI).

Figure 8.2: A wet-snow avalanche in front of the Ryggfonn catching dam that has piled up to a considerable height and also shows some tendency to divert sideways (photo: NGI).

Figure 8.3: A wet-snow avalanche with a thick deposit in steep terrain showing some lateral spreading (photo: NGI).

Snow on the ground is often not entrained in wet-snow avalanches flowing over gentle terrain. Ploughing and compression of the snow on the ground seem to be the dominant processes.

Wet-snow avalanches will in some cases move as a rigid plug with distinct lateral boundaries, in other cases they may move as a pile of loose balls that can widen laterally (Fig. 8.3).

The friction angle of wet snow may be large. Accumulation of wet avalanche snow has been observed at terrain inclinations above 25°. Glide planes at the bottom of the avalanche and shear planes within the avalanche are commonly observed.

Typical accumulation heights are observed to be around 3–5 m in steep terrain. Two avalanches on top of each other may then need more than 8 m high channel walls or deflecting dams to contain most of the snow (Fig. 8.4). In some cases, several hundred thousand m^3

Figure 8.4: Several wet-snow avalanches may fill up the storage capacity for a deflecting channel even in fairly steep terrain as shown here for deflecting dams at Langageiti (left) and Nautagrovi (right) in western Norway (photos: NGI). The figure from Langageiti shows how a part of an avalanche may turn sideways after the avalanche overtops or flows past the downstream end of a deflecting dam.

of wet snow may accumulate along a deflecting dam. The storage capacity should reflect the expected dimensioning avalanche. If several release areas are draining into the same track, this must also be taken into account.

Large wet-snow avalanches may have deposit depths of 10 m or more in gentle terrain (Fig. 8.5). The storage space above dams may then need to accumulate a lot of avalanching snow and should be designed for at least twice the volume of the maximum avalanche in case the return period of such events is short enough to make multiple events in the same winter likely to occur.

To summarise:

- During mild weather/rain situations, several subsequent wet-snow avalanches from different release areas may drain into the same channel/scar/path. Deposit depths can be very large. Necessary height of catching dams may depend more on the volume of the design avalanche than its velocity.

- The channel along a deflecting dam for wet-snow avalanches should be dimensioned for large volumes. A width of several tens of meters is in most cases necessary to contain the snow masses (*cf.* Fig. 8.4). As for catching dams, the design height of deflecting dams may depend more on possible deposit depths in the channel than on the velocity of the avalanche.

- Wet-snow avalanches may turn sharply when encountering obstacles or changes in path geometry. Spreading or turning of avalanches as they flow past the downstream end of deflecting dams must be carefully considered in the design of such dams.

- Wet-snow avalanches have a capacity to carry large amounts of loose materials and

Figure 8.5: Large amounts of wet snow may pile up in flat areas when the front stops and additional volume from the tail of the avalanche accumulates on top of the snow that has come to rest (photo: NGI).

rocks, and may cause both erosion and accumulation at the deflecting dam and in the channel.

9 Braking mounds

Kristín Martha Hákonardóttir and Tómas Jóhannesson

9.1 Introduction

Braking mounds (or retarding mounds) are widely used for protection against dense, wet-snow avalanches, but they are often thought to have little effect against rapidly moving, dry snow avalanches (see for example Norem, 1994; McClung and Schaerer, 1993). Until recently, the design of such mounds has in most cases been based on the subjective judgement of avalanche experts, as there exist no accepted design guidelines for braking mounds. There are, furthermore, no established methods for estimating the retarding effect of avalanche mounds in a quantitative way. The retarding effect is particularly badly known for dry-snow avalanches.

A number of chute experiments at different scales and with different types of granular materials have recently been performed in order to shed light on the dynamics of avalanche flow over and around braking mounds and catching dams, and to estimate the retarding effect of the mounds (Woods and Hogg, 1998, 1999; Hákonardóttir, 2000; Hákonardóttir and others, 2001, 2003d,b,c; Hákonardóttir, 2004). Some of these experiments were carried out as part of the design of avalanche protective measures for the town of Neskaupstaður in eastern Iceland (Figs. D1 and D2) (Tómasson and others, 1998b,a). A review of available hydro-engineering studies on retarding structures for high speed water flow was also carried out as part of the design (Tómasson and others (1998b); this review is summarised in the Appendix of Jóhannesson and Hákonardóttir (2003)). The experiments were carried out for dry, supercritical, granular flow in order to analyse the retarding effect of mounds against rapid, dry-snow avalanches.

This section summarises the main results of the abovementioned studies based on Jóhannesson and Hákonardóttir (2003). Several general recommendations for the practical design of braking mounds are given with references to technical articles and reports that contain more detailed descriptions of the experimental results on which the recommendations are based.

Due to the very different scales, there remain open questions regarding the applicability of the experimental results to natural snow avalanches. An insignificant braking effect at the scales of the experiments would suggest that this effect would also be small for natural snow avalanches. On the other hand, a result indicating a substantial braking effect does not necessarily apply to natural avalanches due to the different physics and scales of the flows, such as compression of the snow during the impact with the mounds and the effect of air resistance on the flow over the mounds. Nevertheless, the experiments may be used to identify certain types of behaviour, which do not strongly depend on scale or material properties, and which may be exploited in the design of avalanche protective measures. The experiments, thus, provide useful indications for designers of retarding structures for snow avalanches in the absence of data from experiments at larger scales and measurements of natural avalanches.

As described in Section 4, the dimensionless Froude number, Fr, given by Equation (4.1) is commonly used to characterise free-surface fluid flows. The design of the abovementioned chute experiments was based on the conjecture that if the Froude numbers were on the same order of magnitude, dynamic similarity between natural snow avalanches and the smaller-scale experimental avalanches would be maintained (see Hákonardóttir and others (2003b) for a further discussion). The Froude number of the smaller scale experiments in 3, 6 and 9 m long

chutes in Reykjavík, Bristol and Davos was Fr ≈ 10. The Froude number in snow experiments in a 34 m long chute at Weissfluhjoch in Davos was within the range of 3–6, varying with each experimental run, due to differences in snow conditions. Six was the highest Froude number allowed by the experimental setup, and somewhat lower than would have been ideal.

Although there exist no generally accepted guidelines for the design of avalanche mounds, Salm (1987) proposed an estimate for the speed reduction of an avalanche that hits several obstacles, such as buildings, spread out over the run-out area of the avalanche, and assumed to cover a fraction, c, of the cross-sectional area of the path. According to this estimate, the speed of the avalanche is reduced by the ratio $c/2$, assuming that the obstacles are sufficiently sturdy and are not swept away by the avalanche. If, for example, $c = 1/2$, this expression predicts that the speed is reduced by 25%, indicating a substantial effect of the obstructions on the avalanche speed. A similar estimate for the speed reduction of an avalanche hitting several rows of trees was proposed by Voellmy (1955). These estimates are not derived from a conceptual model of the flow around obstacles, and it is not clear whether they may be expected to apply to a rapidly moving dry-snow avalanche.

Braking mounds designed to retard rapidly moving dry-snow avalanches, in most cases, are small compared with the height-scale corresponding to the kinetic energy of the avalanche, $u^2/(2g)$, where u is the speed of the flow and g is the gravitational acceleration. In the absence of dissipation, having ascended the mounds, an avalanche would regain the kinetic energy spent upon descending on the downstream side of the mounds. For braking mounds to be as effective as assumed by Salm and Voellmy, substantial energy dissipation must be brought about by flow deflections and mixing introduced as an avalanche flows over and around mounds. Such an effect may be expected to depend to a high degree on various details of the layout and geometry of braking mounds, making the lack of established guidelines for the design of avalanche mounds particularly acute. One may also note that the volumes of the avalanches will typically be so large that only a small fraction of the snow near the front of the avalanche is needed to fill the space upstream of the mounds, thereby effectively burying them and allowing easy overflow of the bulk of the avalanche. For braking mounds to be effective while the avalanche passes over them, they must not become buried by the avalanche.

Experiments to study the effect of braking mounds on snow avalanches have not been performed until recently. Similar structures have, however, been studied extensively for supercritical, free-surface water flow in dam spillways and bottom outlets where they are used to dissipate the kinetic energy of water before it enters the downstream channel (in this context they are termed baffle blocks and baffle piers). The original experiments are described in Peterka (1984) and US Bureau of Reclamation (1987) and they are summarised in many text books on hydraulic engineering, for example Roberson and others (1997). The energy dissipation induced by baffle piers in dam spillways and bottom outlets is principally a shallow flow phenomenon and does not depend on the frictional properties of the fluid in question. The dense core of rapidly moving snow avalanches is a shallow, gravity-driven flow. Energy dissipation by inelastic granular collisions could play a similar role in avalanche flow around and over dissipating structures, as turbulent dissipation by fluid friction in ordinary fluid flow. These studies complement the braking mound experiments with granular materials in an important way, because the scale of the hydraulic structures is much larger than the scale of the experimental chutes and therefore closer to the scale of natural avalanches. The speed of the water flow in spillways is sometimes more than an order of magnitude higher than the speed of the granular materials in the abovementioned chute experiments with mounds. The results of

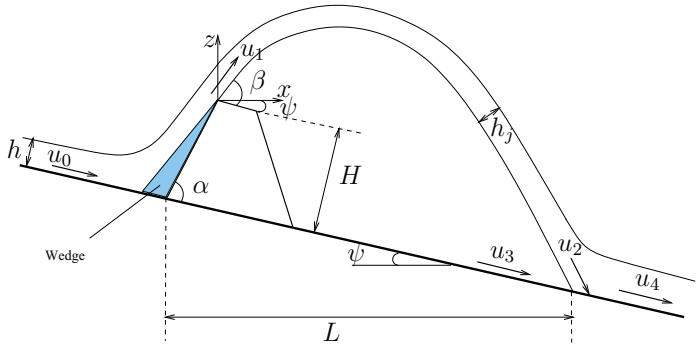

Figure 9.1: A schematic diagram of a jet of length L with upstream flow thickness h and jet thickness h_j. The jet is deflected at an angle β over a mound or a dam of height H positioned in a terrain with inclination ψ. The upstream mound face is inclined at an angle α with respect to the slope. u_0, u_1, u_2, u_3 and u_4 are speed values at different locations along trajectories.

the hydraulic experiments and their implications in the context of snow avalanches, including the importance of the Froude number in both cases, are discussed further by Hákonardóttir and others (2003c).

9.2 Interaction of a supercritical granular avalanche with mounds

The experiments showed that a collision of a supercritical granular avalanche with a row of mounds leads to the formation of a jump or jet, whereby a large fraction of the flow is launched from the top of the mounds and subsequently lands back on the chute (Figs. 9.1 and 9.2). For steep obstacles, particles are initially launched at an angle close to its upstream angle, α. The jet rapidly adjusts to a new angle due to the formation of a wedge behind the upstream face of the mound. This angle is termed the throw angle and is denoted by β. The bulk of the current then passes over the barrier as a coherent, quasi-steady jet (Figs. 9.1 and 9.2). This part of the jet lands farthest away from the mounds.

Energy dissipation takes place during the impact of the avalanche with the mounds and also in the interaction of jets from adjacent mounds. Energy dissipation, furthermore, takes place in the landing of the jets on the chute and the subsequent mixing with material flowing in between the mounds.

The airborne jet that is formed by the collision of the flow with the mounds has important practical consequences for the use of multiple rows of mounds or combinations of rows of mounds and a catching dam. The spacing between the rows must be sufficient so that the material launched from the mounds does not jump over structures farther down the slope.

The trajectory of the jet launched directly over the mounds can be approximated as a projectile motion in two dimensions (Fig. 9.1). Conservation of momentum leads to the equation

$$m\ddot{\mathbf{x}} = \mathbf{F} = m\mathbf{g} - m(f/h_j)\dot{\mathbf{x}}|\dot{\mathbf{x}}| \,, \tag{9.1}$$

where $\mathbf{F}$ is the force exerted on the mass, m, $\mathbf{g}$ is the gravitational acceleration, f is a dimensionless constant representing turbulent drag caused by air resistance, h_j is the thickness of

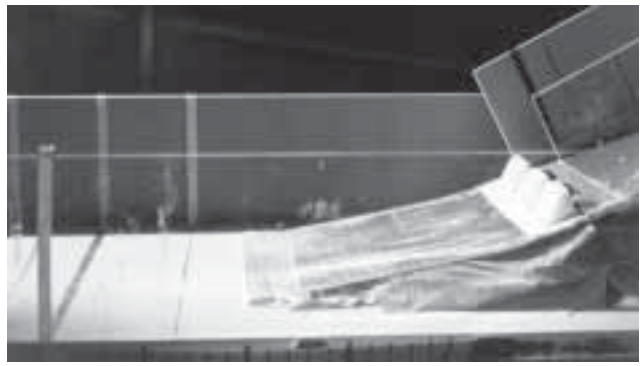

(a)

(b)

Figure 9.2: Photographs of (a) the datum mound configuration and (b) the jet in a quasi-steady state on the 6 m long experimental chute in Bristol (Hákonardóttir and others, 2003c).

the core of the jet, $\mathbf{x} = (x,z)$ is the location of the projectile in horizontal and vertical directions, respectively, with the origin at the top of the mound, and a dot denotes a time derivative. Equation (9.1) can be written as

$$\ddot{x} = -(f/h_j)\dot{x}\sqrt{\dot{x}^2+\dot{z}^2} \tag{9.2}$$

$$\ddot{z} = -g-(f/h_j)\dot{z}\sqrt{\dot{x}^2+\dot{z}^2}\,. \tag{9.3}$$

The initial conditions at $t = 0$ are

$$x = z = 0 \qquad \text{at} \qquad t = 0$$

and

$$\dot{x}(0) = u_1\cos(\beta-\psi) \qquad \text{and} \qquad \dot{z}(0) = u_1\sin(\beta-\psi),$$

where β is the throw angle and ψ is the terrain slope where the mounds are situated. The horizontal length of the jump, L (Fig. 9.1), can be found by solving the two equations given appropriate values of u_1, β and f/h_j. Recommended values for these parameters for natural snow avalanches are discussed below.

Figure 9.3: A photograph of the snow hitting a 60 cm high catching dam in the 34 m long chute at Weissfluhjoch (Hákonardóttir and others, 2003d). A part of the dam broke during this experiment as seen on the photograph.

$\mathbf{u_1}$: The throw speed u_1 may be expressed as

$$u_1 = k\sqrt{u_0^2 - 2gH\cos\psi},$$

where u_0 is the incoming speed, H is the height of the mounds above the snow cover and k is a dimensionless constant representing the energy dissipation involved during the impact of the avalanche with the mounds. The value $k = 1$ corresponds to no energy loss during the impact. The experimental results indicate that k is in the range of 0.5–0.8 for mound and dam heights of 2–3 times the flow depth (Hákonardóttir and others, 2001, Fig. 38), (Hákonardóttir and others, 2003d, Fig. 7), (Hákonardóttir and others, 2003c, Fig. 10), with most of the values falling in the range 0.6–0.7. For natural snow avalanches, it is recommended that the throw length is computed for the three values $k = 0.7$, 0.8 and 0.9 and that the result for $k = 0.8$ be used to calculate the minimum distance between a row of mounds and the next retarding or retaining structures downstream.

β: Figure 9.4 shows theoretical curves for inviscid, irrotational flow of a fluid over an obstacle where gravity effects are neglected Yih (1979). The experimental results indicate that the theory gives an upper bound for the throw angle, β. For mounds with $H/h \approx$ 2–3 and $\alpha = 90°$, the theoretical β should be reduced by 20–25°, for $\alpha = 75°$, β should be reduced by 10–20° and for $\alpha = 60°$, it should be reduced by 0°–10°. It is recommended that the throw angle β be chosen based on these considerations.

$\frac{f}{h_j}$: The turbulent drag on the jet, caused by air resistance, is represented by the dimensionless constant f, and depends on the jet thickness, h_j, and the speed of the airborne flow (Eqs. (9.2) and (9.3)). Air resistance does not affect the flow on the small scale of the granular experiments (including the snow experiments) and the experimental trajectories are

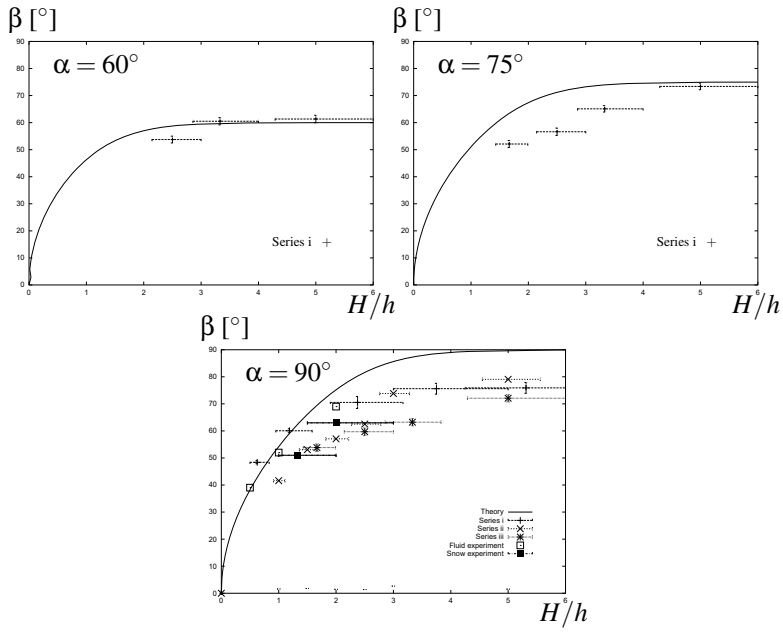

Figure 9.4: The throw angle, β, plotted against the non-dimensional mound height, H/h, for different angles between the upstream faces of the mounds and the slope, α. The points denote experimental results and the solid lines are theoretical predictions. 'Series i, ii and iii' are results from experiments described in Hákonardóttir and others (2003c) using glass particles on 3, 6 and 9 m long chutes. 'Snow experiments' denotes experiments with snow on the 34 m long chute at Weissfluhjoch described in Hákonardóttir and others (2003d), and 'Fluid experiment' denotes an experiment described in Yih (1979).

therefore well reproduced using $f = 0$ in equations (9.2) and (9.3). On the other hand, full-scale experiments with water jets suggest that between 0–30% of the initial kinetic energy of the jet may be lost during the jump (see Hager and Vischer, 1995; Novak and others, 1989; US Bureau of Reclamation, 1987). The dense core of an avalanche is less dense (density in the range of 100–400 kg m^{-3}) than water (density of 1000 kg m^{-3}). Therefore, it is reasonable to assume that an avalanche jet will be affected by air resistance at least to the same extent as a jet of water, leading to a shortening of the jet. By taking $f \approx 0.01$ and $h_j \approx 2$–4 m we obtain $f/h_j = 0.0025$–$0.005\,\mathrm{m}^{-1}$. In order to reduce the kinetic energy of a fluid jet with a speed of 40 m s^{-1} by 30%, as suggested by Novak and others (1989), f/h_j needs to have a value of $f/h_j \approx 0.004\,\mathrm{m}^{-1}$, which fits into the range given above. Here, it is recommended that the value of $f/h_j = 0.004\,\mathrm{m}^{-1}$ is adopted in computations of the throw length.

Given the above recommended values of u_1, β and f/h_j, the ordinary differential equations (9.2) and (9.3) may be solved numerically in order to obtain the throw length for determining the minimum longitudinal spacing of retarding and retaining structures in the design of braking mounds.

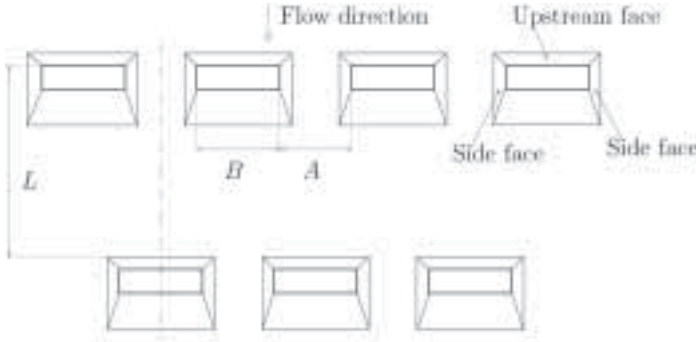

Figure 9.5: Plan view of two staggered rows of braking mounds. The minimum horizontal distance between the two rows, L, is found according to the procedures outlined in § 9.2. Recommendations regarding the geometry and layout of the mounds are given in § 9.3. B is the top breadth of a mound and A is the distance between the tops of two adjacent mounds. A should be similar to or shorter than B, and B should be similar to the height of the mounds, H, above the snow cover.

9.3 Recommendations regarding the geometry and layout of the mounds

The chute experiments with granular materials lead to the following recommendations for the geometry of avalanche braking mounds.

1. The height of the mounds, H, above the snow cover should be 2–3 times the thickness of the dense core of the avalanche. Increasing the height of the mounds beyond this, for a fixed width of the mounds, does not significantly reduce the run-out according to experiments.

2. The upstream face of the mounds should be steep. For the chute experiments with glass beads (ballotini), $\alpha \approx 60^\circ$ was sufficient since a steeper upstream face only marginally improved the energy dissipation. This result may not be appropriate for natural snow avalanches because of the different physical properties of the materials.

3. The aspect ratio of the mounds above snow cover, H/B, should be chosen close to 1.

4. The mounds should be placed close together with steep side faces, so that jets launched sideways from adjacent mounds interact. Many short mounds were found to be more effective than fewer and wider mounds for the same area of the flow path covered by mounds.

If there is sufficient space in the terrain for a second row, it should be staggered with respect to the first row (Fig. 9.5). As discussed in the following subsection, the retarding effect of the second row may be expected to be somewhat less than the effect of the first row, although this is not well constrained by the available experiments (Hákonardóttir and others, 2001).

9.4 Retarding effect

It is important to be able to quantify the reduction in flow velocity provided by braking mounds in addition to defining an optimum layout and geometry of the mounds. An estimate of this retardation cannot be made from full-scale observations of natural events and must therefore be based on the results of chute experiments. There are many technical difficulties associated with direct measurements of the flow speed of granular materials in the chute experiments, in particular for measurements of the speed of the flow downstream of the landing point of the jet, as mentioned in Section 7. In most of the experiments, the speed reduction was not directly measured. Rather, the effect of the mounds for reducing the maximum and centre-of-mass run-out distance was measured.

The most effective single row mound configurations in the 3, 6 and 9 m long chutes with mound heights of 2–3 times the flow thickness were found to shorten the maximum run-out beyond the mounds by about 30% in the experiments with small glass beads (ballotini), and by a similar amount for sand in the 9 m long chute (Hákonardóttir and others, 2001). The reduction in the run-out corresponding to the centre of mass was greater, *i.e.* between 40–50%. The reduction in maximum run-out for two staggered rows of mounds for experiments in the 3 and 9 m long chutes was found to be in the approximate range of 40–50% and the reduction in the run-out corresponding to the centre of mass was greater than 50%.

The relative run-out reduction may be crudely interpreted as a relative reduction in the kinetic energy of the granular material by assuming that the slowing down of the avalanche in the run-out zone is brought about by frictional forces between the bed and the moving material that are approximately proportional to the weight of the material (Coulomb friction). A relative run-out reduction of about 30% (the maximum run-out) to 40–50% (the centre of mass run-out) then corresponds to a reduction in the speed of an avalanche by about 15–30% by one row of mounds. For two mound rows, a run-out reduction by 40–50% or more corresponds to a speed reduction of 20–30% or more. This interpretation of run-out reduction in terms of speed reduction is so crude that it is not possible to say whether it is more appropriate to use the relative reduction in the maximum run-out or in the run-out corresponding to the centre of mass.

In experiments with snow in the 34 m long chute at Weissfluhjoch (Hákonardóttir and others, 2003d), the avalanche speed just upstream of the mounds (u_0), as well as the speed after the landing of the jet (u_4) (*cf.* Fig. 9.1) was measured. The velocity of the control avalanche in the absence of mounds at the landing location of the jet (u_{cont}) could also be estimated. There is considerable uncertainty in the measurements of both the velocity and the flow thickness in the Weissfluhjoch experiments, but the results indicate a ratio $u_4/u_{\mathrm{cont}} \approx 0.8$ for mounds that are about 1.3 times higher than the flow thickness.

Despite experimental uncertainties, available results indicate that braking mounds have a substantial retarding effect on supercritical granular flows. Furthermore, the retarding effect does not seem to vary much with the scale of the chutes over the range of scales (lengths of the chutes in the range 3–34 m), velocities (flow speeds upstream of the obstacles in the range 2.6–7.5 m s^{-1}), and experimental materials covered by the experiments. For one row of mounds designed according to the recommendations given above, it is recommended that the relative speed reduction is estimated as 20%. It is not possible to specify in detail how the energy dissipation caused by the mounds is divided between the initial impact, the interaction between adjacent jets, air resistance and energy lost in the landing of the jet, and mixing with

material flowing between the mounds. This will depend, among other things, on the slope and shape of the terrain in which the mounds are located. For simplicity, it is recommended that the assumed speed reduction is applied at the location of the upper faces of the mounds in model simulatations of avalanche flow in the absence of mounds. This assumption should only be applied for mounds located in the run-out zone of avalanches. Higher up the avalanche path, where the terrain is steeper, it will not provide reasonable results. However, this is not an important restriction since mounds are not likely to be located outside the run-out zone.

It appears from the experimental results that a second row of mounds has less relative effect on the flow velocity than the initial row. This is also indicated by the hydraulic experiments with baffle piers in dam spillways and bottom outlets (Peterka, 1984). Here, it is recommended that a second row of mounds is assumed to reduce avalanche speeds by 10%, in addition to the 20% reduction provided by the first row.

It needs to be stressed that the above recommendations are based on an incomplete understanding of the complex dynamics of granular avalanches that hit obstructions. Nevertheless, we believe that the chute experiments and the above recommendations derived from them, provide useful indications for designers of retarding structures for snow avalanches, in the absence of data from experiments at larger scales and measurements of natural avalanches.

10 The effect of dams on powder-snow avalanches

Florence Naaim-Bouvet, Mohamed Naaim, Thierry Faug and Dieter Issler

Both deflecting and catching dams are usually built with the goal of preventing the dense part of avalanches from entering into vulnerable territory. Dry-snow avalanches of considerable size often form an accompanying suspension layer (the "powder-snow cloud", see Figs. 4.1 and 10.1) that may have a long run-out distance and considerable destructive power. It is therefore of interest in the dam design process and in hazard zoning after the construction of a dam to estimate the effect of a dam on powder-snow avalanches (PSAs), and, in particular, to estimate the effect of a dam on the suspension layer accompanying dense-flow avalanches.

There are virtually no observations of the interaction of PSAs with man-made dams available; some inferences can be drawn, however, from the behaviour of PSAs on natural counterslopes. The main source of our present understanding are laboratory experiments since the 1990s and numerical simulations carried out in the past ten years. The main findings will be summarised in Subsection 10.2, and tentative design recommendations formulated in Subsection 10.3.

It is important to note that there are many observational and experimental findings suggesting the existence of an intermediate flow regime between dense flow and suspension flow. This so-called fluidised flow is sometimes implicitly accounted for as part of the dense flow, sometimes as part of the PSA. Considerable confusion seems to result from this fuzziness of the traditional notions. As will be discussed more precisely below, the full-scale dam at the test site Ryggfonn may appear much less efficient than expected from laboratory granular-flow experiments (see Section 7) because fluidised flow often occurred in Ryggfonn without being explicitly accounted for, while granular-flow experiments at the laboratory scale do not attain this regime. For this reason, a brief discussion (Subsection 10.1) of the present knowledge of the formation and physical properties of PSAs sets the stage for the discussion of dam-related issues.

Figure 10.1: A powder-snow avalanche running over flat terrain (photo: Pierre Beghin / Cemagref).

10.1 Properties of powder-snow avalanches

A brief characterisation of the main flow regimes of snow avalanches was given in Section 4. So far, only indirect estimates of the density of snow avalanches can be made, based on theoretical considerations of the mechanics of granular flow. However, it is hoped that direct measurements with capacitance sensors will soon give more reliable information about this important quantity. Density estimates influence the assessment of the effect of dams on PSAs in two ways: First, the pressure exerted by a PSA is directly proportional to the density, which seems to vary by an order of magnitude. Second, the run-up height may substantially exceed the simple estimate based on kinetic energy as given by Equation (3.2), for low-density PSAs.

The latter assertion can be demonstrated in the following way: Assume that the kinetic energy of the PSA per unit volume immediately after the impact on the obstacle is given by $T_i = \rho u_i^2/(2\lambda_{\mathrm{PSA}})$, where ρ is the density, u_i is the speed immediately before impact, and $1/\lambda_{\mathrm{PSA}}$ is the fraction of kinetic energy of the PSA remaining after the impact. Note that λ_{PSA} may differ substantially from the λ-parameter used in Equations (3.2) and (3.3) to calculate the run-up of the dense part of avalanches on dams. During an ascent by of height $h_{u,\mathrm{PSA}}$, the kinetic energy decreases by the increase in potential energy, $\Delta T = -\Delta V = -(\rho - \rho_a) g h_{u,\mathrm{PSA}}$, with air density $\rho_a \approx 1$–$1.3\,\mathrm{kg\,m^{-3}}$ depending on altitude and temperature. Omitting the weak friction at the underlying snow surface, the maximum run-up height thus becomes

$$h_{u,\mathrm{PSA}} = \frac{u_i^2}{2g\lambda_{\mathrm{PSA}}} \cdot \frac{\rho}{\rho - \rho_a}. \tag{10.1}$$

For dilute PSAs, the extra factor $\rho/(\rho - \rho_a)$ is substantially larger than 1. Air entrainment, which is the main mechanism that reduces the speed of PSAs flowing over flat terrain, does not directly reduce the run-up height because it merely distributes the kinetic energy over a larger mass, the entrained air being neutrally buoyant. However, the pressure significantly diminishes due to entrainment because both the density and velocity decrease.

The vertical structure of the head of fully developed PSAs implies that the speed u_i used in (10.1) is different from the front speed. Laboratory measurements with ultrasonic sensors (Keller, 1996; Naaim-Bouvet and others, 2002) showed that bed-parallel internal velocities near the bed typically reach 1.5–1.8 times the front speed, u_f, and vertical velocities may be up to 0.6–0.9 times the front speed. As a rule of thumb, one may assume that $u_i^2 \approx 1.5 u_f^2$.

Observations on large PSAs corroborate these simple considerations. The run-up height of the PSA part in the 1999-02-25 avalanche at the Swiss test site Vallée de la Sionne exceeded 250 m, with an estimated front speed of $50\,\mathrm{m\,s^{-1}}$ at the beginning of the run-up. In the 1997 Brenva avalanche (Courmayeur, Italy), the front velocity was estimated at $70\,\mathrm{m\,s^{-1}}$, and the PSA cleared an approximately 500 m high mountain shoulder. The simple conclusion is that man-made dams are unable to stop large PSAs. The question is, to which degree can they reduce the impact pressure downstream of the dam?

Tentative, but potentially important inferences may be drawn if one compares videos of the front of dry-snow avalanches developing a suspension layer to FMCW radar measurements at Vallée de la Sionne (Gauer and Issler, 2004), pressure measurements at Ryggfonn (Gauer and others, 2007) and Vallée de la Sionne (Schaer and Issler, 2001), and observations of avalanche deposits (Issler and others, 1996), as well as laboratory experiments on the formation of turbidity currents (Mohrig and Marr, 2003). All these observations are compatible with, and strongly suggest, that the suspension layer is largely created by the fluidised layer

and remains coupled to it essentially until the latter comes to a stop. The front speed of the avalanche corresponds to the speed of the fluidised layer while the dense part may be much slower (sometimes 50–60% of the front speed). In contrast, laboratory experiments with granular materials, on which much of the new recommendations of the preceding sections is based, did not attain the fluidised flow regime. One should thus consider that they in the first place model the behaviour of the dense-flow regime in dry-snow avalanches.

It may thus be conjectured that the surprisingly low effectiveness of the Ryggfonn dam (and presumably all other catching dams as well) in stopping dry-snow avalanches might be due mainly to the occurrence of fluidised flow. In a number of cases, the dam retained a large fraction of the avalanche mass even though it was overrun by a large distance. The deposit profiles are compatible with the notion that the dense part was stopped by the dam while a large portion of the fluidised part overflowed it. Besides its much higher velocity (corresponding to a run-up height three to four times larger than for the dense part, according to Equation (3.2), the fluidised regime may have additional properties that reduce the energy loss at impact on the dam and may allow it to overflow obstacles more easily. If future research corroborates this interpretation, the shock-theory based design principles may be applied with greater confidence (and possibly with reduced speed) for the dense part of dry-snow avalanches while it must be expected that the fluidised part of large avalanches will often overrun the dams. However, the fluidised part would exert smaller pressures downstream of the dam than the dense part would have without the dam, and deposit only a modest fraction of the avalanche mass in the area that is to be protected.

10.2 Results of laboratory experiments and numerical simulations on the interaction of PSAs with obstacles

Laboratory experiments studying the impact of the suspension layer on dams were carried out with various measurement techniques at Cemagref (Beghin and Closet, 1990; Augé and others, 1995; Naaim-Bouvet and others, 2002, 2003, 2004; Primus and others, 2004) and with arrays of ultrasonic sensors at ETH Zürich by Keller and Issler (1996). Naaim-Bouvet and others (2003) and Sampl and others (2004) numerically simulated non-Boussinesq situations that are impossible to reproduce in their experimental approach, and developed empirical improvements of depth-averaged flow models to account for the extra mass gain and momentum loss during the passage over an obstacle. Strictly speaking, the cited laboratory experiments have in common that they apply to PSAs in the so-called Boussinesq regime, in which $\rho - \rho_a \ll \rho_a$. It appears likely that PSAs that have separated from the dense and fluidised layers and do not entrain large quantities of snow, are in the Boussinesq regime. However, these conditions are not met during impact with a retaining or deflecting dam. The abovementioned laboratory experiments thus only apply if the suspension layer is still relatively dilute at the dam location, and detaches from the fluidised layer upon impact.

Front behaviour. In experiments with the upstream dam front perpendicular to the ground and the dam height comparable to the flow height, the front of the PSA was observed to shoot vertically up before "jumping" over the dam. The laboratory flows and numerical simulations (Fig. 10.2) strikingly resemble observations and interpretation of measurements at Ryggfonn as described in Section 11 (see Figs. 11.1 and 11.13), even though the Ryggfonn dam deflects

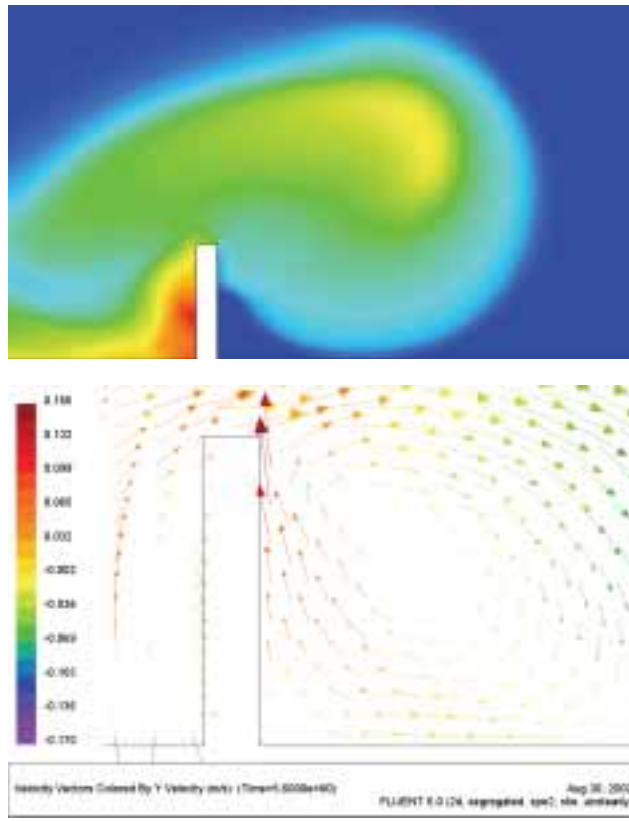

Figure 10.2: Numerical simulation of the impact of a PSA on a vertical wall. The wall height is 0.6 times the flow height before the impact, the density is 1.2 times ambient density, and the Froude number is 0.6. The colours in the upper figure indicate the density distribution (1000 kg m^{-3} is blue and 1200 kg m^{-3} is red). The upper figure is from Naaim-Bouvet and others (2003) and the lower one from Pain (2002).

the flow by less than 60°. The dimensionless jump length diminishes with increasing dam height, see Figure 10.3, and the front velocity of the PSA near the dam is substantially reduced by the impact, see Figure 10.4. In the laboratory experiments using gravity currents, the jump length was found to be essentially independent of the incident velocity. However, numerical simulations with a density ratio of 10 (Naaim-Bouvet and others, 2004), far outside the Boussinesq regime, found the jump length to grow with increasing approach velocity. The effects of buoyancy and incorporation of ambient fluid are stronger in the Boussinesq regime than in the non-Boussinesq regime, and they are negligible in dense granular flows in air. A recirculation zone forms downstream of the dam within the distance corresponding to the jump, with high turbulence and the near-ground flow velocity directed upstream. In real PSAs, considerable deposition of snow is expected to occur in this area. In practice, such conditions may occur in avalanche paths where the dam must be placed near the beginning of the run-out zone and the suspension layer has not fully matured yet, exhibiting a flat "forehead" and a flow height of 10–20 m.

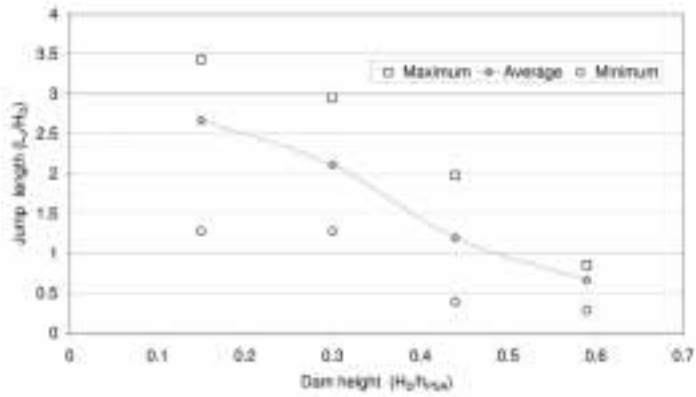

Figure 10.3: Dimensionless jump length of a powder-snow avalanche overflowing a dam. The jump length is given in units of the dam height. (2D Cemagref experiments.)

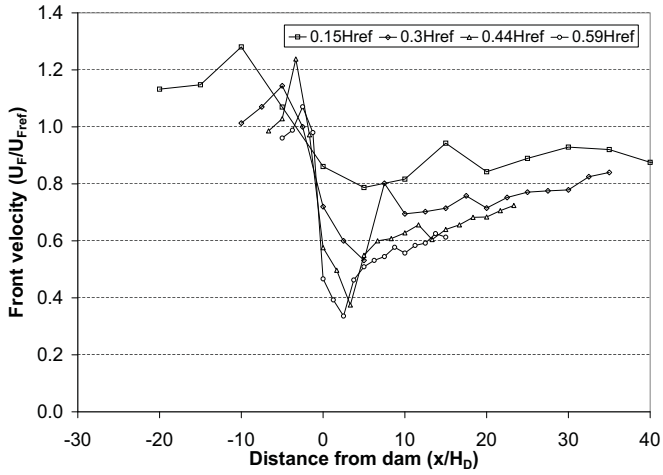

Figure 10.4: Relative reduction in front velocity of a powder-snow avalanche overflowing a dam. (2D Cemagref experiments.)

Velocity reduction due to a dam. The velocity measurements in the laboratory experiments yielded the following main results:

1. The maximum internal velocities parallel to the slope (near the ground in the undisturbed flow) were approximately 1.5–1.8 times the front speed without a dam; the maximum velocities perpendicular to the ground were approximately equal to the front speed.

2. In the presence of a dam, the peak velocity parallel to the slope increases locally in the upper part of the cloud by up to 20% as the PSA flows over the obstacle whereas the mean velocity (averaged over the head) tends to diminish.

3. Downstream of the dam after reattachment of the flow, the velocity reduction relative to the undisturbed flow was small (Cemagref experiments) or negligible (ETH experiments) for dam heights of approx. 0.15 times the flow height just before impact.

4. For a dam height of approx. 0.3 times the flow height, the velocity reduction was 15–20% in all experiments.

5. For a dam height of approx. 0.4 times the flow height, the Cemagref experiments showed a velocity reduction of 20–25%, while the ETH experiments indicated approx. 40%—a value attained by the Cemagref experiments only with dams of height 0.6 times flow height.

6. The dams are significantly more effective in an open slope configuration (3D) than in a laterally confined geometry (2D).

7. The obstacle leads to a reduction in the vertical velocity downstream of the vortex zone but just above the dam (see Fig. 10.2), the vertical velocity is approximately 2–3 times the vertical velocity without the dam for dam heights in the range 0.2–0.8 times the flow height.

8. In the vortex zone downstream of the dam (see Fig. 10.2), negative horizontal velocities appear near the ground. This effect becomes more pronounced with increasing dam height. The negative horizontal velocity peak decreases with distance from the dam.

In view of as yet poorly understood differences between the results from different experiments, we recommend to adopt the more conservative results where the experiments do not fully agree.

Density and turbulence. In the ETH experiments, particle concentration could be measured—albeit with large uncertainties—at one location approximately two flow heights downstream of the dam. The results depend strongly on the dam height, with a marked increase of maximum concentration at the lowest dam height. These results are far from being understood. We will assume here that the density is not strongly affected by a dam.

The same experiments were also analysed with respect to the fluctuations in the velocity and concentration values. The velocity fluctuations were found to be largely unaffected by low dams (0.15 times flow height) and to increase by 20 and 50% for dam heights of approximately 0.3 and 0.4 times flow height, respectively. This means that the obstacle increases turbulence significantly if it is high enough, and peak pressures in turbulent eddies are much higher than the mean pressure.

The effect of different dam orientations and shapes. The experiments by Beghin and Closet (1990) and Keller and Issler (1996) yielded compatible results concerning the effect of deflecting dams. The ETH experiments showed that many results depend sensitively on the front shape and flow density. Nevertheless, the main findings were that the effectiveness is similar to that of a retaining dam if the deflection angle is 60°, and somewhat reduced if it is 30°. The pressure reduction behind a deflection dam with deflection angle of 30° is ca. half the reduction behind a retaining dam of the same height.

The ETH experiments compared traditional dams with an upstream slope angle of 45° to walls perpendicular to the ground. The velocity reduction effect depended on the flow density, but the overall result was that a wall with a height of 0.27 times the flow height, on average, had the same effect as a dam with a height of 0.4 times the flow height. The Cemagref experiments (Caccamo, 2008) showed a smaller difference between a wall and a dam with lower upstream slope angles (45° and 60°). In particular, the difference was found to be negligible far away from the dam.

In addition, the effect of vertical panels on the upstream face of the wall was studied. It was expected that they would reduce turbulence and be particularly effective for deflecting dams. However, no significant and consistent effects could be observed.

Effect of retarding mounds. A series of experiments has been carried out at Cemagref in order to study the effect of retarding mounds on PSAs (Primus and others, 2004). The experiments showed that the retarding effect of a row of mounds results from the deviation of the flow over and around the mounds. A part of the flow jumps over the obstacles, forms jets and lands back on the ground, and another part is channelled between the mounds, leading to a local acceleration and spreading downstream of the mounds. Kinetic energy is dissipated during the impact with the mounds, in mixing of jets from adjacent mounds, in the airborne jets and during the impact and mixing at the landing.

Retarding mounds can be characterised by their shape (width and height), the gap between adjacent mounds, the number of rows and the distance between rows. The potential number of combinations is infinite but a few representative configurations have been tested: the proportion of the cross-sectional area that is blocked by the mounds was equal to 0.72 and the ratio between the dam height and the PSA flow height was equal to 0.44. In the tested configurations, the variation in width and spacing between mounds had no effect on the decrease in front velocity. Regarding the maximum internal horizontal velocities, it was shown to be more efficient to build up a row of wide mounds with large spacing rather than narrow mounds that are closer together. A second row of mounds increases the retarding effect, but two rows of mounds are less efficient than a single catching dam of the same height.

10.3 Tentative recommendations for assessing the impact of powder-snow avalanches below dams

With regard to the suspension layer (the pure PSA), the results from the laboratory experiments are expected to hold in Nature as well. The main recommendations that can be based on the laboratory experiments and modelling studies described above, can be summarised as follows:

1. With realistic dam heights, it is not possible to completely contain or deflect the suspension layer. Nevertheless, PSA pressure can be significantly reduced by appropriately designed and dimensioned dams. However, such pressure reduction is only relevant for hazard zoning if requirements for avalanche safety are formulated in terms of acceptable pressures and event frequencies (or risk), rather than demanding complete absence of avalanche effects for some limit event frequency.

2. An evaluation of PSA impact pressure below a dam has to start by defining a reference PSA for a given scenario. The flow height at the dam location needs to be determined

because effects depend on the ratio of dam versus flow height. Pressure reduction factors at downstream locations may then be determined relative to the pressure distribution of the reference PSA.

3. If a dam is located where the PSA is not fully developed yet, the flow height is often around 20 m or less. Dams of realistic heights (15–25 m) have a strong effect on the velocity of the PSA. For such cases, laboratory experiments indicate pressure reductions of 50–75% below the dam.

4. The effect of the dam on the PSA diminishes sharply if the dam height is reduced to less than ca. 0.4 times the local flow height. At 0.2 times the flow height, the effect must be assumed to be negligible.

5. The laboratory experiments do not indicate high impact pressures at ground level in the recirculation zone with intensified turbulence immediately downstream of the dam while an increase in flow velocities is observed at higher levels in the powder cloud. It is, nevertheless, recommended that the reduction in impact pressures in the wake of the dam that is described in the preceding four items is not applied within a distance of $\sim$2–3 dam heights downstream of the crown of the dam.

6. Deflecting dams are more effective in deviating the PSA if they are positioned at 45–60° to the flow rather than at only 30°, in contrast to the design principles with regard to dense-flow avalanches. The velocity reduction in the PSA part overflowing the dam is then similar as for a retaining dam.

7. Vertical walls may have a stronger effect on PSAs than conventional earth dams of the same height. To obtain the same effect, some experiments indicate that a dam with side slopes corresponding to loose materials must be approximately 50% higher than a corresponding wall with an upstream face normal to the terrain. Other experiments indicate a smaller effect, particularly far away from the dam. It is recommended that the above numbers for PSA impact pressure reductions are applied irrespective of the shape of the dam.

After surpassing the dam, the powder cloud will continue to propagate downstream and typically slow down on level terrain, mainly due to entrainment of ambient air. On steep slopes, the PSA may, however, regain some of the kinetic energy lost during the impact with the dam. In case of comparatively level terrain downstream of the dam, the slowing down and reduction in density due to entrainment of ambient air will lead to a reduction in impact pressure with distance from the dam that may be relevant for hazard zoning below the dam. No general rules for the pressure decrease with distance from the dam can be given, but a dedicated study, usually including numerical simulations, will be needed in each case.

11 Loads on walls

Peter Gauer and Tómas Jóhannesson

Traditional avalanche dams built from loose materials are strong and stable against relevant loads, including dynamic loads from impacting avalanches, if the dams are properly designed according to the geotechnical principles summarised in Section 15. On the other hand, dynamic loads from avalanches need to be explicitly taken into account in the design of some dam structures in the run-out zones of avalanches, such as concrete walls and retarding mounds with steep upper sides. This section presents design recommendations for such loads. In addition to being useful for the design of dams and mounds, the recommendations are also of relevance to other structures such as buildings located in avalanche-prone terrain, which are otherwise not the subject of these guidelines.

11.1 Impact forces on a wall-like vertical obstacle

We first consider the impact of an incompressible fluid of width, W_a, onto a wall of width, W_{wall}, perpendicular to the flow (see Fig. 11.2). It is assumed that the wall is sufficiently wide so that a major part of the avalanche does not flow around it. This is a slight variation of the well known problem of a free jet impinging on a wall in hydraulics. Applying the momentum equation in integral form to the control volume, V, including a small portion of the fluid in contact with the wall, one obtains the impact force normal to the wall

Figure 11.1: An avalanche impinging upon the catching dam at the NGI test site Ryggfonn. There is an obvious increase in depth as the avalanche hits the dam. (Photo: NGI.)

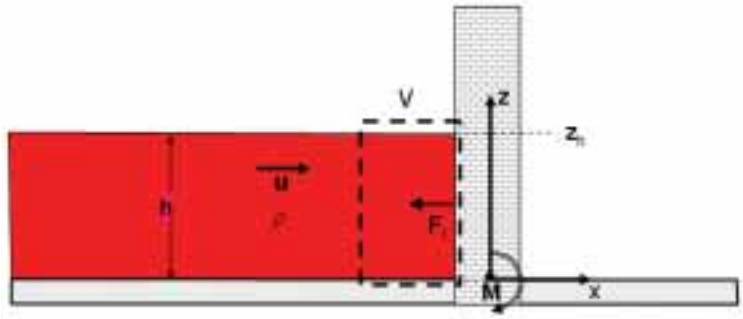

Figure 11.2: A schematic illustration of the impact of an incompressible fluid onto a wall.

$$F_{Ix} = \int_{\mathcal{A}} (\rho u_x (\mathbf{u}\cdot\mathbf{n}) + \rho g z)\, dA = \left[\rho h \alpha \overline{u}_x^2 + \rho g \frac{h^2}{2}\right] b\,. \tag{11.1}$$

Here, a hydrostatic pressure distribution is assumed within the flow. $\mathbf{n}$ is a unit vector perpendicular to the wall surface. The contact area, $\mathcal{A}$, is equal to bh, where b is the smaller of the widths of either the avalanche or the wall, *i.e.*, $b = \min(W_a, W_{wall})$. $\overline{u}_x$ is depth-averaged velocity perpendicular to the wall, and the factor $\alpha \approx 1$ accounts for a non-uniform velocity profile.

Furthermore, if one disregards the hydrostatic component on the right hand side of (11.1), which may be justified for $\mathrm{Fr} = u_x/\sqrt{gh} \gtrsim 2.5$, one obtains

$$\frac{F_{Ix}}{\mathcal{A}} \approx \rho \overline{u}_x^2\,. \tag{11.2}$$

This is a widely used expression for the impact pressure on large obstacles (*e.g.* Gruber and others, 1999b, see also Appendix F.1). However, the derivation is an oversimplification of the problem. Equation (11.1) holds true, *e.g.*, in a steady case where the flow is stopped or deflected at an angle of 90°, but not during the first milliseconds of a vigorous impact. Schaerer and Salway (1980), for example, observed a short pressure peak, which was several times a base pressure (of magnitude approximately given by half the impact pressure expressed by Equation (11.2)) about which the pressure fluctuated after the initial peak (*cf.* Fig. 11.3).

Detailed investigations of short-lived peaks and fluctuations of impact forces on structures on a millisecond time-scale are hard to carry out due to oscillations of the structures themselves and the measurement devices that are induced by the applied loading. New measurement techniques based on inverse analysis (Berthet-Rambaud and others, 2008) make it possible to account for this effect, which may affect some of the impact pressure measurements that are described in the available scientific literature.

Initial peak pressure

Let us consider a flow in a confined setting first (*cf.* Fig. 11.4). As soon as the flow hits the wall, the fluid next to the wall is stopped abruptly, and a pressure wave travels upstream with a celerity C_p, causing the fluid to decelerate. Within a short time interval $\Delta t = t_i - t_0$, a fluid

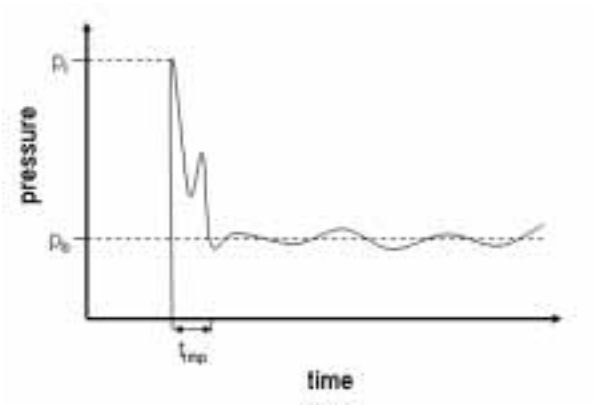

Figure 11.3: A schematic diagram of impact pressure on a vertical obstacle in the dense flow part of a dry-snow avalanche as a function of time, as determined by Schaerer and Salway (1980).

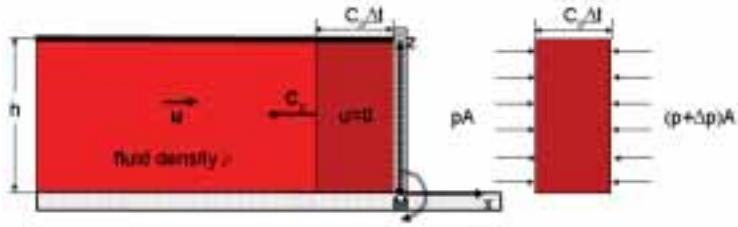

Figure 11.4: Definition sketch for the analysis of the so-called water hammer. In a confined setting, also the upper boundary is given by a fixed wall.

element of mass $m = \rho C_p \Delta t \mathcal{A}$ is stopped. Applying the principle of linear impulse to this fluid element yields

$$-\rho C_p \Delta t \mathcal{A} u_x = \int_{t_0}^{t_i} R\,dt \;, \tag{11.3}$$

where $\int R\,dt$ is the impulse of the resultant force, which is given by

$$R = [p\mathcal{A} - (p+\Delta p)\mathcal{A}] \;. \tag{11.4}$$

Combining (11.3) and (11.4), we get

$$\Delta p = \rho C_p u_x \;. \tag{11.5}$$

In this case, the impact pressure is linear in the velocity perpendicular to the wall. In an elastic medium the celerity of the pressure (sonic) wave is given by

$$C_p = \sqrt{\frac{E_b}{\rho}} \;, \tag{11.6}$$

where E_b is the bulk elastic modulus of the fluid. For water, C_p is about $1440\,\mathrm{m\,s^{-1}}$; for air, C_p equals $330\,\mathrm{m\,s^{-1}}$. In multi-phase flows, like an avalanche, C_p depends on the particle con-

centration. For a snow avalanche, it might be as low as approximately $30\,\mathrm{m\,s^{-1}}$ (see below). The so-called water hammer as described above is a well known problem in hydraulics (*cf.* Franzini and Finnimore, 1997, Ch. 12.6). It is encountered in hydroelectric plants, during a sudden closing of a pipeline. In this case, it is observed that the duration of the pressure peak depends on the length of the pipe and the celerity. In contrast to the confined setting used in the description above, in the case of an avalanche hitting a wall-like obstacle, the flow is usually only partly confined by the ground surface and the neighbouring flow. At the upper boundary, atmospheric pressure is maintained, allowing the flow to spread out, which leads to a reduction of the excess pressure throughout the flow. Experiments on water waves (Cooker and Peregrine, 1995) indicate a non-uniform pressure profile with increasing pressure with increasing distance from the free surface. This type of distribution was also observed for the distribution of maximum impact pressures in full-scale avalanche experiments by Kotlyakov and others (1977). Furthermore, it might also be reasonable to assume that the duration of the peak pressure is on the order of $O(h/C_p)$, *i.e.*, the time needed by the pressure wave to reach the free surface. In the case of an avalanche, however, the wave propagation might not be fully elastic. It might spread as a plastic wave with a lower propagation speed, or as a shock wave with increasing propagation speed. A transition from elastic to plastic wave propagation is accompanied by a reduction of the maximum peak pressure. On the other hand, the duration of the pressure peak increases, which may have to be accounted for in the design of structures.

Experiments by Bachmann (1987) with snow blocks, for $0.5 < \mathrm{Fr}_1 < 3$, indicate that the ratio of the peak pressure to the pressure corresponding to the density and flow velocity in the undisturbed flow is given by $p_{peak}/(\rho_1 {u_1}^2) \approx 3$. Similar values for the pressure ratio were observed by Schaerer and Salway (1980) in their measurements on full-scale avalanches at Rogers Pass. They determined a ratio of 3.3 for small sized load cells (645 mm^2) and of 2.4 for large ones (6450 mm^2). Fr_1 ranged between 6.2 and 8.5. They also noted that their values are in agreement with other reported values, which range from 2 to 5. For example, the reported values by Kotlyakov and others (1977) correspond to a ratio of about 4.8.

Calculations by Kulibaba and Eglit (2008) and Eglit and others (2007) suggest that the ratio $p_{peak}/(\rho_1 u_1^2)$ is a function of the Mach number, $M_1 = u_1/C_{p1}$, where C_{p1} is the speed of sound within the flowing avalanche. The ratio is also weakly dependent on the flow height. Figure 11.5 shows a re-plot of their results, which implies that the pressure ratio decreases with increasing Mach number. The speed of sound, C_{p1}, is a function of the solid concentration in the mixture of air and snow forming the avalanche. It depends further on a scale for the particle diameter, and on the density and other physical properties of the particles (*cf.* Fan and Zhu, 2005, Ch. 6). Figure 11.6 shows the expected range for the speed of sound within a snow avalanche as a function of the bulk density. No direct measurements of the speed of sound in snow avalanches are currently available.

The calculations by Kulibaba and Eglit (2008) and Eglit and others (2007) suggest that the ratio $p_{peak}/(\rho_1 u_1^2)$ is a function of u_1, h_1, and ρ_1. With increasing u_1, the ratio decreases; with increasing h_1 the ratio increases; and, in general, as ρ_1 increases, the celerity decreases causing the Mach number to increase and the pressure ratio tends to decrease.

Loading after the initial peak

On longer time-scales than the duration of the pressure peak, an avalanche will start to spread out sideways and splash up if it suddenly meets a wide obstacle such as a wall and is thus

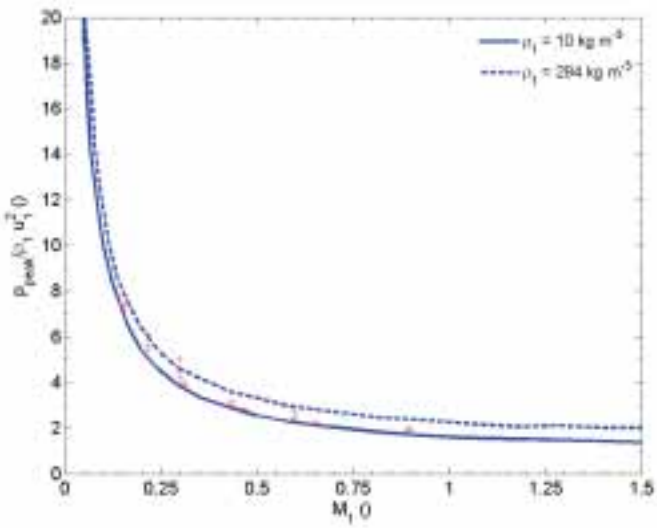

Figure 11.5: The pressure ratio, $p_{peak}/(\rho_1 u_1^2)$, as a function of the Mach number of the flow. Solid line: high density avalanche; dashed line: low density avalanche; after Eglit and others (2007). Red crosses denote values given in Kulibaba and Eglit (2008).

prevented from moving ahead. Simultaneously, the mixture of snow and air close to the wall will be compressed and stopped. This leads to a piling up in front of the wall and a propagation of a wave, which travels upstream through the incoming avalanche at a speed **w** (Fig. 11.7). The wave front is a non-material singularity as avalanche snow passes through it. It marks the boundary between the stopped deposit (or deflected avalanche flow) and the moving avalanche farther upstream. The conservation equations of mass and momentum lead to the following jump conditions across this discontinuity.

$$\int_\Sigma [\![\rho(\mathbf{u}-\mathbf{w})\cdot\mathbf{n}]\!]\, dA \;=\; 0\,, \tag{11.7}$$

$$\int_\Sigma [\![\rho\mathbf{u}(\mathbf{u}-\mathbf{w})\cdot\mathbf{n}]\!] - [\![\mathbf{t}\cdot\mathbf{n}]\!]\, dA \;=\; \mathbf{0}\,, \tag{11.8}$$

where, as in Section 4, the jump bracket $[\![f]\!] = f_2 - f_1$ denotes the difference between the enclosed function on the forward and rearward sides of the singular surface Σ. The evaluation position is denoted by the subscripts 1 and 2, respectively, and **n** is a unit normal vector onto the singular surface pointing in the direction of the movement of the shock. **w** is the propagation velocity of the singular surface (wave front) and $\mathbf{t}\cdot\mathbf{n}$ describes the normal stress onto its respective side. If one assumes an effective width of the singular surface, b, the jump conditions in (11.7) and (11.8) can be written as

$$[\![\rho h(\mathbf{u}-\mathbf{w})\cdot\mathbf{n}]\!]\, b \;=\; 0\,, \tag{11.9}$$

$$\left[[\![\rho h\mathbf{u}(\mathbf{u}-\mathbf{w})\cdot\mathbf{n}]\!] - \left[\!\!\left[\int_0^h \sigma_x dz \right]\!\!\right]\mathbf{n} \right] b \;=\; \mathbf{0}\,, \tag{11.10}$$

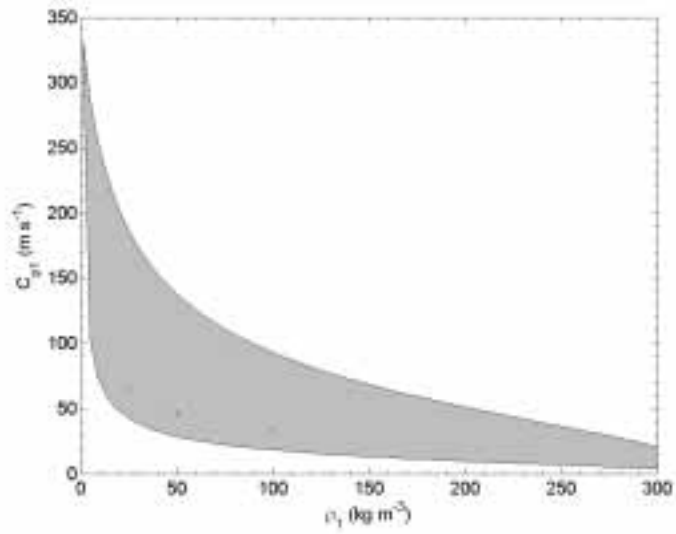

Figure 11.6: Expected range for the speed of sound within a snow avalanche as function of the bulk density. Red crosses are values given by Kulibaba and Eglit (2008).

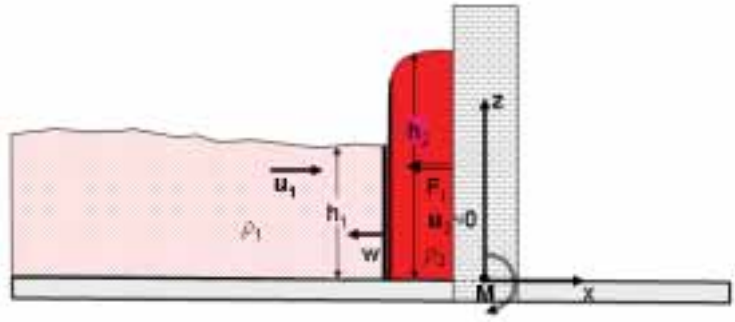

Figure 11.7: A schematic drawing of the impact of an avalanche onto a wall assuming a compressible shock.

where discontinuities in shear stresses within the flow have been neglected. From mass balance, (11.9), $\mathbf{w}$ can be derived using the approximation $\mathbf{u_2} \cdot \mathbf{n} \approx \mathbf{0}$, *i.e.*, the normal velocity of the avalanche behind the shock is zero. Then,

$$\mathbf{w} \approx -\frac{(\mathbf{u_1} \cdot \mathbf{n})\,\mathbf{n}}{(\rho_2 h_2/\rho_1 h_1) - 1} \; . \tag{11.11}$$

The ratio $\rho_2 h_2/(\rho_1 h_1)$ is clearly larger than one. In case the ratio is smaller than two, the wave propagates faster upstream than the incoming avalanche downstream. Figure 11.8 shows the ratio between shock and incoming flow speed versus incoming Froude number for several values of the density ratio ρ_2/ρ_1 (the shock depth, h_2, is determined as described below). Using (11.11) and assuming a hydrostatic pressure distribution within the flowing part of the

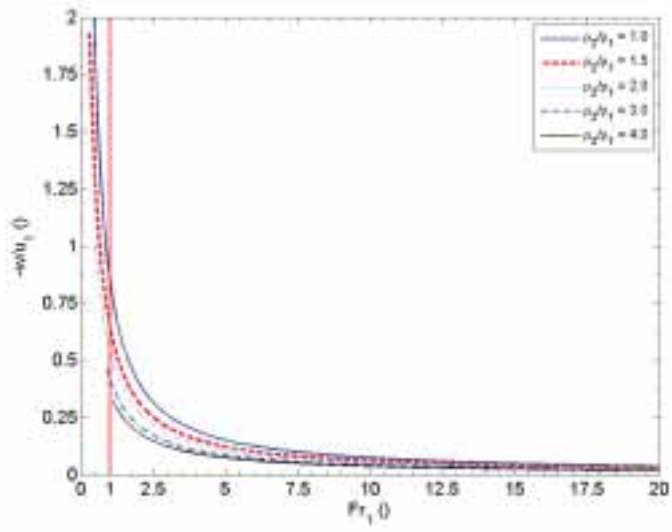

Figure 11.8: The ratio between shock and incoming flow speed versus incoming Froude number, Fr_1.

avalanche, as well as a uniform velocity profile, one obtains from (11.8)

$$\left[\rho_1 h_1 u_1^2 \left(1+\frac{\rho_1 h_1}{[\![\rho h]\!]}\right)+\rho_1 g \frac{h_1^2}{2}\right] b = \left[-\int_0^{h_2} (\sigma_x)_2 dz\right] b \,. \tag{11.12}$$

If one further neglects the influence of friction at the bottom and the upper surface, the right hand side is approximately equal to the normal force imparted to the wall. One then has

$$F_{Ix} = \rho_1 u_1^2 \left[\left(1+\frac{1}{(\rho_2 h_2/\rho_1 h_1)-1}\right)+\frac{1}{2\,\mathrm{Fr}_1^2}\right] h_1 b \,, \tag{11.13}$$

where $\mathrm{Fr}_1 = u_1/\sqrt{g h_1}$ is the incoming Froude number. The dynamic impact force estimated from (11.12) is thus greater by approximately $\rho_1 u_1^2 ((\rho_2 h_2/\rho_1 h_1)-1)^{-1} h_1 b$ than the stress estimated by (11.1).

The jump $[\![\rho h]\!]$ itself depends on the impact pressure and the compressibility of the snow-air mixture, as well as on the ability of the avalanche to change direction. For laterally extended obstacles this primarily means the ability to increase its height in the stagnation layer downstream of the shock (h_2). Voellmy (1955) proposed the following compressibility relation for snow,

$$\frac{\rho}{\rho_0} = \frac{1+\frac{p}{p_0}}{1+\frac{\rho_0}{\rho_F}\frac{p}{p_0}} \,, \tag{11.14}$$

where ρ_0 is the initial density of the snow, $p_0 \approx 1000\,\mathrm{hPa}$ is the atmospheric pressure, and p is the dynamic overpressure. For the values of the upper limit density, ρ_F, Voellmy (1955) gives the values 800 kg m^{-3} for dry fine-grained snow, 600 kg m^{-3} for dry large-grained snow, and 1000 kg m^{-3} for water-saturated snow. Figure 11.9 shows the densification curve for various

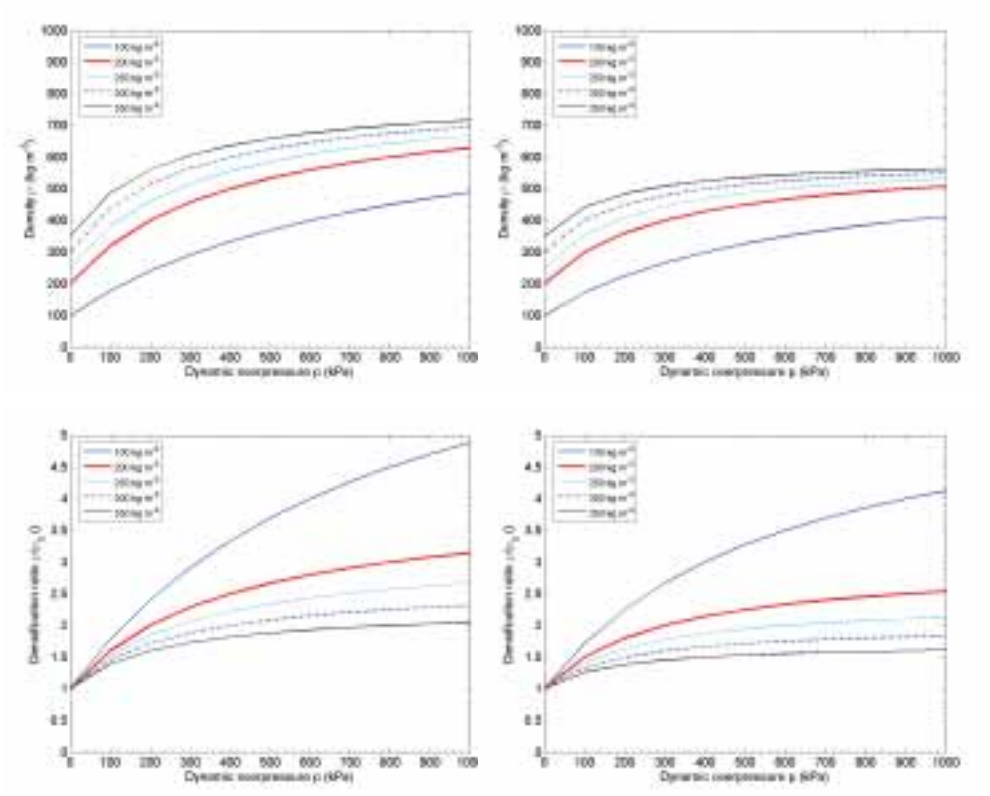

Figure 11.9: Densification of snow according to (11.14) with initial density, ρ_0, as parameter. Left hand side, $\rho_F = 800\ \mathrm{kg\,m^{-3}}$ and right side $\rho_F = 600\ \mathrm{kg\,m^{-3}}$. The lower row shows the respective densification normalised by the initial density.

initial densities. A comparison between measurements and Voellmy's relation is given by Voellmy (1955). From these plots, it is apparent that typical values for the ratio ρ/ρ_0 range between 1.5 and 3 during instantaneous compression. Instantaneous compression means that the duration is too short for the encapsulated air to escape. Hence, due to consolidation, observed density in avalanche deposits can be higher than at impact. Although the presented measurements are for initially intact snow, it is reasonable to assume that similar relationships hold for flowing densities. Kotlyakov and others (1977) obtained similar ratios. They, however, compared the density of the snow deposit in front of a wall (200–600 $\mathrm{kg\,m^{-3}}$) with the density of snow clods in the avalanche snow (150–400 $\mathrm{kg\,m^{-3}}$).

No approach enables estimates of the increase in avalanche depth independent of density changes. However, the flow depth at a dam downstream of the shock, as a function of Froude number of the incoming flow and for a given density ratio, was derived by Hákonardóttir and others (2003a) based on depth-integrated dynamics, assuming hydrostatic stress and lateral confinement.

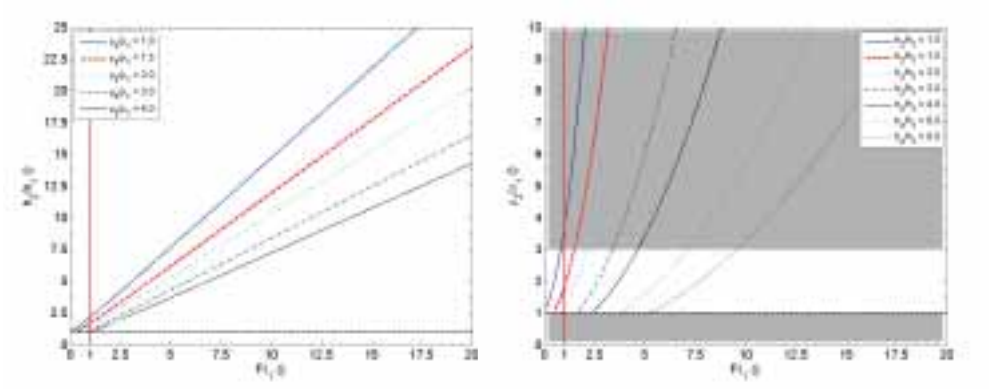

Figure 11.10: *Left:* The ratio between shock depth and depth of the approaching flow versus the incoming Froude number, Fr_1. The density ratios between 1 and 4 are chosen to correspond to possible density ratios in snow avalanches. *Right:* The ratio ρ_2/ρ_1 *vs.* incoming Froude for varying shock depths. The white area depicts the most likely combinations.

$$\frac{\rho_2}{\rho_1}\left(\frac{h_2}{h_1}\right)^2 - \frac{h_2}{h_1} - 1 + \left(\frac{\rho_2}{\rho_1}\frac{h_2}{h_1}\right)^{-1} - 2\,\mathrm{Fr}_1^2 = 0\,. \tag{11.15}$$

Currently, there is also no reliable approach to estimate the effect of a non-hydrostatic stress distribution during impact, or of lateral flow, on the increase in flow depth and density by the dam. The ratio h_2/h_1 is plotted in Figure 11.10 as a function of Fr_1 for different density ratios for a wide obstacle, where h_2 is found from (11.15). An increase in the density ratio lowers the height h_2. The right panel of the figure shows a similar plot for the density ratio ρ_2/ρ_1.

The left panel of Figure 11.11 shows the intensity factor $1 + (\rho_2 h_2/\rho_1 h_1 - 1)^{-1}$ from Equation (11.13) as a function of the incoming Froude number, Fr_1. For $\mathrm{Fr}_1 > 2.5$, which is a reasonable value for fast moving catastrophic avalanches, the difference between (11.13) and (11.1) is smaller than 25%. That is, the force onto the wall is similar according to the two expressions. However, the point of action is lifted, causing an increase in the moment about the foot point. Due to an increase in flow depth, the pressure onto the wall after the first impact by the avalanche front can be reduced proportional to h_1/h_2 for Froude numbers greater than 2. For Froude numbers smaller than 2, the impact force might be increased by a factor between 1 and 2, and even more for $\mathrm{Fr} < 1$, but this situation does not normally arise in dry-snow avalanches.

Figure 11.12 depicts the pressure factor as a function of the incoming Froude number. This reduction, however, is most likely to be nonuniform, as the snow close to the sliding surface is more confined by the surrounding flow. Furthermore, the loading during the initial impact, before the shock has formed, will presumably be distributed over a vertical distance on the order of the upstream flow depth h_1. In this case, the curve $h_2/h_1 = 1$ would be more representative. It should also be noted that this comparatively high initial impact pressure, which is not redistributed by a shock, may affect an area somewhat above the bottom of the wall in case a wedge is formed by the first front, and the flow that immediately follows is deflected slightly upwards somewhat later during the initial impact.

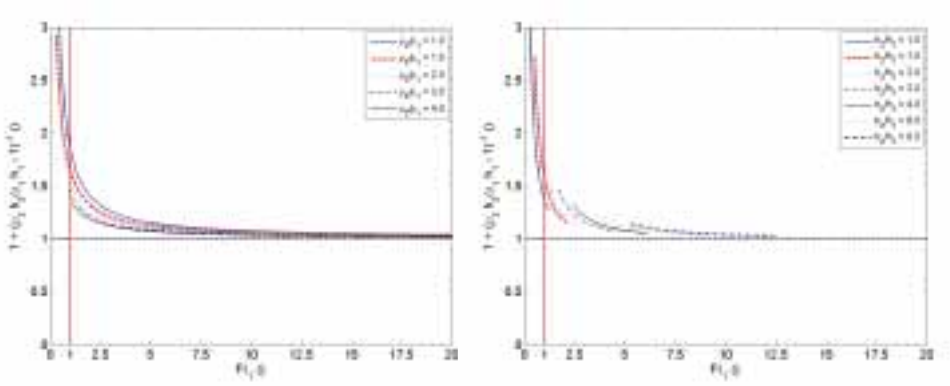

Figure 11.11: Intensity factor $f(\mathrm{Fr}_1) = 1 + (\rho_2 h_2/\rho_1 h_1 - 1)^{-1}$ versus Fr_1. *Left:* ρ_2/ρ_1 taken as parameter; $h_2/h_1 \geq 1$. The density ratios between 1 and 4 are chosen to correspond to density ratios in snow avalanches. *Right:* h_2/h_1 taken as parameter; densification ρ_2/ρ_1 ranges between 1 and 5.

An approach to directly account for the compressibility of avalanches in impact pressure analysis can be found in recent papers by Eglit and others (2007) and Kulibaba and Eglit (2008) as already mentioned in the preceding discussion of initial peak pressure. However, detailed measurements with high spatial and temporal resolution are required to verify those results.

Impacts of solid bodies

In addition, it should be noted that snow avalanches may contain large clods, stones, tree trunks and other debris that, on impact, can create considerable local forces with short durations. This type of loading is discussed in a separate section below.

Horizontal and vertical shear forces

As the avalanche changes its flow direction, it creates not only a normal force at the wall, but also considerable horizontal and vertical shear forces. The vertical component, in particular, was mentioned by Voellmy (1955) as a major cause for the observed destructions of buildings. He estimated the vertical force to be in the range of 0.3 to 0.5 times the normal forces. He also noted that the vertical component may be directed downward on obstacles in steep terrain. In addition to shear forces, up-lifting can be caused by upward motion of the avalanche below balconies or the ledge of a roof. This situation corresponds to a confined setting, in which the ratio h_2/h_1 is restricted and high pressures can occur. However, no quantitative measurements have been made of those effects.

11.2 Determining design loads

The construction of a building or wall-like structure in avalanche-prone regions requires the assessment of reasonable loads, *i.e.*, estimates of the total maximum force, $\mathbf{F_m}$, and moment, $\mathbf{M}$, due to avalanches. Here, a rectangular wall is considered that is wide enough such that

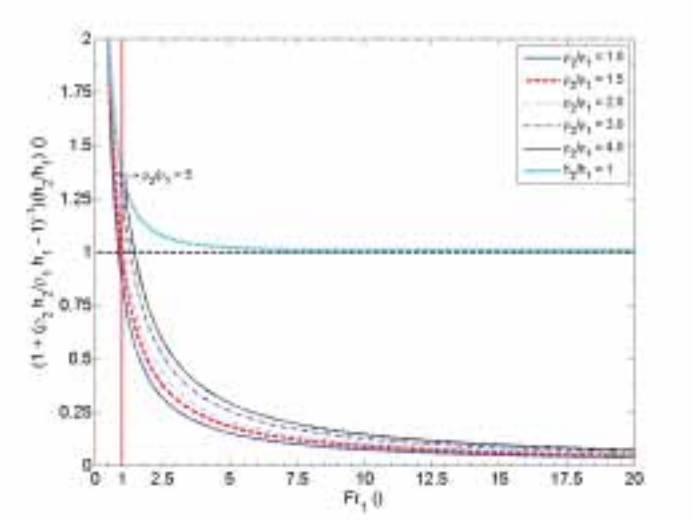

Figure 11.12: Pressure factor $(1+(\rho_2 h_2/\rho_1 h_1-1)^{-1})(h_1/h_2)$ versus Fr_1. The density ratios between 1 and 4 are chosen to correspond to possible density ratios in snow avalanches. In addition, the pressure factor for $h_2/h_1 = 1$ (confined setting) is shown. The mark indicates the point, at which the densification would become larger than 5.

a major portion of an avalanche will not flow horizontally around it, and major parts of the avalanche are at least laterally confined by the neighbouring flow.

In determining the impact load, it is assumed that relevant parameters characterising the avalanche (such as speed, density, structure of the head, *etc.*) are known. Such parameters may be defined using numerical simulations of the flow in accordance with avalanche type, or from field observations.

Figure 11.13 shows a schematic diagram of the impact pressure distribution on a wall due to an avalanche together with the coordinate system and notation used in the following discussion.

The following recommendations are based on Norem (1991), but with some modifications of coefficients. Swiss recommendations for the determination of impact forces on walls are described in Appendix F, and compared with the recommendations given here in figures and tables in Appendix E.

In general, three flow regimes are distinguished for the determination of the impact force on wall-like structures:

- dense flow
- fluidised flow (also referred to as saltation layer)
- suspension flow (powder part)

In addition, the force transmitted through the snowpack is included. *However, static snow loads from the snowpack on the ground or previous avalanche deposits are not considered.*

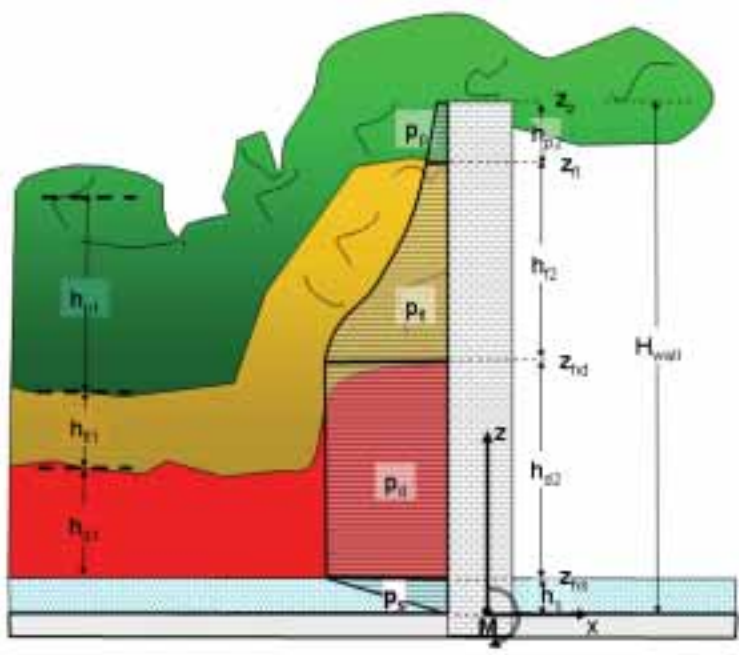

Figure 11.13: A schematic drawing of the impact pressure distribution due to an avalanche on a wall.

Under some circumstances, loading corresponding to some of the flow regimes listed above does not need to be considered. Small or wet avalanches may not be accompanied by a fluidised layer or a powder cloud in the run-out zone, and powder-snow avalanches may need to be considered independent of other flow regimes in some cases. This must be decided on a case-by-case basis by an avalanche expert.

The loads recommended below are in all cases *calculated loads*, which need to be multiplied by appropriate *safety factors* to yield *design loads* to be applied in the design. The safety factors depend on the design methodology and may be specified by national or international standards or guidelines, or reflect safety requirements specified by the customer. The safety factors may also depend on whether the impact pressure due to an avalanche is considered an *accidental load* or not. Assuming an accidental load would be typical for an avalanche with a long return period that endangers a settlement, but not for exposed structures that are frequently hit by avalanches.

Pressure transmitted through the snowpack

Measurements from the full-scale test site Ryggfonn, western Norway, show that avalanche forces can be transmitted through the snowpack on the ground (*cf.* Gauer and others, 2007). For simplicity, a linear pressure distribution will be assumed within the snowpack down to a maximum depth of $2h_d$, *i.e.*

$$p_s(z) = p_d \frac{z - z_0}{h_s - z_0} \quad \text{for } z > z_0, \quad \text{and } p_s(z) = 0 \quad \text{for } z <= z_0 \,, \tag{11.16}$$

where $z_0 = \max(h_s - 2\,h_d, 0)$ and p_d is the dynamic pressure of the avalanche calculated at the lower boundary of the flow (see Eq. (11.20)) in the next paragraph) and h_s is snow depth before the avalanche falls. Thus, the force normal onto a rectangular wall exerted by an avalanche through the snowpack is

$$F_{sx} = \frac{b\,(h_s - z_0)}{2}\,p_d\ , \tag{11.17}$$

and the corresponding moment about the y-axis is

$$M_{sy} \approx b\,p_d \int_{z_0}^{h_s} z\,\frac{z - z_0}{h_s - z_0}\,dz = \frac{1}{3}\,(2\,h_s + z_0)\,F_{sx}\ . \tag{11.18}$$

The contribution to a total lift force is negligible, *i.e.*,

$$F_{sz} \approx 0\ . \tag{11.19}$$

Dense flow

The pressure within the dense flow is assumed to be uniformly distributed along the wall. This is certainly a simplification as there is most likely an increasing pressure with depth. On the other hand, a uniform pressure distribution gives an overestimate of the moment and is, therefore, more conservative. The pressure is computed from (11.13) as

$$p_d \approx \rho_1\,u_1^2 \left[f(\mathrm{Fr}_1) + \frac{1}{2\,\mathrm{Fr}_1^2} \right] \frac{h_1}{h_2}\ . \tag{11.20}$$

ρ_1 is often set to a rather high value of $300\,\mathrm{kg\,m^{-3}}$ for safety reasons but other values for ρ_1 can be used based on expert judgement. The factor $f(\mathrm{Fr}_1)$ accounts for effects due to compressibility of the snow and other effects of the assumed flow dynamics (see Figs. 11.10 and 11.11). A good estimate might be $f(\mathrm{Fr}_1) \approx 1.2$. Reasonable estimates for h_2/h_1 are in the range of 3 to 8 for vertically unconfined settings (Fig. 11.10). The contact area, $\mathcal{A}$, is equal to $b\,H_e$, where $b = \min(W_a, W_{wall})$, and $H_e = \min(h_2, H_{wall} - h_s)$. The height above ground of the upper boundary of the dense flow is given by

$$z_{hdf} = z_{hs} + h_2\ , \tag{11.21}$$

and the height of the upper layer still effecting the wall is equal to

$$z_{hd} = \min(z_{hdf}, H_{wall})\ . \tag{11.22}$$

During the first instant of the impact, peak pressures of several times p_d may occur for durations t_{imp} on the order of $O(h_1/|\mathbf{w}|)$, which is probably a reasonable estimate for the time needed for the pressure wave to reach the free surface. The shock speed $|\mathbf{w}|$ is here used as an order of magnitude estimate for the speed of an internal pressure wave, C_p. It decreases with increasing Fr_1 (see Fig. 11.8). t_{imp} is probably on the order of 0.1 s. During this time, the pressure decreases from its initial peak value and approaches the recommended mean value on longer time-scales. Simultaneously, the flow height increases from $h = h_1$ to $h = h_2$. Comparing the curve labelled $h_2/h_1 = 1$ with the other curves, Figure 11.12 gives

an indication of the relative difference between the peak pressure, p_{peak}, and p_d. As already discussed, a rough estimate for p_{peak} based on experiments is

$$p_{peak} = 3\,\rho_1\,u_1^2\ . \tag{11.23}$$

where $\rho_1\,u_1^2$ is the "impact pressure" corresponding to the density and flow velocity in the undisturbed flow (*cf.* Eq. (11.2)). It is clear from the summary of available experiments and theoretical analyses given earlier in this section, that there is no unique, well-defined value for the pressure ratio, $p_{peak}/(\rho_1\,u_1^2)$, that applies to all snow avalanches. A value of approximately 3 may be a reasonable order of magnitude estimate under many conditions and is recommended here for design purposes.

The peak pressure should be assumed to affect an area with height on the order of h_1 simultaneously. A short-lived pulse in moment load corresponding to the pressure peak also has to be accounted for. For the estimate of this moment pulse, the point of attack of the pressure peak should be assumed to be at a minimum distance $h_s + h_1$ from the ground. This accounts for a possible, small vertical deviation of the main stream due to a build-up of a wedge near the bottom of the obstacle before the pressure peak reaches its maximum, for instance if the dense part of the avalanche is preceded by a fluidised head. The peak load in the impact pressure from the dense flow should be assumed to act independently from the loading due to the fluidised layer and the powder part described below.

It is debatable whether the full magnitude of the pressure peak needs to be taken into account over the entire contact area of laterally extended obstacles because the front of real avalanches is characterised by geometrical irregularities and will not hit the entire contact area simultaneously. Based on the current understanding of the dynamics of the impact process, it is not possible to make a detailed recommendation regarding a maximum size of the area over which the pressure peak on a wall is assumed to act. Here it is recommended that the pressure peak is taken into account for sensitive structures where failure endangers public safety or leads to costly damage. For other structures, it may, based on expert judgement, be permissible to accept a higher risk and work with a smaller area than the total contact area or ignore the pressure peak altogether in the design.

The normal force onto the wall is

$$F_{dx} = \rho_1\,u_1^2\left[f(\mathrm{Fr}_1) + \frac{1}{2\,\mathrm{Fr}_1^2}\right]\frac{h_1}{h_2}\,(z_{hd} - z_{hs})\,b\ . \tag{11.24}$$

The vertical component of the force (tangential force) can be approximated by

$$F_{dz} = c_1\,F_{dx}\ . \tag{11.25}$$

According to Voellmy (1955), c_1 is approximately between 0.3 and 0.5. New experimental results from laboratory measurements indicate that c_1 in dry-snow avalanche ranges between 0.1 and 0.4 whereas in wet-snow and slushflows, it ranges between 0.3 and 0.6 (Margreth and Platzer, 2008). Observation of impact pressures on a large load plate suggest that there is an upper limit of shear stress that can be transferred before shear failure within the flowing snow occurs (Sovilla and others, 2008b). In this case, the tangential shear force may be given as

$$F_{dz} = \min(c_1\,F_{dx}, \tau_y\,\mathcal{A})\ , \tag{11.26}$$

The critical shear stress τ_y is likely to be on the order of 10 kPa.

The moment about the y-axis is

$$M_{dy} \approx b \int_{z_{hs}}^{z_{hd}} z\, p_d\, dz \approx \frac{z_{hs} + z_{hd}}{2} F_{dx} \,. \tag{11.27}$$

Here, the contribution due to the vertical component of the force (Eqs. (11.25) and (11.26)) is omitted. However, in the case of vertical forces acting on a balcony or a ledge, its contribution to the moment can be considerable, and has to be accounted for.

The factor $\frac{h_1}{h_2}$ in Equation (11.20) typically leads to a substantial reduction in the recommended mean impact pressure compared with the impact pressure given by Equation (11.2), which corresponds to the density and velocity in the undisturbed flow upstream of the obstacle. Equation (11.20) implies a redistribution of the total impact force over a larger area than corresponds to the upstream flow depth, and this leads to a higher moment load compared with a more concentrated force closer to the ground. The equation is only intended to be used for computing total impact force on the whole wall and total moment load. Because of the poor understanding of the impact process, Equation (11.20) should not be interpreted to give an estimate of the local impact pressure at a particular time. Where an estimate of the scale of the local impact pressure at a particular time is needed, for example in the computation of peak impact pressure (see above) or in calculations of loads due to impacts of solid bodies (see Section 13), it is recommended that $\rho_1 {u_1}^2$ is used as an estimate of the impact pressure in preference to p_d given by Equation (11.20).

Fluidised layer

Within the so-called fluidised or saltation layer, the dynamic pressure is assumed to decrease with increasing height,

$$p_{fl}(z) = p_{zhfl} + \left(p_d - p_{zhfl}\right) \left(\frac{z_{hfl} - z}{z_{hfl} - z_{hd}} \right)^{n_f} \,. \tag{11.28}$$

Based on Norem (1991), the height of the fluidised layer is assumed to be

$$(h_{fl})_2 = c_e\, (0.1\,\mathrm{s})\, u_1 \,, \tag{11.29}$$

where c_e is an expansion factor that accounts for the increase in flow height at impact; a value in the range $1 < c_e < 3$ might be reasonable. *This expression and the chosen value of c_e have a large effect on the final result and need to be investigated further.* The height of the upper boundary of the fluidised layer over ground is

$$z_{hfl} = z_{hd} + (h_{fl})_2 \,, \tag{11.30}$$

and the effective upper limit on the wall is equal to

$$z_{fl} = \min(z_{hfl}, H_{wall}) \,. \tag{11.31}$$

The pressure at the upper boundary may be approximated by

$$p_{zhfl} = \rho_e \frac{(u_1)^2}{2} \,, \tag{11.32}$$

where the effective density is set to $\rho_e = 15\,\mathrm{kg\,m^{-3}}$. In this case, the contribution from the fluidised layer to the total force is given by

$$F_{flx} = \left[p_{zhfl}\,(z_{fl} - z_{hd}) + \frac{(p_d - p_{zhfl})}{n_f + 1} \left((z_{hfl} - z_{hd}) - \frac{(z_{hfl} - z_{fl})^{n_f+1}}{(z_{hfl} - z_{hd})^{n_f}} \right) \right] b \qquad (11.33)$$

and the vertical component is

$$F_{flz} = \min(c_1 F_{flx}, \tau_y A)\ . \qquad (11.34)$$

The moment about the y-axis is

$$\begin{aligned} M_{fly} &= \left[p_{zhfl} \frac{(z_{fl}^2 - z_{hd}^2)}{2} + \frac{(p_d - p_{zhfl})}{(z_{hfl} - z_{hd})^{n_f}} \left(\frac{z_{hfl}(z_{hfl} - z_{hd})^{n_f+1}}{n_f + 1} - \frac{(z_{hfl} - z_{hd})^{n_f+2}}{n_f + 2} \right. \right. \\ &- \left. \left. \left(\frac{z_{hfl}(z_{hfl} - z_{fl})^{n_f+1}}{n_f + 1} - \frac{(z_{hfl} - z_{fl})^{n_f+2}}{n_f + 2} \right) \right) \right] b\ . \end{aligned} \qquad (11.35)$$

Norem (1991)[2] proposed a value of 4 for the shape factor exponent n_f, which would give a rapid decrease in pressure within the fluidised layer above the dense flow. However, measurements indicate that the decrease might be slower than this. Therefore, $n_f = 1$ is recommended, which is a more conservative choice. *However, this choice needs to be further investigated.*

The pressure at the lower boundary, p_d, and at the upper boundary, p_{zhfl}, is given by equations (11.20) and (11.32), respectively. As mentioned above, some measurements indicate that the decrease of dynamic pressure through the fluidised layer may be slower than proposed by Norem (1991). This depends on the assumed thickness of the dense flow which is not well constrained, since the transition between the dense core and the fluidised layer takes place over a range in flow depth rather than at a well defined distance from the bottom of the flow as explained in Section 4. Therefore, $n_f = 1$ is chosen and, for simplicity, it is assumed that the transition from the dense core to the fluidised layer takes place where the density has dropped considerably from the characteristic density of the dense core, so that within the fluidised layer the magnitude of the impact pressure declines rapidly with distance from the bed.

If the avalanche is preceded by a fast moving fluidised head, Equations (11.20) to (11.22) with appropriate density, ρ_1, should be used instead of Equations (11.28) through (11.35). p_{zhfl} is then given by (11.20) and is used as lower boundary for the powder part.

Powder part

Within the powder part, it is assumed that the dynamic pressure decreases rapidly with height such that

$$p_p(z) = \max\left(p_{zhfl} \left(\frac{z_{hp} - z}{z_{hp} - z_{hfl}} \right)^3, p_a \right)\ . \qquad (11.36)$$

[2]There is a misprint in the original formula in (Norem, 1991, Eq. (9)), which has been corrected here.

The dynamic pressure at the lower boundary is given by Equation (11.32) or (11.20). The pressure at the upper boundary is

$$p_a = \rho_a \frac{u_1^2}{2} \,, \tag{11.37}$$

where air density $\rho_a \approx 1.2\,\mathrm{kg\,m^{-3}}$. The height of the snow cloud, h_p, is assumed to depend on the travel distance along the track, l_{track}, and the flow velocity, u_1, and is given by

$$h_p = (10^{-5}\ \mathrm{s}^{-2})\, l_{track}\, u_1^2 \,. \tag{11.38}$$

It follows that

$$z_{hp} = z_{hfl} + h_p \,, \tag{11.39}$$

and the effective upper limit on the wall is given by

$$z_p = \min(z_{hp}, H_{wall}) \,. \tag{11.40}$$

The normal force is given by

$$F_{px} \approx \frac{p_{zhfl}}{4} \left[(z_{hp} - z_{hfl}) - \frac{(z_{hp} - z_p)^4}{(z_{hp} - z_{hfl})^3} \right] b \,, \tag{11.41}$$

and the vertical force is defined as

$$F_{pz} \approx 0 \,, \tag{11.42}$$

The corresponding moment about the y-axis is

$$\begin{aligned} M_{py} \;\approx\; & p_{zhfl} \left[\frac{z_{hp}(z_{hp} - z_{hfl})}{4} - \frac{(z_{hp} - z_{hfl})^2}{5} \right. \\ & \left. - \left(\frac{z_{hp}(z_{hp} - z_p)^4}{4\,(z_{hp} - z_{hfl})^3} - \frac{(z_{hp} - z_p)^5}{5\,(z_{hp} - z_{hfl})^3} \right) \right] b \,. \end{aligned} \tag{11.43}$$

The above method for estimating the height of the powder cloud (Eq. (11.38)) is quite crude and should be refined by numerical simulations with a 3D powder-snow avalanche model if possible.

Deflecting angle

Loads often have to be computed for extended walls that are hit by an avalanche at an angle φ. The loading computations described above may then be carried out using the normal component of the velocity, $u_\eta = u_1 \sin\varphi$, instead of u_1 in all expressions for forces and moments, but are otherwise identical. The original value of u_1 is retained in expressions that are used to estimate the thickness of the fluidised and powder parts of the flow. Tangential components of the force may be approximated by (see discussion in the preceding subsection about the dense flow)

$$F_{dy} = \min(c_1 F_{dx}, \tau_y \mathcal{A}) \tag{11.44}$$

and

$$F_{fly} = \min(c_1 F_{flx}, \tau_y \mathcal{A}) \ . \tag{11.45}$$

It may then be advisable to assume an error margin on φ so that, up to a maximum of 90°, 20° are added to the estimated deflecting angle

A practical example of loading computations for a wall, according to the procedure described above, is given in Appendix E.

12 Loads on masts and narrow obstacles

Peter Gauer and Tómas Jóhannesson

Impact forces by snow avalanches on narrow obstacles are important for the design of many constructions in avalanche-prone terrain, such as masts of electrical power lines, ski lifts, and cable cars (Fig. 12.1). The design of such objects is mostly outside the scope of this book, but the design of some retarding objects, such as short concrete walls to break up the avalanche flow, is principally similar to the design of other narrow obstacles supposed to withstand dynamic loads. This section, therefore, presents design recommendations for dynamic loads due to snow avalanches on narrow obstacles.

A narrow obstacle is here defined as an obstacle with a width on the same scale or smaller than the flow depth. For such obstacles, the flow is not laterally confined, as for flow against an extended wall. Deviation of the flow around the obstacle and sideways propagation of internal shocks during impact, may then be dynamically as important or more important for determining impact loads than deviation and shock propagation in the vertical direction.

An important question in connection with such impact forces on high obstacles that extend

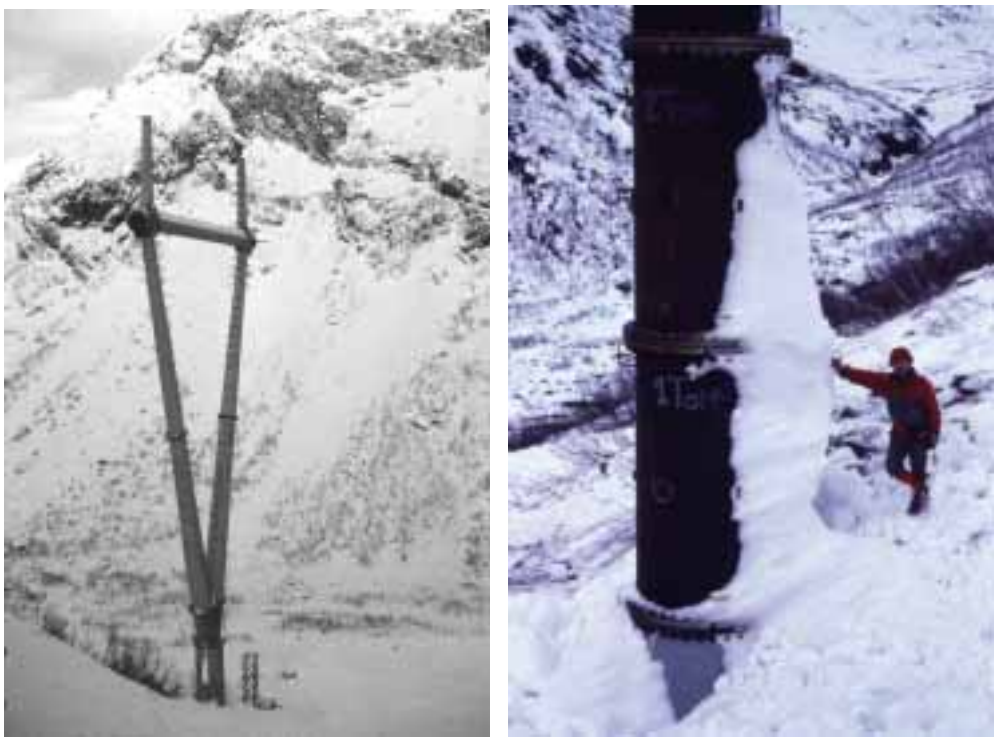

Figure 12.1: A mast built for studying impact forces on electrical power lines (left), and an instrument tower (right) that has just been hit by an avalanche in the Ryggfonn avalanche path in western Norway. The power line mast was broken several times by avalanches during the investigation period. (Photos: NGI.)

through the flow is how they depend on the width and cross-sectional shape of the obstacle for a given velocity and depth of the oncoming flow. Widely used engineering guidelines imply that a significant fraction of the dynamic pressure impacts the obstacle simultaneously over a substantial part of the full height range corresponding to the run-up of the avalanche.

12.1 Forces on immersed bodies

The drag force, F_D, on a body submerged (or partly immersed) in a flow can be viewed as having two components: a pressure drag, F_p, and a friction drag, F_f (*e.g.* Franzini and Finnimore, 1997, Ch. 9). The pressure drag is also referred to as form drag because it depends largely on the form or shape of the immersed body. It is equal to the integral of all pressure components in the direction of motion exerted on the surface of the body. Commonly, the pressure drag is related to the dynamic pressure, $\rho u_\infty^2/2$, acting on the projected area, A, of the body normal to the flow. Thus,

$$F_p = C_p A \frac{\rho u_\infty^2}{2} , \tag{12.1}$$

where ρ is the density of the flow and u_∞ the flow velocity upstream of the body. The coefficient C_p depends on the geometry of the body, as well as factors that define the flow state, such as the Reynolds number, Re, or the Froude number, Fr.

The friction drag along a body is equal to the integral of the shear stress along the surface in the direction of motion. Similar to the pressure drag, the friction drag, also referred to as skin friction, is commonly expressed as a function of the dynamic pressure. Thus,

$$F_f = C_f B L \frac{\rho u_\infty^2}{2} . \tag{12.2}$$

where L is the length of the surface parallel to the flow and B the width of the surface. Similarly to C_p, C_f depends on the geometry of the body, as well as factors that define the flow. Equation (12.2) gives the drag on only one side of an immersed body. Hence, the total frictional component of the drag force is twice that if the flow is around two sides of the body.

The total drag force on a body is the sum of the pressure and the friction drag

$$F_D = F_p + F_f . \tag{12.3}$$

However, it is customary to express the total drag on a body by a single equation

$$F_D = C_D A \frac{\rho u_\infty^2}{2} , \tag{12.4}$$

Thus, the drag factor C_D describes the combined action of dynamic pressure and friction on the body. Consequently, it is a function of the flow regime and depends on factors like the Reynolds number, Re, Froude number, Fr, and the geometry of the obstacle. If one considers a granular flow, C_D might also depend on the particle concentration, size, and restitution coefficient, as well as on the ratio of the particle diameter to the size of the obstacle. Generally, drag coefficients have to be determined experimentally.

In the case of a free-surface flow, *i.e.*, if the obstacle is only partly immersed, a fluid-free zone, "vacuum", can develop behind the obstacle (*cf.* Fig. 12.2). The depth and extent of this zone depends on the flow velocity and properties of the flow. In addition to the dynamic

Figure 12.2: Fluid "vacuum" in the wake behind partly immersed obstacles in water (photos: P. Gauer).

drag, an unbalanced static load may be imparted onto the obstacle. For a hydrostatic pressure distribution (normal to the bottom of the flow), the additional quasi-static load is given by

$$F_{static} = W \int_{h_{dn}}^{h_{up}} \Delta\rho \, g^* \, (h_{up} - z) dz = \Delta\rho \, g^* \, W \, \frac{(h_{up} - h_{dn})^2}{2} \, , \tag{12.5}$$

where $\Delta\rho = \rho - \rho_a$ is the difference between the fluid density and the air density, and $g^* = g\cos\psi$ is the slope-corrected acceleration of gravity. W is the obstacle width across the flow. h_{up} and h_{dn} are the flow depths upstream and downstream of the obstacle, respectively.

The total drag force can then be rewritten as

$$F_{D_t} = \left(C_D + \frac{f_s(h_{up}/h_\infty, h_{dn}/h_\infty, W/h_\infty, \Delta\rho/\rho)}{\mathrm{Fr}_\infty^2} \right) A_\infty \, \frac{\rho \, u_\infty^2}{2} \, , \tag{12.6}$$

where the (slope corrected) Froude number is defined as $\mathrm{Fr}_\infty = u_\infty / \sqrt{g^* \, h_\infty}$, h_∞ is the upstream flow depth, $A_\infty = W \, h_\infty$, is the cross-sectional area of the upstream flow, h_{up} the run-up height upstream of the obstacle, and h_{dn} the flow depth immediately behind the obstacle as before. The notation A_∞, Fr_∞, u_∞, h_∞, h_{up} and h_{dn} is used rather than the subscripts 1 and 2 as in the preceding section, because the flow around masts analysed here is not discussed in terms of an upstream shock. It is reasonable to assume that the function $f_s(h_{up}/h_\infty, h_{dn}/h_\infty, W/h_\infty, \Delta\rho/\rho)$ is also a function of other dimensionless groups, which may involve u_∞. The contribution from the quasi-static component might become negligible for $\mathrm{Fr}_\infty \gg 1$.

It should be noted that a distinction is typically not made between the dynamic drag factors defined by Equations (12.4) and (12.6), respectively, in reporting of experiments with loading of obstacles. The cited drag factors usually represent the effective factor defined by Equation (12.4) without accounting separately for the static loading. The effective drag factor may be

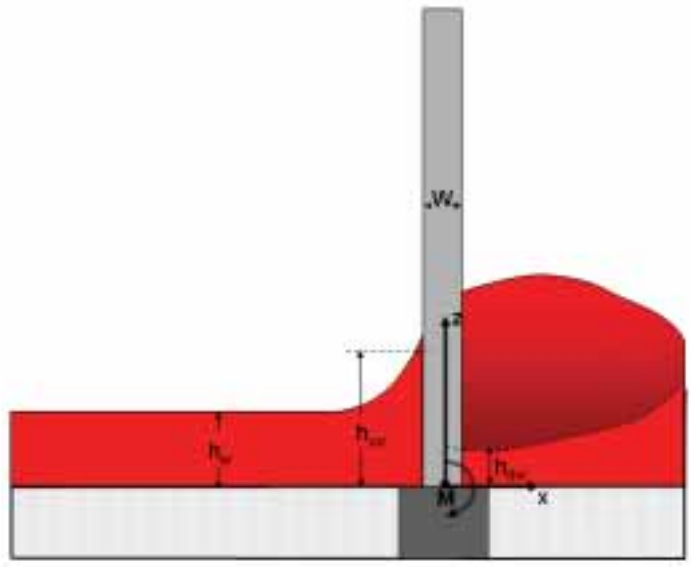

Figure 12.3: A schematic drawing of fluid "vacuum" behind a partly immersed obstacle.

denoted by C_D^*, in case there is a need use different symbols for the different concepts, *i.e.*,

$$C_D^* = \left(C_D + \frac{f_s(h_{up}/h_\infty, h_{dn}/h_\infty, W/h_\infty, \Delta\rho/\rho)}{\mathrm{Fr}_\infty^2} \right) . \tag{12.7}$$

For $\mathrm{Fr}_\infty < 1$, the quasi-static load may dominate the drag. For example, this is the case during snow creep and gliding (see Section 14). In the case of water, the "vacuum" zone diminishes as the flow speed goes to zero, and the static force upstream and downstream of the obstacle balance each other. In contrast to this, avalanche snow has a cohesive strength that may prevent the "vacuum" behind the obstacle from closing, causing a static load from avalanche deposits on the obstacle even after the avalanche movement has stopped.

The overall drag on a small obstacle may be considerably reduced in a free-surface flow compared with a confined setting due to the increased possibility of the material to flow around the obstacle.

12.2 Dynamic drag coefficients

From fluid mechanics, it is well known that C_D can vary by several orders of magnitude depending on the flow regime. There is only a limited set of reliable measurements available from real avalanches. Those, however, indicate that C_D values can vary considerably depending on the regime of the avalanche flow, *i.e.*, whether the flow is more or less fluidised or frictionally dominated, or whether the avalanche is of a dry or wet type, or even slush-like.

Despite this, the value of C_D used for a rectangular cross section in dry-snow avalanches is commonly set to 2, *cf.* Mellor (1968). This holds true for the powder part as well as for the dense part, even if not explicitly stated. Norem (1991) sets up equations for computing the coefficient, connecting it with the Reynolds number, Re. As he notes, even though Re is often

in the range of 4 to 1000, it can be in the range of 0.1 to 4 when snow avalanches are coming to a halt in their run-out area. If Re is expected to range from 4 to 1000, the coefficient C_D may by analogy with fluid flow be expected to lie in the range of 1 to 4. Finally, Norem proposed a value of 2.5 for dry-snow avalanches and 6.3 for wet-snow avalanches, based on impact pressure measurements from the Ryggfonn test site. Salm and others (1990) recommended a C_D of 2 for small rectangular obstacles, and C_D = 1 for cylindrical ones, in combination with a density of 300 kg m^{-3}.

Systematic investigations of drag factors in snow avalanches are not available. Some considerations can be found in (Bozhinskiy and Losev, 1998, Chapter 5.6). Schaerer and Salway (1980) reported values ranging from 2 to 3.4 for the front part, and from 0.86 to 0.96 for the body (values are adapted to the form of Eq. (12.4)). However, they related those values to the front velocity, which probably overestimates the velocity within the body and so causes significant underestimation of the C_D values. McClung and Schaerer (1985) also provided some considerations.

Pfeiff and Hopfinger (1986) conducted laboratory experiments with dense suspensions of polystyrene particles in water. They found good agreement with the classical correlation $C_D(\mathrm{Re})$ that is valid in Newtonian fluids, if they calculated the Reynolds number using the apparent viscosity of the suspension. Gauer and Kvalstad (unpublished) used numerical simulations and experimental results to determine the drag coefficient for mud flows hitting a cylinder. They obtained the relationship $C_D = 24/\mathrm{Re} + 1$, with $\mathrm{Re} = \rho\ u_\infty^2/k$, where k is the yield stress of the mud in simple shear. This means that there are two contributions to the drag force, one independent of the speed and the other growing with the square of the speed. Pazwash and Robertson (1975), conducting experiments with discs, spheres, an ellipsoid, and flat plates, obtained similar results for the force on bodies immersed in a Bingham fluid. They proposed the formulation $C_D = C_{D0} + k_p \mathrm{He}/\mathrm{Re}$, where C_{D0} is a constant depending on the form of the body, k_p is a plasticity factor also depending on the form of the body, $\mathrm{He} = \rho k L^2/\mu_B^2$ is the Hedstrom number and $\mathrm{Re} = \rho u_\infty L/\mu_B$ the Reynolds number. L is a horizontal length-scale and k and μ_B the yield stress and Bingham viscosity, respectively.

Chehata and others (2003) conducted experiments with dense granular flows around an immersed cylinder in a confined setting and found that $C_D \propto \mathrm{Fr}^{-2}$, resulting in a velocity independent drag force. The Froude number was defined by $\mathrm{Fr} = u_\infty/\sqrt{g(D+d)}$, where D is the cylinder diameter and d the particle diameter. The velocities in their experiments were less than 1 m s^{-1}, and Fr was less than 1. For similar conditions but with a free surface, Wieghardt (1975) made experiments with moving rods in sand. In those cases, the drag factor might be approximated by $C_D \approx 24/5\,\mathrm{Fr}^{-2}\sqrt{h/D}$, where h is the flow height, and $\mathrm{Fr} = u_\infty/\sqrt{gh}$. Wassgren and others (2003) performed numerical simulations of dilute granular flows around an immersed cylinder in a confined setting. They found that C_D increases with increasing Knudsen number[3] and decreases with increasing upstream Mach number. In both cases, C_D approaches an asymptote. Besides this, they concluded that the drag coefficient decreases with decreasing restitution coefficient, e, of the particles. Taking parameters that might be relevant in dilute dry avalanches ($D = 0.6$ m, $d \approx 0.05$ m, $c_\infty \approx 0.2$, $e \approx 0.1$–0.3), C_D would vary only between 1 and 3, so that 2 seems to be a reasonable approximation for this flow regime.

On the other hand, Hauksson and others (2007), in their laboratory experiments, found

[3]The ratio between the upstream particle free-path length and the cylinder diameter; $\mathrm{Kn} = \pi d/(8 c_\infty D)$, where c_∞ is the upstream particle concentration, ranging from 0.08 to 0.3 in the simulations.

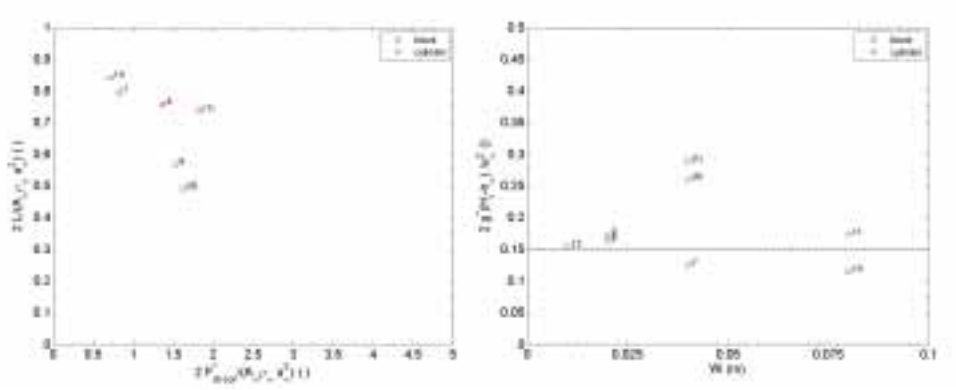

Figure 12.4: Normalised load on an obstacle in a granular free-surface flow *vs.* normalised static load, left panel. The data are adapted from Hauksson and others (2007). Numbers in parentheses indicate their different experiments. Right panel, observed climbing heights plotted against the width of the obstacle.

rather low C_D values ranging from ca. 0.5 for cylindrical obstacles to ca. 0.8 for rectangular blocks. They used fine-grained granular material (glass beads) in a free-surface flow at a Froude number of approximately 13 and upstream volume fraction of approximately 0.55 (Kn numbers between $8 \cdot 10^{-4}$ and $3 \cdot 10^{-3}$). There is a difference in their experimental setup compared with many of the studies described above, in that they measured the total force on obstacles extending through a free-surface flow. Figure 12.4 shows their estimated C_D values plotted against the (corrected) static load defined by

$$F^*_{st-cor} = \Delta\rho \, g^* W \, \frac{h_{up}^2 - \Delta h^2}{2} \, . \tag{12.8}$$

Here, $\Delta h = \max(h_{up} - h_{obs}, 0)$, which is the difference by which the climbing height, h_{up}, exceeded the obstacle height, h_{obs}, in several cases. For those cases, the experiment number is set in parenthesis in the figure. The difference is used to calculate the static load that was actually imparted on the obstacle. Note that for this experimental configuration, h_{dn} (*cf.* Eq. (12.5)) may be assumed to be zero. The figure does not show a rise in C_D with climbing height that might be expected from Equations (12.5) and (12.6), although the data points are rather few for each of the two obstacle geometries to draw definite conclusions. This indicates that a separately defined static load (*cf.* Eq. (12.6)) is comparatively unimportant for the high Froude number flow of these experiments. Figure 12.4 also shows the observed climbing height normalised with the climbing height corresponding to the flow velocity plotted against the width of the obstacle. It shows that although there are substantial variations in the climbing height between different experiments, it does not seem to depend consistently on the obstacle width.

If one assumes that $(h_{up} - h_\infty) \sim u_\infty^2$, then C_D^* (*cf.* Eqs. (12.5) and (12.6)) is function of u_∞^2, rather than a function of Fr_∞^{-2}. The dependency of C_D^* on Fr cannot be analysed based on the experiments of Hauksson and others (2007) because they were only carried out for a single value of the Froude number. On the other hand, Holzinger and Hübl (2004) reported laboratory experiments with impact forces on debris flow breakers, which suggest a decrease

of C_D with increasing Froude number. Also, measurements from the full-scale avalanche test site at Vallée de la Sionne, Switzerland, suggest a similar Froude number dependency (Sovilla and others, 2008a). The measurements imply that the combination ρC_D decreases with increasing Fr. Recently, Thibert and others (2008) obtained similar results at the Lautaret avalanche test site, France.

Yakimov and others (1979) measured forces acting on wedge-shaped obstacles located in an avalanche path. The wedges had upstream angles of $\alpha = 60^\circ, 90^\circ, 120^\circ$ and 150°, with an angle between the flow velocity and the wedge surfaces of $0.5\,\alpha$. The flow depth was equal to the height of the wedge H, or (in some experiments) larger than H. The normal component of the force on the wedge surface was measured as a function of time. Yakimov and others proposed the following empirical estimates for the drag factor

$$C_{D\max} = 0.025\alpha; \qquad C_{D\infty} = 1.2 \qquad \text{if} \quad \alpha > 90^\circ \,. \tag{12.9}$$

$C_{D\max}$ is the drag factor at maximum force, and $C_{D\infty}$ the factor during stationary flow. According to Equation (12.9), both are independent of the Froude number and do not depend on the flow or obstacle geometry apart from α.

12.3 Determining design loads

The construction of mast-like structures in avalanche-prone regions requires the assessment of reasonable loads, *i.e.*, an estimate of the total maximum force, $\mathbf{F_m}$, due to avalanches. Even, more important is an estimate of the maximum moment, $\mathbf{M}$, about the foot point of the mast, or about the footing of the foundation.

In the determination of the impact load it is assumed that relevant parameters characterising the avalanche (such as speed, density, structure of the head *etc.*) are known. Such parameters may be defined using numerical simulations of the flow in accordance with avalanche type, or from field observations.

Figure 12.5 shows a schematic diagram of the impact pressure distribution due to an avalanche on a mast. Here, p_s denotes the pressure transmitted from the avalanche through the snowpack on the ground, and $h_s = z_{hs}$ is the snow depth, p_d is the impact pressure due to the dense part, and $h_d = z_{hd} - z_{hs}$ is the flow depth of the dense layer. Similarly, p_{fl} is the impact pressure due to a fluidised layer and $h_{fl} = z_{hfl} - z_{hd}$ is the height of this layer. Finally, p_p is the dynamic pressure within the suspension layer (powder part), and $h_p = z_{hp} - z_{hfl}$ is the height of the suspension layer. One should keep in mind that all pressures might vary with height.

The total force in x direction is given by

$$\begin{aligned} F_{mx} &= \int_0^{z_{hs}} A(z)\, p_s(z)\, dz + \int_{z_{hs}}^{z_{hd}} C_D(z) A(z)\, p_d(z)\, dz \\ &\quad + \int_{z_{hd}}^{z_{hfl}} C_D(z) A(z)\, p_{fl}(z)\, dz + \int_{z_{hfl}}^{z_{hp}} C_D(z) A(z)\, p_p(z)\, dz \,. \end{aligned} \tag{12.10}$$

As mentioned in the previous subsection, the drag coefficient C_D depends on the flow. Hence, it might not be constant within the whole avalanche, and may vary from layer to layer. The moment, M, about the foot point of the mast is given by

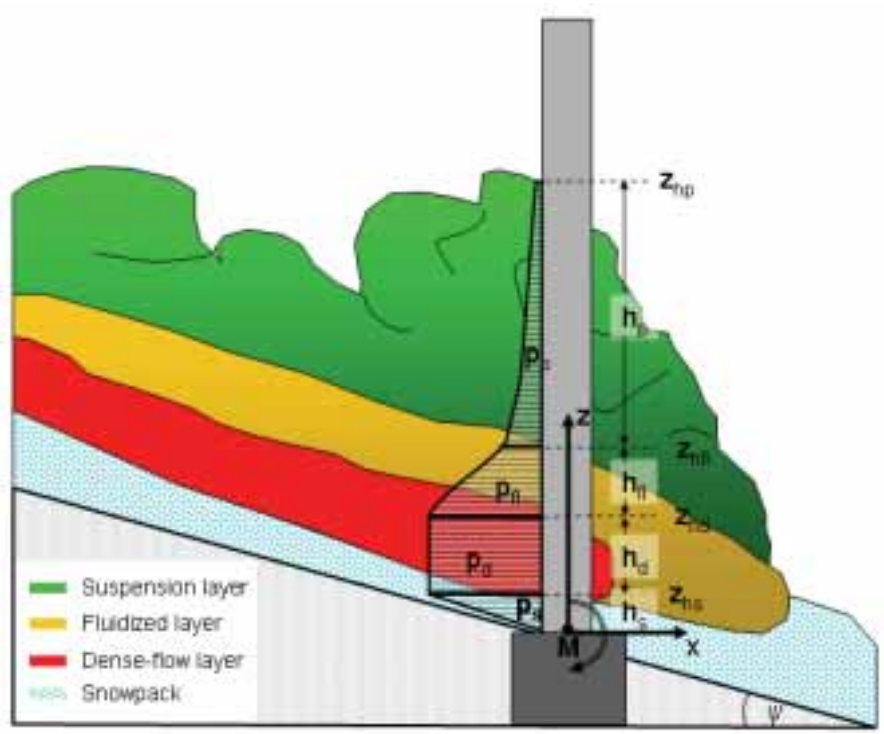

Figure 12.5: A schematic diagram of the impact pressure distribution due to an avalanche on a mast-like structure according to the recommendations described here.

$$M = \int_0^{z_{hs}} z\, p_s(z) A(z)\, dz + \int_{z_{hs}}^{z_{hd}} z C_D(z) A(z)\, p_d(z)\, dz + \int_{z_{hd}}^{z_{hfl}} z C_D(z) A(z)\, p_{fl}(z)\, dz + \int_{z_{hfl}}^{z_{hp}} z C_D(z) A(z)\, p_p(z)\, dz\,. \qquad (12.11)$$

The following recommendations are based on Norem (1991), as in the previous section about loads on walls, but with some modifications of coefficients. Swiss recommendations are, as for the wall loads, described in Appendix F, and are compared with the recommendations given here in Appendix E.

In general, three flow regimes are distinguished for the determination of the impact force on narrow obstacles (Fig. 12.5):

- dense flow
- fluidised flow (also referred to as saltation layer)
- suspension flow (powder part)

In addition, the force transmitted through the snowpack is included. As for loads on a wall, *static snow loads from the snowpack on the ground or previous avalanche deposits are not considered.*

Full-scale experiments (Gauer and others, 2007) show that the largest pressures do not necessarily occur during the passage of the front. This has to be taken into account by a choice of appropriate values for speed and density.

As for loads on a wall, loading corresponding to some of the flow regimes listed above may not need to be considered in some cases. This must be decided on a case-by-case basis by an avalanche expert.

As further discussed in the previous section about walls, the loads recommended below are in all cases calculated loads, which need to be multiplied by appropriate safety factors to yield design loads to be applied in the design.

Pressure transmitted through the snowpack

Measurements from the full-scale test site at Ryggfonn, western Norway, show that avalanche forces can be transferred through the snowpack (*cf.* Gauer and others, 2007). As for loads on a wall, a linear pressure distribution is, for simplicity, assumed within the snowpack down to a maximum depth of $2\,h_d$, *i.e.*,

$$p_s(z) = p_d \frac{z - z_0}{h_s - z_0} \text{ for } z > z_0, \text{ and } p_s(z) = 0 \text{ for } z <= z_0 \,, \tag{12.12}$$

where $z_0 = \max(h_s - 2\,h_d, 0)$ and p_d is the dynamic pressure of the avalanche calculated at the lower boundary of the flow (see Eq. (12.15) below). Hence, the force on the mast exerted by an avalanche through the snowpack is

$$F_{sx} = \frac{W\,(h_s - z_0)}{2}\, p_d \,, \tag{12.13}$$

where W is the width of the mast across the flow. The corresponding moment about the y-axis is

$$M_{sy} \approx \frac{1}{3}\,(2\,h_s + z_0)\, F_{sx} \,. \tag{12.14}$$

Dense flow

The dynamic pressure within the dense flow is assumed to be

$$p_d = \rho_d \frac{u_f^2}{2} \,, \tag{12.15}$$

where u_f is the front velocity of the avalanche, and ρ_d is set to $300\,\mathrm{kg\,m^{-3}}$, which is a rather high value for fast moving dry-snow avalanches. This comparatively high value for ρ_d is chosen for safety reasons, in part for taking loading fluctuations due to individual snow clods into account as discussed below. The height above ground of the upper boundary of the dense flow is

$$z_{hdf} = h_d + z_{hs} \,, \tag{12.16}$$

and the effective height of the mast affected by the dense flow is

$$z_{hd} = \min(z_{hdf}, H_{mast}) \,. \tag{12.17}$$

Then, the force exerted by the dense flow on the mast is

$$F_{dx} = C_D^* W \left(z_{hd} - z_{hs}\right) p_d \ . \tag{12.18}$$

The corresponding moment about the y-axis is

$$M_{dy} \approx \frac{z_{hs} + z_{hd}}{2} F_{dx} \ . \tag{12.19}$$

The effective drag coefficient C_D^* is given by

$$C_D^* = C_D + \frac{f_s(h_d)}{\mathrm{Fr}^2} \ . \tag{12.20}$$

Table 12.1 gives recommendations for the dynamic drag coefficient C_D. Measurements on a wet-snow avalanche (*cf.* Gauer and others, 2007) indicate that $f_s(h_d)$ might be approximated by

$$f_s(h_d) \approx 4.8 \sqrt{\frac{h_d}{W}} \ , \tag{12.21}$$

which is similar to the value proposed by Wieghardt (1975) and also comparable to loads due to snow-creep and gliding (see Section 14).

As for loads on walls, a short lived initial pressure peak, lasting for ca. $t_{imp} = 0.1\,\mathrm{s}$, in the impact force due to the dense flow, and the corresponding moment load, might be taken into account. The recommended magnitude of the peak for narrow structures with a square or blunt shape (*cf.* Table 12.1) is $p_{peak} = 2\,\rho_d\,u_f^2$. No drag factor is used and the peak pressure should be assumed to affect an area corresponding to the width of the obstacle and with height on the order of h_d simultaneously. A peak pressure is only specified for square or blunt narrow obstacles and not for obstacles with a round or a triangular shape (*cf.* Table 12.1). The point of attack of the force to estimate the moment load should be assumed to be at a minimum distance $h_s + h_d$ from the ground.

The recommended magnitude of the peak pressure on square narrow obstacle is chosen somewhat lower than for walls, where a factor of 3 was used (see the previous section). This is due to the flexibility of the flow to diffuse the peak pressure towards the sides, in addition to upward propagation towards the free surface. As for walls, the peak load should be assumed to act independently from the loading due to the fluidised layer and the powder part described below.

It is debatable whether the peak pressure needs to be taken into account for narrow obstacles because pressure fluctuations due to individual snow clods are likely to be relatively more important for narrow obstacles and one might argue that the safety margin introduced by the comparatively large density could also absorb the extra loading due to the pressure peak. As for walls, it is recommended that the pressure peak is taken into account for sensitive structures where failure endangers public safety or leads to costly damage or disturbances of important distribution networks. For other structures, it may, based on expert judgement, be permissible to accept a higher risk and ignore the pressure peak in the design.

Fluidised layer

The dynamic pressure within the fluidised layer is assumed to decrease with increasing height in the same manner as assumed previously for loads on a wall:

$$p_{fl}(z) = p_{zhfl} + \left(p_d - p_{zhfl}\right) \left(\frac{z_{hfl} - z}{z_{hfl} - z_{hd}} \right)^{n_f} . \tag{12.22}$$

The pressure at the lower boundary, p_d, is given by Equation (12.15) and the pressure at the upper boundary is set to

$$p_{zhfl} = \rho_e \frac{u_f^2}{2} , \tag{12.23}$$

where the effective density is again assumed to be $\rho_e = 15\,\mathrm{kg\,m^{-3}}$. The height of the fluidised layer is set to

$$h_{fl} = (0.1\,\mathrm{s})\, u_f . \tag{12.24}$$

It follows that

$$z_{hfl} = z_{hd} + h_{fl} , \tag{12.25}$$

and the effective upper limit on the mast is equal to

$$z_{fl} = \min(z_{hfl}, H_{mast}) . \tag{12.26}$$

In this case, the contribution from the fluidised layer to the total force is given by

$$F_{flx} = C_D W \left[p_{zhfl} \left(z_{fl} - z_{hd}\right) + \frac{\left(p_d - p_{zhfl}\right)}{n_f + 1} \left(\left(z_{hfl} - z_{hd}\right) - \frac{\left(z_{hfl} - z_{fl}\right)^{n_f+1}}{\left(z_{hfl} - z_{hd}\right)^{n_f}} \right) \right] , \tag{12.27}$$

and the corresponding moment about the y-axis is

$$\begin{aligned} M_{fly} &= C_D W \left[p_{zhfl} \frac{\left(z_{fl}^2 - z_{hd}^2\right)}{2} + \frac{\left(p_d - p_{zhfl}\right)}{\left(z_{hfl} - z_{hd}\right)^{n_f}} \left(\frac{z_{hfl} \left(z_{hfl} - z_{hd}\right)^{n_f+1}}{n_f + 1} \right. \right. \\ &- \left. \left. \frac{\left(z_{hfl} - z_{hd}\right)^{n_f+2}}{n_f + 2} - \left(\frac{z_{hfl} \left(z_{hfl} - z_{fl}\right)^{n_f+1}}{n_f + 1} - \frac{\left(z_{hfl} - z_{fl}\right)^{n_f+2}}{n_f + 2} \right) \right) \right] . \end{aligned} \tag{12.28}$$

Norem (1991)[4] proposed a value of 4 for n_f. However, as mentioned in Section 11, the choice of $n_f = 1$ is recommended here, as measurements indicate that the pressure decrease within the fluidised layer might be slower than corresponding to $n_f = 4$. If the avalanche is preceded by a fast moving fluidised head, Equations (12.15) to (12.17) with appropriate density ρ should be used instead of Equations (12.22) through (12.28). In this case, p_{zhfl} is given by (12.15) and used as lower boundary for the powder part.

Powder part

Within the powder part, as for loads on a wall, it is assumed that the dynamic pressure decreases rapidly with height such that

[4]There is a misprint in the original formula in (Norem, 1991, Eq. (9)), which has been corrected here.

$$p_p(z) = \max\left(p_{zhfl}\left(\frac{z_{hp}-z}{z_{hp}-z_{hfl}}\right)^3, p_a\right) . \tag{12.29}$$

The dynamic pressure at the lower boundary, p_{zhfl}, is given by Equation (12.23) or (12.15). The pressure at the upper boundary is

$$p_a = \rho_a \frac{u_f^2}{2} , \tag{12.30}$$

where air density $\rho_a \approx 1.2\,\mathrm{kg\,m^{-3}}$. The height of the snow cloud, h_p, is assumed to depend on the travel distance along the track, l_{track}, the flow velocity, u_1, and is given by

$$h_p = (10^{-5}\ \mathrm{s}^{-2})\, l_{track}\, u_f^2 . \tag{12.31}$$

It follows that

$$z_{hp} = z_{hfl} + h_p , \tag{12.32}$$

and the effective upper limit on the mast is given by

$$z_p = \min(z_{hp}, H_{mast}) . \tag{12.33}$$

The force due to the powder part is then

$$F_{px} \approx C_D W \frac{p_{zhfl}}{4}\left[(z_{hp}-z_{hfl}) - \frac{(z_{hp}-z_p)^4}{(z_{hp}-z_{hfl})^3}\right] , \tag{12.34}$$

and the corresponding moment about the foot point is

$$\begin{aligned} M_{py} \;\approx\; & C_D W\, p_{zhfl}\left[\frac{z_{hp}(z_{hp}-z_{hfl})}{4} - \frac{(z_{hp}-z_{hfl})^2}{5}\right. \\ & \left. - \left(\frac{z_{hp}(z_{hp}-z_p)^4}{4\,(z_{hp}-z_{hfl})^3} - \frac{(z_{hp}-z_p)^5}{5\,(z_{hp}-z_{hfl})^3}\right)\right] . \end{aligned} \tag{12.35}$$

As remarked in the previous section about loads on walls, the above method for estimating the height of the powder cloud (Eq. (12.31)) is quite crude and should be refined by numerical simulations with a 3D powder-snow avalanche model if possible.

Recommended drag coefficient C_D

As discussed in Section 12.2, there is considerable uncertainty about the choice of the right dynamic drag coefficient, C_D, for avalanche flow. Table 12.1 gives an overview of recommended values for C_D for design purposes.

Due to the current lack of available quantitative values, no explicit dependency of C_D and ρ on the flow velocity is included in these recommendations (see discussion in Subsection 12.2). This may change in the future, when more direct measurements become available. Studies of avalanche impact are an ongoing research. Generally, observations from avalanche experiments suggest that the mean density within the avalanche decreases with increasing

Table 12.1: Recommended drag coefficients C_D for various mast geometries.

Flow regime	Obstacle form	C_D	
Through snowpack	no distinction	1.0	
		dry	wet
Dense flow	◯	1.5	3.0–5.0
	△	1.5	3.0–6.0
	□	2.0	4–6
Fluidised layer (Saltation)	◯	1.0	
	△	1.5	
	□	2.0	
Powder Part	◯	1.0	
	△	1.5	
	□	2.0	

speed; the avalanche becomes more and more fluidised. At the same time, the mean C_D value also appears to decrease. The use of the recommended values for C_D in Table 12.1 will, therefore, lead to an overestimate of the actual (mean) impact pressure for high velocities. On the other hand, measurements show that impacts of single particles (snow clods) in the fluidised layer can cause peak pressures on the order of 1 MPa (Schaer and Issler, 2001). Using $\rho_d = 300\,\mathrm{kg\,m^{-3}}$, in combination with the recommended values for C_D in Table 12.1 without regard to flow velocity, is intended as a compromise in order to take into account the effect of impacts of snow clods. Impacts of solid bodies such as rocks advected with the flow can cause even higher pressure peaks as described in Section 13. In slow-moving, wet-snow avalanches ($u < 5\,\mathrm{m\,s^{-1}}$), C_D values may exceed the recommended values by a factor on the order of 10, but usually, faster moving avalanches will determine the load.

A practical example of loading computations for a mast, according to the procedure described above, is given in Appendix E.

13 Loads due to impacts of solid bodies

Peter Gauer

In addition to impact forces due to snow loads, it must also be considered that avalanches may contain large snow clods, stones, tree trunks and other kinds of debris that on impact can cause high short-term impact forces locally with durations on the order of 1–100 ms. These impacts, if not damped by protection measures or snowcover, can cause considerable damage. Figure 13.1 shows an example of the damage of a concrete structure caused by the impact of part of a steel pylon that was advected with an avalanche.

It is not possible to formulate general rules on how to deal with this type of loading, as the type and amount of the advected debris depends on the avalanche path, and must to a large extent be subjectively evaluated in each case.

13.1 Local impacts

In areas where boulder and debris impacts can be expected, it is necessary to consider single solid impacts, which can lead to localised high impact loads. A first estimate of the impact load due to boulder impact, for example, can be obtained using the Hertz's equation describing elastic impacts (*cf.* Johnson, 2001, Ch. 11). A sketch of a boulder impact onto a plane wall is shown in Figure 13.2. The impact force according to Hertz's formula is

$$F_I = \frac{4}{3} R^{1/2} E^* \delta^{3/2} \,, \tag{13.1}$$

Figure 13.1: Damage caused by an impact of solid debris at the NGI test site Ryggfonn (photo: NGI; Avalanche event 20000217 13:55).

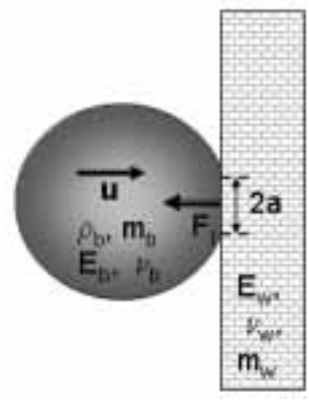

Figure 13.2: A sketch of a boulder impact

where $1/R = 1/R_b + 1/R_w$ and $1/E^* = (1-\nu_b^2)/E_b + (1-\nu_w^2)/E_w$. E_b and E_w are the elastic moduli of the boulder and wall, respectively. Likewise, ν_b and ν_w are the respective Poisson ratios, and R_b and R_w are the radii or characteristic dimensions of the boulder and the wall. In the case of a boulder impacting onto a plane wall, $R_w = \infty$ and $R \approx R_b$. δ is the compression during impact, of which the maximum is given by

$$\delta^* = \left(\frac{15}{16} \frac{m u^2}{R^{1/2} E^*} \right)^{2/5} , \tag{13.2}$$

where $1/m = 1/m_b + 1/m_w$ is the effective mass and u is the velocity at impact. In the case of an elastic impact, the total time of impact t_i is given by

$$t_i = 2.87 \left(\frac{m^2}{R E^{*2} u} \right)^{1/5} . \tag{13.3}$$

For circular point contact, the radius of the contact area is then

$$a = \left(\frac{3}{4} \frac{F_I R}{E^*} \right)^{1/3} = (R\delta)^{1/2} , \tag{13.4}$$

and the maximum contact pressure

$$p_0 = \left(\frac{3 F_I}{2\pi a^2} \right) = \frac{3}{2\pi} \left(\frac{4E^*}{3R^{3/4}} \right)^{4/5} \left(\frac{5}{4} m u^2 \right)^{1/5} . \tag{13.5}$$

As soon as the maximum contact pressure beneath the surface reaches a critical value of about $1.6Y$, Y being the yield stress of the softer body, plastic failure occurs. For a sphere impinging on a wall, Equation (13.5) then reduces to

$$\frac{\rho_b u^2}{Y} = 26 (Y/E^*)^4 , \tag{13.6}$$

where $\rho_b = m/((4/3)\pi R_b^3)$ is the density of the impacting body. This equation gives an estimate of the impact speed necessary for the onset of failure. After that, plastic deformation

Table 13.1: Order of magnitude estimates for the Young's moduli of typical solid debris in avalanches.

	Young's modulus GPa	Poisson ratio ()	Yield strength[‡] MPa	Density (kg m^{-3})
Concrete	20	0.15	20[†]	2500
Ice	9.1	0.33	10[⋆]	916
Iron (cast)	120	0.3	200	7000
Rock (Granite)	50	0.25	100[†]	2600
Steel	200	0.3	300	7850
Wood	0.5	0.4[*]	70[†]	500

[‡] causing plastic deformation but not a catastrophic failure
[†] ultimate strength; causing a catastrophic failure
[⋆] the yield strength of ice varies over a wide range depending on the time-scale of the loading
[*] highly anisotropic

occurs, which reduces the intensity of the contact pressure pulse. In this sense, Hertz's formula gives an upper value of the maximum contact pressure. From the onset until full plastic failure, the mean contact pressure, p_Y, increases from about $1.1Y$ to $3Y$. During plastic failure, the contact area and contact time increase. This increase has to be taken into account for sensitive structures. The order of magnitude of the impact time during plastic failure can be estimated as

$$t_p \approx 2\left(\frac{\pi m}{8 R p_Y}\right)^{1/2} . \tag{13.7}$$

An approximation for the radius of the contact area during failure is

$$a^* \approx R\left(\frac{8}{3}\frac{\rho_b u^2}{p_Y}\right)^{1/4} , \tag{13.8}$$

where ρ_b is the density of the impacting body. According to Johnson (2001, Ch. 11), $\rho_b u^2/Y < 10^{-6}$ gives the limit for elastic impacts, thereafter plastic failure occurs. $\rho_b u^2/Y \sim 10^{-1}$ gives the limit for the shallow indentation theory given by Equations (13.6) to (13.8).

Table 13.1 gives order of magnitude estimates for the Young's moduli of typical solid debris in avalanches. The (compressive) strength of many materials is ca. 2–3 orders of magnitude lower than their Young's modulus.

13.2 Determining design loads

For practical purposes, the Gebäudeversicherung Graubünden proposes the following procedure (GVA, 1994) for loading of structures in the blue zone in Switzerland where avalanche speeds are lower than $10\,\mathrm{m\,s^{-1}}$. The impact of a point load (boulder or tree) is assumed to occur simultaneously with the impact of the dense part of the avalanche. The impact of the point load can occur anywhere within the reach of the dense flow. The design impact force is given by the relation

$$F_I = 3.3\,\rho_1\,u_1^2 \qquad \text{[N]}\,, \tag{13.9}$$

where $\rho_1\,u_1^2$ is a scale for the "impact pressure" corresponding to the density and flow velocity in the undisturbed flow. The contact area is assumed to be $0.05\,\text{m}^2$, which corresponds to a disc with a diameter 0.25 m, giving a local impact pressure of

$$p_I = 66.6\,\rho_1\,{u_1}^2 \qquad \text{in (Pa)} \tag{13.10}$$

on the contact area.

As for loads on walls and narrow obstacles described in the previous sections, the recommended loads are calculated loads, which need to be multiplied by appropriate safety factors to yield design loads to be applied in the design. Loads due to impacts of solid bodies will in most cases be considered accidental loads in which case a safety factor equal to 1 will typically be adopted.

This recommendation implies that the assumed point impact load is roughly equivalent to an assumed scale for the impact pressure of the dense core of the avalanche (corresponding to the density and flow velocity in the undisturbed flow), integrated over an area of somewhat more than $3\,\text{m}^2$. It also implies that the local impact pressure is larger than the assumed scale for the impact pressure of the dense core by one to two orders of magnitude over areas that are a few tens of cm across. This means that point loads will sometimes be the determining factor in the design of objects that need to withstand avalanche loads, and they often need to be carefully considered in the choice of materials for and the layout of constructions.

Similar expressions as Equations (13.9) and (13.10) have in some cases been used for higher speeds than $10\,\text{m}\,\text{s}^{-1}$ for sensitive structures but no formal recommendations regarding the values of the numerical coefficients on the right hand sides of the equations exist in that case.

It should be noted that Equations (13.9) and (13.10) often give lower estimates than those resulting from the Hertzian or the plastic failure approach (see also the example in Section E.3). These lower estimates might be justified if debris within the avalanche only rarely hits the structure without being damped by the surrounding avalanche snow. However, sensitive structures should also be designed according to the Hertzian or the plastic failure approach.

Point loads often need to be considered for walls or other objects that are hit by an avalanche at an angle φ. As for wall loads, the point loads are then calculated using the normal component of the velocity, $u_\eta = u_1 \sin\varphi$, instead of u_1. Otherwise, all expressions for forces and moments but are identical. Again it is recommended to use an error margin on φ so that, up to a maximum of 90°, 20° are added to the estimated deflecting angle

A practical example of impact loading computations, according to the procedure described above, is given in Appendix E.

14 Loads due to static snow pressure

Peter Gauer

Static loads due to snow pressure are often important for the design of narrow obstacles, which were discussed in the preceding section, and can exceed dynamic loads due to avalanche impacts in some areas with an abundant snow cover. The knowledge of snow pressure on narrow structures, such as masts of electrical power lines, ski lifts or cableways, is still limited, and the following recommendations for design loads are based on empirical considerations.

14.1 Static snow pressure

As the snowpack moves slowly and continually downslope, it generates forces onto obstacles parallel and perpendicular to the slope. Two types of movement of the snowpack can be distinguished: snow creep and snow glide (see Figure 14.1). The gliding velocity u_0 can vary within a wide range between zero to several metres per day. Snow creep (v) is the result of vertical settlement (w) of the snow cover and internal shear deformation parallel to the slope (u). Typical creep rates are on the order of mm to cm per day. At the ground, the snow creep is zero.

During the downward motion, the snow causes a pressure on any obstacle in its path. The snow pressure depends mainly on snow depth, and density, slope angle, a gliding factor, and an efficiency factor. The efficiency factor accounts for extension of the influence zone, which depends on the strength of the snowpack, and can be much larger then the obstacle size. The

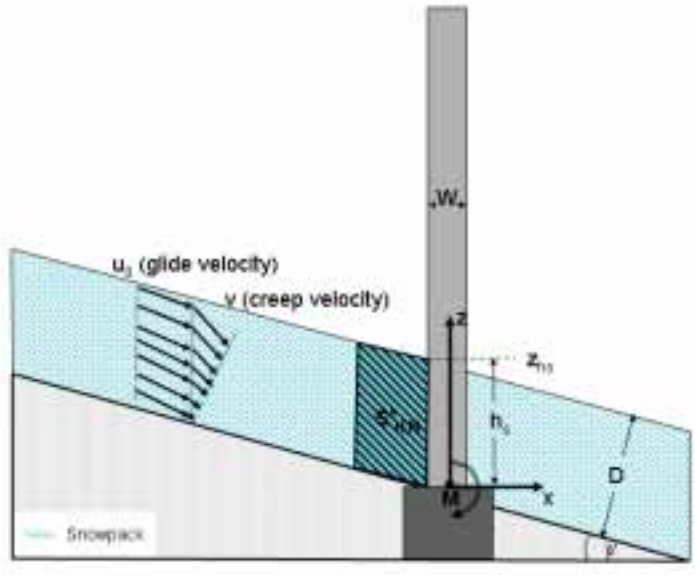

Figure 14.1: A schematic diagram of the creep and glide movement of the snowpack and snow pressure acting on a mast.

gliding factor is a measure for the speed of the snowpack. Higher speeds give the snowpack less time to redistribute stresses around an obstacle, and therefore cause higher loads.

14.2 Determining design loads

The following recommendation follows the approach by Margreth (2007), which is based on the Swiss Guidelines (1990). The snow load per unit length due to snow creep and gliding on a narrow obstacle is

$$S'_{N,M} = \frac{\rho_s}{1000} g \frac{H_s^2}{2} K N \eta_F \frac{W}{D} \qquad [\mathrm{kN\,m^{-1}}] \,. \tag{14.1}$$

The moment per unit length about the foot point is

$$M'_{N,M} = \frac{H_s}{2} S'_{N,M} \qquad [\mathrm{kNm\,m^{-1}}] \,. \tag{14.2}$$

To get the total snow pressure $S_{N,M}$, $S'_{N,M}$ needs to be multiplied by the snow thickness perpendicular to the terrain, $D = H_s \cos\psi$. Similarly, $M'_{N,M}$ needs to be multiplied by D to obtain the total moment. ρ_s is the density of the snowpack in $\mathrm{kg\,m^{-3}}$, g the acceleration due to gravity, and H_s the vertical snow depth. The creep factor, K, depends on the snow density and the slope angle, ψ, and is approximately given by the Swiss Guidelines (1990) as

$$K = \left(2.5 \left(\frac{\rho_s}{1000} \right)^3 - 1.86 \left(\frac{\rho_s}{1000} \right)^2 + 1.06 \left(\frac{\rho_s}{1000} \right) + 0.54 \right) \sin(2\psi) \,. \tag{14.3}$$

The gliding factor, N, depends on the roughness and exposition of the terrain according to the Swiss Guidelines (1990) as given in Table 14.1. The efficiency η_F is defined in relation to the snow thickness perpendicular to the ground, D, and the width of the structure, W. It accounts for end-effect forces, which are higher in a relative sense for narrow obstacles than for wide ones. This arises because, mainly due to three-dimensional viscous flow of the snowpack around the object, the influence width of a narrow obstacle is much larger than the width of the object itself. The efficiency is given as

$$\eta_F = 1 + c \frac{D}{W} \,, \tag{14.4}$$

where the non-dimensional constant c accounts for the intensity of snow gliding and the snow depth. Recommended values for c for Switzerland is given in in Table 14.2.

Table 14.1: Gliding factor, N, for different surface types according to the Swiss Guidelines (1990).

Ground classification		Gliding factor N		Gliding intensity:
		Slope exposition:		
		WNW-N-ENE	ENE-S-WNW	
I	- Big boulders, rocks > 0.3 m	1.2	1.3	small
II II	- Large bushes > 1 m, bumps, mounds > 0.5 m - Scree 0.1–0.3 m	1.6	1.8	medium
III	- Short grass - Bushes < 1 m - Fine rubble alternating with grass and small shrubs - Grass with indistinct cow trails	2.0	2.4	strong
IV	- Smooth long-bladed grass - Smooth rock plates with stratification planes parallel to the slope - Swampy depressions	2.6	3.2	extreme

Table 14.2: c-factors for calculation of the efficiency η_F (Eq. 14.4) for different snow gliding intensity and slope exposition (*cf.* Margreth, 2007).

Gliding intensity and situation	Ground classification		c-factor intensity:
	Slope exposition:		
	WNW-N-ENE	ENE-S-WNW	
Small	Class I-III	–	0.6
Medium	Class IV	Class I-II	1.0
Strong	–	Class III	1.5
Extreme and big snow depth (>2-3 m)	–	Class IV	2.0
Extreme and small snow depth (<2-3 m)	–	Class IV	6.0

15 Geotechnical issues

Karstein Lied

15.1 Introduction

For an avalanche expert it is of importance to have a basic knowledge of the construction principles of retaining and deflecting dams.

It is important to taka geotechnical issues into account when building dams and walls to ensure stability of the construction, reduce maintenance costs and increase lifetime. Although avalanche specialists typically do not perform geotechnical analysis themselves, they should know which building principles must be applied, and what to recommend to the client concerning the general build-up of a dam. In addition to having some knowledge of geotechnical principles, avalanche specialists must also be aware that geotechnical investigations and calculations should always be performed by specialists in the geotechnical field, to ensure sufficient stability of the dam and the ground under it.

Avalanche dam constructions usually have heights ranging between 10–25 m, and lengths of 50–500 m or more (Fig. 15.1). Volumes are usually on the order of 10^4 to 10^5 m^3. Construction costs are therefore high. Dam construction without proper regard to geotechnical principles may lead to fatal failures of the dam, with serious damage as a result (Fig. 15.2).

15.2 Location and design

The location of the dam is usually the first issue to decide in dam planning. The dam must be located in such a way that it protects the whole exposed object or area in question, and it must

Figure 15.1: Deflecting dam and braking mounds at Seljalandsmúli in Ísafjörður, northwestern Iceland. The dam is 650 m long and 16 m high, and the braking mounds are 7 m high. The total volume of fill material in the dam and mounds is 360,000 m^3. (Photo: Tómas Jóhannesson.)

Figure 15.2: Failure in an avalanche retaining dam. The dam height is 8 m. (Photo: Karstein Lied.)

have the correct dimensions to secure the exposed object. It should be planned in such a way that the cost/benefit is optimised. It should, therefore, neither be too large, nor too small.

To optimise the height and length of the dam, and therefore the costs, it is of importance to locate the dam far down the avalanche path, as close to the protection area as possible. This is also an important issue concerning the construction itself, as it is usually cheaper to carry out the construction work on flat ground instead of on a steep mountain slope.

Both deflecting and retaining dams can be made shorter and lower as they are located closer to the object to be protected. If a dam is located farther uphill, one must ensure that the dam is long enough to prevent the avalanche from circumventing the dam and hitting the area or object to be protected. The chance of this happening increases rapidly with increasing distance between the dam and the exposed object.

When an optimal location has been determined, a decision has to be made about the type of dam, and the dam dimensions must be calculated:

- the length of the dam crown,
- the effective height of the dam, and
- the storage volume upstream of the dam.

These calculations are described in detail in Sections 5 to 8.

Various geotechnical aspects in the design and construction of several avalanche dams built in Iceland since 1996 have recently been described by Indriðason (2008).

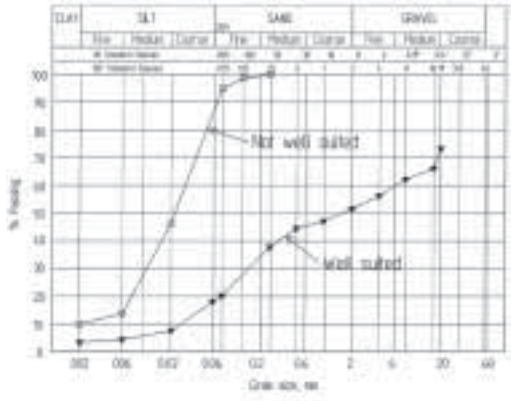

Figure 15.3: Grain distribution curves, two examples.

15.3 Construction materials

Many different types of materials are used for avalanche deflecting and retaining dams or walls, depending on what is found to be the most cost-effective solution in each case. The construction materials normally consist of:

- loose deposits: rocks, gravel, sand, and/or
- reinforced earth, or
- concrete.

15.4 Dams made of loose deposits

Ground investigations

Before the construction starts, ground investigations must be carried out to ensure that the soils are usable for the construction and that the stability of the underlying ground is sufficient. As part of the ground investigations one must:

- check the depth to the underlying bedrock and the amount of loose deposits, and
- collect soil samples for geotechnical testing in the laboratory.

It is common to make pits in the construction area, both at the dam site itself and in the excavation area, and collect samples of materials. Core drillings may also be used in fine-grained soils. Soil samples must be analysed in a geotechnical laboratory. A sieve analysis is important and should always be performed. The sieve analysis provides grain-distribution curves, which specify the relative amounts of the different types of materials in the sample (clay, silt, sand, gravel), see Figure 15.3. In special cases, triaxial tests are performed to calculate the angle of repose of the masses.

Based on the soil samples, geotechnical experts must calculate the global stability of the ground, the stability of the dam, and make a detailed plan for its construction (slope angles of the fill, build-up of the dam, erosion protection, drainage of the dam area, *etc.*).

Dam construction

A dam is most commonly constructed of natural soils found at the dam site or in the vicinity of the dam. A dam built in mass balance has a clear economical advantage.

Mass balance means that excavation is done just above the dam, and that all excavated masses are used in the dam fill. The fill volume may then also be reduced, as the effective dam height is the sum of the fill itself and the depth of the excavated area.

When dealing with earth fill dams, and especially with dams in which fine-grained materials are used, the following points must be assessed:

- quality of the earth materials,
- treatment of organic material in the ground,
- design of the dam,
- design of the excavation area,
- water, drainage and erosion protection.

Quality of the earth materials

All kinds of loose materials, from clay, silt, sand, gravel to rocks may in principle be used for the construction of a dam. In fine-grained, cohesive materials such as clay and silt, the drainage of water is very slow. Due to heavy rainfall, pore pressures might build up during or following the construction phase and reduce the stability of the dam.

A rule of thumb is that if more than 10% of the dam fill consists of fine-grained materials, one has to make extra precautions in the construction to ensure that the water drainage from the body of the dam is sufficient to ensure satisfactory stability of the dam. This results in higher construction costs. It is therefore a clear advantage to use coarse-grained, frictional materials, such as gravel and rocks, for dams made of loose deposits.

Organic materials

If organic masses are present they must be removed before the construction, both under the dam itself and from the excavation area. If the organic materials are not removed, they will be compressed under the weight of the dam. Bog material will settle by up to 90%. Organic layers may contain weak layers, especially in sloping terrain, and act as failure planes.

Design of the dam

Fine-grained cohesive materials will not be stable with inclinations steeper than 1:2. For friction materials such as sand and gravel, the maximum steepness of the dam sides should not exceed 1:1.5 (34°) to obtain a satisfactory stability. For coarser frictional materials one can obtain a stable inclination of the dam sides up to 1:1.25 (39°).

In steep dams, one should use dry walls, reinforced earth or concrete (see the section below). As described in Sections 5 to 7, steep inclinations are advantageous for the effectiveness of the dam.

In conclusion, the slope of loose materials should not be steeper than the figures given below:

- Fine-grained materials, 1:2

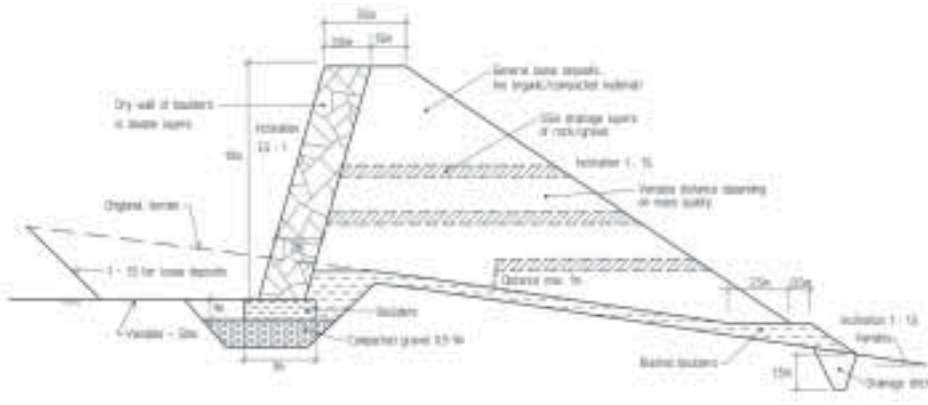

Figure 15.4: A principle sketch of a dam with a dry wall.

- Sand, gravel, 1:1.5
- Loose layered rocks, 1:1.25
- Dry walls with rocks, 3.5:1–4:1
- Reinforced earth, geotextiles, 4:1

Fine-grained masses must be sorted out from the excavation. If one decides to use fine-grained materials in the dam, such materials must be built into the dam in combination with coarser material to ensure sufficient drainage. A common practise is to make a horizontally layered construction with alternating coarse-grained and fine-grained layers (see Figure 15.4). The thickness of the layers should not exceed 0.5 m, and they should be levelled out and compacted by heavy machinery.

Design of the excavation area

The excavation area above the dam must be made broad enough to prevent the avalanche from jumping over the dam from the uphill natural terrain surface. A minimum width of the excavation area should be about 50 m. The width depends on the velocity and volume of the avalanche, and must be evaluated in each particular case. The layout of the excavation area must ensure that the effective height of the dam is retained; it must not be so deep and narrow that the dam ends up in a “ditch”.

The sides of the cut must be gentle enough to ensure stability of the earth masses along the cut, and should normally not be steeper than 1:1.5. Coarser deposits (gravel, boulders) are stable up to 1:1.25, and if clay and silt make up for most of the cut, the inclination should not be steeper than 1:2.

Water, drainage, and erosion protection

If water occurs in the excavation, precautions must be taken to keep the construction masses as dry as possible, since water-soaked masses are difficult to handle. If the water content of the masses is high, the angle of repose is lower, and it will be difficult to obtain the designed inclinations of the fill during the construction. Water built into the dam also reduces the

stability of the dam. Usually, the water content in the dam materials is at its highest during the construction, especially if much fine-grained soils are used. The construction period is therefore often a critical phase for the stability of the dam.

Surface streams and brooks must be diverted from the dam area. If possible, the flowing water should be directed around the dam along the base of the upper fill, or kept completely away from the dam area. The dam and the excavated area should be designed in such a manner that ponding of water above the dam cannot occur. If necessary, one may lead the water in culverts underneath the dam, but there is always the possibility that such culverts may become blocked, either by avalanche snow or earth materials. If ponding of water behind a dam is possible, the dam should be designed for hydrostatic pressures. Some countries have special regulations concerning this problem.

The weight of the dam may block natural drainage channels in the ground and force groundwater upwards into the dam itself, thereby reducing the stability of the dam. A high ground water table can be avoided by making ditches underneath the base of the dam to ensure sufficient drainage. In addition, the bottom layer of the dam should always be constructed from self-draining materials.

Both the dam sides and the sides of the cut should be protected against water erosion. This can be done by the use of different kinds of vegetation or geotextiles to stabilise the surface.

Water courses in the dam area must be protected against erosion by stones, boulders, or other suitable materials, unless the water flows on the bedrock.

Advantages and disadvantages

The advantages of using natural loose deposits for the construction are mainly:

- Materials are often at hand.
- Natural loose deposits are cheaper than other materials.
- Maintenance costs are low.
- The appearance of the constructions is more easily accepted by the public as the visual impact is less than for an "artificial" structure such as a concrete dam.

The disadvantages of dams made purely of loose deposits are many:

- Dams built of loose materials require much space. A 15 m high dam with an inclination of 1:1.5 on horizontal ground is, including the width of the dam crown (2–4 m), 45–50 m wide at the base. When the excavation area is included, one needs at least about 100 m for the construction. As dams are built in the run-out zone, the terrain is often sloping, and with increasing terrain inclination the lower fill will rapidly increase in width and volume.
- The volume of a dam per unit length is roughly proportional to $h^2 \cot\alpha$, where h is the vertical dam height and α the inclination of the dam sides. As a consequence, the volume increases rapidly with the dam height. Although unit prices per m^3 decrease with the volume of the dam, high dams with natural side inclinations will be costly.

Figure 15.5: A catching dam for wet snow avalanches and debris flows. Dry wall with backfill of earth materials, height 12 m, inclination 1:1. Ullensvang, Norway. (Photo: Karstein Lied.)

- It is difficult to obtain steep enough dam sides by using earth materials, and such dams are therefore less effective than dams with the same height made of concrete or reinforced earth.
- For deflecting dams in steep terrain, the effective inclination of the dam sides (measured perpendicular to the dam axis), decreases with increasing terrain inclination. The angle of repose in such cases is found along a plane between the direction of the cross section and the longitudinal dam axis.

15.5 Dams with steep sides

It is possible to increase the inclination of dam sides by the use of materials such as:

- dry walls,
- reinforced earth,
- concrete, steel.

As mentioned earlier, a steep upstream side of the dam increases the effect of the dam.

Dry walls consist of a "masonry" of boulders with a back fill of other earth materials, see Figures 15.5 and 15.6. The boulders should not be smaller than about 0.5 m^3, and be built up in bonded layers. Experience has shown that dry walls with inclinations of up to 4:1 (76°) are stable, provided that the foundation is adequate, and that the dry wall itself is designed to withstand the earth pressure from the backfill. To withstand the earth pressure, the thickness of the dry wall must increase with the height of the dam. The ratio of the thickness of the dry wall to the dam height should not be less than 1:5. Therefore, a 10 m high dam needs a 2 m thick dry wall. To increase the stability, it is advantageous to tilt the boulders a little into the wall.

Figure 15.6: A river outlet trough a dam (photo: Karstein Lied).

The foundation of the dry wall must consist of materials that are not subjected to frost heave (sand, gravel, boulders), and both the foundation and the backfill must be drained. Calculations to ensure sufficient global stability, as well as stability of the dam itself, are necessary.

As for the use of reinforced earth, many solutions are possible, and different commercial products are available on the market. The reinforcement may consist of nets or gabion boxes of galvanised steel, or net constructions of polymers, such as polyethylene, polypropylene, polyester, *etc*. The reinforcement is applied as the outer cover of the dam, and makes it possible to build dams with inclinations of 4:1 or more. Earth materials (usually gravel or stones) are embedded into the cases or into the nets, and are kept in place by additional anchors built into the dam. All such constructions must be designed by geotechnical experts to ensure a safe and optimal layout.

A combined defence structure system consisting of two rows of 10 m high braking mounds and a 17 m high steep catching dam has been constructed above the town of Neskaupstaður in eastern Iceland, see Figures 15.7, 15.8 and 15.9. The dam and mounds are designed in combination with 1200 m of supporting structures in the avalanche starting zone (not shown on the map). The dam is 400 m long, and the mounds are 10 m wide at the top and 30 m wide at the bottom. The uppermost 14 m of the upstream side of the dam have a slope of 4:1. It is built from reinforced loose materials with a front constructed from 0.5 m high steel-mesh steps, which are anchored into the dam fill with long steel rods. The lowest 3 m of the face of the dam are built from loose materials with a slope of 1:1.5. The upstream sides of the mounds have the same slope as the steep part of the dam, and are built with the same kind of steel reinforcement.

Concrete constructions are well known as deflectors and for catching purposes. They have an advantage over constructions made of earth materials because a vertical wall is more effective for dissipating the kinetic energy of the avalanche. Furthermore, concrete walls

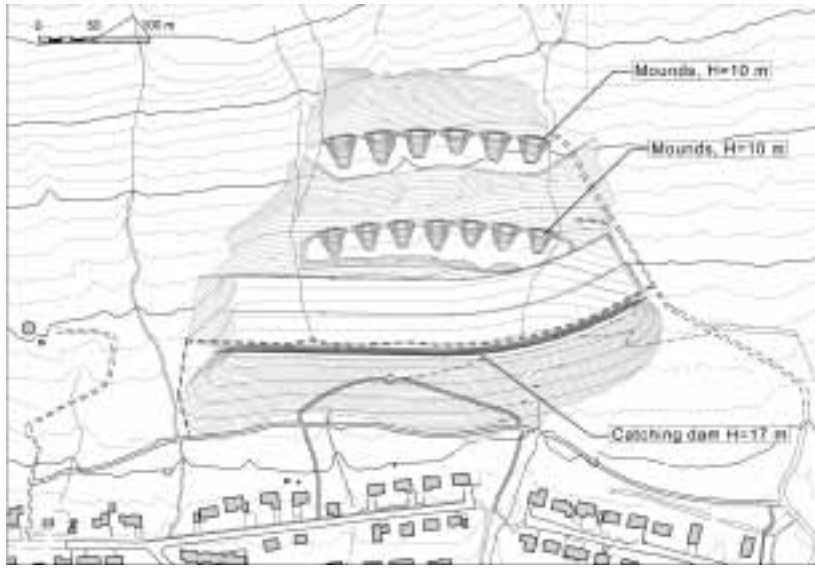

Figure 15.7: Plan view of combined braking mounds and a catching dam, made from reinforced earth. Neskaupstaður, eastern Iceland (designed by VST Consulting Engineers Ltd. and Forverk Consulting Engineers Ltd. in Reykjavík, Iceland, and Cemagref in Grenoble, France).

Figure 15.8: A row of 10 m high braking mounds at Neskaupstaður (see map in Fig. 15.7) (photo: Tómas Jóhannesson).

are more slender than dams made of natural deposits only, and consequently need much less space. The major drawbacks are high costs and visually displeasing constructions.

Concrete walls are usually made as slab concrete dams, reinforced with ribbing (see Figure 15.10). For such slender constructions, the avalanche impact pressure must be carefully cal-

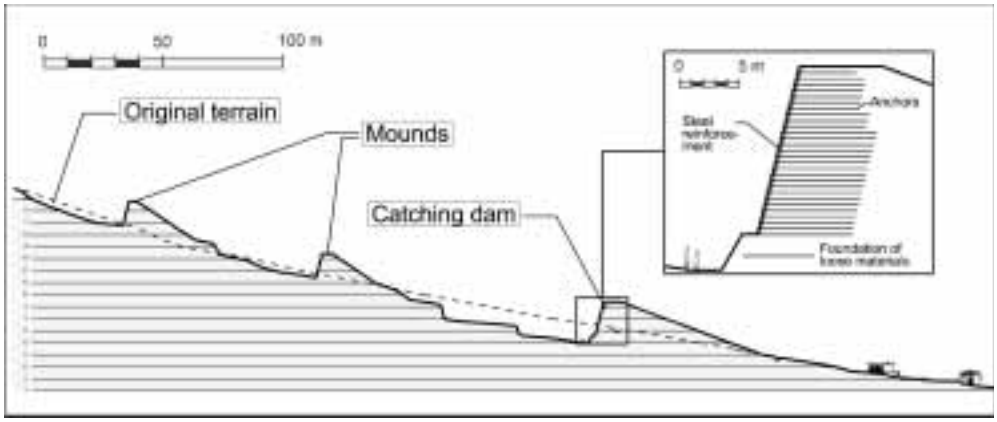

Figure 15.9: A vertical section of a dam and braking mounds at Neskaupstaður (see map in Fig. 15.7).

Figure 15.10: A concrete diverting dam at Odda, Norway (height 8 m, length 200 m) (photo: Karstein Lied).

culated, as the walls must withstand the pressure without tilting or being displaced. For these reasons, the foundations are especially important. In bedrock, the foundations are usually made by steel tension anchors (ribbed bars) in boreholes with cement grout. In loose deposits, one must ensure that the ground is able to withstand the weight of the concrete construction plus the loads from the avalanche impact. A foundation platform of concrete is normally used as a base for the wall. The base must be frost proof, and the area around it well drained.

A 10 m high and 113 m long retaining wall made as a shell construction, founded on bedrock at Ullensvang in Norway (Lied and others, 1998), is shown in Figure 15.11. A shell construction can take higher loads than a straight wall for the equivalent amount of concrete, and was therefore more cost-effective.

Steel constructions may also be used for deflecting and retaining purposes. However, such constructions are not common, as they tend to be more costly than constructions from other materials.

Figure 15.11: A retaining dam made of six 20 m wide and 10 m high reinforced concrete shells at Ullensvang, Norway (designed by NGI and Instanes AS, Norway). Maximum design avalanche impact force is 92 kPa. Each shell has four vertical steel anchors, each with a capacity of 2800 kN, drilled 12–14 m into the bedrock. Tilting moment on each shell is 59,000 kNm, and shear force is 8500 kN. (Photo: Ulrik Domaas.)

16 Unresolved issues

Several issues need to be investigated further in order to improve avalanche dam design criteria beyond the guidelines proposed here. The most important issues that must be addressed are listed below. Since the main focus of this book is on avalanche–dam interactions, the points raised here address dam design criteria. There are also various unresolved issues regarding avalanches loads on structures (as mentioned in Sections 11 to 14), but these are not considered here.

Loss of momentum during the impact with the dam: The proposed values of the k-factor (Eq. (5.14)) are based on weak arguments. In particular, dam overflow data from the full-scale Ryggfonn test site in Norway indicate that very little energy loss occurs above a dam with a side slope of about 40°. These results may be interpreted as an indication that, for overflowing avalanches, the loss of kinetic energy during the impact with the dam equals *on the order of half the potential energy corresponding to the freeboard of the dam*. This means that λ is on the order of 0.5 in this case, rather than 1.5–2, as proposed in Section 5! These results are very disconcerting and need to be analysed further. They may indicate the lack of some fundamental dynamic process in the analysis of overflow, as summarised in this report. Observations of run-up marks on natural obstacles for real snow avalanches indicate, however, that much more energy than this is in many cases lost during impacts with abrupt obstacles. Run-up marks and data of avalanche overrun need to be analysed further to resolve this discrepancy.

The maximum deflecting angle φ_{max}: The requirement that φ be at least 10° smaller than φ_{max} needs to be discussed further. Is the rather arbitrary value of 10° appropriate, or should some other value be chosen?

Effect of terrain slope towards the dam on the shock height: Hydraulic jumps in fluid flow in sloping channels are affected by the channel slope, which leads to an increase in flow depth downstream of the jump for positive slopes (see Chow, 1959). This effect, which arises from the action of the gravitational force over the length of the jump, can be taken into account by an adjustment of the Froude number based on empirical data of water flows. However, granular jumps have been observed to be considerably shorter than water jumps (see Hákonardóttir, 2004), and the gravitational force is assumed to be to a large extent balanced by frictional forces. Therefore, it is not clear to what extent this effect of terrain slope should be taken into account for design criteria for avalanche dams. If dams are constructed in areas, where avalanches may be expected to be slowing down, one might even argue that this is equivalent to fluid flow in an up-sloping channel, where this effect acts in the opposite direction.

Effect of entrainment and deposition: Deposition may be an important process during avalanche impacts, and entrainment might have an effect under some circumstances. However, these effects have been omitted here.

Effect of the saltation and powder parts: A major limitation of the dynamic description of the impact process developed here, results from the depth-averaged formulation of the shallow flow of the avalanche dense core. Consequenctly, the saltation and powder components are ignored. These components may lead to important overflow in some

cases, and may cause substantial impact on structures below the dam, which cannot be evaluated based on the simplified dynamic framework. This limitation needs to be addressed in further studies.

References

Alþingi. 1997. Act on Protective Measures against Avalanches and Landslides, Reykjavík.

Arnalds, Þ., K. Jónasson and S. Sigurðsson. 2004. Avalanche hazard zoning in Iceland based on individual risk, *Annals of Glaciology*, **38**, 285–290.

Arnalds, Þ., S. Sauermoser and H. Grímsdóttir. 2001a. Hazard zoning for Neskaupstaður. Technical report, *Report 01010*, IMO, Reykjavík.

Arnalds, Þ., S. Sauermoser and H. Grímsdóttir. 2001b. Hazard zoning for Ísafjörður, Siglufjörður and Neskaupstaður. General report, *Report 01009*, IMO, Reykjavík.

Augé, A., F. Ousset and O. Marco. 1995. Effet d'une digue sur l'écoulement d'un aérosol, Sivardière, F., ed., Actes du colloque ANENA, "Les apports de la recherche scientifique à la sécurité neige, glace et avalanche", Chamonix (France), May 30 to June 3, 1995, Cemagref Editions, Antony Cedex, 235–240.

Bachmann, O. 1987. Energy loss of snow blocks passing through a supporting structure, Salm, B. and H.U. Gubler, eds., Avalanche Formation, Movement and Effects, IAHS Publ. 162, 613–622.

Baillifard, M.-A. 2007. Interaction between snow avalanches and catching dams, Ph.D. thesis, ETH Zürich, Zürich.

Barbolini, M., L. Natale, M. Cordola and G. Tecilla. 2004. Linee Guida metodologiche per la perimetrazione delle aree esposte al pericolo di valanghe (In Italian with an abstract in English), *Neve e Valanghe*, **53**, 6–13.

Beghin, P., and J.-F. Closet. 1990. Effet d'une digue sur l'écoulement d'une avalanche poudreuse, *Informations Techniques 77/3*, CEMAGREF Division Nivologie, Grenoble.

Berthet-Rambaud, P., A. Limam, D. Baroudi, E. Thibert and J.-M. Taillandier. 2008. Characterization of avalanche loading on impacted structures: a new approach based on inverse analysis, *Journal of Glaciology*, **54**(185), 324–332.

BFF/SLF. 1984. Richtlinien zur Berücksichtigung der Lawinengefahr bei raumwirksamen Tätigkeiten, Bundesamt für Forstwesen (Swiss Federal Office of Forestry) and Eidg. Institut für Schnee- und Lawinenforschung (SFISAR), Bern.

Bozhinskiy, A. N., and K. S. Losev. 1998. The Fundamentals of Avalanche Science, *Mitt. 55*, Eidg. Institut für Schnee- und Lawinenforschung, Davos.

BUWAL/WSL. 1990. Richtlinien für den Lawinenverbau im Anrissgebiet (Guidelines for defence structures in starting zones), Bundesamt für Wald und Landschaft (Swiss Federal Office of Forests and Landscape) and Eidg. Forschungsanstalt für Wald, Schnee und Landschaft (Swiss Federal Institute for Forest, Snow and Landscape Research), Bern.

Caccamo, P. 2008. Experimental assessment of the influence of a dam on powder snow avalanche impact: the case study of Taconnaz, Master's thesis, University of Milano, Cemagref, Milano, Italy, and Grenoble, France.

Chapman, C. J. 2000. High Speed Flow, Cambridge University Press, Cambridge, UK.

Chehata, D., R. Zenit and C. R. Wassgren. 2003. Dense granular flow around an immersed cylinder, *Physics of Fluids*, **15**(6), 1622–1631.

Chow, V. T. 1959. Open-channel hydraulics, McGraw-Hill Inc., New York.

Chu, T., G. Hill, D. M. McClung, R. Ngun and R. Sherkat. 1995. Experiments on granular flow to predict avalanche runup, *Canadian Geotechnical Journal*, **32**, 285–295.

Cooker, J. M., and D. H. Peregrine. 1995. Pressure-impulse theory for liquid impact problems, *Journal of Fluid Mechanics*, **297**, 193–214.

Cui, X., J. M. N. T. Gray and T. Jóhannesson. 2007. Deflecting dams and the formation of oblique shocks in snow avalanches at Flateyri, Iceland, *J. Geophys. Res.*, **112**(F04012).

Domaas, U., and C. B. Harbitz. 1998. On avalanche run-up heights on deflecting dams: Centre-of-mass computations compared to observations, Hestnes, E., ed., 25 Years of Snow Avalanche Research, Voss 12–16 May 1998, NGI Report 203, Norwegian Geotechnical Institute, Oslo, 94–98.

Egli, T. 1999. Richtlinie Objektschutz gegen Naturgefahren, Gebäudeversicherungsanstalt des Kantons St. Gallen, St. Gallen, Switzerland.

Eglit, M. E. 1983. Some mathematical models of snow avalanches, Shahinpoor, E., ed., Advances in the mechanics and the flow of granular materials, Houston, Texas, vol. 2 of *Trans. Tech. Publ.*, 577–588.

Eglit, M. E., V. S. Kulibaba and M. Naaim. 2007. Impact of a snow avalanche against an obstacle. Formation of shock waves, *Cold Region Science and Technology*, **50**(1–3), 86–96.

Fan, L.-S., and C. Zhu. 2005. Principles of Gas-Solid Flows, Cambridge Series in Chemical Engineering, Cambridge University Press.

Faug, T., P. Gauer, K. Lied and M. Naaim. 2008. Overrun length of avalanches overtopping catching dams: Cross-comparison of small-scale laboratory experiments and observations from full-scale avalanches, *Journal of Geophysical Research – Earth Surface*, **113**, F03009.

Faug, T., M. Naaim, D. Bertrand, P. Lachamp and F. Naaim-Bouvet. 2003. Varying dam height to shorten the run-out of dense avalanche flows: developing a scaling law from laboratory experiments, *Surveys in Geophysic*, **24**, 555–568.

Faug, T., M. Naaim and A. Fourriére. 2007. Dense snow flowing past a deflecting obstacle: An experimental investigation, *Cold Regions Science and Technology*, **49**(1), 64–73.

Faug, T., M. Naaim and F. Naaim-Bouvet. 2004. An equation for spreading length, centre of mass and maximum run-outs shortenings of avalanche flows by obstacle, *Cold Region Science and Technology*, **39**(2/3), 141–151.

Franzini, J. B., and E. J. Finnimore. 1997. Fluid Mechanics with Engineering Applications, McGraw-Hill.

Gauer, P., and D. Issler. 2004. Possible erosion mechanisms in snow avalanches, *Annals of Glaciology*, **38**, 384–392.

Gauer, P., D. Issler, K. Lied, K. Kristensen, H. Iwe, E. Lied, L. Rammer and H. Schreiber. 2007. On full-scale avalanche measurements at the Ryggfonn test site, Norway, *Cold Regions Science and Technology*, **49**, 39–53.

Gauer, P., and K. Kristensen. 2005. Avalanche Studies and Model Validation in Europe, SATSIE: Ryggfonn measurements. Overview and dam interaction, *NGI Report 20021048-10*, Norwegian Geotechnical Institute, Oslo.

Gray, J. M. N. T., Y.-C. Tai and S. Noelle. 2003. Shock waves, dead-zones and particle-free regions in rapid granular free surface flows, *J. Fluid Mech*, **491**, 161–181.

Gray, J. M. N. T., M. Wieland and K. Hutter. 1999. Gravity-driven free surface flow of granular avalanches over complex basal topography, *Proc. R. Soc. Lond. A*, **455**, 1841–1874.

Gruber, U., P. Bartelt and S. Margreth. 1999a. Anleitung zur Berechnung von Fliesslawinen, *Kursunterlagen/course material*, Eidg. Institut für Schnee- und Lawinenforschung, Davos.

Gruber, U., P. Bartelt and S. Margreth. 1999b. Neue Berechnungsmethoden in den Lawinengefahrenkartierung, *Tech. Rep. Part III*, Eidg. Institut für Schnee- und Lawinenforschung, Davos.

GVA. 1994. Vorschriften für bauliche Massnahmen an Bauten in der blauen Lawinenzone, Gebäudeversicherung Graubünden, Chur, Switzerland.

Hager, W. H. 1992. Energy Dissipators and Hydraulic Jump, Kluwer Academic Publishers, Dordrecht.

Hager, W. H., and D. L. Vischer. 1995. Energy Dissipators, Balkema Publishers, Dordrecht.

Haraldsdóttir, S. H. 1997. Snjóflóðasaga Neskaupstaðar (Avalanche history of Neskaupstaður), *Report R97002*, IMO, Reykjavík.

Harbitz, C. B., and U. Domaas. 1997. Run-out distance: Mapping of natural deflecting dams, *Report 581210-1*, Norwegian Geotechnical Institute, Oslo.

Harbitz, C. B., and U. Domaas. in prep. Mapping of natural deflecting dams and application of a centre-of-mass model, *Report 581210-2*, Norwegian Geotechnical Institute, Oslo.

Harbitz, C. B., U. Domaas and A. Engen. 2001. Design of snow avalanche deflecting dams, *Report 589000-4*, Norwegian Geotechnical Institute, Oslo, also in: *Proceedings of the 9th Interpraevent 2000 Congress, 26^{th} – 30^{th} June 2000*, Villach, Austria, **1**, 383–396.

Hauksson, S., M. Pagliardi, M. Barbolini and T. Jóhannesson. 2007. Laboratory measurements of impact forces of supercritical granular flow against mast-like obstacles, *Cold Regions Science and Technology*, **49**, 54–63.

Hogg, A. J., J. M. N. T. Gray and X. Cui. 2005. Granular vacua, R. Carcia-Rojo, H. J. Herrmann and S. McNamara, eds., Powders and grains 2005, A. A. Balkema, Rotterdam, 929–933.

Holzinger, G., and J. Hübl. 2004. Belastung eines Murbrechers: Abgeleitet aus Laborversuchen (Impact forces on a debris flow breaker: Derived from laboratory experiments), Mikos, M. and D. Gutknecht, eds., 10. Kongress Interpraevent 2004, 24.–27. Mai 2004, Riva del Garda, Trient, vol. 3, 131–139.

Hákonardóttir, K. M. 2000. Retarding effects of breaking mounds—avalanches, Master's thesis, University of Bristol, School of Mathematics, Bristol, England.

Hákonardóttir, K. M. 2004. The interaction between snow avalanches and dams, Ph.D. thesis, University of Bristol, School of Mathematics, Bristol, England.

Hákonardóttir, K. M., and A. J. Hogg. 2005. Oblique shocks in rapid granular flows, *Physics of Fluids*, **17**, 077101.

Hákonardóttir, K. M., A. J. Hogg and T. Jóhannesson. 2003a. A laboratory study of the interaction between supercritical shallow flows and dams, *Report 03038*, IMO, Reykjavík.

Hákonardóttir, K. M., A. J. Hogg, T. Jóhannesson, M. Kern and F. Tiefenbacher. 2003b. Large-scale avalanche braking mound and catching dam experiments with snow. A study of the airborne jet, *Surveys in Geophysics*, **24**, 543–554.

Hákonardóttir, K. M., A. J. Hogg, T. Jóhannesson and G. G. Tómasson. 2003c. A laboratory study of the retarding effects of braking mounds on snow avalanches, *Journal of Glaciology*, **49**(165), 191–200.

Hákonardóttir, K. M., T. Jóhannesson, F. Tiefenbacher and M. Kern. 2001. A laboratory study of the retarding effect of braking mounds in 3, 6 and 9 m long chutes, *Report 01007*, IMO, Reykjavík.

Hákonardóttir, K. M., T. Jóhannesson, F. Tiefenbacher and M. Kern. 2003d. Avalanche braking mound experiments with snow. Switzerland — March 2002, *Report 03023*, IMO, Reykjavík.

Indriðason, H. D., F. Sigurðsson, G. G. Tómasson and K. M. Hákonardóttir. 2008. Avalanche protections in Iceland designed by VST Consulting Engineers Ltd.: Experience and

examples, Jóhannesson, T., E. Hestnes, G. Eiríksson and J. Gunnarsson, eds., International Symposium on Mitigative Measures against Snow Avalanches, Egilsstaðir, Iceland, 11–14 March 2008, Association of Chartered Engineers in Iceland, Reykjavík, 124–129.

Indriðason, J. S. 2008. Avalanche protection—Some aspects of design and construction, Jóhannesson, T., E. Hestnes, G. Eiríksson and J. Gunnarsson, eds., International Symposium on Mitigative Measures against Snow Avalanches, Egilsstaðir, Iceland, 11–14 March 2008, Association of Chartered Engineers in Iceland, Reykjavík, 188–195.

Irgens, F., B. Schieldrop, C. B. Harbitz, U. Domaas and R. Opdahl. 1998. Simulations of dense-snow avalanches on deflecting dams, *Annals of Glaciology*, **26**, 265–271.

Issler, D. 1999. Berücksichtigung der Staublawinen in der Gefahrenkartierung, *Kursunterlagen/course material*, Eidg. Institut für Schnee- und Lawinenforschung, Davos.

Issler, D. 2003. Experimental information on the dynamics of dry-snow avalanches, Hutter, Kolumban and Nina Kirchner, eds., Dynamic Response of Granular and Porous Materials Under Large and Catastrophic Deformations, Springer, Berlin, vol. 11 of *Lecture Notes in Applied and Computational Mechanics*, 109–160.

Issler, D., P. Gauer, M. Schaer and S. Keller. 1996. Staublawinenereignisse im Winter 1995: Seewis (GR), Adelboden (BE) und Col du Pillon (VD), *Internal Report 694*, Eidg. Institut für Schnee- und Lawinenforschung, Davos.

Johnson, K. L. 2001. Contact Mechanics, Cambridge University Press, Cambridge, U.K.

Jóhannesson, T. 2001. Run-up of two avalanches on the deflecting dams at Flateyri, northwestern Iceland, *Annals of Glaciology*, **32**, 350–354.

Jóhannesson, T., and K. M. Hákonardóttir. 2003. Remarks on the design of avalanche braking mounds based on experiments in 3, 6, 9 and 34 m long chutes, *Report 03024*, IMO, Reykjavík.

Jóhannesson, T., K. M. Hákonardóttir, C. B. Harbitz and U. Domaas. 2008. Background for the determination of dam height in the SATSIE dam design guidelines, *Report 08003*, IMO, Reykjavík.

Jónasson, K., Þ. Arnalds and S. Sigurðsson. 1999. Estimation of avalanche risk, *Report R99001*, IMO, Reykjavík.

Keller, S. 1996. Physikalische Simulation von Staublawinen – Experimente zur Dynamik im dreidimensionalen Auslauf, *Mitteilung 141*, Versuchsanstalt für Wasserbau, Hydrologie und Glaziologie, ETH Zürich, Zürich.

Keller, S., and D. Issler. 1996. Staublawinen über Dämme und Mauern im Labor: Zusammenstellung aller Resultate und Auswertung. Bericht zuhanden des Schweiz. IDNDR-Komitees, *Internal Report 697*, Eidg. Institut für Schnee- und Lawinenforschung, Davos.

Kotlyakov, V. M., B. N. Rzhevskiy and V. A. Samoylov. 1977. The dynamics of avalanching in the Khibins, *Journal of Glaciology*, **19**(81), 431–439.

Kulibaba, V.S., and M. E. Eglit. 2008. Numerical modeling of an avalanche impact against an obstacle with account of snow compressibility, *Annals of Glaciology*, **49**, 27–32.

Larsen, J. O. 1998. Snow-creep forces on masts, *Annuals of Glaciology*, **26**, 19–21.

Lied, K., B. Instanes, U. Domaas and C. B. Harbitz. 1998. Snow avalanche at Bleie, Ullensvang, January 1994, Hestnes, E., ed., 25 Years of Snow Avalanche Research, Voss 12–16 May 1998, Norwegian Geotechnical Institute, Oslo, vol. 203, 175–181.

Lied, K., and K. Kristensen. 2003. Snøskred. Håndbok om Snøskred, Vett & Viten as., Oslo.

Margreth, S. 1998. Velocity profiles. Siglufjörður, Iceland, *Technical report*, SLF, Davos.

Margreth, S. 2004. Avalanche control structures, Grenoble, course material presented at the

Université Européenne d'Eté, session 2004, Courmayeur: "Avalanches: Risque, zonage et protections".

Margreth, S. 2007. Snow pressure on cableway masts: Analysis of damages and design approach, *Cold Regions Science and Technology*, **47**(1–2), 4–15.

Margreth, S., and K. Platzer. 2008. New findings on the design of snow sheds, Jóhannesson, T., G. Eiríksson, E. Hestnes and J. Gunnarsson, eds., International Symposium on Mitigative Measures against Snow Avalanches Egilsstaðir, Iceland, 11–14 March 2008, Association of Chartered Engineers in Iceland, 32–37.

McClung, D., and P. Schaerer. 1993. The Avalanche Handbook, The Mountaineers, Seattle, USA.

McClung, D. M., and P. A. Schaerer. 1985. Characteristics of flowing snow and avalanche impact pressures, *Annals of Glaciology*, **6**, 9–14.

Mellor, M. 1968. Cold Regions Science and Engineering, *Part III: Engineering, Section A3: Snow Technology. Avalanches*, Cold Regions Research & Engineering Laboratory, Hanover, New Hampshire.

Mohrig, D., and J. G. Marr. 2003. Constraining the efficiency of turbidity current generation from submarine debris flows and slides using laboratory experiments, *Marine Petrol. Geol.*, **20**, 883–899.

Naaim-Bouvet, F., M. Naaim, M. Bacher and L. Heiligenstein. 2002. Physical modelling of the interaction between powder avalanches and defence structures, *Natural Hazards Earth Systems Sciences*, **2**, 193–202.

Naaim-Bouvet, F., M. Naaim and T. Faug. 2004. Dense and powder avalanches: Momentum reduction generated by a dam, *Annals of Glaciology*, **38**, 373–378.

Naaim-Bouvet, F., S. Pain, M. Naaim and T. Faug. 2003. Numerical and physical modelling of the effect of a dam on powder avalanches motion: Comparison with previous approaches, *Surveys in Geophysics*, **24**, 479–498.

NGI and VA. 2003. Snjóflóðavarnir á Seyðisfirði. Aldan og Bakkahverfi. Frumathugun (Avalanche protection measures for Seyðisfjörður. Aldan and Bakkahverfi. Appraisal), *Report NGI:20021036/VA:VA-0156*, Norwegian Geotechnical Institute and Verkfræðistofa Austurlands, Egilsstaðir, Iceland.

Norem, H. 1990. Ryggfonn-Prosjektet, *NGI Report 581200-16*, Norwegian Geotechnical Institute, Oslo, Norway, (in Norwegian).

Norem, H. 1991. Estimating snow avalanche impact pressures on towers, Gubler, H.U., ed., Proceedings of a Workshop on Avalanche Dynamics, 14–19 May 1990, Mitt. 48, Eidg. Institut für Schnee- und Lawinenforschung, Davos, 42–56.

Norem, H. 1994. Snow Engineering for Roads, *Tech. rep.*, Norwegian Public Roads Administration, Oslo.

Novak, P., A. I. B. Moffat, C. Nalluri and R. Narayanan. 1989. Hydraulic Structures, Unwin Hyman, London, UK.

Pain, S. 2002. Simulation numérique de l'interaction entre une avalanche aerosol et une digue d'arrêt, Master's thesis, Université Joseph Fourier, Cemagref, Grenoble, France.

Pazwash, H., and J. M. Robertson. 1975. Forces on Bodies in Bingham Fluids, *Journal of Hydraulic Research*, **13**(1), 35–55.

Peterka, A. J. 1984. Hydraulic design of stilling basins and energy dissipators, *Engineering Monograph 25*, US Bureau of Reclamation, US Department of the Interior, Denver.

Pfeiff, C. F., and E. J. Hopfinger. 1986. Drag on cylinders moving through suspensions with

high solid concentrations, *PhysicoChemical Hydrodynamics*, **7**(2/3), 101–109.

Primus, M., F. Naaim-Bouvet, M. Naaim and T. Faug. 2004. Physical modeling of the interaction between mounds or deflecting dams on powder avalanches, *Cold Regions Science and Technology*, **39**, 257–267.

Roberson, J. A., J. J. Cassidy and M. H. Chaudhry. 1997. Hydraulic Engineering, Houghton Mifflin Company, Boston, *etc.*

Rudolf-Miklau, F., and F. Schmid. 2004. Implementation, application and enforcement of hazard zone maps for torrent and avalanche control in Austria, *Forstliche Schriftenreihe 18*, Universität für Bodenkultur, Wien.

Salm, B. 1987. Schnee, Lawinen und Lawinenschutz, Vorlesungsskript, ETH, Zürich.

Salm, B., A. Burkard and H. U. Gubler. 1990. Berechnung von Fliesslawinen. Eine Anleitung für Praktiker mit Bleispielen, *Mitteilung 47*, Eidg. Institut für Schnee- und Lawinenforschung, Davos.

Sampl, P., F. Naaim-Bouvet and M. Naaim. 2004. Interaction between dams and powder avalanches: Determination of simple friction laws for shallow water avalanche models, *Cold Regions Science and Technology*, **39**, 115–131.

Sauermoser, S. 2006. Avalanche hazard mapping—30 years experience in Austria, Proceedings of the 2006 International Snow Science Workshop, Telluride, Colorado, ISSW USA, Colorado, USA, 314–321.

Schaer, M., and D. Issler. 2001. Particle densities, velocities and size distributions in large avalanches from impact-sensor measurements, *Annals of Glaciology*, **32**, 321–327.

Schaerer, P. A., and A. A. Salway. 1980. Seismic and impact-pressure monitoring of flowing avalanches, *Journal of Glaciology*, **26**(94), 179–187.

Sigurðsson, F., G. G. Tómasson and H. D. Indriðason. 2003. Snjóflóðavarnir í Neskaupstað. Tröllagiljasvæði. Frumathugun (Avalanche appraisal study for the Tröllagil area, Neskaupstaður), *Report VST:2001.1006*, VST Consulting Engineers, Reykjavík.

Sigurðsson, F., G. G. Tómasson and F. Sandersen. 1998. Avalanche defences for Flateyri, Iceland. From hazard evaluation to construction of defences, Hestnes, E., ed., 25 Years of Snow Avalanche Research, Voss 12–16 May 1998, NGI Report 203, Norwegian Geotechnical Institute, Oslo, 254–258.

SLF. 1990. Richtlinien für den Lawinenverbau im Anbruchgebiet., Eidg. Forstdirektion and Eidg. Inst. Schnee- und Lawinenforsch., Bern.

Sovilla, B., M. Schaer, M. Kern and P. Bartelt. 2008a. Impact pressures and flow regimes in dense snow avalanches observed at the Vallée de la Sionne test site, *Journal of Geophysical Research, Earth-Surfaces*, **113**, F01010.

Sovilla, B., M. Schaer and L. Rammer. 2008b. Measurements and analysis of full-scale avalanche impact pressure at the Vallée de la Sionne test site, *Cold Regions Science and Technology*, **51**, 122–137.

The Ministry for the Environment. 2000. Regulation on hazard zoning due to snow- and landslides, classification and utilisation of hazard zones and preparation of provisional hazard zoning, Reykjavík.

Thibert, E. L., D. Baroudi, A. Limam and P. Berthet-Rambaud. 2008. Avalanche impact pressure on an instrumented structure, *Cold Regions Science and Technology*, **xxx**, doi:10.1016/j.coldregions.2008.01.005.

Tómasson, G. G., F. Sigurðsson and F. Rapin. 1998a. The avalanche situation in Neskaupstaður, Iceland. A preliminary defensive plan, Hestnes, E., ed., 25 Years of Snow Avalan-

che Research, Voss 12–16 May 1998, NGI Report 203, Norwegian Geotechnical Institute, Oslo, 283–287.

Tómasson, G. G., F. Sigurðsson and F. Rapin. 1998b. Neskaupstaður. Avalanche defence appraisal. Drangagil area, *Report VST:97.202/Cemagref:97-024*, VST Consulting Engineers and Cemagref, Reykjavík.

US Bureau of Reclamation. 1987. Design of small dams. 3rd edn., US Department of the Interior, Washington, DC.

Vilhjálmsson, R., and Ó. Ingþórsson. 2008. The role of landscape architects in the design team. Why landscape architects are needed in the design team of large scale projects!, Jóhannesson, T., E. Hestnes, G. Eiríksson and J. Gunnarsson, eds., International Symposium on Mitigative Measures against Snow Avalanches, Egilsstaðir, Iceland, 11–14 March 2008, Association of Chartered Engineers in Iceland, Reykjavík, 196–199.

Voellmy, A. 1955. Über die Zerstörungskraft von Lawinen, *Schweizerische Bauzeitung (Sonderdruck aus dem 73. Jahrgang)*, **73**(12, 15, 17, 19, 37), 3–25.

VS and NGI. 1997. Frumathugun á snjóflóðavörnum (Avalanche defence appraisal), *Report*, Verkfræðistofa Siglufjarðar and Norwegian Geotechnical Institute, Siglufjörður, Iceland.

VST and Cemagref. 1998. Neskaupstaður. Avalanche defences. Protection plan for the residential area, *Report VST:97.202/Cemagref:97-024*, VST Consulting Engineers and Cemagref, Reykjavík.

VST and NGI. 1996. Flateyri. Avalanche defence appraisal, *Report VST:96.201/NGI:964022-1*, VST Consulting Engineers and Norwegian Geotechnical Institute, Reykjavík.

Wassgren, C. R., J. A. Cordova, R. Zenit and A. Karion. 2003. Dilute granular flow around an immersed cylinder, *Physics of Fluids*, **15**(11), 3318–3330.

Whitham, G. B. 1999. Linear and Nonlinear Waves, John Wiley & sons, Inc., New York, *etc.*

Wieghardt, K. 1975. Experiments in granular flow, *Annual Review of Fluid Mechanics*, **7**, 89–114.

Woods, A. W., and A. J. Hogg. 1998. Snow avalanches. Models of particle-laden currents and avalanche protection measures, *Tech. rep.*, University of Bristol, Centre for Environmental and Geophysical Research, School of Mathematics, Bristol.

Woods, A. W., and A. J. Hogg. 1999. Experiments on granular flows passing over obstacles on an inclined chute, *Tech. rep.*, University of Bristol, Centre for Environmental and Geophysical Research, School of Mathematics, Bristol.

Yakimov, Yu. L., I. E. Shurova and Tz. I. Stavskii. 1979. Eksperimentalnoe issledovanie vzaimodeistvija snezhnogo potoka s klinovidnimi prepjatstvijami (Experimental study of an interaction of a snow flow with wedge-shaped obstacles), *Report 2145*, Institute of Mechanics, Moscow State University.

Yih, C.-S. 1979. Fluid Mechanics, West River Press, Ann Arbor, USA.

A Summary of the dam design procedure

It is proposed that the design height of *both catching and deflecting dams* be determined based on essentially the *same dynamic principles*, and be carried out in a stepwise fashion according to the following list.

The required dam height, H, normal to the terrain, is the sum of the run-up of the design avalanche on the dam side, h_r, and the snow depth on the terrain upstream of the dam, h_s,

$$H = h_r + h_s \ , \quad \text{where} \quad h_r = \max(H_{cr} + h_{cr}, h_2 + \Delta H_{\psi_\perp} + \Delta H_\kappa) \ ,$$

(Eq. (5.3)). The steps are as follows (see Figs. 4.1, 4.2, 5.1, 5.2, 5.3 and 5.4 and Appendix B for explanations of the meaning of the variables; equation numbers given in the text following each equation refer to equations in the main text where the same equations are given with additional explanations):

1. Estimate appropriate design values for the velocity and flow depth of the avalanche at the location of the dam, u_1, h_1, and for the snow depth on the terrain upstream of the dam, h_s.

2. For a deflecting dam, determine the deflecting angle φ (for a catching dam, $\varphi = 90^\circ$).

3. Compute the Froude number of the flow, Fr, according to

$$\mathrm{Fr} = \frac{u_1}{\sqrt{g \cos(\psi)\, h_1}}$$

   (Eq. (4.1)).

4. Determine the momentum loss coefficient, k, according to

$$k = 0.75 \text{ for } \alpha > 60^\circ \ , \quad k = 0.75 + 0.1(60^\circ - \alpha)/30^\circ \quad \text{for} \quad 30^\circ \le \alpha \le 60^\circ \ ,$$

   (Eq. (5.14). k represents the loss of momentum normal to the dam axis during impact, and depends on the angle of the upper dam side with respect to the terrain, α.

5. Compute the sum of the critical dam height, H_{cr}, and the corresponding critical flow depth, h_{cr}, according to

$$(H_{cr} + h_{cr})/h_1 = \frac{1}{k} + \frac{1}{2}(k\,\mathrm{Fr}\sin\varphi)^2 - \frac{1}{2}(\mathrm{Fr}\sin\varphi)^{2/3}$$

   or

$$H_{cr} + h_{cr} = \frac{h_1}{k} + \frac{(u_1 \sin\varphi)^2}{2g\cos\psi} k^2 (1 - k^{-2}(\mathrm{Fr}\sin\varphi)^{-4/3})$$

   (Eqs. (5.6) and (5.7)) (see Fig. 5.5). The dam height above the snow cover must be greater than $H_{cr} + h_{cr}$. If the dam height above the snow cover is lower than H_{cr}, the avalanche may overflow in a supercritical state. If the dam height is lower than $H_{cr} + h_{cr}$, the front of the avalanche may overflow the dam while a shock is being formed. Note that some overflow may occur in the initial impact due to splashing, even when this criterion is satisfied.

6. Compute the flow depth, h_2, downstream of a shock upstream of the dam according to

$$h_2/h_1 = (2\sqrt{(6\mathrm{Fr}_\perp^2+4)}\cos\delta+1)/3\ ,$$

where δ is defined as

$$\delta = \frac{1}{3}\left(\frac{\pi}{2} - \tan^{-1}\left(\frac{9\mathrm{Fr}_\perp^2-8}{\mathrm{Fr}_\perp\sqrt{27(16+13\mathrm{Fr}_\perp^2+8\mathrm{Fr}_\perp^4)}}\right)\right)\ ,$$

(Eqs. (5.10) and (5.11)) (see Fig. 5.7). $\mathrm{Fr}_\perp = \mathrm{Fr}\sin\varphi$ is the "Froude number" corresponding to the component of velocity normal to the dam, $|u_\eta| = u_1\sin\varphi$. The dam height above the snow cover, h_r, must also be greater than h_2.

7. The requirements expressed by the previous two items in the list are shown graphically in Figure 5.11. The design dam height above the snow cover, $h_r = H - h_s$, corresponding to given values of h_1 and $|u_\eta|$, may be read directly off the higher of the two curves (representing supercritical overflow and flow depth downstream of a shock, respectively).

8. For a *deflecting dam*, check whether an attached, stationary, oblique shock is dynamically possible, by verifying that the deflecting angle, φ, is smaller than the maximum deflecting angle, $\varphi_{\max}$, corresponding to the Froude number Fr according to

$$\varphi_{\max} = \frac{\pi}{2} - \frac{2^{3/4}}{\mathrm{Fr}^{1/2}} - \frac{2^{1/4}}{6\,\mathrm{Fr}^{3/2}}$$

(Eq. (5.13)) (see Fig. 5.8). It is recommended that φ be at least 10° smaller than $\varphi_{\max}$. If a dam does not satisfy this requirement, the flow depth downstream of the shock, h_2, in item 5 must be calculated for $\varphi = 90^\circ$. The dam is thus dimensioned as a catching dam with regard to the flow depth downstream of the shock, while the criterion based on supercritical overflow in item 4 is computed with the original value of φ as before.

9. If the terrain normal to the dam axis slopes towards the dam, the height of a *deflecting dam* derived from shock dynamics (see item 5) must be increased by $\Delta H_{\psi_\perp}$ according to

$$\Delta H_{\psi_\perp} = \frac{\sqrt{2}\tan\psi_\perp}{2\,\mathrm{Fr}\cos\varphi}\,\xi$$

(Eq. (6.2)). The dam height corresponding to supercritical overflow ($H_{cr}+h_{cr}$, see item 4) is not increased due to this effect.

10. If the dam axis is curved, the height of a *deflecting dam* derived from shock dynamics (see item 5) must be increased by ΔH_κ according to

$$\Delta H_\kappa = \frac{\sqrt{2}\,(u_1\cos\varphi)^2}{2\,\mathrm{Fr}\cos(\varphi)\,g\,\cos(\psi)\,R_\kappa}\,\xi$$

(Eq. (6.3)). This term may be in addition to $\Delta H_{\psi_\perp}$ in case that the upstream terrain slopes towards the dam as described in the previous item. The dam height corresponding to supercritical overflow ($H_{cr}+h_{cr}$, see item 4) is not increased due to this effect.

11. Compute the vertical dam height, H_D, from $H = h_r + h_s$ using

$$H_D = \frac{\cos\psi - \sin\varphi \sin\psi \cot\alpha}{1 - \cos^2\varphi \sin^2\psi} H$$

(Eq. (5.1)).

12. For a *deflecting dam*, evaluate the extent of the region affected by an *increased run-out distance*, caused by the interaction of the avalanche with the dam (see Section 6.6). The construction of a dam leads to increased avalanche risk within this area. Also, evaluate the *lateral spreading of the avalanche downstream of the dam* (see Section 6.7). Possible lateral spreading limits the area protected by the dam.

13. For a *catching dam*, compute the available storage space per unit width upstream of the dam according to

$$S = \int_{x_0}^{x_1} z_l - (z_s + h_s) dx$$

(Eq. (7.1)), where z_l represents the elevation of a straight line from the top of the dam towards the mountain with a slope in the range 0–10°. The *storage per unit width* or *storage area*, S, must be larger than the volume of the avalanche divided by its width (see Fig. 7.1).

The main new features of this procedure to dimension dams are:

- The dam design is based on a *consistent dynamic description* of the interaction of shallow granular flow and an obstacle.
- *Shock dynamics* are used to derive run-up heights on dams, which under some conditions determine the dam height.
- The necessary dam height to prevent *supercritical overflow* is also used to derive run-up heights on dams, which determines the design-dam height under other conditions.
- A *maximum allowable deflecting angle*, derived from shock dynamics, limits the range of possible deflecting angles of deflecting dams.
- *Momentum loss during impact with a dam* is calculated in the same way for both catching and deflecting dams from the component of velocity normal to the dam.
- Avalanche flow along deflecting dams becomes *channelised*, which may lead to a substantial *increase in run-out* in the direction of the channelised flow.
- A consistent dynamic framework makes it possible to account for the *slope of the terrain* on which a dam is located, and a *curvature of the dam axis* in the dam design.

In practice, these requirements are accounted for in an iterative process, in which the dam location, the slope of the upstream face and the deflecting angle of the dam are varied to minimise construction cost, while taking into account other relevant conditions, such as distance to the protected settlement, availability of suitable construction materials, and various environmental aspects.

The above procedure is not applicable for wet-snow avalanches or slushflows. Qualitative considerations about dams against wet-snow avalanches are given in Section 8.

B Notation

The following list defines the main variables used to describe the geometry of the terrain and the dam, the flow of the (dense core of the) avalanche at the dam location and variables used in the analysis of loads on structures. Figures 4.1, 4.2, 5.1, 5.2 and 5.3 provide schematic illustrations of the meaning of the variables.

α Angle of the dam side with respect to the sloping terrain in the direction normal to the dam axis in a plane normal to the upstream terrain. α is also used to denote a factor that accounts for a non-uniform vertical velocity profile of the avalanche in impact pressure calculations.

α_s The steepest inclination of the dam side.

δ, δ^* Compression and maximum compression during the impact of a solid body with a wall.

Δ Widening of a shock along a deflecting dam, $\Delta = \theta - \varphi$.

η_s Width of a shock in the direction normal to the dam axis.

θ Shock angle for a stationary, oblique shock upstream of a deflecting dam.

λ An empirical parameter describing the effect of momentum loss during the impact and the effect of friction of the avalanche against the upstream side of the dam in the traditional expression for design dam height.

μ Friction coefficient for Coulomb friction.

ν_b, ν_w, ν Poisson ratio of a boulder, a wall and an effective Poisson ratio, respectively.

ξ Distance along the dam axis from the upstream end of a (possibly curved) deflecting dam.

ρ Density.

ρ_a Density of air, approximately $1.2\,\mathrm{kg\,m^{-3}}$ near sea level.

σ_x Longitudinal stress.

τ_y Critical shear stress in the flow of an avalanche parallel to a wall.

ϕ Internal friction angle of avalanching snow.

φ Deflecting angle of the dam ($\varphi = 90^\circ$ for a catching dam) in a sloping coordinate system aligned with the terrain.

φ_h Deflecting angle of the dam ($\varphi_h = 90^\circ$ for a catching dam) in the map plane, *i.e.* the angle between horizontal projections of the avalanche direction and the dam axis.

φ_{lsp} Maximum lateral spreading (in terms of the angular width of the fan) beyond the dam axis formed at the downstream end of a deflecting dam.

$\varphi_{\max}$ Maximum deflecting angle for which an attached, stationary, oblique shock may be formed.

ψ Slope of the terrain at the location of the dam.

$\psi_\perp$ Slope of the terrain in the direction normal to the dam axis.

$\mathcal{A}$ The contact area of a body hit by an avalanche.

A Projected area of a body submerged or partly immersed in a flow normal to the flow direction.

A_∞ Projected area of a body submerged or partly immersed in a flow normal to the flow direction corresponding to flow depth upstream of the body.

b Effective width of the area of a wall that is hit by an avalanche, *i.e.* the minimum of the avalanche width and the width of the wall, *i.e.*, $b = \min(W_a, W_{wall})$.

c Propagation speed of a shock or a discontinuity in avalanche flow.

C_D Drag factor.

C_D^* Effective drag factor corresponding to the total drag force due to pressure drag, friction drag and unbalanced static load.

C_p**,** C_f Drag factors related to the pressure distribution and the skin friction in the flow around a body. C_p is also used to denote the celerity of a pressure wave.

d Particle diameter.

D Cylinder diameter.

E_b**,** E_w**,** E^* Elastic moduli of a boulder, a wall and an effective elastic modulus, respectively. E_b is also used to denote the bulk elastic modulus of a fluid.

E_c Energy dissipated by the "effective" dam that is hit by an avalanche.

E_n Kinetic energy of an avalanche at the upstream base of a dam that is hit by an avalanche.

f A dimensionless constant representing turbulent drag caused by air resistance on an airborne jet that is formed during the impact of flow against a mound or a dam.

F_D Total drag force.

F_I Impact force due to the impact of a solid body.

F_{Ix} Impact force normal to a wall.

$\mathbf{F_m}$**,** $\mathbf{M}$ Total force and moment on an object hit by an avalanche.

F_p**,** F_f Pressure drag and friction drag on a body submerged or partly immersed in a flow.

F_{sx}**,** F_{dx}**,** F_{flx}**,** F_{px} Total normal force onto an obstacle from the snowpack (s), dense flow (d), fluidised part (fl) and powder part (p) of an avalanche.

F_{sz}, F_{dz}, F_{flz}, F_{pz} Total lift force onto an obstacle from the snowpack (s), dense flow (d), fluidised part (fl) and powder part (p) of an avalanche.

Fr Froude number, $\mathrm{Fr} = \frac{u}{\sqrt{g\cos(\psi)\,h_1}}$.

$\mathrm{Fr}_\perp$ "Froude number" corresponding to the component of the velocity normal to the dam, $\mathrm{Fr}_\perp = \mathrm{Fr}\sin\varphi$.

Fr_∞ Froude number corresponding to flow depth and flow velocity upstream of a body submerged or partly immersed in a flow.

g Gravitational acceleration, $g = 9.8\,\mathrm{m\,s^{-2}}$.

h_1 Flow depth of the oncoming avalanche upstream of any disturbance to the flow caused by the dam.

h_2 Flow depth downstream of a shock that is formed in the flow against a dam.

h_∞ Flow depth upstream of a body submerged or partly immersed in a flow.

h_b Flow depth of an avalanche at the upstream base of a dam that is hit by an avalanche.

h_{cr} Critical flow depth. Depth of flow over a dam with height H_{cr} at the top of the dam.

h_{fb} Free board height of a dam, *i.e.* the dam height measured from the top of the snow cover and previous avalanche deposits upstream of the dam.

h_r Run-up height or design dam height, depending on the context, above the snow cover, $h_r = \max(H_{cr} + h_{cr}, h_2 + \Delta H_{\psi_\perp} + \Delta H_\kappa)$.

h_s, h_d, h_{fl}, h_p Height of the snowpack (s), and the flow height of dense flow (d), fluidised part (fl) and powder part (p) of an avalanche.

h_u, h_f, h_s Contributions to the vertical dam height, H_D, in the traditional design criterion for dam height, Equation (3.1). h_u is the required height due to the kinetic energy or the velocity of the avalanche, h_f is the thickness of the flowing, dense core of the avalanche and h_s is the thickness of snow and previous avalanche deposits on the ground on the upstream side of the dam before the avalanche falls.

h_{up}, h_{dn} Run-up height upstream of an obstacle and flow depth immediately downstream of an obstacle extending through the flow.

H Dam height measured in the direction normal to the sloping terrain.

H_{cr} Critical dam height. The maximum height of a dam over which uninterrupted, supercritical flow may be maintained.

H_D Vertical dam height measured in a vertical cross section normal to the dam axis in a horizontal plane.

H_{mast} Height of a mast.

H_{wall} Height of a wall that is hit by an avalanche.

ΔH_{κ} Extra deflecting dam height due to the effect of the curvature of the dam axis.

$\Delta H_{\psi_{\perp}}$ Extra deflecting dam height due to terrain slope towards the dam.

He Hedstrom number, $\mathrm{He} = \rho k L^2/\mu_B^2$ (L is a length-scale and k and μ_B the yield stress and the Bingham viscosity, respectively).

k Relative reduction in normal velocity in the initial impact with the dam.

Kn Knudsen number, *i.e.*, ratio between the upstream particle free-path length to the obstacle diameter.

l_{cont} Run-out length in a control experiment without a dam measured from the location of dams in other experiments.

l_{ovr} Overrun length measured from the top of a dam that is scaled by an avalanche.

l_{track} Travel distance along the track from the starting zone.

L, h_j, β Horizontal length, thickness and initial throw angle of an airborne jet or a jump that is formed in the impact of flow against a mound or a dam.

m_b, m_w, m Mass of a boulder, a wall and an effective mass, respectively.

m_r Estimated fraction of the total deposit mass which surpassed the crown of a dam that is hit by an avalanche.

M_{ovr} The mass of the part of the deposit of an avalanche which surpassed the crown of a dam.

M_{sy}, M_{dy}, M_{fly}, M_{py} Total moment onto an obstacle about an axis at ground level from the snowpack (s), dense flow (d), fluidised part (fl) and powder part (p) of an avalanche.

M_{tot} The total mass of the deposit of an avalanche.

$M_{N,M}$, $M'_{N,M}$ Moment load and moment load per unit length due to snow pressure for a narrow obstacle, respectively.

n_f Shape factor exponent describing the decrease in dynamic pressure with height within the fluidised layer.

p_0 Atmospheric pressure ($\approx$ 1000 hPa).

p_a Dynamic pressure corresponding to the density of air and the front velocity of the avalanche, $p_a = \rho_a u_f^2/2$.

p_s, p_d, p_{fl}, p_p Pressure within the snowpack (s) and dynamic pressure in the dense flow (d), fluidised part (fl) and powder part (p) of an avalanche.

p_{peak} Peak pressure.

p_I Local impact pressure due to the impact of a solid body.

r Vertical run-up of an avalanche measured in a vertical section normal to a dam or obstacle axis in a horizontal plane.

R_b, R_w, R Radius or size-scale for a boulder, a wall and an effective radius or scale, respectively.

R_κ Radius of curvature of the dam axis.

Re Reynolds number, $\mathrm{Re} = \rho L u/\mu$ (L is a length-scale and μ is viscosity).

S Storage space per unit width of the avalanche above a catching dam.

$S_{N,M}$, $S'_{N,M}$ Snow pressure load and snow pressure load per unit length for a narrow obstacle, respectively.

$\mathbf{t}$ Stress tensor.

t_{imp} Duration of a short-lived peak pressure at the first instant of the impact of an avalanche with an obstacle.

u_1 Velocity of the oncoming avalanche upstream of any disturbance to the flow caused by the dam.

u_2 Velocity downstream of a shock that is formed in the flow against a dam.

u_∞ Flow velocity upstream of a body submerged or partly immersed in a flow.

u_0, u_1, u_2, u_3, u_4 The speed of an avalanche at different locations in the path as it overflows a mound or a dam.

u_b Front velocity of an avalanche at the upstream base of a dam that is hit by an avalanche.

u_f Front velocity.

u_i Internal (bed-parallel) velocity within a powder-snow avalanche or the powder layer of a dry-snow avalanche.

$\mathbf{w}$ Propagation velocity of a singular surface or discontinuity where the velocity, thickness and density of an avalanche change discontinuously.

W Width of an obstacle.

W_a Width of an avalanche.

W_{wall} Width of a wall that is hit by an avalanche.

x, y, z A coordinate system with the x,y-axes in the plane of the terrain near the dam location with the x-axis in the direction of the oncoming flow upstream of the dam. x and z may also, depending on the context, be used to denote horizontal and vertical coordinates.

z_b, z_s z-coordinates of the bottom and surface of an avalanche. z_s may also, depending on the context, be used to denote the vertical height of the surface of an avalanche.

Y Yield stress.

Quantities with a prime, for example F', denote the corresponding quantity without the prime per unit length.

C Deflecting and catching dams—Practical examples

Tómas Jóhannesson, Carl B. Harbitz and Ulrik Domaas

In this appendix, the dam height expressions derived in Sections 5 to 7 are applied to four practical examples where dams have been designed and constructed according to traditional design procedures. The design dam height according to the new criteria can thus be compared with traditionally determined dam heights in each case. The geometry of the terrain, the assumed properties of the design avalanche, *i.e.* the velocity, flow direction and flow depth at the dam location, and the principal layout and geometry of the dam, and thus the deflecting angle of deflecting dams, are taken from technical dam design documentation and are not reevaluated here. The purpose of the discussion is to demonstrate how the new dam design criteria are applied in practice, and to make a quantitative comparison between the traditional and new criteria, but not to make an independent assessment of suitable protective measures for the respective settlements.

C.1 Deflecting dams at Flateyri

Two 15–20 m high and 600 m long deflecting dams forming a wedge, and a 10 m high and 300 m long connecting catching dam, were built at Flateyri in northwestern Iceland during the years 1996–1998 (Figs. 3.3 and C1). The dams were built following a catastrophic avalanche that occurred on 26 October 1995, killed 20 people and caused great economical losses. The dams were designed by VST Consulting Engineers Ltd. together with the Norwegian Geotechnical Institute (NGI) (VST and NGI, 1996; Sigurðsson and others, 1998). The chosen design avalanches reach far into the settlement, and are assumed to correspond to a return period of 500–1000 years (Fig. C1). Flow velocities of the design avalanches were modelled with several 1D dynamic models: The PCM-model, the NIS-model, the VSG-model and an Icelandic dynamic model. Table C1 summarises the relevant properties of design avalanches, as well as the dam height components according to the design documentation and the new dam height criteria. The dams are built from loose materials taken from thalus cones below the Skollahvilft and Innra-Bæjargil gullies. The central part of the cones was largely removed to construct the dams, and the reshaped landscape above the dams was formed to direct the avalanche flow away from the dams as much as possible. The upstream dam sides have slopes of 1:1.25, but the down facing dam sides have a slope of 1:1.4. The total volume of fill material in the dams is 730–800,000 m^3.

Although the geometry of the mountainside and the dams at Flateyri is simple compared with many other avalanche paths where dams have been constructed, the determination of the deflecting angles for the dams is nontrivial. The avalanches from both paths are highly channelised. They flow out of rather narrow gullies that open onto an unconfined mountainside near 200 m a.s.l. The flow depth within the gullies may be expected to be quite large, and the avalanches will widen considerably in the first few hundred metres after their escape from lateral confinement. The avalanche flow out of the gullies will, furthermore, initially be directed at an angle to the direction of steepest descent, and the flow direction may be assumed to be slightly deflected by gravity, as the avalanche flows towards the dam. Both these effects tend to reduce the deflecting angle at which the avalanche hits the dam, particularly for the upper part of the dam, and they can be estimated result in changes of several degrees each. The best

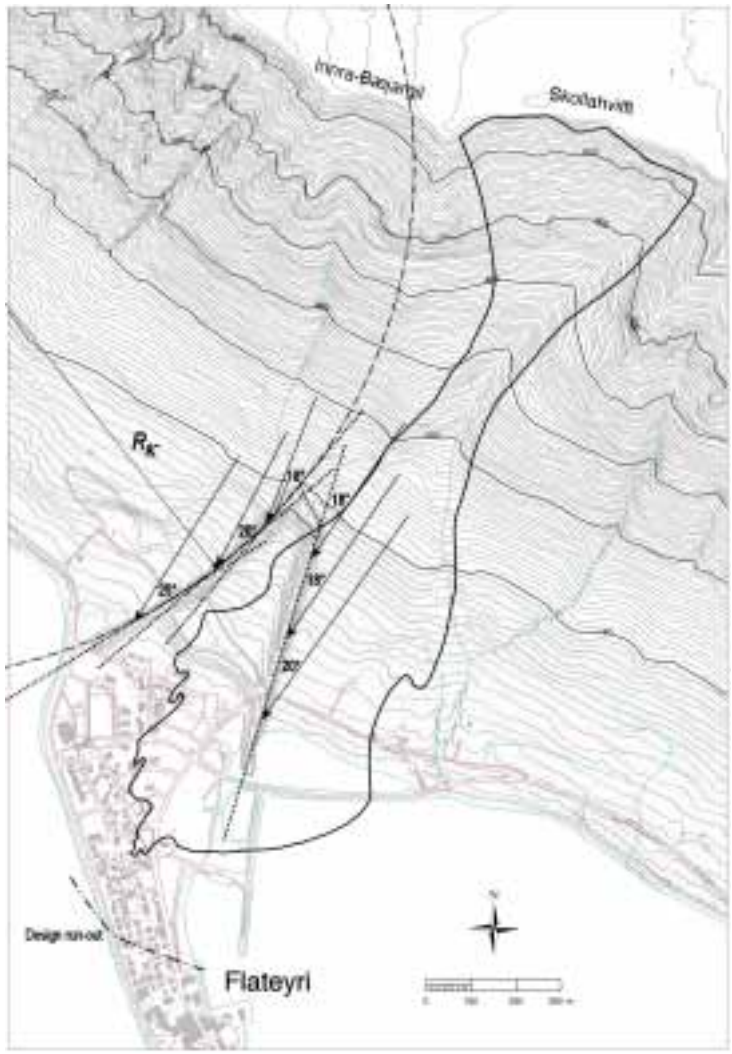

Figure C1: Deflecting dams at Flateyri, northwestern Iceland. Arrows indicate flow direction, dotted lines show the local direction of the dam axis and the dash-dotted curve is a circle fitted to the dam axis of the Innra-Bæjargil dam. The solid curve shows the outline of the catastrophic avalanche on 26. October 1995.

way to estimate the effect on the deflecting angle of various complex terrain features, such as encountered at Flateyri, is to use 2D avalanche simulations to model the flow towards the dam. It is also possible to use more qualitative methods to estimate the widening of the flow as the avalanche flows out of the gully, as well as the change in flow direction due to lateral slope, but such methods will not be described here as, they are generally inferior to simulations with 2D models that are now widely available.

Table C1 lists the different dam height components found with the traditional and new dam design criteria. The first point to notice is that flow depth downstream of the shock determines

Table C1: Design parameters and dam height for the Skollahvilft and Innra-Bæjargil avalanche dams at Flateyri, according to the traditional and the new design criteria. The first number in the H_D column for traditional design is the sum $h_u + h_1 + h_s$, where $h_u = (u_1 \sin\varphi_h)^2/(2g)$ (Eq. (3.3) with $\lambda = 1$), and the second number after the arrow ($\Rightarrow$) is the dam height according to the appraisal report. The Skollahvilft dam is almost straight so the curvature of the dam axis is assumed to be zero ($R_\kappa \to \infty$) in that case. The Innra-Bæjargil dam is slightly curved and, for simplicity, the radius of curvature for the entire dam is estimated to be $R_\kappa \approx 1150$ m. The dam height is specified at three locations for each dam, upper ("u", approximately 100 m from the upper dam end), middle ("m", near the middle of the dam) and lower ("l", approximately 100 m from the lower dam end), see Figure C1. Assuming that the upper lateral margin of the avalanche hits the dam near its upper end, this implies ξ = 100, 300, and 500 m at these three locations for each dam (*cf.* Eqs. (6.2) and (6.3)). Storage above the dams does not need to be considered for deflecting dams. See Appendix B for explanations of the variables in each column.

Dam and location	**Design avalanche and dam geometry**						**Traditional design**		**New criteria**								
	u_1	h_1	h_s	ψ	$\psi_\perp$	φ_h	h_u	H_D	H_{cr}	h_{cr}	$H_{cr}+h_{cr}$	h_2	$\Delta H_{\psi_\perp}$	ΔH_κ	h_r	H	H_D
	($m\,s^{-1}$)	(m)	(m)	(°)	(°)	(°)	(m)	(m)	(m)	(m)	(m)	(m)	(m)	(m)	(m)	(m)	(m)
Skollahv., u.	55	3	2	17	4	18	14.7	19.7 ⇒ 20	3.7	6.3	10.0	14.9	0.5	0.0	15.4	17.4	16.0
Skollahv., m.	50	3	2	8	2	18	12.2	17.2 ⇒ 18	2.8	6.0	8.8	13.9	0.8	0.0	14.8	16.8	16.0
Skollahv., l.	40	2	2	16	3	20	9.5	13.5 ⇒ 15	2.4	4.2	6.6	9.8	2.1	0.0	12.0	14.0	12.7
I-Bæjarg., u.	55	2	3	16	4	18	14.7	19.7 ⇒ 20	4.8	4.8	9.6	11.9	0.4	1.5	13.8	16.8	15.5
I-Bæjarg., m.	45	2	3	13	6	20	12.1	17.1 ⇒ 18	3.6	4.6	8.1	10.9	2.3	3.6	16.8	19.8	18.3
I-Bæjarg., l.	35	1	3	7	3	25	11.2	15.2 ⇒ 15	4.5	2.8	7.3	7.2	1.8	3.1	12.2	15.2	14.3

the dam height rather than supercritical run-up. The dam height term h_2 is 2–5 m larger than $H_{cr} + h_{cr}$, except for the lower part of the Innra-Bæjargil dam where these terms are similar. This confirms the importance of taking the run-up corresponding to flow depth downstream of the shock into account in this case.

The supercritical run-up, $H_{cr} + h_{cr}$, is calculated from Equation (5.6) or (5.7), assuming that momentum loss during the impact occurs. This is 5–7.5 m lower than the traditional estimate, $h_1 + h_u = h_1 + (u_1 \sin\varphi_h)^2/(2g)$ according to Equation (3.3) (with $\lambda = 1$, as assumed in the dam design by VST and NGI). This difference to a large extent is caused by the assumption in the new criteria that momentum is lost during impact with the dam. Without momentum loss, the difference between $H_{cr} + h_{cr}$ and $h_1 + h_u$ is within the range of 1.5–3.5 m. The remaining difference is caused by the assumption underlying Equations (5.6) and (5.7) that uninterrupted flow over the dam must be supercritical at the top of the dam. In this case, it turns out that the supercritical run-up component H_{cr} in several cases is smaller than the critical flow depth h_{cr}, indicating that the run-up contribution, corresponding to the thickening of the flow as it flows up the dam side, is an important part of the supercritical run-up.

The run-up components $\Delta H_{\psi_\perp}$ and ΔH_κ, corresponding to terrain slope towards the dam and curvature of the dam axis, respectively, are several metres each for the moderate terrain slopes and dam curvatures encountered at Flateyri.

Finally, the transformation of the dam height from height normal to the terrain to vertical height, reduces the dam height by a few metres, partly counteracting the increase in dam

Figure C2: Deflecting dams at Siglufjörður, northern Iceland. The larger Strengsgil dam is 18 m high and the smaller Jörundarskál dam is 15 m high. (Photo: Reynir Vilhjálmsson.)

height arising from $\Delta H_{\psi_\perp}$ and ΔH_κ in this case.

The vertical dam height H_D according to the new criteria is similar to the dam height according to the traditional criteria, except for the uppermost part of the dams, where the new criteria lead to approximately 4 m lower dams. This is in agreement with the qualitative discussion at the beginning of Section 6, where it is pointed out, based on observations of run-up marks on terrain obstacles, that maximum run-up is reached downstream of the location at which the avalanche first meets the deflecting landscape. The overall agreement between new and traditional criteria for the dams at Flateyri is better than may generally be expected, because flow depth downstream of dam-induced shocks is not as close to $h_1 + h_u$ according to the traditional criteria, for other combinations of flow velocity and deflecting angle. Furthermore, the agreement partly arises because of counteracting effects that may not be expected to cancel each other in other circumstances, under which, the terrain slope or the dam curvature, for example, are more pronounced than at Flateyri.

The run-up components $\Delta H_{\psi_\perp}$ and ΔH_κ amount to several metres each at some locations along the Flateyri dams (Table C1). Since the dams at Flateyri are located in comparatively flat terrain and have a gentle curvature, these new terms may be expected to be quite large relative to other run-up components for dams in steep terrain or dams with comparatively sharp bends for which those terms may be substantially larger.

C.2 Deflecting dams at Siglufjörður

A 700 m long and 18 m high deflecting dam was built below the gullies Innra- and Ytra-Strengsgil at Siglufjörður in northern Iceland during the years 1997–1999, and a smaller 200 m long and 15 m high deflecting dam below the nearby Jörundarskál avalanche path (Figs. C2 and C3). The dams were designed by Verkfræðistofa Siglufjarðar (VS) and the Norwegian Geotechnical Institute (NGI) (VS and NGI, 1997). The Swiss Federal Institute of Avalan-

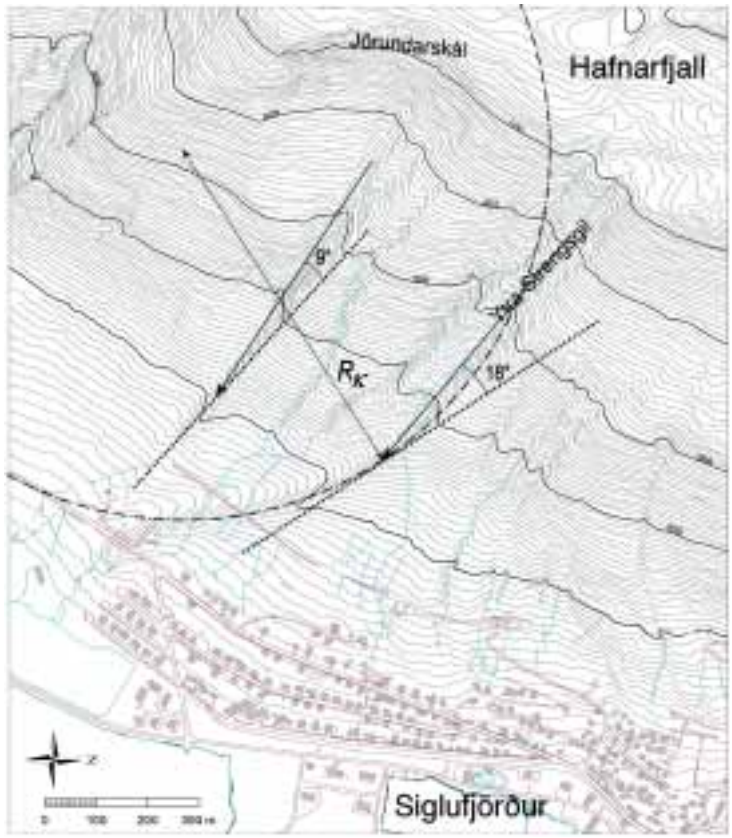

Figure C3: Deflecting dams at Siglufjörður, northern Iceland. Arrows indicate flow direction. The dotted lines show the local direction of the dam axis, and the dash-dotted curve is a circle fitted to the dam axis of the Strengsgil dam.

che Research (SLF) provided additional consultation regarding modelling of the velocity of design avalanches at dam locations (Margreth, 1998). The chosen design avalanches reach beyond the shoreline, and are assumed to correspond to a return period of several thousand years. Table C2 summarises the relevant properties of design avalanches, as well as the dam height components according to the design documentation and the new criteria. Several alternatives for estimating the run-out of the design avalanche, modelling of the flow velocity and flow depth at the dam location, and computing run-up on the dams were explored in the design of the dams by VS and NGI. Table C2 shows avalanche model results obtained by the PCM model, as well as the part of the run-up computations that are most similar to traditional dam design as described in Section 3. The design of the lower part of the Strengsgil dam included computations of run-up due to the curvature of the dam axis, which are not described here. The dams are built from loose materials, excavated from the hillside upstream of the dams, forming a $\sim$50 m wide channel at the dam. The upstream dam sides were constructed with a slope of 1:1.5, but the down facing dam sides have a slope of 1:1.5 to 1:2. The total volume of fill material in the dams is 480,000 m^3.

Table C2: Design parameters and dam height for the Strengsgil and Jörundarskál avalanche dams at Siglufjörður, according to the traditional and the new design criteria. The first number in the H_D column for traditional design is the sum $h_u + h_1 + h_s$, where $h_u = (u_1 \sin\varphi_h)^2/(2g)$ (Eq. (3.3) with $\lambda = 1$), and the second number after the arrow ($\Rightarrow$) is the dam height according to the appraisal report. The Jörundarskál dam is almost straight, so the curvature of the dam axis is assumed to be zero ($R_\kappa \to \infty$). The Strengsgil dam is curved and, for simplicity, the radius of curvature for the entire dam is estimated to be $R_\kappa \approx 700$ m. The dam height is specified at two locations. The upper one ("u") is near the opening of the gully at 150 m a.s.l. where the distance from the uppermost contact of the avalanche with the dam is assumed to be ξ = 50 m (*cf.* Eqs. (6.2) and (6.3)). The lower location ("l") near 100 m a.s.l., at the lower limit of the flow out of the gully towards the dam. The distance from the uppermost contact of the avalanche with the dam is assumed to be ξ = 200 m at this location. The distance from the uppermost contact of the Jörundarskál avalanche with the dam is assumed to be ξ = 200 m at the location considered for the smaller Jörundarskál dam. Storage above the dams does not need to be considered for deflecting dams. See Appendix B for explanations of the variables in each column.

Dam and location	**Design avalanche and dam geometry**						**Traditional design**		**New criteria**								
	u_1	h_1	h_s	ψ	$\psi_\perp$	φ_h	h_u	H_D	H_{cr}	h_{cr}	$H_{cr}+h_{cr}$	h_2	$\Delta H_{\psi_\perp}$	ΔH_κ	h_r	H	H_D
	(m s^{-1})	(m)	(m)	(°)	(°)	(°)	(m)	(m)	(m)	(m)	(m)	(m)	(m)	(m)	(m)	(m)	(m)
Strengsgil, u.	46	4	5	21	7	18	10.3	19.3 $\Rightarrow$ 18	1.4	6.8	8.2	15.1	0.6	1.5	17.1	22.1	19.5
Strengsgil, l.	45	3	4	12	4	18	9.9	16.9 $\Rightarrow$ 18	2.0	5.6	7.6	12.7	1.2	4.8	18.7	22.7	20.9
Jörundarskál	48	7	4	27	4	9	2.9	13.9 $\Rightarrow$ 15	0.0	6.3	6.3	13.9	1.8	0.0	15.8	19.8	19.7

Table C2 shows that flow depth downstream of the shock determines the dam height rather than supercritical run-up. The dam height term h_2 is 5–7.5 m larger than $H_{cr} + h_{cr}$, which is a larger difference than was found for the Flateyri dams in the preceding section.

The supercritical run-up, $H_{cr} + h_{cr}$, assuming momentum loss during the impact, is 3.5–6 m lower than $h_1 + h_u = h_1 + (u_1 \sin\varphi_h)^2/(2g)$ (no momentum loss as assumed in the dam design by VS and NGI). For most relevant values of flow velocity and flow depth, flow depth downstream of the shock represents a more important design criterion than supercritical run-up for rather low deflecting angles, say $\varphi < 15°$. The rather low dam height required to prevent supercritical run-up according to the new design criteria for low deflecting angles does, however, not lead to overall lower required dam heights, because the flow depth downstream of the shock, h_2, will most often be somewhat larger than the run-up, $h_1 + h_u$, according to the traditional criteria.

The run-up components $\Delta H_{\psi_\perp}$ and ΔH_κ, corresponding to terrain slope towards the dam and curvature of the dam axis, respectively, turn out to add several metres to the design dam height at Siglufjörður. The effect of the curvature of the axis of the Strengsgil dam is particularly important at the lower point considered in Table C2, where ΔH_κ becomes almost 5 m. This indicates that these components, which are ignored in traditional design of avalanche dams, may be quite important under some circumstances.

The new design criteria imply a 1.5–3 m larger dam height for the Strengsgil dam and an about 5 m larger dam height for the Jörundarskál dam than the original design. This indicates that the height and effectiveness of these dams should be analysed in more detail using a 2D avalanche model to simulate the retardation of possible overflow into the area between the

dams and the settlement. The effectiveness of the dams against the chosen design avalanche appears to depend on the additional safety provided by the distance between the dam and the protected area (100–200 m for the Strengsgil dam and ∼300 m for the Jörundarskál dam).

C.3 Catching and deflecting dam at Seyðisfjörður

A 380 m long catching dam and a 180 m long deflecting dam were built on the Brún shelf at 650 m a.s.l. on the Bjólfur mountain above the town of Seyðisfjörður in eastern Iceland during the years 2003–2005 (Figs. 3.2 and C4). Both dams are 20 m high with the uppermost 10 m of the upstream dam side having a slope of 4:1, while the lowermost 10 m have a slope of 1:1.5. The dams were designed by the Norwegian Geotechnical Institute (NGI) and Verkfræðistofa Austurlands (VA) (NGI and VA, 2003). The dams are intended as a first step of safety measures for the western part of the town, but a decision has not been made whether further structural measures will be implemented or whether some part of the settlement will be relocated to a safer location. The design avalanches were chosen based on PCM model runs (using the parameters $\mu = 0.15$ and $M/D = 400$–500 m), with the aim to reduce the frequency of avalanches from the upper starting zones of the mountain that are able to pass the shelf and continue down the lower part of the mountainside. Such avalanches are thought to be responsible for most of the avalanche risk in the settlement below Bjólfur, both directly and indirectly, by causing the release of secondary avalanches from the lower starting zones below 650 m a.s.l. Table C3 summarises the relevant properties of design avalanches, as well as dam height components according to the design documentation and the new criteria. The total volume of fill material in the dams is 220,000 m^3.

The dams are located high up in the mountain, where observations indicate a great accumulation of snow compared the flat lowland, and a high frequency of avalanches that reach the dams. Due to the excessive snow depths and in order to account for the possibility of multiple releases of avalanches during the same winter, a rather high value $h_s = 8$ m was chosen for the snow depth on the terrain above the dams. During times of great snow depth near the dams, the lower part of the dams with the more gentle slope are largely covered with snow, so that the steep, upper part of the dam sides will be closer to the surface over which the approaching avalanche flows.

The reshaped terrain upstream from the catching dam is nearly flat, but the terrain upstream of the deflecting dam slopes away from the dam in the lateral direction. The lateral slope, which varies from more than 10° to approximately 0° along the axis of the deflecting dam, leads to a slight advantage for the dam, as the dam height component $\Delta H_{\psi_\perp}$ becomes negative in this case.

Table C3 shows that flow depth downstream of the shock determines the dam height for both dams rather than supercritical run-up, and that the design dam height according to the new criteria is slightly higher for the catching dam, but slightly lower for the deflecting dam compared with the original design.

It is appropriate to end this description by pointing out that the Seyðisfjörður catching dam was overflowed by a medium-sized avalanche in April 2006 as mentioned in Section 5 (see Fig. C4). This avalanche left little stopped snow on the upstream side of the dam but deposited an approximately 65 m wide tongue consisting of snow clods of various sizes on the back side of the dam. The avalanche stopped just above the upper edge of the depression Kálfabotn, which is located in the mountainside immediately below the shelf at Brún.

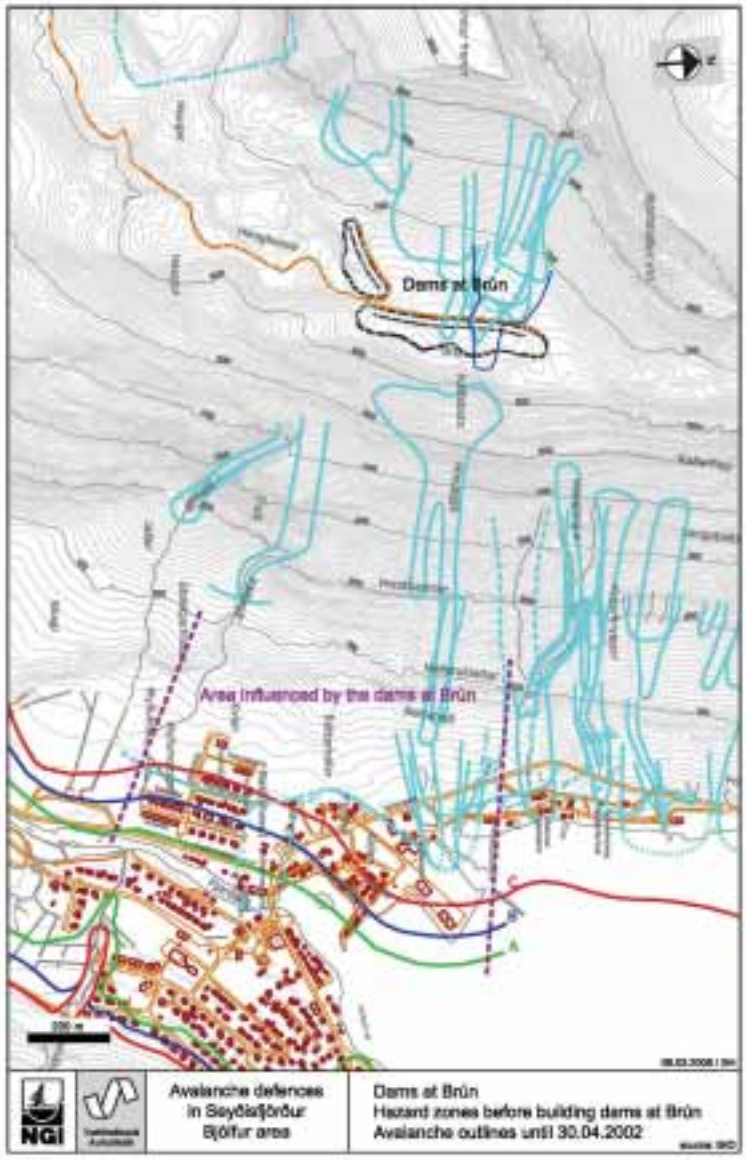

Figure C4: Dams at Seyðisfjörður, eastern Iceland (black curves). The map also shows the outlines of avalanches recorded before the construction of the dams (light blue curves, one highly uncertain tongue is drawn with question marks), the outline of an avalanche in April 2006 that overflowed the dam (dark blue curve) and the hazard zoning for the town before the dams were built (green, blue and red curves). The figure is based on a map showing avalanche outlines until 2002 provided by Sigurjón Hauksson at Verkfræðistofa Austurlands.

Table C3: Design parameters and dam height for the catching and deflecting dam at Brún in Bjólfur in Seyðisfjörður, according to the traditional and the new design criteria. The first number in the H_D column for traditional design is the sum $h_u + h_1 + h_s$, where $h_u = u_1^2/(2g\lambda)$ or $h_u = (u_1 \sin\varphi_h)^2/(2g\lambda)$ (Eqs. (3.2) and (3.3)), and the second number after the arrow ($\Rightarrow$) is the dam height according to the appraisal report. In the first two lines in the table, the energy dissipation parameter λ was chosen to be equal to 2.0 for the catching dam, and 1.5 for the deflecting dam as in the original design of the dams. The coefficient k, describing loss of momentum during the initial impact with the dam in the new design framework, was given the value $k = 0.75$, which is appropriate for a steep dam with $\alpha > 60°$. In the last two lines in the table (marked with a "*" in the first column), the energy dissipation parameter λ was chosen to be equal to 1.0 for both dams (similar to assumptions used in the original design for other deflecting dams described in this appendix), the momentum loss coefficient k was given the value $k = 1$ (to obtain maximum supercritical run-up consistent with the new design framework), and snow depth on the terrain above the dams was specified $h_s = 4$ m (similar to snow depth on the terrain when the catching dam was overflowed by an avalanche in 2006, see discussion near the end of this section about the Seyðisfjörður dams). Two cases with slightly different values for u_1 (19–20 and 29–30 m s^{-1}), h_1 (2–2.5 m for the catching dam), and φ_h (33–35° for the deflecting dam) were considered in the design. For simplicity, the average values of the two alternatives are used in the table. The curvature term ΔH_κ is irrelevant for the catching dam, which is almost straight in any case. The deflecting dam is slightly curved, and the radius of curvature is estimated to be $R_\kappa \approx 450$ m. The distance from the uppermost contact of the avalanche with the deflecting dam is assumed to be $\xi = 100$ m at the location considered in the table. Storage above the deflecting dam does not need to be considered and does not turn out to be determining for the dam height in case of the catching dam. See Appendix B for explanations of the variables in each column.

Dam	**Design avalanche and dam geometry**						**Traditional design**		**New criteria**								
	u_1 (m s^{-1})	h_1 (m)	h_s (m)	ψ (°)	$\psi_\perp$ (°)	φ_h (°)	h_u (m)	H_D (m)	H_{cr} (m)	h_{cr} (m)	$H_{cr}+h_{cr}$ (m)	h_2 (m)	$\Delta H_{\psi_\perp}$ (m)	ΔH_κ (m)	h_r (m)	H (m)	H_D (m)
Catching dam	19.5	2.25	8	0	0	90	9.7	19.9 ⇒ 20	5.2	5.8	11.0	14.5	0.0	0.0	14.5	22.5	22.5
Deflecting dam	29.5	2	8	0	∼10	34	9.2	19.2 ⇒ 20	3.3	4.8	8.1	11.7	−2.3	1.7	11.2	19.2	19.2
Catching dam[1]	19.5	2.25	4	0	0	90	19.4	25.6	12.9	5.8	18.7	14.5	0.0	0.0	18.7	22.7	22.7
Deflecting dam[1]	29.5	2	4	0	∼10	34	13.9	19.9	8.7	4.8	13.5	11.7	−2.3	1.7	13.5	17.5	17.5

[1]See discussion at the end of the section.

Scattered snow clods from the avalanche were strewn all over the Kálfabotn depression, but a secondary avalanche was not released from there. The tongue on the back side of the dam was approximately 100 m long and ∼10–30 cm in thickness. This overflow cannot be explained by the dynamic framework that underlies the new design criteria unless the avalanche was flowing at considerably higher speed than was assumed in the design of the dam.

The last two lines of Table C3 show run-up according to the traditional and new design criteria with no momentum loss during the impact with the dam ($\lambda = 1$ and $k = 1$). The snow depth on the terrain above the dam is, furthermore, reduced from the design value of $h_s = 8$ m to $h_s = 4$ m which is closer to the snow depth when the 2006 avalanche fell. This makes the supercritical run-up the more important run-up component but the calculated run-up height for the catching dam is almost the same as before (the moderate increase in the dynamic run-up is approximately compensated by the decrease in the snow depth). The critical dam height plus

Figure C5: Deflecting dam at Langageiti, western Norway, after the second avalanche during the winter 1998/99 (photos: NGI). The second avalanche overtopped the lower part of the dam. The first avalanche overtopped the uppermost part of the dam. Arrows on the photo to the right show the assumed flow direction of the second avalanche; the red curve shows the outer extension of the flow, the dotted blue curve shows the outer extension of the deposits; the light blue area shows deposits of the first avalanche.

the snow depth on the terrain $H_{cr} + h_s = 12.9 + 4.0 = 16.9$ m is lower than the dam height in this case, so a shock should form although some initial splashing would be expected due to the critical flow depth of $h_{cr} = 6.8$ m being greater then the remaining dam height $H_D - (H_{cr} + h_s)$. It thus seems hard to reconcile the total overflow of the 2006 avalanche with the new design criteria even for no momentum loss during the initial impact unless of course the avalanche velocity was considerably higher than assumed here.

C.4 Deflecting dams at Nautagrovi and Langageiti

Two deflecting dams were built at Gudvangen, Aurland Municipality, in western Norway in 1998. The Nautagrovi dam is 300 m long and 15 m high in the upper part, descending gently to 8 m in the lower part, whereas the Langageiti dam is 570 m long and 11 m high in the upper part, descending gently to 7 m in the lower part (Fig. C5). The dams deflect avalanches from two neighbouring gullies away from a small inhabited area that includes a hotel building between the gullies. The dams, which were designed by the Norwegian Geotechnical Institute (NGI) (Harbitz and others, 2001), are located in a quite steep hillside and the Langageiti dam has a curved axis providing an interesting example to compare the traditional and new dam design criteria. The total volume of fill material in the Nautagrovi dam is 60,000 m^3 and 80,000 m^3 for the Langageiti dam.

The dams were hit by two medium-sized wet-snow avalanches each in the winter 1998/99 (Harbitz and others, 2001) (see also Fig. 5.12, a photograph on the title page and discussion in Jóhannesson and others (2008)). The avalanches hitting the Nautagrovi dam were successfully deflected with an estimated vertical run-up of 7 m on both occations. The Langageiti dam was slightly overflowed by both avalanches, implying a run-up in excess of 11 m, but the main part

Table C4: Design parameters and dam height for deflecting dams at Nautagrovi and Langageiti in Gudvangen according to the original design by NGI and the new design criteria. The oncoming flow depth h_1 and snow depth on the terrain h_s for the Nautagrovi dam are not given as separate numbers by Harbitz and others (2001) but only their sum $h_1 + h_s = 6.5$ m. Here, h_1 is defined as 2 m and h_s is given a value of 6.5 m − 2 m = 4.5 m because of the possibility of multiple avalanches in one winter, which is the reason for the comparatively high value of 6.5 m for $h_1 + h_s$. Two values separated by a "/" are given for h_1 and h_s for the Langageiti dam. The dam height as described by Harbitz and others (2001) is determined from h_u alone and therefore the value for h_1 and h_s in the original design are given as zero (the values before the "/"). In the calculations of the dam height according to the new design criteria, $h_1 = 2$ m and $h_s = 2$ m are somewhat arbitrarily assumed here (the values after the "/"). The deflecting angle φ is given in the table rather than φ_h as in Tables C1, C2 and C3 because this is the quantity given in the design by NGI. The first number in the H_D column for the original design is the sum $h_u + h_1 + h_s$, where h_u is the calculated run-up due to the velocity of the oncoming flow according to the methodology applied by NGI in the design. The second number after the arrow ($\Rightarrow$) is the dam height according to the original design. The gullies are rather narrow so that the avalanche flow that is deflected along the dams may be assumed to extend out of upstream avalanche flow towards the shock. For this reason, the distance from the uppermost contact of the avalanche with the dam to the locations considered in the table are assumed to be $\xi = 100$ m for the Nautagrovi dam and $\xi = 200$ m for the Langageiti dam. The uppermost part of the Nautagrovi dam has a radius of curvature in the range 200–260 m, but the lower half of the dam is almost straight. The radius of curvature at the considered location is here given an intermediate value of $R_\kappa \approx 400$ m. The Langageiti dam is curved and the radius of curvature is estimated to be $R_\kappa \approx 600$ m. The coefficient k describing loss of momentum during the initial impact was computed according to Equation (5.14). Storage above the dam does most often not need to be considered for deflecting dams. In this case, storage above the Nautagrovi dam is indirectly used as an argument for the rather high value of h_s, but does not otherwise enter the determination of the dam height. See Appendix B for explanations of the variables in each column.

Dam	**Design avalanche and dam geometry**						**Original design**		**New criteria**								
	u_1	h_1	h_s	ψ	$\psi_\perp$	φ	h_u	H_D	H_{cr}	h_{cr}	$H_{cr}+h_{cr}$	h_2	$\Delta H_{\psi_\perp}$	ΔH_κ	h_r	H	H_D
	($m\,s^{-1}$)	(m)	(m)	(°)	(°)	(°)	(m)	(m)	(m)	(m)	(m)	(m)	(m)	(m)	(m)	(m)	(m)
Nautagrovi	25	2	4.5	22	13	34	7.5	$14 \Rightarrow 14$	2.6	4.4	7.0	10.5	3.5	1.7	15.7	20.2	16.5
Langageiti	40	0/2	0/2	36	15	18	10.9	$10.9 \Rightarrow 11$	2.8	4.3	7.0	10.0	4.0	4.5	18.5	20.5	15.8

of the avalanches was successfully deflected in both cases.

Table C4 summarises the relevant properties of design avalanches, as well as the dam height components according to the original design and the new criteria. The design used a methodology developed at NGI (Irgens and others, 1998; Harbitz and others, 2001), which is not directly comparable with the traditional design as described in Section 3. This involves computing the trajectory of a point-mass on the sloping dam side based on assumptions regarding momentum loss during the initial impact with the dam and friction in the curved movement up the dam side, and a final empirical adjustment of the run-up height. The value in the h_u column for the original design in Table C4 is the run-up calculated according to this method. For comparison, the traditional velocity run-up component $h_u = (u_1 \sin\varphi_h)^2/(2g\lambda)$, which is tabulated for the previous examples from Flateyri, Siglufjörður and Seyðisfjörður

in this section (Tables C1, C2 and C3), is $h_u = 7.3$ m for Nautagrovi and $h_u = 11.3$ m for Langageiti, which is close to the values found from the point-mass trajectories. For this computation, the energy dissipation parameter λ was chosen to be equal to 1.5 for the Nautagrovi dam and 1.0 for the Langageiti dam in accordance with the original design where a greater initial momentum loss is assumed for the Nautagrovi dam owing to the large angle of incidence.

The dams are located in unusually steep terrain where there is substantial difference between dam height normal to the terrain and vertical dam height (Eq. (5.1)). One also needs to take into account the difference between φ and φ_h and a difference between the slope in the direction of the steepest inclination of the dam side and the direction normal to the dam axis. Based on the values of ψ and φ in Table C4, and the steepest inclination $\alpha_s = 39^\circ$ assumed in the dam design, one may calculate $\varphi_h = 36$ and 22°, and $\alpha = 48$ and 33°, for the Nautagrovi and Langageiti dams, respectively, from Equations (6.1) and (5.2).

Table C4 shows that the dam heights according to the new criteria are for both dams determined by flow depth downstream of the shock, which is about 3 m greater than the dam height needed to prevent supercritical overflow. The run-up components $\Delta H_{\psi_\perp}$ and ΔH_κ, corresponding to terrain slope towards the dam and curvature of the dam axis, are several metres each and add in combination approximately 5 m to the height (normal to the terrain) of the Nautagrovi dam, and more than 8 m to the height of the Langageiti dam. Transformation to vertical dam height reduces the design height by approximately 4 m. In the final result, the vertical dam height is somewhat higher than according to the original design, in particular for the Langageiti dam. The increase in the height of the Langageiti dam results mainly from the omission of the terms h_1 and h_s in the original design, whereas the corresponding terms are included in the design based on the new criteria.

C.5 General considerations

For almost all the examples described above, it was found that flow depth downstream of the shock determines the dam height rather than supercritical run-up, if momentum loss during the initial impact was assumed. In fact, Figure 5.11 shows that for $h_1 > 2$–3 m, flow depth downstream of the shock is greater than supercritical run-up for dam heights lower than ca. 15–20 m. Flow depth downstream of the shock is, therefore, according to the new design criteria, the deciding factor for the design dam height for many or most dams that are actually built. It is only for dams higher than 15–20 m, especially for rather shallow design avalanches, that supercritical run-up determines the dam height. As explained in Section 5, supercritical run-up according to the new design criteria is most often lower than the dam height determined from the traditional criteria, in particular for deflecting dams for which $\lambda = 1$ was often used in traditional design. The dam height requirement arising from the new criterion involving flow depth downstream of the shock is, however, in many or most practical cases, slightly higher than the traditionally determined dam height, especially for curved deflecting dams or when the terrain slopes towards the dam where the new dam height terms ΔH_κ and $\Delta H_{\psi_\perp}$ become important. Therefore, the new criteria will in many cases lead to somewhat higher dams than determined from the traditional methodology.

D Integrated protective measures—A practical example

Tómas Jóhannesson

Avalanche dams are sometimes built in combination with other protective measures, such that the combined effect of several types of constructions needs to be taken into account in the design. Protective measures that were built during the years 1999–2002 for the Drangagil area at Neskaupstaður in eastern Iceland are an example of a comparatively complex system of this kind. They consist of ∼1250 m long and $D_k = 3.5$–4 m high snow nets (1000 m of which have been installed), thirteen 10 m high braking mounds with steep upper faces in two staggered rows, and a 400 m long, 17 m high, steep catching dam (Figs. D1, D2, 15.7, 15.9

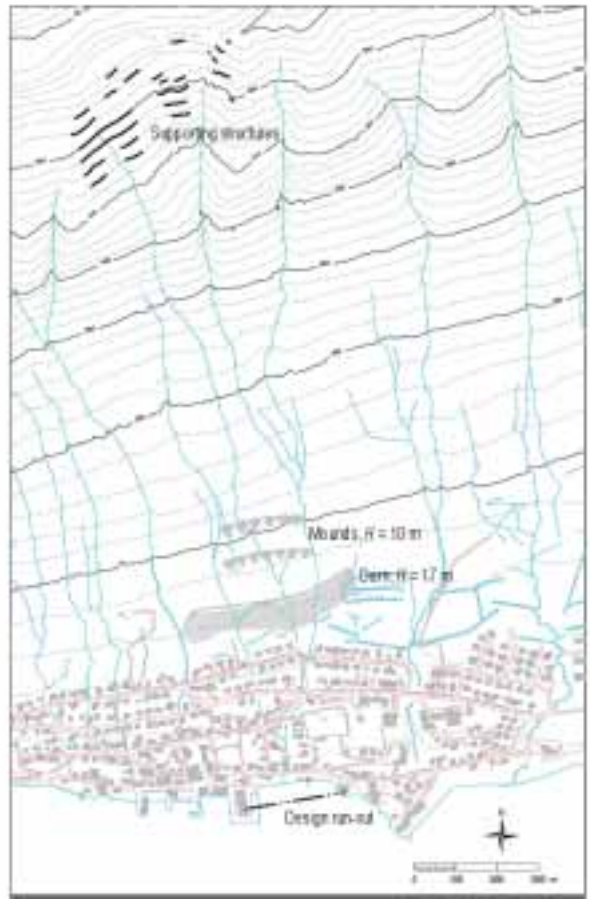

Figure D1: Protective measures in the Drangagil area at Neskaupstaður, eastern Iceland. The map shows the position of the supporting structures in the starting zone, two rows of braking mounds beneath the gully and a dam just above the uppermost houses. A closer map view, a photograph, and a vertical cross-section of the dam and mounds are shown in Figures 15.7, 15.8 and 15.9 in Section 15. Hazard zoning before and after the construction of the protection measures is shown in Figure G3.

Figure D2: The braking mounds at Neskaupstaður and the catching dam behind them. Each mound is 10 m high and the catching dam is 17 m high. (Photo: Tómas Jóhannesson.)

and G3). The protective measures were designed by VST Consulting Engineers Ltd. and Cemagref (Tómasson and others, 1998b,a).

D.1 Hazard situation

The avalanche hazard situation in Neskaupstaður is unfavourable and not suitable for any single type of protective measures. The town of ∼1400 inhabitants stretches along a narrow shoreline below a long mountainside that reaches up to 700–900 m a.s.l., with many starting areas for snow avalanches. More than 90% of the settled area is within hazard zones (Arnalds and others, 2001b,a). Several historical avalanches are reported to have reached far into the currently settled area (Haraldsdóttir, 1997).

The upper part of the mountain is characterised by several wide bowls that narrow downwards and merge with gullies halfway down the mountainside. The gullies open onto an unconfined run-out zone with a slope between 10 and 20° that is several hundred metres long above most of the settlement. Snow depths in the middle of the bowls and in the gullies are greater than what can be reasonably accommodated by supporting structures, but supporting structures can be used in much of the bowls outside the areas of the greatest snow depths.

There is insufficient space in the run-out area for deflecting dams, except near the inner and outer limits of the town, because of the elongated shape of the settlement along the coast. Modelled avalanche speeds in the run-out area are so high, that catching dams of practical height cannot be used to stop the avalanches before they reach the inhabited area. A general assessment of potential protective measures for the whole town by VST and Cemagref (1998) concluded that combined protection measures with supporting structures, braking mounds and catching dams are the best option to protect most of the town. On the basis of this conclusion, more detailed designs of protective measures have been established for the Drangagil and Tröllagil avalanche paths (Tómasson and others, 1998b; Sigurðsson and others, 2003).

The measures for Drangagil have been constructed, and construction in the Tröllagil area is scheduled to start in 2009. An overview of the design of the protective measures for the Drangagil and Tröllagil avalanche paths is given by Indriðason and others (2008), together with descriptions of protective measures at several other locations in Iceland.

D.2 Design of the Drangagil protection system

The protection system for the Drangagil avalanche path is based on the idea that, in order to provide acceptable safety for the settlement, all available options for protective measures need to be used in combination, although each of them individually is insufficient to reach the targeted safety. The chosen design avalanche reaches approximately 100 m beyond the shoreline, and has a modelled speed between 30 and 40 $\mathrm{m\,s^{-1}}$ in the run-out area above the settlement. This is a very high velocity, as in the case of Neskaupstaður a deflecting dam is not feasible due to the layout of the town. Supporting structures in that part of the main starting zone, where snow depths are not too great, are used to reduce the volume and run-out of the design avalanche, and consequently the speed of the avalanche in the run-out area. The available space in the upper part of the run-out area is utilised for two rows of braking mounds that retard the avalanche and further reduce flow speeds to a level that makes it possible to stop the avalanche by a catching dam located just above the uppermost houses. The design challenge is to choose the most effective combination of the three types of protective measures, to provide the required safety.

Table D1 summarises the relevant properties of design avalanches, as well as the dam height components according to the design documentation and the new dam height criteria. The speeds in the table for the alternatives with braking mounds are determined in accordance with the methodology that was used in the appraisal report to estimate the retarding effect of the two rows of braking mounds. This assumes that the combined effect of both rows of mounds, and the slowing down of the avalanche from the landing point of the jet to the catching dam, leads to a lowering by a factor of 0.6 of the flow speed from the impact speed at the upper row of mounds. The speed reduction according to the methodology developed in Section 9 about braking mounds is described in a separate subsection below. The speed $u_1 = 27\,\mathrm{m\,s^{-1}}$ at the dam location for the "dam + supp. struct." alternative is not explicitly given in the design documentation, and is calculated on the basis of other quantities that are tabulated there.

D.3 Comparison of four alternatives

The "dam only" alternative leads to an impractical dam height of over 40 m, requiring a volume of fill material to build the dam on the order of 1,400,000 $\mathrm{m^3}$. The dam height for this alternative is similar according to the traditional and new criteria. In this case, the dam height according to the new criteria is determined by supercritical run-up.

The "dam + mounds" alternative was explicitly evaluated in the appraisal report and compared with the alternative with both supporting structures and mounds. The dam height for this alternative is approximately 2 m higher according to the new criteria compared with the traditional ones, and is determined by the flow depth downstream of the shock. The report recommended the alternative with supporting structures ("dam + s. struct. + mounds") in favour of this alternative. The alternative with supporting structures was judged to have a more

Table D1: Design parameters and dam height for the catching dam at Drangagil in Neskaupstaður, according to the traditional and the new design criteria. The first number in the H_D column for traditional design is the sum $h_u + h_1 + h_s$, where $h_u = u_1^2/(2g\lambda)$ (Eq. (3.2)), and the second number after the arrow ($\Rightarrow$) in the second and forth lines of the table is the actually chosen dam height according to the appraisal report. Due to an increase in the excavation depth upstream of the dam, the design height of the dam was modified from 15 to 17 m during the technical design phase. The H_D value in the table is taken from the original appraisal report and does not take into account this change. The energy dissipation parameter λ was chosen to be equal to 2.0. Four alternatives are shown, a dam without any other protective measures, a dam with two rows of braking mounds in the run-out zone, a dam in combination with supporting structures in the starting zone, and a dam in combination with supporting structures in the starting zone plus two rows of braking mounds in the run-out zone. The second and fourth alternatives are described in the appraisal report. The other two are shown here for comparison. The deflecting angle is $\varphi_h = 90°$, the slope perpendicular to the dam axis $\psi_\perp = \psi$, and the dam height components $\Delta H_{\psi_\perp} = \Delta H_\kappa = 0$ for catching dams. φ_h, $\psi_\perp$, $\Delta H_{\psi_\perp}$, and ΔH_κ, therefore, do not need to be specified in this case. Storage above the dam does not turn out to be determining for the dam height. See Appendix B for explanations of the variables in each column.

Dam and location	**Design avalanche and dam geometry**				**Traditional design**		**New criteria**						
	u_1	h_1	h_s	ψ	h_u	H_D	H_{cr}	h_{cr}	$H_{cr}+h_{cr}$	h_2	h_r	H	H_D
	(m s^{-1})	(m)	(m)	(°)	(m)	(m)	(m)	(m)	(m)	(m)	(m)	(m)	(m)
Dam only	32	3	2.5	10	36.8	42.3	29.4	11.0	40.5	31.6	40.5	43.0	40.5
Dam + mounds	23	3	2.5	10	13.2	18.7 $\Rightarrow$ 19	7.3	7.9	15.2	19.7	19.7	22.2	20.9
Dam + supp. struct.	27	3	2.5	10	18.3	23.8	11.8	8.7	20.5	22.8	22.8	25.3	23.9
Dam + s. struct. + mounds	19	3	2.5	10	9.4	14.9 $\Rightarrow$ 15[1]	4.2	7.0	11.2	16.9	16.9	19.4	18.3

[1]The dam height was increased to 17 m in the technical design.

proven effectiveness, however, it was estimated to be ∼20% more expensive. Furthermore, the higher flow velocity in the alternative without supporting structures leads to a longer jump length from the upper row of mounds, as described below, and a greater chance that the avalanche jumps over the lower row of mounds, which does then not effectively slow down the avalanche before it hits the catching dam.

Based on avalanche modelling, the supporting structures, which cover about one third of the main starting zone in Drangagil, are assumed to reduce the velocity of the avalanche at the location of the upper row of braking mounds by ∼15%. This lowers the flow velocity at the dam location for both the alternative with and without mounds (the third and fourth lines in Table D1). In both cases, the calculated dam heigh according to the new criteria is determined by the flow depth downstream of the shock rather than by supercritical run-up. The dam height for the alternative without mounds is similar according to the traditional and new criteria, but the dam height for the alternative with mounds is approximately 3 m higher according to the new criteria.

The alternative with braking mounds was recommended in the appraisal report based on preliminary studies, indicating that properly designed braking structures could effectively reduce the speed of granular flows. These studies were later expanded in work that led to the guidelines for the design of braking mounds described in Section 9.

Table D2: Throw length of a jet formed by the impact with the first row of braking mounds at Drangagil, Neskaupstaður.

Alternative	**Design avalanche** Impact velocity, u_0 ($\mathrm{m\,s^{-1}}$)	**Throw length**, L $k = 0.7$ (m)	$k = 0.8$ (m)	$k = 0.9$ (m)
Dam + mounds	38	65	79	94
Dam + supp. struct. + mounds	32	48	59	71

D.4 Braking mounds

The braking mounds below Drangagil satisfy the geometrical requirements described in Subsection 9.3. That is, i) their height above the snow cover ($10 - 2.5 = 7.5$ m) is in the range of 2–3 times the estimated thickness of the dense core of the avalanche ($h_1 = 3$ m); ii) they are steep; iii) the aspect ratio is close to 1 if the top width of the mounds (10 m) is used, but somewhat lower than 1 if the half-width is used; and iv) they are placed side by side close to each other in two staggered rows. The remaining requirement of Section 9 states that the separation of the two rows (80 m) should be large enough to ensure that the trajectory of the jet formed by the avalanche during the impact with the first row should land upstream of the second row.

The trajectory of the jet was computed according to the methodology outlined in Subsection 9.2 for the two alternatives with mounds in Table D1 (the second and fourth lines), using the parameters $k = 0.7$, 0.8 and 0.9, $\beta = 60^\circ$ ($\alpha \approx 86^\circ$), and $f/h_j = 0.004\,\mathrm{m^{-1}}$ (Table D2). The results show that jets corresponding to the alternative with supporting structures land upstream from the second row of mounds for all three values of the energy dissipation parameter k. For the higher velocity, corresponding to the alternative without supporting structures, the jet is found to land upstream of the second row of mounds for $k = 0.7$, and barely so for $k = 0.8$, but the throw length $L > 80$ m for $k = 0.9$. If the alternative without supporting structures had been chosen it would, therefore, have been advisable to increase the separation of the rows slightly. Finally, the jet formed by the impact with the second row should land upstream of the catching dam. Since the flow velocity at the impact with the second row is lower than the impact velocity with the first row, and the distance to the catching dam, for practical reasons, is greater than the separation between the two rows of mounds, it is easy to see that the second requirement is satisfied.

The velocity reduction, according to the recommendation given in Section 9, should be estimated as a 20% relative reduction in speed for an impact with one row of mounds, and an additional 10% for a second row. This reduction should be applied at the location of the mounds in a model computation that takes into account the effect of terrain friction between the mounds and the dam to further reduce the flow speed. The modelled variation of the speed between the two rows of mounds, and from the second row to the catching dam, depends on the avalanche model used in the design. Here, for simplicity, a square root variation of the speed with horizontal distance, calibrated to match the speeds and distances given in the appraisal report, will be used to illustrate these computations. For the alternative with

supporting structures, the speed is found to be reduced from 32 to 25.6 m s^{-1} by the impact with the first row of mounds. The speed is further reduced to 22.5 m s^{-1} when the flow hits the second row of mounds, to 20.3 m s^{-1} by the impact with the second row and to $\sim$14 m s^{-1} by the flow over the 120 m distance from the second row of mounds to the catching dam. Similarly, for the alternative without supporting structures, the flow velocity is reduced from 38 m s^{-1} at the upper row of mounds to $\sim$20 m s^{-1} at the impact with the catching dam. This speed reduction is somewhat greater than assumed in the appraisal report of 1998, in which in both cases, the speed at the dam was calculated to be $\sim$19 m s^{-1} and $\sim$23 m s^{-1} (Table D1) for the alternatives with and without supporting structures, respectively. Design dam heights corresponding to the flow speeds $u_1 = 14$ and 20 m s^{-1} according to the new design criteria are 14 and 19 m, respectively, which is close to the original design dam heights from the appraisal report (the fourth and second lines in Table D1). Overall, according to the new criteria, the design dam height at Drangagil is, therefore, found to be consistent with the dimensions determined in the original design, although there are (comparatively small) compensating differences in intermediate results of dam height calculations.

E Loads on structures—Practical examples

Peter Gauer

E.1 Load on a wall

In the following, two examples are given for the determination of the design force on a 20 m high and 100 m long wall in the lower part of an avalanche path. The assumed location of the wall is approximately 900 m downstream of the starting zone. Input parameters are summarised in Table E1. A velocity of 25 m s^{-1} and a density of 150 kg m^{-3} are used in example e1, and a velocity of 10 m s^{-1} and a density of 250 kg m^{-3} in example e2. These values for the flow density are used rather than 300 kg m^{-3} based on an assumption that the density decreases with increasing velocity. As described in Section 11, a density of 300 kg m^{-3} is often chosen for safety reasons and the choice of a lower value must be based on expert judgment. In both cases, the density downstream of the shock, ρ_2, is assumed to be 500 kg m^{-3}; the wall friction factors, c_1 and μ, are set to 0.3; the shape factor, n_f, is 1; and the expansion factor for the height of the fluidised layer $c_e = 2$ is used.

Table E1: Example input: Load on a wall.

Parameter	Symbol		Value	
			e1	e2
Height of the wall	H_{wall}	(m)	20	
Width of the wall	W_{wall}	(m)	100	
Distance along the track	l_{track}	(m)	900	
Height of snowpack / deposits	h_s	(m)	1.5	
Flow height (dense flow)	h_1	(m)	2	
Front velocity	u_1	(m s^{-1})	25	10
Density (dense flow)	ρ_1	(kg m^{-3})	150	250

Using the assumptions above one obtains:

Parameter		e1	e2
Froude number	Fr_1	5.6	2.3
Intensity factor	$f(\mathrm{Fr}_1)$	1.07	1.24
Density ratio	ρ_2/ρ_1	3.3	2.0
Flow height ratio	h_2/h_1	4.6	2.6

Figure E1 depicts the pressure distribution according to the recommendation given in Section 11. It should be noted that the derivation of the Swiss recommendations is not momentum conserving and leads to an overall higher total force normal to the wall. The initial peak impact pressure, which lasts on the order of 0.1 s, is considerably higher than the recommended mean value. For sensitive structures, in particular, it is important to account for this load. During this time, the pressure decreases from its initial peak value and approaches the recommended mean value. Simultaneously, the flow height increases from $h = h_1$ to $h = h_2$. The area on the wall affected by the pressure peak is, however, restricted to the upstream flow

Table E2: Comparison of the calculated loads on a wall for the example according to the recommended approach and the Swiss recommendation; example e1. Dynamic forces and moments per metre length of the wall are given.

Force	Recommend. ($kN\,m^{-1}$)	Swiss ($kN\,m^{-1}$)	Moment	Recommend. ($kNm\,m^{-1}$)	Swiss ($kNm\,m^{-1}$)	Remarks
F'_{peak}	563	–	M'_{peak}	1969	–	expert judgment
F'_{sx}	17	–	M'_{sy}	17	–	
F'_{dx}	204	375	M'_{dy}	1234	938	
F'_{stau}	–	1196	M'_{stauy}	–	9255	$\lambda = 2.5$
F'_{flx}	67	–	M'_{fly}	849	–	
F'_{px}	7	–	M'_{py}	111	–	
F'_{totx}	295	1571	M'_{toty}	2211	10192	
F'_{totz}	81	471				

Table E3: Comparison of the calculated loads on a wall for the example according to the recommended approach and the Swiss recommendation; example e2. Dynamic forces and moments per metre length of the wall are given.

Force	Recommend. ($kN\,m^{-1}$)	Swiss ($kN\,m^{-1}$)	Moment	Recommend. ($kNm\,m^{-1}$)	Swiss ($kNm\,m^{-1}$)	Remarks
F'_{peak}	150	–	M'_{peak}	525	–	expert judgment
F'_{sx}	10	–	M'_{sy}	10	–	
F'_{dx}	66	60	M'_{dy}	276	150	
F'_{stau}	–	31	M'_{stauy}	–	128	$\lambda = 2.5$
F'_{flx}	14	–	M'_{fly}	100	–	
F'_{px}	0.2	–	M'_{py}	2	–	
F'_{totx}	90	91	M'_{toty}	387	278	
F'_{totz}	24	27				

depth of the avalanche, h_1. The figure shows the initial impact peak acting over an area directly above the snowpack. As mentioned in Section 11, one needs to allow for a possible higher point of attack of the peak force by up to h_1. Table E2 gives the calculated forces for example e1 and Table E3 for example e2. If one uses $\rho_1 = 300\,kg\,m^{-3}$ in example e1, the initial peak force, F'_{peak}, would be $1125\,kN\,m^{-1}$ and M'_{peak} would be $3938\,kNm\,m^{-1}$; the total mean force, F'_{totx}, would be $536\,kN\,m^{-1}$ instead of $295\,kN\,m^{-1}$, and the total mean moment, M'_{toty}, $4936\,kNm\,m^{-1}$. Note that, as discussed in Section 11, it is a question of expert judgement whether the initial peak pressure is taken into account in the design or not.

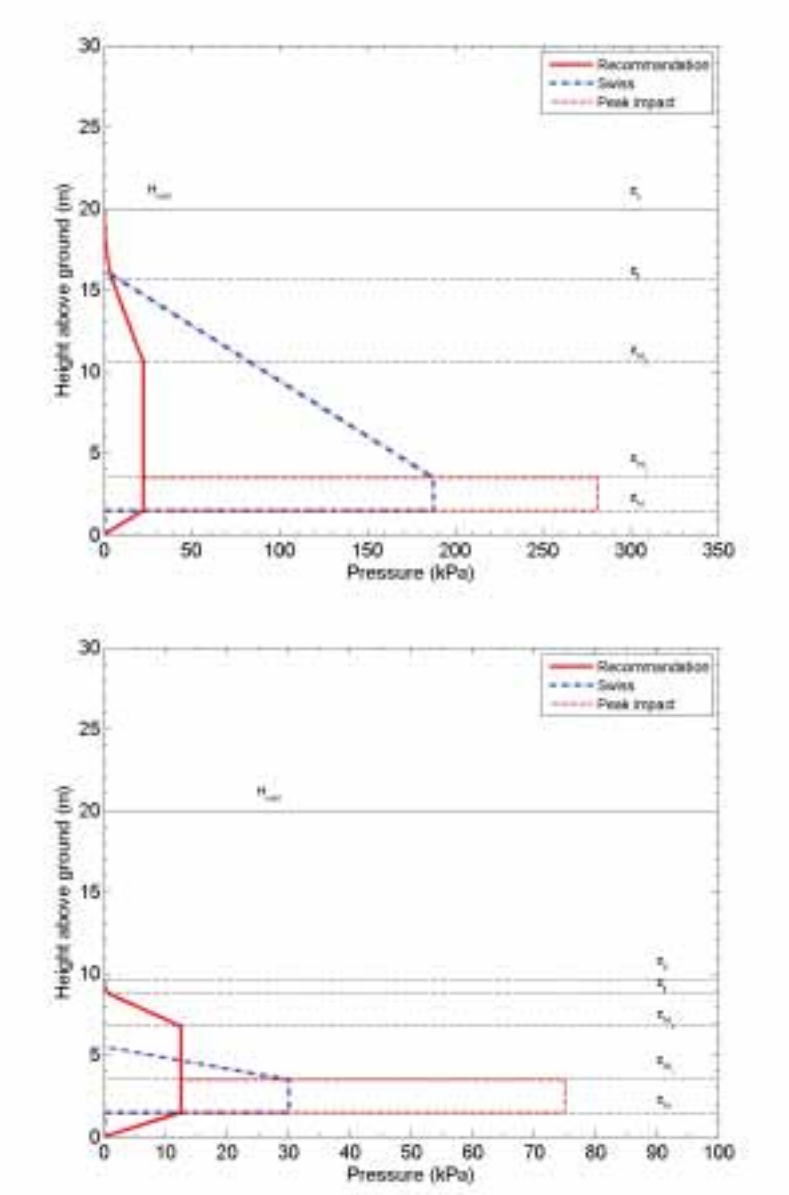

Figure E1: Distribution of impact pressure on a wall for the example, according to the recommendation. An initial impact pressure peak with a magnitude of $3\rho_1 {u_1}^2$, which may be taken into account in design depending expert judgment, is shown. Also shown is a comparison with Swiss recommendations. Top: example e1; Bottom: example e2.

E.2 Load on a mast

In the following, an example is given for the determination of the design force on a 1.5 m wide cylindrical mast in an avalanche path. The assumed location of the mast is approximately 900 m downstream of the starting zone. Input parameters are summarised in Table E4. No considerations about return periods are given. The recommended loading according to the Swiss recommendations (Gruber and others, 1999b) (see Appendix F.2) is also given for comparison.

Table E4: Example input: Load on a mast.

Parameter	Symbol		Value
Diameter of the round mast	W	(m)	1.5
Height of the round mast	H_{mast}	(m)	20
Distance along the track	l_{track}	(m)	900
Height of snowpack	h_s	(m)	1.5
Front velocity	u_f	($\mathrm{m\,s^{-1}}$)	30
Density (dense flow)	ρ_d	($\mathrm{kg\,m^{-3}}$)	300
Flow height dense flow	h_d	(m)	2.0

Figure E2 depicts the distribution of the dynamic pressure, $\rho u_f^2/2$ (*i.e.* the pressure is not factored by C_D), according to recommendation given in Section 12 and compares it with the Swiss recommendations (see F.2). It should be noted that the derivation of the Swiss recommendation is not momentum conserving and thus allows an overall higher total force normal to the mast. Table E5 gives the calculated forces for both cases. The figure and table both show the peak pressure, $p_{peak} = 2\rho_d u_f^2$, which may be taken into account for square or blunt obstacles depending expert judgment, even though the peak pressure does not need to be taken into account for the cylindrical mast considered here.

Table E5: Comparison of the calculated loads on a mast for the example according to recommended approach and the Swiss recommendation. The reduction factor $f(W/h_d) = 0.55$ is found by interpolating the values tabulated in Table F2.

Force	Recommend. (kN)	Swiss (kN)	Moment	Recommend. (kNm)	Swiss (kNm)	Remarks
F_{peak}	1620	–	M_{peak}	5670	–	expert judgment
F_s	152	0	M_s	152	0	
F_d	608	405	M_d	1519	1012	
F_{stau}	–	1023	M_{stau}	–	7024	$\lambda = 2.5$
F_{fl}	319	–	M_{fl}	1450	–	
F_p	21	–	M_p	166	–	
F_{tot}	1100	1428	M_{tot}	3287	8036	

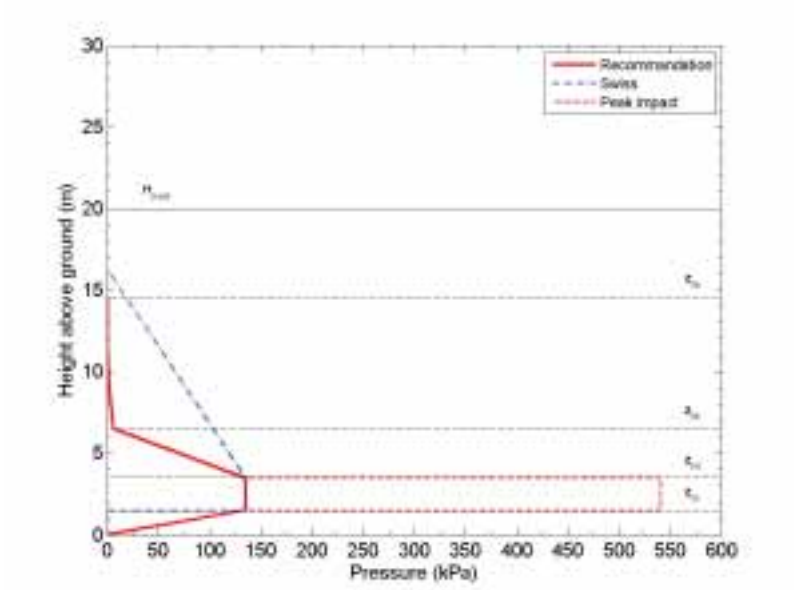

Figure E2: Distribution of dynamic pressure on a mast for the example according to recommended approach and the Swiss recommendation. An impact pressure peak $p_{peak} = 2\rho_d u_f^2$, which may be taken into account for square or blunt obstacles depending expert judgment, is also shown.

E.3 Load due to impacts of solid bodies

The example considers an impact of a rock with a diameter of 0.3 m onto a 5 m high, 5 m wide, and 0.3 m thick concrete wall. The avalanche speed is assumed to be 25 m s^{-1} and the density 300 kg m^{-3}. Table E6 summarises the input parameters and Table E7 various calculated parameters as well as the estimated pressures and forces. The recommended loads according to GVA (1994) are lower than the theoretical values found by the Hertzian or the plastic failure approach. However, as mentioned in Section 13, the impact of a solid body will in most cases be damped by the surrounding snow and therefore the lower recommended values may be justified. It should be noted that the loading according to the Hertzian or the plastic failure approach depends largely on the choice of the size of the impacting body. The difference in the loading according to the different approaches mostly reflects the choice of the size of the boulder rather than indicating a fundamental difference between the methodologies.

Table E6: Example input: Load due to impacts of solid bodies.

Parameter	Symbol		Value
Avalanche speed	u_1	m s^{-1}	25
Avalanche density	ρ_1	kg m^{-3}	300
Volume of the wall	V_w	m^3	7.5
Young's modulus for concrete	E_c	GPa	20
Poisson ratio for concrete	ν_c		0.15
Yield (ultimate) stress of concrete	Y	MPa	20
Density of concrete	ρ_c	kg m^{-3}	2500
Young's modulus for rock	E_r	GPa	50
Poisson ratio for rock	ν_r		0.25
Density of rock	ρ_r	kg m^{-3}	2600
Volume of the rock	V_r	m^3	0.014

Table E7: Comparison of the calculated local impact loads onto a wall for the example according to the recommended, the Hertzian, and the plastic failure approach.

Model parameter	Symbol		Recommendation	Hertzian	plastic
Effective Young's modulus	E^*	GPa		14.8	
Effective radius	R	m		0.15	
Effective mass	m	kg		36.7	
Contact radius	a	m	0.125	0.032	0.078
Contact time	t_i	ms		0.8	2.5
Impact pressure (max)	p_I (p_0)	MPa	12.5	887.5	60
Impact force	F_I	kN	624	4241	1140

E.4 Snow-creep load

The following example shows the determination of the design force for a 1.5 m wide cylindrical mast on a 30° slope. Input parameters are summarised in Table E8 and the calculated loads are given in Table E9. Loading according to the recommendation of Larsen (1998) is given for comparison. Larsen based his recommendation on experiments on snow creep loads on two masts with different diameters at the Norwegian test-site Fonnbu (see Appendix F.3).

Table E8: Example input: Snow-creep load calculation.

Input parameter	Symbol		Value
Diameter of the round mast	W	(m)	1.5
Slope angle	ψ	(°)	30
Snowpack density	ρ	(kg m^{-3})	300
Snow depth	h_s	(m)	1.5
Snow thickness	D	(m)	1.3

Table E9: Example snow-creep load calculation according to the Swiss recommendations (cf. Margreth, 2007), and according to Larsen (1998). The first case according to the Swiss Guidelines corresponds to a situation with low gliding, the second to extreme gliding conditions.

Model parameter	Symbol		Value		
			Swiss		Larsen
Creep factor	K		0.66	0.66	
Gliding factor	N		1.2	2.6	
c-factor	c		0.6	6	
Efficiency factor	η_F		1.52	6.2	
Coefficient	C_L				1.69
Factor	K_L				1.2
Total snow creep load	$S_{N,M}$	(kN)	5.95	52.6	6.52
Total moment	$M_{N,M}$	(kNm)	3.87	34.2	4.24

F Loads on walls and masts—Summary of existing Swiss and Norwegian recommendations

Peter Gauer

F.1 Load on wall-like structures

Swiss recommendations

According to Gruber and others (1999b), the following approach for the determination of the force on extended obstacles is recommended in Switzerland. "Extended" means that a considerable part of the avalanche is deflected by an angle φ, which the obstacle makes with respect to the flow direction of the oncoming avalanche.

Dense flow

The impact pressure normal to wall, p_{dn}, is expressed as

$$p_{dn} = \rho\, u^2 \sin^2 \varphi\ , \tag{F1}$$

where ρ is the density of the avalanche, and u is the speed of the approaching flow. In the case of a vertical wall, φ would be 90°. The tangential pressure is assumed to be

$$p_{dt} = \mu\, p_{dn}\ . \tag{F2}$$

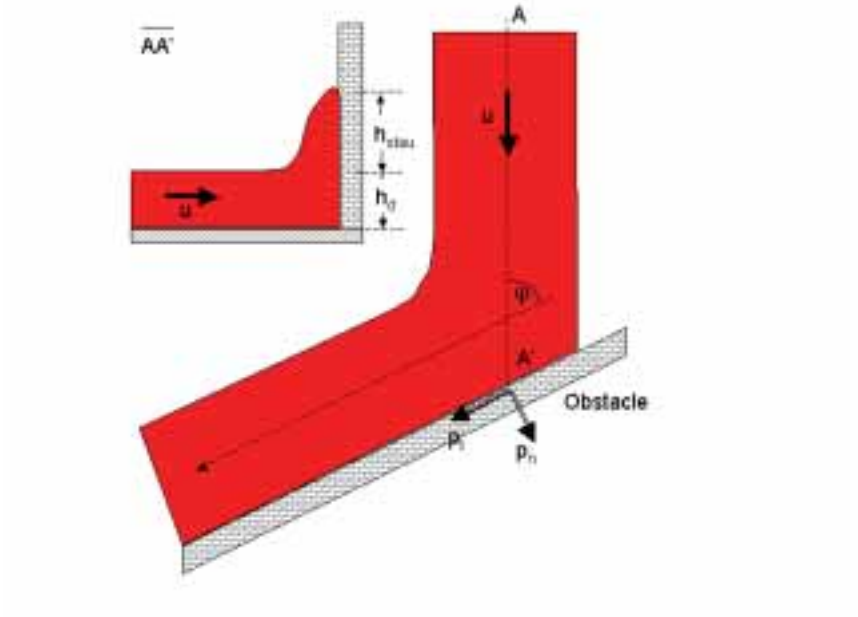

Figure F1: Load on a large obstacle.

For safety reasons, a flow density, $\rho = 300\,\mathrm{kg\,m^{-3}}$ is assumed.

It follows that the normal force acting on a wall with width b is

$$F_{dn} = p_{dn}\,(z_{hd} - z_{hs})\,b\ . \tag{F3}$$

With that, the tangential force

$$F_{dt} = \mu F_{dn}\ , \tag{F4}$$

and the moment

$$M_{dn} = \frac{(z_{hd} + z_{hs})}{2}\,F_{dn}\ , \tag{F5}$$

can be calculated.

Above, the flow depth of the avalanche, the pressure is assumed to decrease linearly within a stagnation (climbing) height, which is given by

$$h_{stau} = \frac{u^2}{2\,g\,\lambda}\ . \tag{F6}$$

For dry, mostly fluidised flows, $\lambda = 1.5$ is proposed. For dense flows, it is assumed that $2 \le \lambda \le 3$. The pressure is given by

$$p(z) = p_{dn}\,\frac{(z_{tot} - z)}{(z_{tot} - z_{hd})}\ . \tag{F7}$$

The force component is

$$F_{stau} = W\,p_{dn}\,\frac{(z_{tot} - z_{hd})}{2}\ , \tag{F8}$$

in case the obstacle is lower than $z_{tot} = z_{hd} + h_{stau}$, and the moment is given by

$$M_{stau} = \frac{z_{tot} + 2z_{hd}}{3}\,F_{stau}\ . \tag{F9}$$

The expressions for F_{stau} and M_{stau} have to be modified slightly if the wall is lower than z_{tot}.

Fluidised/saltation layer and powder part

In Gruber and others (1999b), Issler provides some estimates of the effect of powder-snow avalanches and the saltation layer on an obstacle. He expresses the impact pressure acting on the obstacle as

$$p_{pn} = f\,\rho\,u^2\,\sin^2\varphi\ , \tag{F10}$$

where the factor f is between 0.5 and 1. It is closer to 1: (i) the higher the velocity, u, (ii) the higher the deflection angle, (iii) the higher the density of the powder part, and (iv) the larger the particle size within the flow. For perpendicular impact, $f = 1$ is recommended. Vertical profiles of ρ or p_{pn} are not specified.

The density, ρ, within the saltation layer is assumed to vary between 10 and $50\,\mathrm{kg\,m^{-3}}$, and in the powder part between 1 and $10\,\mathrm{kg\,m^{-3}}$. The depth of the saltation layer is assumed to vary between 1 and 5 m, and the powder part is assumed to be several tens of metres high.

It follows that the force acting on a wall is

$$F_{pn} = p_n (z_{hp} - z_{hd})\, b \tag{F11}$$

and the moment (no profile specified) is given by

$$M_{pn} = \frac{(z_{hp} + z_{hd})}{2} F_{pn} \ . \tag{F12}$$

F.2 Load on mast-like structures

Swiss recommendations

According to Gruber and others (1999b), the following approach for the determination of the force on narrow obstacles is recommended in Switzerland. The impact force is expressed as

$$F_m = C_D A\, p(z) \ . \tag{F13}$$

Here, no distinction is made between different flow regimes. Also, no distinction between dry- or wet-snow avalanches is made. The recommended values for C_D are given in Table F1.

Table F1: Drag coefficients C_D according to the Swiss recommendations.

Flow regime	Obstacle form	C_D
No distinction	◯	1.0
	△	1.5
	□	2.0

The projected area, A, is defined as

$$A = h_{tot}\, W \ , \tag{F14}$$

where W is the width of the obstacle. The total impacted height, h_{tot}, is given by (see also Fig. F2)

$$h_{tot} = h_d + h_{stau} \ , \tag{F15}$$

where h_d is the flow height of the avalanche. The second term on the right hand side describes the climbing height, and is given by

$$h_{stau} = \frac{u_f^2}{2\, g\, \lambda} f(W/h_d) \ . \tag{F16}$$

For dry, mostly fluidised flows, $\lambda = 1.5$ is proposed. For dense flows, $2 \leq \lambda \leq 3$ is assumed. $f(W/h_d)$ is a reduction factor, which depends on the ratio of obstacle width to flow depth. Proposed values for the reduction factor are given in Table F2.

Within the flow height, the pressure is assumed to be constant and given by

$$p_d = \frac{\rho u_f^2}{2} \ . \tag{F17}$$

Table F2: Reduction factor f for loading of masts as a function of the ratio W/h_d.

W/h_d	0.1	0.5	1	2	≥ 3
$f(W/h_d)$	0.1	0.4	0.7	0.9	1

Hence, the force component on the mast from the dense flow is

$$F_d = C_D W p_d (z_{hd} - z_{hs}) \tag{F18}$$

and the moment

$$M_d = \frac{z_{hd} + z_{hs}}{2} F_d \ . \tag{F19}$$

Above the upstream height of the dense part, a linearly decreasing impact pressure is assumed (see Fig. F2), *i.e.*,

$$p(z) = \frac{\rho u_f^2}{2} \frac{(z_{tot} - z)}{(z_{tot} - z_{hd})} \ , \tag{F20}$$

where again $z_{tot} = z_{hd} + h_{stau}$. Consequently, the total force due to the impact pressure above the upstream height of the dense part is

$$F_{stau} = C_D W p_d \frac{(z_{tot} - z_{hd})}{2} \ , \tag{F21}$$

and the moment is

$$M_{stau} = \frac{z_{tot} + 2z_{hd}}{3} F_{stau} \ . \tag{F22}$$

As for loading of walls, a flow density, $\rho = 300\,\mathrm{kg\,m^{-3}}$ is assumed for safety reasons.

The expressions for F_{stau} and M_{stau} have to be modified slightly if the mast is lower than z_{tot}.

F.3 Load due to snow pressure

Based on experiments with snow creep loads on two masts with different diameters at the NGI test-site Fonnbu, Larsen (1998) proposed the following relation for the design load on mast-like constructions.

$$S'_{N,M} = K_L C_L \frac{\rho}{1000} D^2 g \sin\psi \qquad [\mathrm{kN\,m^{-1}}] \ , \tag{F23}$$

where ρ is the average snow density, D the thickness of the snowpack perpendicular to the ground, ψ the slope angle, and g is the acceleration due to gravity. The factor, K_L, depends on D. In his experiments, Larsen (1998) found $K_L = 1.2$ for a snow thickness of 4 m, and $K_L = 0.7$ for a snow thickness of 5 m. The coefficient C_L depends on the mast diameter d

$$C_L = 0.98\, d^{0.63} + 0.42 \ . \tag{F24}$$

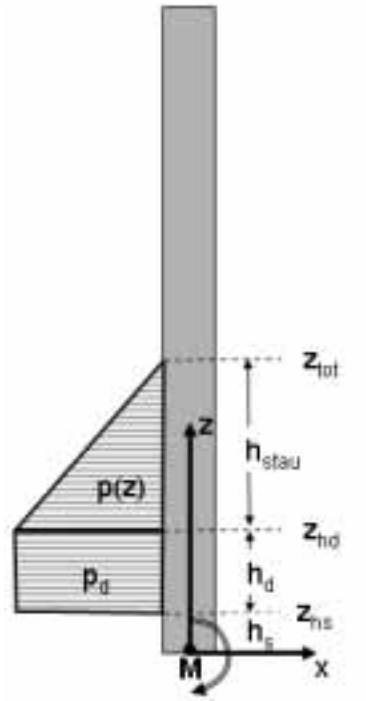

Figure F2: A schematic diagram of the impact pressure distribution due to an avalanche on a mast-like structure according to the Swiss recommendations.

Margreth (2007) notes that this model neglects effects due to snow gliding and is therefore limited to situations without snow gliding. The moment is given by

$$M'_{N,M} = \frac{h_s}{2} S'_{N,M} \qquad [\mathrm{kNm\,m^{-1}}] \,. \tag{F25}$$

G Laws and regulations about avalanche protective measures in Austria, Switzerland, Italy, France, Norway, and Iceland

Massimiliano Barbolini, Dieter Issler, Tómas Jóhannesson, Mohamed Naaim, Karstein Lied and Lambert Rammer

Laws and regulations regarding the adaptation of hazard zoning after avalanche protective measures have been completed, are different in different countries. In France, no changes are made in zoning, so that no relaxation of land use restrictions is made in spite of the improved safety provided by the protective measures. This underlines the policy that protective measures are only intended to improve the hazard situation in existing settlements, and should not lead to increased population density in potentially hazardous areas, especially considering the inherent uncertainty regarding the effectiveness of avalanche protective measures. In most other countries, the hazard zoning is modified after protective measures have been completed, in order to reflect the improved hazard situation. However, the detailed manner in which modifications are made differs between countries. The design requirements for the protective measures are usually expressed in terms of a *minimum return period* of avalanches, which can reach the settlement with a given impact pressure, or a *maximum acceptable risk* in the settlement after protective measures have been constructed. The following sections summarise the laws and regulations that concern avalanche protective measures in some European countries, where snow avalanches constitute a natural hazard.

G.1 Austria

According to the Austrian Constitution (B-VG 1920) the protective against torrents and avalanches falls within the responsibility of the Federal Government. Subsidies are granted by the Government and the Provinces for preventive measures, and area planning is to be carried out in accordance with hazard zone maps. The provisions of the Austrian Forest Act (1975), § 8 b and § 11, are the basis of hazard zoning. Detailed regulations concerning hazard zone maps are laid down in the Ordinance on Hazard Zoning of 1976.

The hazard zone map is to be worked out by an office according to § 102 of the Forest Act (Austrian Service for Torrent and Avalanche Control), which is a subordinate body of the Federal Ministry of Agriculture, Forestry, Environment, and Water Management. The approval of the hazard zone map is granted by the Federal Minister.

According to § 1 of the Ordinance on Hazard Zoning, it is the basis for the planning and execution of the protective measures of the Austrian Service for Torrent and Avalanche Control, as well as for the ranking of these measures according to their urgency (priority list). Hazard zone maps have to be elaborated in such a way that they can serve as a basis for general development planning, building trade, and safety planning. The hazard zone map is only a "directive", but no subsidy can be granted for torrent and avalanche control measures if the hazard zone maps are not taken into account in other aspects of planning. It may be stated that, according to laws and regulations, the hazard map is actually an expert opinion with the character of a forecast.

In accordance with § 6 of the regulations of the Ordinance on Hazard Zoning, hazard zones

Table G1: Hazards zones for snow avalanches in Austria according to the "Directive for hazard zoning" released by the Federal Ministry of Agriculture, Forestry, Environment and Water management (AR = avalanches-red, AY = avalanches-yellow, P = impact pressure, T = thickness of deposits).

Zone	**Design Event**	**Frequent event (1–10 yr recurrence)**
AR	$P > 10\,\mathrm{kPa}$	$P > 10\,\mathrm{kPa}$
	$T > 1.5\,\mathrm{m}$	$T > 1.5\,\mathrm{m}$
AY	$1 < P < 10\,\mathrm{kPa}$	$1 < P < 10\,\mathrm{kPa}$
	$0.2 < T < 1.5\,\mathrm{m}$	$0.2 < T < 1.5\,\mathrm{m}$

have to be determined, taking into account an event with a probability of recurrence of approximately 150 years (design event). Additionally, a "frequent event" with a probability of recurrence of 10 years was defined in the "Directive for Hazard Zoning", released by the Federal Ministry of Agriculture, Forestry, Environment, and Water Management. The determined hazard zones reflect an expert estimation of the sum line of all possibilities for the occurrence of a design event.

The catchment areas of torrents and avalanches are the basis for the designation of natural dangers in the hazard zone map, in accordance with the Forest Act § 99. The most important protection category are hazard zones which mark areas endangered by torrents and avalanches to such an extent that a permanent use for settlement is not possible or only with an unproportionally high effort (red zone) or some impairement (yellow zone). The other zones outlined in the hazard zone maps are: blue areas, which are reserved for future protective measures by the Austrian Forest Engineering Service for Torrent and Avalanche Control; brown areas, which indicate other natural hazards than torrents and avalanches, such as landslides and rock-falls without assessing the intensity and frequency of an event; and purple areas, which show the protection function dependent on the soil composition (terrain). Table G1 shows the criteria used to define hazard zones for avalanches in Austria. Further information about these criteria and hazard zoning in Austria in general is given in Rudolf-Miklau and Schmid (2004) and Sauermoser (2006).

The delineation of hazard zones, reservation areas, and areas indicating other natural hazards is carried out on the basis of state-of-the-art methods, the personal experience of experts, the documentation of historical catastrophe events (the torrent and avalanche chronicle), and the estimated consequences of possible disaster events (scenarios) with a recurrence period of up to 150 years. In principle, it is necessary to clarify for any planned building and land use activity in areas endangered by torrents, avalanches or erosion, whether the plan is compatible with the hazard zoning, and whether the effort for possible protective measures is technically and economically acceptable. Besides their protection effect, protective measures should be in harmony with the use of the building. Improved protection of existing buildings should also be evaluated.

All Building Acts (Building Regulations) of the Austrian provinces contain provisions regarding natural hazards. The building acts regulate how a building permission for a construction site can be issued, considering the safety of the building itself and the natural hazards

that may threaten the site. As a rule, building schemes in hazardous areas are permitted. In most building acts in Austria, an obligatory declaration for a site concerning the suitability for building purposes and the preliminary examination by the building authority prevents building schemes in endangered areas from reaching the official hearing for the building permission. In case of substantial danger, a permission for a new building or rebuilding is only granted if sufficient protective measures can be constructed.

Direct references to the hazard zone map are not made in the building acts of the Austrian provinces except for the Tyrolean Building Act. But the hazard zone map, as a basis for the consideration of natural hazards, becomes effective indirectly via the development plans. The specifications of the development plan and development scheme are legally-binding. Building permissions by the authority have the legal force of an ordinance, thus the object protective measures laid down in these documents must be constructed by the building-owner.

Hazard zone maps can serve as an effective basis (information source) for local safety planning, providing the basic principles for warning and evacuation plans, as well as crisis management. However, until now, these possibilities have hardly been used in Austria. The avalanche warning commissions most likely use the information from the hazard zone maps to assess the situation in avalanche-prone areas (run-out lengths, propagation of avalanches) in order to estimate the area of necessary closings under impending avalanche danger. In Austria, initiatives are taken to build up computer-based crisis information systems. Based on geographical information systems, the hazard zones can be overlaid with other data, for example the number of persons to be evacuated in a given area.

The implementation of permanent protective measures is one of the consequences of hazard zoning. Therefore, assistance of governmental institutions for natural hazard control is frequently requested by the communities for such constructions, and public funds from the federal and provincial governments are requested on a large scale. In Austria, approx. 25 million Euros are currently spent annually on avalanche protective measures and more than 30 million Euros on erosion and torrent control measures. These technical measures have to be designed based on the same parameters as are used in the hazard zoning. In Austria, public funds are only available for projects to protect existing settlements and installations, not to enable new developments. The reduction of hazard zones as a consequence of protective measures is, therefore, limited to these areas and depends on type, function, maintenance and lifespan of these constructions. Especially supporting structures in the starting zone of avalanches have to be considered carefully. The formal reduction of hazard zones after the implementation of protective measures often seems to be more difficult than the first assessment of the reduction of the zones had indicated due to the economical, social and political consequences.

According to the methods described above, legal conditions and administrative regulations, hazard zoning, and construction of protective measures seem to have reached a relative high level of performance and social acceptance in Austria. This situation is based on current knowledge and experience and needs to be developed further. The main points to consider in this future development are:

- Continuous adaptation and verification of the hazard maps in the event of extraordinary natural disasters, to check whether basic environmental factors have changed after the implementation of protective measures.

- Elaboration of “Evacuation Plans” by communities on the basis of avalanche hazard

maps, to ensure that people are not endangered outside their houses in case of high avalanche danger.

- Long-term management of mountain forests, to ensure their protective effect and to prevent the development of new hazard sources.

- Improvement of numerical models in international research programmes.

- Adaptation of national legislative and administrative regulations (*e.g.* "Avalanche Decree" for cabled railways) to an international standard at least within the European Union.

G.2 Switzerland

Protection from snow avalanches and other natural hazards has for a long time been an important responsibility of the Swiss authorities at the communal, cantonal and confederational level. The fundamental legal basis for this activity is the general principle that the state has to protect life, health and property of its citizens. In certain areas, the protective effect of mountain forests was recognised already in the Middle Ages and local laws prohibited logging and grazing in these forests. Avalanche catastrophes in the second half of the 19^{th} century led Johann Coaz, the Federal Forestry Superintendent, to have catastrophic avalanche events in the Swiss Alps systematically observed and catalogued. The Federal Forestry Policy Law of 1876 provided the legal basis for general preservation of protective forests, and for reforestation of mountain slopes, where the growing industry's consumption of firewood and timber, as well as the need of the poor mountain population for pastures, had dangerously reduced the stands and left villages without adequate protection.

Based on this tradition, protection against natural hazards and avalanche research in Switzerland were mostly under the auspices of the federal and cantonal forestry authorities until near the end of the 20^{th} century. Accordingly, it was in the Executive Regulations of 1965, detailing the application of the 1902 Federal Law on the Forestry Police, that the cantons were required to prevent construction in strongly endangered areas and to demand adequate protective measures in less endangered areas. The Confederation will not subsidise protective measures for buildings outside approved construction areas. To this end, the cantons are to elaborate avalanche hazard maps.

In 1979, the Federal Law on Land-Use Planning stipulates that the cantons elaborate the necessary information for the master development plan, and thereby designate the areas endangered by natural hazards and other adverse influences. The communal land-use plans have to be in agreement with the master plan. This implies that the cantons have jurisdiction and responsibility over the avalanche hazard maps, even if they delegate the elaboration of such maps to the communes. The 1991 Federal Law on Forests (WaG) declares the duty of the cantons to secure the starting zones of avalanches that endanger human life or significant property values, and allows federal subsidies of up to 70% of the costs. Passive measures in the run-out zone, such as dams, are not mentioned, but the 1992 Federal Edict on Forests (WaV) details the protective measures against natural hazards in words that do not exclude protection dams. At a yet lower legal level, the Recommendations on Land-Use Planning and

Table G2: Degrees of risk used in the Swiss guidelines for avalanche hazard mapping, their relationship to return period and impact pressure, and their consequences with regard to land-use planning. *DFA*: dense-flow avalanche; *PSA*: powder-snow avalanche.

Zone	**Return period**	**Pressure**	**Consequences and measures**
Red	≤ 30 yr	DFA: any	No construction allowed.
		PSA: > 3 kPa	No reconstruction of old buildings.
	30–300 yr	> 3–30 kPa[1]	
Blue	≤ 30 yr	PSA: < 3 kPa	Construction with reinforcements.
	30–300 yr	DFA: < 3–30 kPa	No buildings open to public.
		PSA: < 3–30 kPa[1], but also > 3 kPa	Evacuation plans.
Yellow	30–300 yr	PSA: < 3 kPa	No constructive measures required.
	> 300 yr	DFA: any	Alarm organisation needed.
White	—	0	No restrictions on land-use, no particular organisational measures required.

[1]Limit pressure depends on return period according to the diagram in Fig. G1.

Natural Hazards[5] explicitly state that passive measures may be used in certain cases to enlarge existing settlement areas or create new ones.

In order to harmonise avalanche hazard maps throughout Switzerland, the Federal Office of Forestry and SLF issued the "Guidelines to Account for Avalanche Danger in Activities Related to Territorial Organisation" in 1984 (BFF/SLF, 1984), following the provisional guidelines of 1975. As such, these guidelines do not have the status of a law passed by Parliament, but only spell out administrative regulation that can be changed when scientific or technical reasons demand it. Nevertheless, they have binding character.

The guidelines pioneered the notion of *risk* as the basis for land-use planning. Mostly, the risk is quantified as the probability of structures being damaged or destroyed, but considerations of human exposure and vulnerability also appear at various places. The threshold for the acceptable residual risk of death from avalanches is considered to be around 10^{-5} per person and year living in an Alpine settlement. However, the guidelines use event frequency and intensity (pressure) as proxies for the local risk.

For hazard mapping in settlement areas, a nominal return period of 300 years has been selected as the threshold beyond which avalanche danger is classified as residual risk. Two or three degrees of danger/risk are differentiated according to frequency (the reciprocal of the return period) and impact pressure, see Table G2 and Figure G1. Associated with these degrees of risk are specific consequences for land use and required active protective measures.

In the 1980s, a method was developed at SLF for calculating run-out distances and pressure distribution of dense-flow avalanches (Salm and others, 1990), based on the Voellmy–

[5]"http://www.are.admin.ch/imperia/md/content/are/are2/publikationen/deutsch/natur_raum_de.pdf" or ". . . /natur_raum_fr.pdf", in German or French.

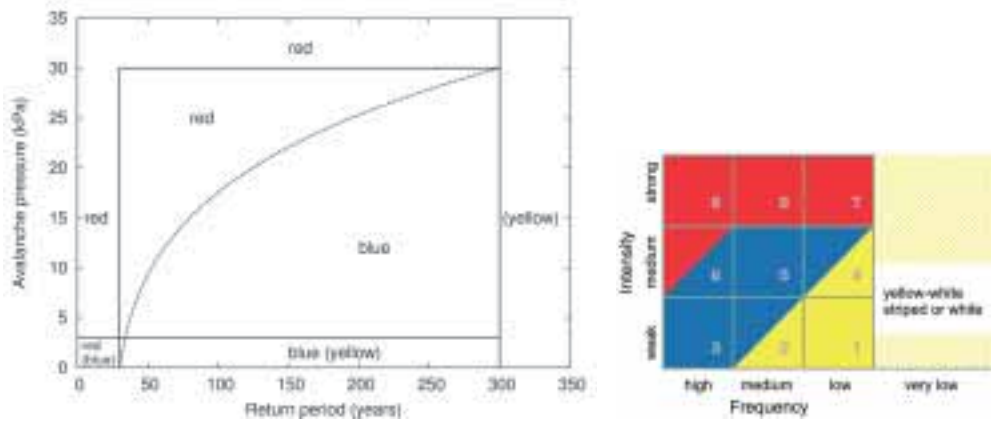

Figure G1: Representation of risk levels as a function of event frequency and intensity. Low frequencies are in the range $3.3–10.0 \cdot 10^{-3}$ per year, high frequencies are $3.3 \cdot 10^{-2}$ per year or higher. Low intensity is associated with pressures below 3 kPa, high intensity corresponds to pressures above 30 kPa. *Left:* Diagram from the 1984 guidelines for snow avalanches. *Right:* New schematic diagram applied to other natural hazards, but not in full agreement with the original diagram for avalanches.

Salm dynamic avalanche model, as well as a statistical approach for determining the initial conditions (*i.e.*, mainly the vertical extent of the starting zone and the fracture depth) as a function of the return period. With the advent of numerical models, the method was adapted (Gruber and others, 1999a) and extended to powder-snow avalanches (Issler, 1999). This calculational procedure has to be followed in all avalanche-hazard mapping work, and is being taught in courses for engineers at ETH Zurich and for practitioners.

Salm and others (1990) also indicate simple methods for estimating the impact forces on objects, as well as the run-up height at wide and narrow obstacles. These methods are based on point-particle considerations as discussed in Sections 11 and 12. SLF is currently working on guidelines for catching and deflecting dams, with similar objectives as the this book. New experimental studies at reduced scale are employed to this purpose.

The 1984 guidelines clearly state that the avalanche hazard maps have to be adapted to newly recognised dangers, reforestation, passive protective measures and new buildings, but it is not specified under which conditions protective measures justify lifting of land-use restrictions. In recent years, efforts were made at various levels to achieve a consensus among the cantonal agencies and practitioners throughout Switzerland, as to the technical conditions for protective measures to be considered effective. At the time of writing, no conclusive results have been obtained, but the following principles are most often applied:

- The endangered areas may be reduced only if the protective measures remain functional with no or little human intervention, or if regular maintenance will be assured over the life cycle of the measure. For example, temporary snow bridges or artificial release devices such as GazEx are not adequate.

- The effectiveness of the measure should be quantifiable and undisputed. In the case of dams, this means that the dam should be constructed according to the general indications given in the guidelines on avalanche calculations (Salm and others, 1990; Gruber

Table G3: Definition of hazard zones for snow avalanches in Italy (Barbolini and others, 2004). T is the return period (years) of avalanches, and P is the impact pressure (kPa) of an avalanche with the indicated return period at the location in question. "$T > 100$ yrs" in the last line of the table indicates that only avalanches with a return period longer than 100 years can reach the location.

Hazard zone	**Hazard level**	**Definition**
Red	High	$T = 30$ yrs and $P > 3$ kPa or $T = 100$ yrs and $P > 15$ kPa.
Blue	Moderate	$T = 30$ yrs and $P < 3$ kPa or $T = 100$ yrs and $3 < P < 15$ kPa.
Yellow	Low	$T = 100$ yrs and $P < 3$ kPa or $T > 100$ yrs.

and others, 1999a; Issler, 1999).

- After a passive protective measure has been completed, the hazard map has to be adjusted on the basis of the best methods and tools then available. In practice this is done in a rather conservative way and only after an adequate observation period.

At the time of writing, no legally binding method for selecting and designing protective measures have been issued, with the exception of the Guidelines for Defence Structures in the Starting Zone (BUWAL/WSL, 1990). General guidelines concerning the choice of protective measures for different types of natural hazard have been issued by the Building Insurance Institution of the Canton of St. Gall (Egli, 1999). They do not have binding legal power but have been well received and serve as a reference work in Switzerland. As mentioned above, guidelines for the design of protection dams are in preparation.

G.3 Italy

A national regulation concerning avalanche hazard mapping does not exist in Italy, and Alpine regions produce their own laws to take snow avalanches into account in land use planning procedures. Recently, as a result of a collaboration project of AINEVA (Italian Association for Snow and Avalanches) and the University of Pavia, new "Guidelines for Avalanche Hazard Mapping" (Barbolini and others, 2004) have been published. This document proposes criteria and methods to be used during different phases of territorial planning in avalanche-prone areas, and represents a reference for the Italian public administrations, which operate in mountainous regions. The mapping criteria proposed in this document exclusively consider urban settlements; traffic roads, electric systems, ski and chair lifts, *etc*. are excluded. The mapping criteria and some relevant aspects of these "Guidelines" are briefly presented below.

Three zones with decreasing degree of hazard are defined on the basis of the return period and impact pressure of avalanches (Table G3).

Red hazard zones include those areas that can be reached relatively frequently by avalanches, even with moderate destructive power, or by rare events with high destructive

potential.

Blue hazard zones include areas reached by residual effects of relatively frequent avalanches, or rarely by avalanches with moderate destructive power.

Yellow hazard zones are those areas that can be reached by the residual effects of rare events. Also, areas reached by extreme events belong to the yellow hazard zone.

Some important aspects of these new guidelines that should be highlighted are:

- The static component of the snow pressure should also be accounted for in the calculation of avalanche impact pressure; this means that the mapping is also based on the deposition depth.
- Monitoring and evacuation plans must be prepared to increase the safety of people living in red, blue and yellow zones.
- Modification of hazard maps after protective measures have been built (or following reforestation) is allowed under certain conditions (no new white areas, that means that the boundaries between red/blue and blue/yellow zones may be moved, but the yellow boundary is not modified; a maintenance plan for the defence measures must be made; *etc*.)

Some general criteria for the updating of hazard zoning is also suggested. On the basis of new information, hazard maps have to be checked and, if necessary, modified. Particular attention has to be paid to:

- historical documentation of past events, not already used in the preparation of the previous hazard map;
- new avalanche events (that is avalanches in areas not registered in the avalanche cadastre) or known events with unexpected extraordinary magnitude;
- natural or artificial modifications to the environment that increase the exposition factor (*e.g.* deforestation of the release area). Up-to-date nivometereological data and the development of new calculation tools also have to be considered as part of the updating of hazard maps.

Factors that can decrease hazard levels have to be considered also, for example, natural reforestation of release areas or the construction of protective measures in the release and/or run-out areas. In order to maintain a control on areas potentially exposed to "extreme" avalanches, the updating of hazard maps should only involve a re-classification of hazard levels, maintaining the earlier total extent of the hazard zones, that is the boundary of the yellow area should remain unchanged. The updating process should be carried out, making use of expert evaluations which:

- consider the effect of reforestation on the release and motion of the snow mass, depending on the type, density and age of the vegetation, as well as its exposure to risk factors that can reduce its efficacy;

Figure G2: An example of the modification of an Italian hazard map after the construction of protective measures: The hazard map before the protective measure were built (left) and an updated map after the construction of protective measures (right) (both snow bridges in the release zone and a deflecting dam in the run-out zone). According to current Italian guidelines, the boundary of the yellow zone has remained unchanged. "Trabuchello" avalanche path, Isola di Fondra community, Brembana Valley, Italy, Central Alps.

- take into account how the protective measures modify release conditions and avalanche dynamics. The life-time of the protective constructions has to be considered as a part of hazard re-classification.

Limitations on land use and specific safety requirements for hazard zones are defined according to the hazard level. Due to the high level of hazard associated with the red zone, construction of new buildings (both residential and commercial) is not allowed in these areas. In the blue (moderate hazard) zones, new constructions are allowed, but with "strong" restrictions (low building indexes, properly reinforced structures, *etc*.). In the yellow (low hazard) zones, new constructions are allowed, with "minor" restrictions (public facilities, like schools and hotels, are not allowed).

Figure G2 shows an example of the original and a revised hazard map from "Trabuchello" avalanche path, Italy, after the construction of protective measures.

G.4 France

France is a country that remains moderately affected by natural disasters. It has an old system of risk prevention. In the middle of the last century, the urbanism code introduced several measures to prevent natural hazards. Articles R-113-2 and R-111-3 allowed the authorities to prohibit construction or to impose requirements on construction in the areas affected by this type of risk. The Code states that "the construction on land threatened by flooding, erosion, landslides, or avalanches may be subject to special construction requirements. The recommendations are set by the national representative at the department level. This concerns all

areas where the phenomenon is considered sufficiently serious and probable. The safety recommendations concern buildings and their occupants." This land use legislation introduced hazard mapping to the Land Use Plan.

On 10 February 1970, an avalanche killed 39 persons at the Val d'Isère ski resort. This disaster highlighted the need for safety planning in mountainous areas and triggered a new step in prevention policy. The development of winter sports and tourism has greatly increased the risk in mountainous areas. The pressure on land use has created new risks caused by an increase in vulnerability.

During the 1970s, the maps of areas exposed to landslide risks (ZERMOS maps) were drawn up by various government agencies. The same was done in avalanche zones with the CLPA maps (location of avalanche phenomena), informative maps detailing the extent of past avalanche events. During the same period, Maps of Areas Exposed to Avalanches (PZEA) were prepared to account for the intensity and frequency of avalanches in urbanised areas. Avalanche mapping covered only avalanche hazard. A system: white for very low hazard, red for high hazard, and blue for moderate hazard or doubtful areas, was adopted.

A new system was established in the early 1980s. It is based on two measures: the PER and CATNAT. The 1982 legislation established the Predictable Natural Hazard maps (PER). The right to compensation and the compensation system called Natural Catastrophes CATNAT were set up in 1984. The law concerned property damage covered by insurance policies. Human life, in particular, was excluded. The CATNAT principle of compensation was balanced by the PER, which contains and even reduces vulnerability. However, between 1982 and 1998, 61,000 insurance claims resulting from natural disasters were filed, showing that this system has not increased prevention. The PER map combines the notions of hazard and vulnerability. Vulnerability must be quantified taking into account direct and indirect potential damage. The hazard study ascertains the reference event and vulnerability is quantified using the event's intensity as a reference. Once the event's intensity and spatial extension are determined, homogeneous areas are defined according to a classification that takes into account the types of construction and economic activity. Hazards and vulnerabilities were difficult to quantify, and the monetary evaluations too time-consuming and too complicated to carry out. The studies were long and expensive. The required consensus between stakeholders and the lack of funding were the main obstacles for the implementation of these plans. Approximately 10,500 municipalities are concerned by risks; 700 PER were started and only 307 were achieved in 1995, evidence of the near failure of this legislation.

One important aspect of the French legislation concerns citizen information. The law of 22 July 1987 created the right of citizens to be informed of the risks to which they are exposed. New documents were set up and disseminated at the national and local levels.

In 1995, the national government simplified the prevention policy against natural hazards within the framework of the above-mentioned environment law. The precautionary principle was retained as the basis for all environmental questions in the 2 February 1995 law. It was stipulated that "the absence of certainty, in terms of scientific and technical knowledge, should not delay the adoption of effective and adequate measures to prevent serious and irreversible risk ... at an economically acceptable cost." This principle led to the adoption of new prevention plans against natural hazards. Following this principle, preventive measures must not only be effective but also proportionate to the risk one is attempting to prevent.

New maps were produced: Prevention of Predictable Risk maps (PPR), which are tools for both information and urban planning regulation that included construction requirements.

Existing maps (R111-3 and PER) were automatically converted into PPR maps. The new procedure was meant to simplify and speed up map design and implementation.

One of the objectives of the PPR programme is to delimit areas directly subjected to risk. For avalanches, the reference event is defined as the avalanche corresponding to the maximum known extension since the middle of the 19^{th} century if this has a return period that is longer than 100 years. If not, the 100-year return period event is determined (statistically, expert assessment) using current knowledge. The intensity of the reference event is determined and mapped. In the area where the pressure is higher than 30 kPa, construction is banned. This area is the red zone. In the area reached by the reference avalanche, but with a pressure lower than 30 kPa, construction is restricted. This area is the blue zone. A methodological guide is currently being prepared.

In addition, the law has provided a complementary solution: procedures for the expropriation of property exposed to major natural hazards (law of 17 October, 1995). To benefit from this particular type of expropriation, a series of conditions are required. Avalanches, landslides and torrential floods are the only types of predictable natural hazards likely to come within this specific expropriation measure.

Unlike PER, the PPR also incorporates human life and the ability to impose use requirements and additional reinforcement for existing constructions. This additional work must be done within a period of 5 years after the adoption of the PPR, and shall not exceed an amount equivalent to 10% of the property's value.

Laws and regulations also state that avalanche zoning should not be modified after avalanche protective measures have been constructed. For example, no relaxation of land use restrictions is made in spite of the improved safety provided by the protective measures in place. This underlines the policy that protective measures are only intended to improve the hazard situation in existing settlements and should not lead to increased population density in potentially hazardous areas, especially considering the inherent uncertainty on the effectiveness of avalanche protective measures. If the construction of a defence structure increases the hazard in specific areas (for example avalanche deviation towards an initially safe area), this must be included in the hazard mapping. Lastly, hazard mapping has to be updated every 10 years.

G.5 Norway

The Building and Planning Act in Norway is the principal legal act concerning snow avalanche and landslide hazard. The legal demands concerning avalanche safety was first established in the Building Act of 1924. The act was put into force for the whole country in 1966. The last revision was made in 2008. The municipality is responsible for maintaining the Planning and Building Act.

Two paragraphs are of special importance concerning snow and landslide hazard: § 25 defines the different Regulation areas:

- Building areas
- Agricultural areas
- Public traffic areas
- Danger areas: "... areas that because of the risk of avalanches, landslides or flooding, or other specific danger, are not allowed to be built out, or can only be developed under

Table G4: Hazard zones for snow avalanches and landslides in Norway. Nominal frequency and return period in the Norwegian Building and Planning Act.

Safety class	**Max. nominal**[1] **frequency per year**	**Return period (years)**	**Type of construction**
1 Small	10^{-2}	> 100	Garages, smaller storage rooms of one floor, boat houses.
2 Medium	10^{-3}	> 1000	Dwelling houses up to two floors, operational buildings in agriculture.
3 Large	$< 10^{-3}$	> 1000	Hospitals, schools, public halls *etc*.
4 Very large	No danger accepted	—	Oil refinery, other big industrial plants, *etc*.

[1]The word "nominal" is used for snow and landslide frequencies, in order to distinguish it from "real". Admittingly it is often impossible or very difficult to calculate the real frequencies of snow and landslides, and subjective judgement by experts is accepted.

special conditions concerning safety."

and § 68, which puts demands on the Building ground:

- "An area can only be disposed of, or built upon if there is sufficient safety against danger or considerable disadvantage because of natural or environmental conditions. The municipality may forbid building, or put forward special requirements for the use of areas mentioned above."

Supplementary details to the paragraphs in the act are described in Technical Regulations, where conditions on the location and safety of buildings are given:

"Buildings must be located and designed to give satisfactory safety against damage from natural hazards such as:

- avalanches and slides
- flooding
- sea
- wind."

According to the Technical Regulations in the law, four classes of snow and landslide frequencies are usually taken into account, see Table G4. The table accounts for both the size of the building, indirectly the number of people occupying the building, and the length of time it is used for residence.

As can be seen from the table, buildings like garages, are allowed to be built, where snow and landslide frequencies are up to 10^{-2} per year. A normal dwelling house should not be exposed to a hazard greater than 10^{-3} per year. The safety for a school or a hospital should be better than 10^{-3} per year, how much better is to be decided by the municipality in each case.

Very large industrial plants and similar buildings should not be exposed to snow and landslide hazard at all.

In addition, the regulation states that rebuilding after fires or other types of repair may be done for class two, when the nominal yearly frequency is lower than $3 \cdot 10^{-3}$.

There are no specifications concerning impact forces from snow avalanches or landslides in the regulations.

Nothing is said specifically concerning the use of safety measures and the effect of safety measures on hazard zones, but the regulations state that: "The safety against snow avalanches and landslides is supposed to be satisfactory when buildings in safety classes 1, 2, and 3, plus the directly adjacent external areas are dimensioned or protected against snow and landslides in such a way that the norm figures in the table are fulfilled. Buildings in class 4 are not to be located in hazard areas." According to this, it is legal to develop areas in hazardous regions, as long as they are protected according to the regulations.

Other legal regulations which are of interest concerning snow and landslide hazard are:

Police Law: The police are responsible for the safety of the inhabitants in dangerous situations.

Working Environment Law: The working environment must be arranged in such a way that employees are not exposed to falling objects or slides.

Natural Hazard Law: National law for compensation caused by natural hazards and for contribution to safety measures.

- Buildings insured against fire are automatically insured against natural hazards.
- Governmental compensation for mitigation measures based on the Natural Hazard Law is about 50%. The county, the municipality and the owner must pay the rest.

River Course Law: Regulates management and control of river courses.

For the protection of road traffic against snow avalanches and landslides, there exist no official laws concerning acceptable snow and landslide frequency, but the Norwegian Road Administration has worked out a set of internal guidelines. According to these guidelines, the frequencies taken into account when defence structures are made, depend mainly on traffic density, type of traffic, importance of the road, and alternative routes when the road is blocked.

G.6 Iceland

The Icelandic regulation on snow and landslide hazard zoning is based on individual risk (The Ministry for the Environment, 2000; Jónasson and others, 1999; Arnalds and others, 2004), *i.e.* the probability of death as a consequence of a snow avalanche or a landslide. The so-called *local risk* (*i.e.* ignoring exposure, see Arnalds and others (2004)) of $0.3 \cdot 10^{-4}$ per year is defined to be acceptable for residential areas, and three types of hazard zones are defined, where the risk is progressively higher, see Table G5. The guidelines for the zoning and utilisation of the hazard zones are tailored to attain the acceptable risk level in residences when the exposure and increased safety provided by reinforcements have been taken into

Table G5: Hazard zones for snow avalanches in Iceland.

Zone	**Lower level of local risk**	**Upper level of local risk**	**Building restrictions**
C	$3 \cdot 10^{-4}$ yr^{-1}	–	No new buildings, except for summer houses[1], and buildings where people are seldom present.
B	$1 \cdot 10^{-4}$ yr^{-1}	$3 \cdot 10^{-4}$ yr^{-1}	Industrial buildings may be built without reinforcements. Homes have to be reinforced and hospitals, schools *etc*. can only be enlarged and have to be reinforced. The planning of new housing areas is prohibited.
A	$0.3 \cdot 10^{-4}$ yr^{-1}	$1 \cdot 10^{-4}$ yr^{-1}	Houses where large gatherings are expected, such as schools, hospitals *etc*., have to be reinforced. The planning of new housing areas is prohibited.

[1]If the local risk is less than $5 \cdot 10^{-4}$ per year.

account. For industrial buildings, the guidelines probably correspond to a somewhat higher risk, but this may be justified by the absence of children.

The Icelandic hazard zoning regulation (The Ministry for the Environment, 2000)[6], which is based on a law from 1997 concerning avalanches and landslides (Alþingi, 1997)[7], states that protective structures "shall only be built to increase the safety of people in areas already populated." The effect of protective structures shall be assessed and/or calculated, and this effect is reflected in an updated hazard zoning, which is issued by the government after the protective measures are completed. This leads to a (partial) relaxation of previous restrictions on the use of land in the protected area. This applies in particular to catching and deflecting dams in avalanche run-out areas and to supporting structures in starting zones. In areas with protective structures, both local risk in the absence of such measures, as well as local risk taking the structures into consideration, shall be shown on the hazard map. Protective measures shall be designed with the aim to increase the safety such that that the risk to humans in the protected area is as near as possible to the acceptable risk as specified by the hazard zoning regulation (see above). However, this goal is not an absolute requirement. Due to the large uncertainty in the design assumptions of avalanche protective measures, the adaptation of the hazard zoning to a large extent is based on the subjective judgement of experts involved in the design of the structures. In order to reflect this uncertainty, the outer boundary of the **A** hazard zone is typically not moved higher up than the line corresponding to the previous boundary of the **C** hazard zone.

Figure G3 shows a hazard map for the Drangagil area in Neskaupstaður, eastern Iceland (Arnalds and others, 2001a), where protective measures consisting of supporting structures,

[6]No. 505/2000, "http://www.vedur.is/snjoflod/haettumat/reglugerd_505_2000_e.pdf"
[7]No. 49/1997, "http://www.vedur.is/snjoflod/haettumat/log_49_1997_e.pdf"

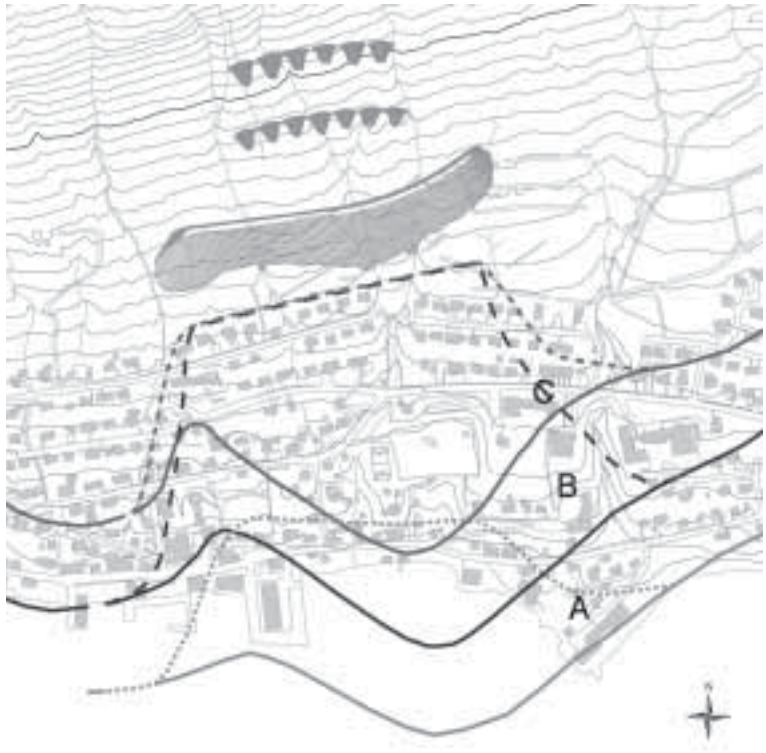

Figure G3: A hazard map for the area below Drangagil in Neskaupstaður, eastern Iceland, showing the estimated local risk both in the absence of protective measures (solid lines) and the estimated local risk after the structures have been fully completed (dashed lines, the **B** and the **C** lines coincide below the dam) (*cf.* Table G5). The protective measures consist of supporting structures (not shown in this figure, but shown in figure D1), 10 m high braking mounds, and a 17 m high catching dam (see also Figures D1 and D2).

braking mounds and a catching dam have been constructed (Tómasson and others, 1998a,b). The map shows the estimated isorisklines in the absence of protective measures, and the estimated local risk after the structures have been fully completed.

European Commission

EUR 23339 - The design of avalanche protection dams — Recent practical and theoretical developments

2009 — 205 pp. — 17.6 x 25.0 cm

ISBN 978-92-79-08885-8
ISSN 1018-5593
DOI 10.2777/12871

How to obtain EU publications

Our priced publications are available from EU Bookshop (http://bookshop.europa.eu), where you can place an order with the sales agent of your choice.
The Publications Office has a worldwide network of sales agents. You can obtain their contact details by sending a fax to (352) 29 29-42758.

This book represents a capitalisation of knowledge from previous EC research projects in the field of Natural hazards and, in particular, the CADZIE and SATSIE projects addressing the problem of avalanches. It is about the design of dams and other protection measures in the run-out zones of wet- and dry-snow avalanches. The book summarises recent theoretical developments and the results of field and laboratory studies, combining them with traditional design guidelines and principles to formulate design recommendations. The findings of the book are relevant to avalanche experts and authorities concerned with protection measures and risk management.

KI-NA-23339-EN-C

Publications Office
Publications.europa.eu

ISBN 978-92-79-08885-8